Soft radiation in Quantum Chromodynamics

ISBN 978-90-9024613-0

Soft radiation in Quantum Chromodynamics

Zachte straling in de kwantumchromodynamica

(met een samenvatting in het Nederlands)

Proefschrift

ter verkrijging van de graad van doctor aan de Universiteit Utrecht
op gezag van de rector magnificus, prof.dr. J.C. Stoof, ingevolge het
besluit van het college voor promoties in het openbaar te verdedigen
op maandag 14 september 2009 des middags te 2.30 uur

door

Gerben Cornelis Stavenga

geboren op 25 juni 1980
te Delft

Promotor: Prof.dr. E.M.L.P. Laenen

Ter nagedachtenis aan mijn moeder.

The material presented in this thesis is based on the following publications:

chapter 2
E. Laenen, L. Magnea, and G. Stavenga,
On next-to-eikonal corrections to threshold resummation for the Drell-Yan and DIS cross sections, Phys. Lett. **B669** (2008), 173–179.

chapter 3
E. Laenen, G. Stavenga, and C.D. White,
Path integral approach to eikonal and next-to-eikonal exponentiation, JHEP **03** (2009), 054.

chapter 4
E. Laenen, L. Magnea, G. Stavenga, and C.D. White,
Next-to-eikonal exponentiation of DY cross sections, in preparation.

chapter 5
S. Frixione, M. Herquet, M.Klasen, E. Laenen, T. Plehn, G. Stavenga, C. Weydert and C.D. White, *Single top production in association with a charged Higgs boson*, in preparation.

Contents

Chapter 1

Introduction

The most fundamental theory of elementary particles according to our current understanding is the "Standard Model" (SM). It has been developed in a 50 year time span, from the late 1920's with the birth of quantum electrodynamics (QED) to the early 1970's when quantum chromodynamics (QCD) emerged as the fundamental theory of the strong force. The Standard Model unifies electromagnetism and the two nuclear forces into one model based on Yang-Mills gauge theories. In 1954 Chen Ning Yang and Robert Mills, inspired by electrodynamics and general relativity, generalized the abelian gauge symmetry of electrodynamics to gauge symmetries based on arbitrary Lie groups. This was a monumental leap of insight, and beauty, in theoretical physics. Yang and Mills tried to use their model as a model for the strong force. They noticed, as others had, that the mass difference between neutrons and protons is small, and proposed to treat them as two different states of the same particle. By analogy to spin states of the electron this property was called isospin. In other words, an SU(2) symmetry is present if the tiny mass difference is ignored. Using this SU(2) as a (non-abelian) gauge group they tried to find a model for the dynamics of the strong nuclear force. Ultimately this failed, because the model predicted massless particles associated with the gauge field, in analogy to photons in QED. These massless particles were not seen, which ruled this theory out. There was evidence, in contrast, for massive photon-like particles. However, a good idea does not have to die, but can live to serve another day. Indeed the idea of Yang and Mills turned out to be correct, after some hurdles were taken. The apparent absence of massless particles, besides the photon, implied the need for a mechanism to give the gauge field mass. This is a non-trivial requirement, because almost all methods that give the gauge field a mass run into inconsistencies. The appropriate method was found by Brout, Englert and Higgs. They discovered that if one makes the vacuum superconducting with respect to the current associated with the gauge field, the gauge field acquires an effective mass. Intuitively this can be understood as follows. A gauge particle is a quantum of the fluctuating of gauge field. A fluctuating magnetic field induces a electric field. In a low-temperature superconductor this electric field creates a current that coun-

teracts the fluctuation of the magnetic field. Within the superconductor, as a result, a magnetic field decays exponentially, a phenomenon known as the Meissner effect. This exponential decay of the force is characteristic of a massive force particle. This mechanism, later named after Higgs, does not ruin the underlying gauge principle and provides the necessary ingredient for the creation of the Weinberg-Salam model for the electromagnetic and the weak force. The Higgs mechanism predicts the existence of a Higgs particle. The Large Hadron Collider (LHC) will hopefully discover this particle and measure its properties.

Another hurdle to be taken was the occurrence of infinities associated with the perturbative quantum field theory calculations. In QED it had been shown by Feynman, Schwinger and Tomonaga, based on work of Kramer and Bethe, that all infinities encountered could be canceled by the renormalization of the mass, field strength and coupling constant. Although the renormalization procedure was consistent and the results in excellent agreement with experiments, people felt uncomfortable with renormalization. As a result much attention went into finding quantum theories that did not suffer from infinities, and research on quantum field theory was not popular. Furthermore, the non-abelian nature of Yang-Mills theory made the proof of renormalization much more difficult. It was not until 1971 that Gerard 't Hooft and Martinus Veltman proved that Yang-Mills theory is renormalizable, even in the presence of the Higgs mechanism. This paved the way for Yang-Mills theories to be considered viable, consistent and predictive theories of nature.

The work of 't Hooft and Veltman together with the Weinberg-Salam model settled the issue of the weak nuclear force. One big problem remained: the description of the strong nuclear force, which behaved very strangely. It was clear at this time from deep inelastic scattering (DIS) experiments carried out at the Stanford Linear Accelerator (SLAC), that protons and neutrons where not fundamental particles, but have substructure. They are actually part of a larger set of particles and resonances called hadrons, to which also pions and kaons belong. Murray Gell-Mann was able to explain a pattern in the spectrum of these hadrons by proposing "quarks" as building blocks of hadronic particles. These quarks were considered to be very tightly bound together in hadrons. On the other hand, to explain the observations from the DIS experiments, Feynman proposed that hadronic particles consist of so-called partons, which behaved like free particles.

From this paradox QCD emerged. The quarks proposed by Gell-Mann are charged under a new gauge force called the "color" force. Each quark can be in three , labeled red, green and blue. Physical quantities are invariant under local mixings of these states, so that an SU(3) symmetry is present. This SU(3) is the gauge group for a Yang-Mills force field. The elementary force particles of this force are aptly called gluons, as the force is so strong that it glues quarks together into the hadronic particles. These quarks together with the gluons are what Feynman called partons.

Although further experiments provided evidence that QCD is the correct theory of the strong force, a full theoretical understanding has not yet been reached, and a number of important questions remain unsettled. The fundamental particles of QCD are the quarks and gluons, but these have never been seen in experiments. Why can't

we see them as free particles? While the detailed answer to this question is not exactly known, apparently the dynamics is such that the force strongly ties colored particles together into neutral particles. This poses another question: if the force is so strong why do quarks and gluons behave like free non-interacting partons inside the hadrons? The answer to this question, at least, has been given by Gross, Politzer and Wilczek and independently by 't Hooft around 1973. QCD is asymptotically free, which means that the force becomes weak at small distance scales. Within the small space of the hadrons the partons are weakly interacting, therefore Feynman's assumption of free non-interacting particles is valid. The answer to the first question is still open and goes under the name of confinement. A lot of progress in understanding confinement has been made, but no scientific consensus has been reached. In every experiment, when we smash hadrons to smithereens, the partons will recombine in such a way that color neutral final state particles are formed. In 1.7 I will discuss confinement a bit further. There is now no doubt that QCD is the correct theory for the strong force. The same can be said for the electroweak force, although the important issues of its symmetry breaking (Higgs mechanism) are not yet experimentally confirmed.

Present-day theoretical particle physics can be roughly divided into two branches. One branch consists of issues associated with quantum gravity, the only known force that so far eludes a description within the framework of quantum mechanics. There are two mainstream candidates, string theory and loop quantum gravity. The problem in this branch is that the gravitational force is so weak that direct experimental input within the foreseeable future is out of the question. The goal then is not to explain experiments, but to explain the Standard Model or extensions of it, explain gravity and explain cosmological phenomena from an era where gravity was important as a quantum theory. Of necessity, this is a top-down approach to physics. The other branch consist of theory relevant for collider experiments. Here the Standard Model or possible extensions and their phenomenology for such experiments are studied, more a bottom-up approach. Of course, there is a fuzzy boundary between these two branches, with much cross-fertilization. The research in this thesis belongs mainly in the second branch. In chapters 2, 3 and 4 the focus is on increasing the accuracy of calculations within QCD by examining all-order effects to help find signals of new physics by discriminating the new from the known. We shall also uncover new structures in the perturbative description of QCD that enable more accurate calculations. Chapter 5 discusses a possible extension of the Standard Model involving additional Higgs particles. We implement the process of top plus charged Higgs production in a next-to-leading order Monte Carlo simulation, which is very useful in order to compare the theory with data.

1.1 Quantum Field Theory

In this thesis various concepts in quantum field theory, such as path integrals and perturbative divergences of various kinds, will play a role in a variety of new settings.

To this end it is appropriate to briefly review these concepts again in a more introductory way. While the presentation is not unlike what can be found in textbooks, it has been structured to match the context of this thesis, and may on occasion present an unusual viewpoint. In classical field theory we are interested in a field that lives on all points in a space or space-time. For instance the electric potential $\phi(x,t)$ is a function of space and time. The dynamics of the field is given by the field equations and is usually derived from Hamilton's principle of least action. This means that the classical field is given by a stationary point of a functional $S[\phi]$, the action, given by the integral over a Lagrangian

$$S[\phi] = \int d^d x L(\phi(x), \partial_\mu \phi(x)). \tag{1.1}$$

The classical field configuration is given by the stationary point

$$\frac{\delta S[\phi]}{\delta \phi(y)} = \int d^d x \left(\frac{\partial L}{\partial \phi} - \partial_\mu \frac{\partial L}{\partial(\partial_\mu \phi)} \right) \delta^d(x-y) = 0, \tag{1.2}$$

from which we can deduce the Euler-Lagrange equation of motion

$$\frac{\partial L}{\partial \phi} - \partial_\mu \frac{\partial L}{\partial(\partial_\mu \phi)} = 0. \tag{1.3}$$

In quantum mechanics we are generally interested in the amplitude to pass from a certain initial state to some final state. In quantum field theory such an amplitude is given by the Feynman path-integral

$$Z = \int_{\phi(t_i)=\phi_i}^{\phi(t_f)=\phi_f} \mathcal{D}\phi \exp\left[\frac{i}{\hbar} S[\phi]\right]. \tag{1.4}$$

Here we integrate over all the possible field configurations that are fixed at initial and final time t_i, t_f. This path-integral is proportional to the required amplitude. For calculations of cross-sections one does not need to fix the fields at the boundary. All we need to know are the so-called n-point Green's functions

$$G(x_1, \ldots, x_n) = \frac{1}{Z} \int \mathcal{D}\phi \; \phi(x_1) \ldots \phi(x_n) \exp\left[\frac{i}{\hbar} S[\phi]\right]. \tag{1.5}$$

All these Green's functions can be obtained from a generating functional

$$Z[J] = \int \mathcal{D}\phi \exp\left[\frac{i}{\hbar}\left(S[\phi] - \int d^d x J(x)\phi(x)\right)\right]. \tag{1.6}$$

In general the integral above is impossible to carry out exactly, except when the action is quadratic in ϕ. To be specific, let us take ϕ^4 theory as an example. The action of this

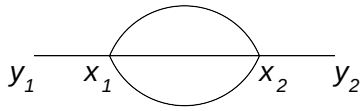

Figure 1.1: Graph corresponding to $J(y_1)G(y_1,x_1)G(x_1,x_2)^3G(x_2,y_2)$

theory is given by

$$\begin{aligned} S[\phi] &= \int d^dx \left(\frac{1}{2}\partial_\mu\phi\partial^\mu\phi - \frac{1}{2}m^2\phi^2 - \frac{1}{4!}\lambda\phi^4\right) = S_0[\phi] + S_I[\phi], \\ S_0[\phi] &= \int d^dx \frac{1}{2}\phi\hat{A}\phi, \quad \hat{A} = -\partial_\mu\partial^\mu - m^2 = \hat{p}^2 - m^2 \\ S_I[\phi] &= -\int d^dx \frac{1}{4!}\lambda\phi^4. \end{aligned} \tag{1.7}$$

Using this we can write eq. (1.6) as

$$Z[J] = \exp\left[\frac{i}{\hbar}S_I\left[i\hbar\frac{\delta}{\delta J}\right]\right]\int \mathcal{D}\phi \exp\left[\frac{i}{\hbar}\left(S_0[\phi] - \int d^dx J(x)\phi(x)\right)\right], \tag{1.8}$$

which is a formal expression in that we define the first exponential as its power series. The identity is only valid when the RHS is regarded as an asymptotic series in λ. This is so because in deriving the above formula integration and summation had to be interchanged. Due to the non-compactness of the integration domain this is not valid as a strict identity, but is allowed as an asymptotic identity in λ. The path-integral on the RHS can be performed analytically because it is a Gaussian integral after completing the square. Up to an overall normalization we have

$$\begin{aligned} Z[J] &= \exp\left[\frac{i}{\hbar}S_I\left[i\hbar\frac{\delta}{\delta J}\right]\right]\exp\left[-\frac{i}{\hbar}\frac{1}{2}JGJ\right] \\ &= \exp\left[\frac{i}{\hbar}S_I\left[i\hbar\frac{\delta}{\delta J}\right]\right]\left[\exp\left[i\hbar\frac{1}{2}\frac{\delta}{\delta\phi}G\frac{\delta}{\delta\phi}\right]\exp\left[-\frac{i}{\hbar}J\phi\right]\right]_{\phi=0} \\ &= \left[\exp\left[i\hbar\frac{1}{2}\frac{\delta}{\delta\phi}G\frac{\delta}{\delta\phi}\right]\exp\left[\frac{i}{\hbar}S_I\left[i\hbar\frac{\delta}{\delta J}\right]\right]\exp\left[-\frac{i}{\hbar}J\phi\right]\right]_{\phi=0} \\ &= \left[\exp\left[i\hbar\frac{1}{2}\frac{\delta}{\delta\phi}G\frac{\delta}{\delta\phi}\right]\exp\left[\frac{i}{\hbar}\left(S_I[\phi] - J\phi\right)\right]\right]_{\phi=0}. \end{aligned} \tag{1.9}$$

Here G is the two point Green's function, the inverse of the differential operator $\hat{A}$ in eq.(1.7). We used shorthand notation $J\phi = \int d^dx J(x)\phi(x)$ and $JGJ = \int d^dx d^dy J(x)G(x,y)J(y)$. There is a simple pictorial (see fig. 1.1) description for the terms generated by performing the functional differentiations in the last line. If we expand the last exponential in powers of ϕ the only contributions to $Z[J]$ are generated by acting with $\frac{\delta}{\delta\phi}$ precisely

enough times to remove all ϕ's. A typical term takes the form

$$\exp\left[i\hbar\frac{1}{2}\frac{\delta}{\delta\phi}G\frac{\delta}{\delta\phi}\right]\frac{(-i\lambda)^n}{\hbar^n 4!^n n!}\left(\int d^dx\phi(x)^4\right)^n\frac{(-i)^m}{\hbar^m m!}\left(\int d^dxJ(x)\phi(x)\right)^m\Big|_{\phi=0}. \quad (1.10)$$

If m is odd this term vanishes when we put ϕ to zero. Furthermore we must act precisely $2n+m/2$ times with the derivative operator. Therefore this expression becomes

$$\frac{1}{(2n+m/2)!}\left(i\hbar\frac{1}{2}\frac{\delta}{\delta\phi}G\frac{\delta}{\delta\phi}\right)^{2n+m/2}\frac{(-i\lambda)^n}{\hbar^n 4!^n n!}\left(\int d^dx\phi(x)^4\right)^n \times\frac{(-i)^m}{\hbar^m m!}\left(\int d^dyJ(y)\phi(y)\right)^m\Big|_{\phi=0}. \quad (1.11)$$

Each derivative operator cancels two ϕ's, let us say $\phi(z_1)$ and $\phi(z_2)$, and replace this pair by a factor $i\hbar G(z_1,z_2)$. If we interpret $i\hbar G(z_1,z_2)$ as a line between the two points z_1 and z_2 then after all differentiations we obtain a set of terms, where each term is a graph with vertices located at $x_1,\ldots,x_n$ and $y_1,\ldots,y_m$. The vertices located at one of the x_i have 4 lines and the vertices located at y_i have one line. In general many terms are generated that are isomorphic to each other. Two terms which have isomorphic graphs are related by relabeling of the coordinates in the integral and give the same contribution. Generically the number of isomorphic terms thus found cancel all the factorial factors in eq. (1.11) except for diagrams with extra internal symmetry. Summarizing, perturbative theory gives

$$Z[J]=\sum_G\frac{1}{\mathrm{sym}(G)}\mathcal{F}(G), \quad (1.12)$$

where we sum over all graphs consisting of vertices of degree one (source terms) and four (interactions). Here $\mathrm{sym}(G)$ gives the symmetry factor of the diagram and $\mathcal{F}(G)$ the corresponding expression for the Feynman diagram in terms of propagators and vertices. From eq. (1.11) it is easy to see that every line comes with a factor $\hbar$ while every vertex comes with a factor $\frac{1}{\hbar}$. The total power in $\hbar$ is given by

$$\#\text{lines}-\#\text{vertices}=\#\text{loops}-\#\text{connected components}, \quad (1.13)$$

where we used Euler's network formula for graphs.

As proved in 3.A, Z can also be written as the exponent of the sum of connected graphs

$$Z[J]=\exp\left[\sum_G^{\text{conn}}\frac{1}{\mathrm{sym}(G)}\mathcal{F}(G)\right]. \quad (1.14)$$

Therefore the power of $\hbar$ in the exponent is given by $\#\text{loops}-1$. The graph expansion is thus an expansion in powers of $\hbar$. If $\hbar$ is very small then small variations of the action produces large oscillations of the exponent. These oscillations integrate to zero,

except when the action is stationary. One expands the integral around the classical stationary point, which should be reliable when $\hbar$ is small. The perturbative expansion is thus equivalent to the semi-classical expansion.

In theories such as ϕ^4 theory where we have translational invariance it is convenient to switch to momentum space. Momenta then flows through the lines and is conserved at every vertex, except at the J vertices. The J vertex is a source (or sink) for particles with momentum. In momentum space, the two point Green's function, or propagator becomes especially simple

$$G(p) = \frac{i\hbar}{p^2 - m^2 + i\varepsilon}. \tag{1.15}$$

If a graph has no loops (ie. a "tree" graph) momentum conservation at each vertex fixes all the momenta of the propagators. For graphs containing loops, momentum conservation does not fix the momentum flowing through each line. Therefore we must integrate over all loop momenta. Also note that calculating diagrams in momentum space matches the physics of actual experiments, where one collides particles of definite momenta and measures the momenta of the produced particles.

The most well-known way to calculate quantities in QFT is by using this semi-classical approximation, or loop expansion. We can think of quantum effects as minor corrections to the classical solution and include them order by order in a systematic perturbative expansion. There are only a few examples of QFT's that can be solved exactly and even then almost always in some specific limit. This is in contrast to quantum mechanics where many different systems have known exact solutions. The difference is that QFT is quantum system of infinite many degrees of freedom, making exact analytic calculations difficult. Even within perturbation theory the infinitely many degrees of freedom make life hard because they give rise to divergent coefficients in perturbation series. It is to such divergences that we now turn our attention.

There are two types of divergences in the perturbative expansion of QFT's. The UV divergences are in a sense entropic divergences: states receive corrections from all other states. Though the coupling to very highly energetic states is suppressed by their energy difference, the number of such very highly energetic states increases so rapidly with energy that the net effect is divergent. For example, in our ϕ^4 theory we obtain the following contribution for a four point interaction (see fig. 1.2)

$$(-i\lambda)^2 \frac{1}{2} \int \frac{d^d l}{(2\pi)^d} \frac{i}{l^2 - m^2 + i\varepsilon} \frac{i}{(l+P)^2 - m^2 + i\varepsilon}. \tag{1.16}$$

This expression is clearly divergent for $d = 4$. This diagram describes the scattering of two initial particles with total momentum P, by first interacting to form a two particle state with momenta $P - l, l$ and then another interaction to form the final state. Although the amplitude to produce a highly energetic state is suppressed by the denominators there are so many highly energetic states to be integrated over that a divergent contribution to the amplitude is produced. These divergences are normally absent in QM where the number of degrees of freedom is finite. UV divergences are therefore a generic feature of QFT, and they become worse in higher dimensions.

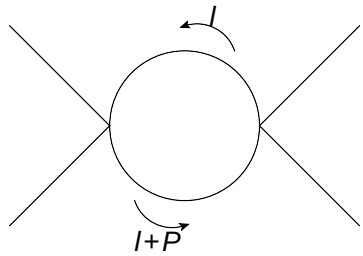

Figure 1.2: Virtual correction to 4-point interaction.

The other type consists of infrared (IR) and collinear (COL) divergences. States receive corrections from states with almost the same energy, that couple very strongly to each other. To see how these divergences arise, let us take the same amplitude (1.16), but now set the mass zero and consider the scattering of zero momentum particles $P = 0$. The integrand is singular at $l^2 = 0$, sufficiently so to make the integral diverge. Going to higher dimensions typically reduces the IR/COL divergences. These divergences also occur in ordinary QM. In this thesis IR/COL divergences play an important role: in particular their origin, how to handle and remove them and their consequences. In order to develop intuition about these divergences we will show some examples of IR divergences in QM toy models and QED/QCD in this chapter. We demonstrate that, in a sense, these divergences are predominantly artefacts of our calculational technique. In other words, there might be so far unknown calculational methods in which these divergences are manifestly absent. Indeed a full understanding of QCD would include the effects of confinement and therefore be free of IR and COL divergences due to the absence of massless particles.

Due to the proliferation of divergences in calculations, theoretical high energy physics requires mastering the art of juggling with infinities. Many expressions are divergent and great care must be taken to obtain meaningful answers. The most general way to deal with infinite expressions is to regularize them by changing them first to convergent expressions. In general a "cut-off" parameter is introduced that governs such a regularization. The limit in which the cut-off is removed will be singular and the expression must be reorganized consistently such that a convergent limit is obtained. There are any number of ways to regulate expressions. Some are more convenient, some are more physical, but physics should not and must not depend on our choice of regularization.

The UV divergences are handled by renormalization. If a theory is renormalizable the particular regularization method is not important because differences between regularization schemes can be absorbed into a finite number of parameters. These parameters are not directly measurable, therefore not physical. They are known as bare parameters. When one calculates measurable observables one obtains finite and regularization scheme independent results. Therefore renormalizable theories meet the criteria to serve as a theory of nature by being consistent and predictive. The fact that

a renormalizable theory is independent on the regularization scheme is most easily seen in the BPHZ [1] renormalization method. In the BPHZ renormalization method one can renormalize a QFT without introducing any regularization. In this method the UV infinities are handled at the level of integrands, before performing the integration. By using the BPHZ renormalization method, in combination with some explicit regularization, one can show that artefacts coming from a particular regularization choice are absorbed into the definition of bare coupling parameters, which are unphysical anyway. The resulting expression for physical meaningful quantities are finite and independent of the method of regularization. The question now arises: why do we use regulators when it is not necessary according to the BPHZ method? There are two reasons for this. The first is that regularization using the dimensional regularization method turns out to be much more convenient than BPHZ. The second reason is that in the presence of massless particles BPHZ renormalization becomes very cumbersome, because it is based on expanding integrands around zero momentum, which is a singular expansion point. Dimensional regularization allows an arbitrary subtraction point. Moreover in the presence of a gauge symmetry BPHZ is hard to apply, in contrast to dimensional regularization, which easily respects the gauge symmetry.

Theories that are not renormalizable require an infinite number of parameters to absorb the ambiguities introduced by the regularization procedure. Although these theories are less predictive, they still have use in physics. For instance, the four fermion theory of weak interaction is an accurate and useful model for the weak interaction at low energies at tree level. The non-renormalizability of the theory reflects the sensitivity of the theory to its "UV completion" around the electroweak breaking scale. Indeed the Weinberg-Salam model provides this UV completion at this scale as the theory for the weak interaction. One can understand the four fermion theory then as an effective theory at lower energy. Usually the low energy limit of a theory will be a renormalizable theory, but in this case the low energy renormalizable limit of the Weinberg-Salam model would be a free theory. There are no renormalizable interactions terms that respect all the symmetries of the full theory. Therefore the non-renormalizable interaction term is the only remaining interaction, and its effects are therefore visible. This explains also why the weak force is so small at low energy scales.

It is common to view the Standard Model as a low energy approximation to an as yet unknown full, completely finite, theory of nature (string theory has been proposed). If one reverses this view and regards the full theory as a regularization of the QFT, then one concludes that precisely the class of renormalizable theories are independent of this particular regularization. If one is interested in the low energy limit of the physics of some system, much lower than the fundamental scales of the system, one expects to arrive at a theory that is independent of the precise physics at the fundamental scale. These theories are then given by the class of renormalizable theories. Thus the historical search for renormalizable theories of nature was fruitful not because nature is described by renormalizable theories, but it was fruitful because no matter how nature precisely works a renormalizable theory will describe the low energy limit. Given the probable scale for the fundamental laws of nature, the Planck

mass, $\approx 10^{18}$ GeV and the scales we probe in experiments ≈ 1000 GeV we see that we are in the extremely low energy regime of physics and renormalizable theories should be the context in which we work. Renormalization and the UV infinities, then, are not a nuisance but rather reflect deep concepts about the degrees of freedom relevant to the scales at hand.

This leaves us with the IR/COL divergences. These do not originate from unknown high energy physics, but from long distance physics instead. They only occur in theories with massless particles, because at long distances only the massless degrees of freedom are relevant. These divergences either indicate that a theory is inconsistent or that our calculation is inconsistent. No theory with IR/COL divergences that is inconsistent, ie. in which the infinite volume limit cannot be defined, is known to the author, but it is a logical possibility. For all theories with IR/COL divergences the divergences are a consequence of "wrong" calculations, by which is meant calculations for quantities that are not physical or a wrong set of perturbative states is used. The adjective "wrong" refers to naive calculations that one would do in direct analogy with calculations in theories without divergences. The solution to handling IR/COL divergences is not as unique and uniform as the renormalization procedure handled UV divergences. In different theories different solutions are possible. In QED with a massive electron the IR divergences are canceled by the Bloch-Nordsieck mechanism which involves adding virtual to real contributions. In massless QED and QCD one has to factorize COL divergences. In the non-linear sigma model one can either solve the theory non-perturbatively such that no IR divergences are present at any stage in the calculation, or one can factorize IR divergences in the context of the operator product expansion (OPE). Except for non-perturbative solutions where the divergences are absent, all the other techniques of solving the problem of divergences use a regulator to control them. But, again, physics must of course be insensitive to the choice of regulator.

In this thesis we shall use dimensional regularization for most cases. It proves to be the most convenient regularization because it preserves most of the symmetries and because it regularizes both UV and IR/COL divergences. It is however rather unphysical because it changes the number of space-time dimensions n to arbitrary complex numbers $d = n - 2\varepsilon$. We shall see later how one can see it as a short cut for calculations with more physical regulators, such as a cut-off scale and non-zero masses.

Our focus shall be on the IR/COL divergences as they occur particularly in QCD. In what follows, I will first give a brief introduction to UV divergences in QFT's from a path integral perspective, and their regularization. After this I will discuss some simple examples of IR divergences so as to get an impression of their origin.

1.2 Infinities in Quantum Field Theory

To discuss UV divergences we focus on Euclidean field theory. We work in a n-dimensional Euclidean space with fields collectively denoted by $\phi(x)$. An action $S[\phi]$

specifies the dynamics and is taken to be positive definite. We are interested in the Euclidean analog of eq.(1.6), which is

$$Z[J] = \int \mathcal{D}\phi \exp[-S[\phi] + \int d^d x J(x)\phi(x)]. \tag{1.17}$$

In the above equation we integrate over all field configurations, that is all functions on the n-dimensional space. Note that a definition of the integration measure is not as easy as it is for ordinary integration. Typical actions consist of a quadratic kinetic term and a potential term

$$S[\phi] = \int d^n x \left(\frac{1}{2}\partial_i\phi\partial_i\phi + V[\phi]\right). \tag{1.18}$$

The kinetic term becomes large for violently fluctuating fields, which suppresses such field configurations in the integration. It is best to see the kinetic term as part of the measure. In one dimension this Euclidean path-integral exists formally and the measure, including the kinetic exponent, is called the Wiener measure. A typical function with respect to the Wiener measure is a continuous but nowhere differentiable function. So, as long as the potential term does not contain derivatives and is well-behaved for large values of the fields, we have a well-defined integration and we will not encounter infinities due to short distance (UV) fluctuations. In the presence of derivatives in the potential more care must be taken. It is then possible to encounter infinities, so that the need for renormalization arises, even in quantum mechanics [2]. In particular the ordering problems of non-commuting canonical operators in quantum mechanics may be appearing as infinities. The path-integral as stated above integrates over fields defined on the real line. A rigorous definition must entail a integration over fields defined on a finite interval $[-T, T]$. The limit $T \to \infty$ may be divergent.

In two or more dimensions the kinetic term is not large enough to suppress the short distance fluctuations. Typical configurations are no longer continuous and products of fields at the same point become ill-defined. The higher the dimension the stronger the short distance fluctuations become. This severely constrains the possible terms in the potential. In general dimensions only a mass term can be inserted as this amounts to a Gaussian integral which can be performed analytically. Physically this corresponds to a free theory and is not of particular interest here. In dimensions two to four however one can add a limited set of potential terms and still obtain a meaningful theory[3]. In these cases the divergent structure is such that the theory is renormalizable, but one needs a regularization to tame the divergences.

One way to regularize is changing the kinetic term to

$$S_{\text{kin}}[\phi] = \int d^n x \frac{1}{2}\phi\left(-\partial_i\partial_i \exp\left[-\lambda\partial_j\partial_j\right]\right)\phi \quad \lambda > 0. \tag{1.19}$$

The extra exponent produces an extremely strong suppression for strongly fluctuating fields, enough that at least within perturbation theory the typical field configurations

that dominate the path integral is smooth. Here λ is a cut-off and the limit $\lambda \to 0$ removes the regulator regaining and the ordinary kinetic term. Note that this regularization is only possible in Euclidean space due to the positive definite metric. Even more rigorous would be a lattice regularization which can serve as a completely non-perturbative definition of the path-integral, because it reduces the path-integral to an ordinary finite dimensional integral. However the regularization in (1.19) gives simpler expressions and provides a smooth transition to dimensional regularization.

Within such a regulated theory products of fields and derivatives thereof are well defined within perturbation theory. Local products of the fields are called composite fields. They appear as terms in the Lagrangian, but are in fact of more general interest. In particular they appear in the operator product expansion which we will discuss below. In the limit where the cut-off is removed the composite operators become singular and are therefore in need of renormalization to make them finite. This renormalization is an additional renormalization, beyond the renormalization of the parameters of the Lagrangian. Let $O_n(x)$ denote the set of composite fields. The structure of renormalization is

$$O_n(x) = \sum_k Z_{nk}(\lambda) \left[O_k\right](x), \tag{1.20}$$

where on the LHS we have the "bare" composite field and the operators between brackets are the renormalized, finite, composite fields. The Z factors are singular when $\lambda \to 0$. The dimension of the renormalized operators $[O_k]$ must be lower or equal to the dimension of O_n, otherwise Z_{nk} must contain a positive power of λ for dimensional reasons and will vanish in the limit $\lambda \to 0$. This reasoning only holds if all the coupling constants have zero or positive mass dimension, which is true for renormalizable theories. The above structure shows that operators mix with each other and the precise mixing will depend on the renormalization scheme, i.e. one can always include some extra finite piece in the Z-factors. A natural renormalization scheme is the minimal subtraction, in which the Z factors are pure poles in λ. This works fine except in the presence of logarithmic singularities $\log \lambda$, which are logarithms of a dimensionful quantity. We can introduce a scale μ and extend the minimal subtraction scheme by the additional rule that Z contains only $\log \lambda\mu$. Now varying μ varies the amount of mixing by a finite amount, so we have

$$\left[O_n\right]_{\mu'}(x) = \sum_k G_{nk}(\mu', \mu) \left[O_k\right]_{\mu}(x). \tag{1.21}$$

Taking the derivative with respect to μ' at $\mu' = \mu$ we get the renormalization group equation

$$\mu \frac{d}{d\mu} \left[O_n\right]_{\mu}(x) = \sum_k \gamma_{nk}(\mu) \left[O_k\right]_{\mu}(x). \tag{1.22}$$

Another way to regulate a composite field and one which occurs very often in QFT, is to consider product of fields at different points. This would give us

$$\lim_{y \to x} \left[O_n\right](x) \left[O_m\right](y) = \sum_k Z_{nm,k}(x) \left[O_k\right](x). \tag{1.23}$$

Here Z may also have a non-trivial tensor structure, because x is a vector. This equation is not only useful as method of regularization of composite operators through point splitting, but it is also interesting as it gives information about the behavior of Green's functions when to operators get close to each other, a question in which one is often interested in QFT. We now explore this issue further.

1.2.1 Operator product expansion

Suppose we are interested in the product of two ϕ operators close to each other in ϕ^4 theory for example. We consider the correlator

$$\langle \phi(x)\phi(0)\tilde{\phi}(p_1)\dots\tilde{\phi}(p_n)\rangle, \tag{1.24}$$

of two phi fields close together ($x \approx 0$) and other long wavelength length fields ($p_i \approx 0$). Then the long wavelength fields cannot resolve the small distance and the two close-by operators seem to be at the same point. Therefore Wilson postulated that we would have

$$\langle \phi(x)\phi(0)\tilde{\phi}(p_1)\dots\tilde{\phi}(p_n)\rangle = \sum_n c_n(x)\langle O_n(0)\tilde{\phi}(p_1)\dots\tilde{\phi}(p_n)\rangle, \tag{1.25}$$

where $O_n(x)$ are higher dimensional operators and $c_n(x)$ are called Wilson coefficients. The x dependence of the correlator has been factored out and is summarized by the $c_n(x)$.

Within the regulated theory the exponential cut-off selects extremely smooth fields. So one expects that we can Taylor-expand the fields as follows

$$\langle \phi(x)\phi(0)\tilde{\phi}(p_1)\dots\tilde{\phi}(p_n)\rangle = \sum_n \frac{1}{n!}x^{\mu_1}\dots x^{\mu_n}\langle (\partial_{\mu_1}\dots\partial_{\mu_n}\phi(0))\,\phi(0)\tilde{\phi}(p_1)\dots\tilde{\phi}(p_n)\rangle. \tag{1.26}$$

Within perturbation theory this is indeed possible [4] and in fact gives the exact answer as it amounts to expand the Fourier factor $\exp(ixp)$ in x: the cut-off provides a suppression strong enough to interchange the integration and summation and we precisely get the LHS. The local product on the RHS diverges when we remove the cut-off, but we can replace the $\partial^n\phi(0)\phi(0)$ combination by finite renormalized operators, see eq. (1.20). So we get

$$\begin{aligned}\langle \phi(x)\phi(0)\tilde{\phi}(p_1)\dots\tilde{\phi}(p_n)\rangle &= \sum_{n,k} Z^k_{\mu_1\dots\mu_n}(\lambda,\mu)\frac{1}{n!}x^{\mu_1}\dots x^{\mu_n}\langle [O_k]_\mu(0)\tilde{\phi}(p_1)\dots\tilde{\phi}(p_n)\rangle \\ &= \sum_k c^k(x,\mu,\lambda)\langle [O_k]_\mu(0)\tilde{\phi}(p_1)\dots\tilde{\phi}(p_n)\rangle \\ c^k(x,\mu,\lambda) &= \sum_n Z^k_{\mu_1\dots\mu_n}(\lambda,\mu)\frac{1}{n!}x^{\mu_1}\dots x^{\mu_n}.\end{aligned} \tag{1.27}$$

The index k also includes possible Lorentz indices. The correlation function on the LHS is finite and the renormalized operators on the RHS are finite when the cut-off is removed. Therefore the coefficients c^k are also finite. Taking the limit $\lambda \to 0$ we then obtain

$$\langle \phi(x)\phi(0)\tilde{\phi}(p_1)\dots\tilde{\phi}(p_n)\rangle = \sum_k c^k(x,\mu)\langle [O_k]_\mu(0)\tilde{\phi}(p_1)\dots\tilde{\phi}(p_n)\rangle, \tag{1.28}$$

which is Wilson's ansatz. The coefficients can be calculated by matching the LHS and RHS order by order in perturbation theory. They are governed by a renormalization group equation, are independent of the other fields in the correlator, and describe physics at short distances. Therefore the coefficient cannot depend on large distances, and are finite when one takes all masses to be zero. This property of the coefficient functions, called IR safety[1], will return in later chapters.

1.2.2 Non-perturbative OPE

We discussed the operator product expansion from a perturbative point of view. A more heuristic but more intuitive and insightful discussion of the OPE is provided by a path-integral viewpoint. Let us review the correlator of fields with two nearby points within the path-integral formulation of QFT

$$\langle \phi(x)\phi(0)\phi(y_1)\dots\tilde{\phi}(y_n)\rangle = \frac{1}{Z}\int \mathcal{D}\phi\ \phi(x)\phi(0)\phi(y_1)\dots\tilde{\phi}(y_n)\exp\left[-S[\phi]\right]. \tag{1.29}$$

Let us first divide space into two regions, one region "I" of size R containing the points 0 and x, and one region "O" complementary to this. The path-integral can be rewritten as

$$\begin{aligned}\frac{1}{Z}\int \mathcal{D}\phi\ \phi(x)\phi(0)\phi(y_1)\dots\phi(y_n)\exp\left[-S[\phi]\right] = \\ \frac{1}{Z}\int \mathcal{D}\phi_O \int \mathcal{D}\phi_I \phi_I(x)\phi_I(0)\phi_O(y_1)\dots\phi_O(y_n)\exp\left[-S[\phi_O]-S[\phi_I]\right],\end{aligned} \tag{1.30}$$

where the path-integral over the fields in the inside region has some appropriate boundary condition for the field ϕ_I to match the field ϕ_O at the boundary. We define

$$Z_I[\partial\phi_O] = \int \mathcal{D}\phi_I \exp\left[-S[\phi_I]\right], \tag{1.31}$$

which is the normalization of the path-integral over the inside region depending on the outside field through the boundary. Relabeling ϕ_I to ϕ'_I in eq.(1.30) and inserting the identity in the form of

$$\frac{1}{Z_I[\partial\phi_O]}\int \mathcal{D}\phi_I \exp\left[-S[\phi_I]\right] = 1, \tag{1.32}$$

[1] Recall that we are in Euclidean space. Collinear safety will be addressed further below.

we obtain

$$\frac{1}{Z}\int \mathcal{D}\phi_O \int \mathcal{D}\phi_I \left(\frac{1}{Z_I[\partial\phi_O]}\int \mathcal{D}\phi_I'\phi_I'(x)\phi_I'(0)\exp\left[-S[\phi_I']\right]\right) \\ \phi_O(y_1)\dots\phi_O(y_n)\exp\left[-S[\phi_O]-S[\phi_I]\right]. \quad (1.33)$$

This is just

$$\frac{1}{Z}\int \mathcal{D}\phi\langle\phi_I'(x)\phi_I'(0)\rangle_{\partial\phi}\phi(y_1)\dots\phi(y_n)\exp\left[-S[\phi]\right], \\ \langle\phi_I'(x)\phi_I'(0)\rangle_{\partial\phi} = \frac{1}{Z_I[\partial\phi]}\int \mathcal{D}\phi_I'\phi_I'(x)\phi_I'(0)\exp\left[-S[\phi_I']\right] \quad (1.34)$$

The correlator is a function of x and can be expanded around $x = 0$ and its coefficients depend on the boundary. The boundary of the inside region is a sphere of radius R. Hence R is much smaller than the distance to the other points. Therefore the correlator acts as a local operator and we can expand it in a basis of local operators,

$$\langle\phi(x)\phi(0)\rangle_{\partial\phi} = \sum_k c^k(x,R)\left[O_k\right]_R(0). \quad (1.35)$$

In this way we also obtain the operator product expansion. In this derivation R is both a UV cut-off for the local operators and an IR cut-off for the coefficients. In this sense it is analogous to μ. Of course, like μ, the result does not depend on the particular value of R.

1.3 Regularization

So far we regularized with an explicit cut-off. Though physical and intuitive, it becomes unwieldy in real calculations. The method preferred in the literature and used in this thesis will be dimensional regularization. It regularizes a field theory while preserving almost all symmetries. For this reason it is technically the simplest and the most widely used regularization. For QCD calculations a major advantage is that it regularizes IR/COL[2] divergences at the same time. A downside of dimensional regularization is that it tends to obscure the underlying physics. It mixes divergences of different origin, which sometimes need to be disentangled. We will encounter this in chapter 5.

The clearest way of introducing the logic of dimensional regularization is to observe that if a theory is renormalizable with a particular regularization, then it should be so for any regularization. We now consider a theory that is renormalizable with a regularization similar to that of eq. (1.19), and show how we can relate this to dimensional regularization, thus providing a link between a real physical regularization

[2]See section 1.3.2 for the explanation of collinear divergences.

and dimensional regularization. In practice we shall not bother with such links in later chapters.

We work in a Euclidean signature and replace every propagator $\Delta(p) = (p^2 + m^2)^{-1}$ by $\Delta(p)\exp[-\lambda(p^2+m^2)]$, and consider only massive fields. This is basically the regularization of (1.19). All Feynman diagrams are manifestly finite because the integrand does not have singularities and the exponential fall-off ensures convergence at large momenta. We can therefore calculate the integrals in arbitrary integer dimensions (d), with a natural continuation to complex dimensions[3]. The expression for a particular Feynman diagram G is then given by

$$G(\lambda) = \int \frac{d^d l_1}{(2\pi)^d} \cdots \frac{d^d l_n}{(2\pi)^d} I(l_1, \ldots) \exp[-\lambda(\sum p_i (l_j)^2 + m^2)], \tag{1.36}$$

where I is the usual Feynman integrand without regularization and for every internal propagator i we have a term in the exponent. Now we can perform a Mellin transform $G(\lambda)$ to get

$$\begin{aligned} \int_0^\infty d\lambda \lambda^{s-1} G(\lambda) &= G(s)\Gamma(s) \\ G(s) &= \int \frac{d^d l_1}{(2\pi)^d} \cdots \frac{d^d l_n}{(2\pi)^d} I(l_1, \ldots) \frac{1}{(\sum p_i^2 + m^2)^s}. \end{aligned} \tag{1.37}$$

Here $G(s)$ could be viewed as another regularization of G, where in the end the limit $s \to 0$ must be taken. However in general there is a problem with this interpretation. If the integral converges for $\Re s > 0$ then this is indeed a valid regularization and we would find a singularity of G at $s = 0$. However if the integral only converges for $\Re s > k$ for some positive k then the limit $s \to 0$ cannot be taken. Because G is an analytical function of s one can analytically continue G to the whole complex plane and then take the limit $s \to 0$, but now it is not so clear that this is a proper regulator for the expression. Nevertheless we take this regularization seriously. It is called the zeta function regularization and has the advantage that no explicit cut-off scale is present. How should we interpret $G(s)$? To see how note that we can recover the physical $G(\lambda)$ by an inverse Mellin transform

$$G(\lambda) = \frac{1}{2\pi i} \int_{c-i\infty}^{c+i\infty} d\lambda \lambda^{-s} G(s)\Gamma(s). \tag{1.38}$$

Here c must be large enough for the Mellin transform in eq. (1.37) to converge in the neighborhood of $\lambda = 0$. As $G(s)$ is an analytic function of s it can be continued to a meromorphic function on the whole complex plane, with isolated poles. Now we can shift the integration contour to the left until it lies in the left-half complex plane, adding residues whenever we pass through a pole of $G(s)$. In this way we obtain terms with a negative powers of λ that are divergent. If $G(s)$ has a pole at $s = 0$ then $\Gamma(s)$ also has a pole there, and we get a logarithmic divergence when we push

[3] In the absence of Levi-Civita tensors.

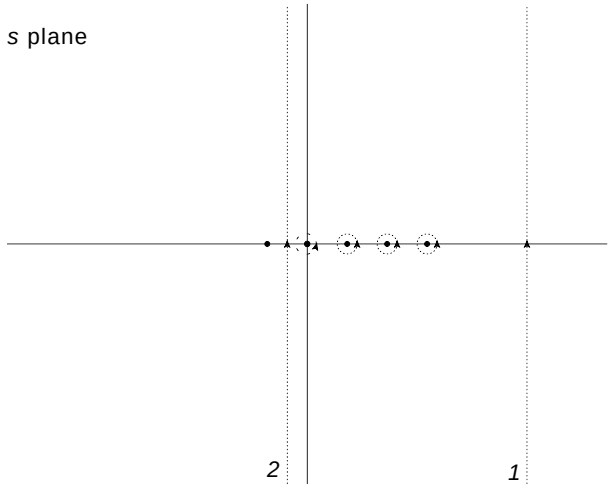

Figure 1.3: Contour in complex s-plane, with poles on the real axis. Moving the original contour 1 to where contour 2 lies, residues of the poles are picked up.

the contour through the pole at $s = 0$. When the integration contour lies in the left-half plane, the integration vanishes in the limit $\lambda \to 0$. The power of dimensional regularization now becomes apparent. Both $G(\lambda)$ and $G(s)$ were complex functions of the dimension d. The poles of $G(s)$ lie on the real axis with $s - d/2$ integer. So if we decrease the dimension slightly the poles are slightly shifted to the left. If $d = 4 - 2\varepsilon$, the pole of $G(s)$ at $s = 0$ is shifted to $s = -\varepsilon$. We move the integration contour to the left-half plane at $c = -\varepsilon/2$ then we pick up possible poles of $G(s)$ near the positive integers and we pick up the pole of Γ at $s = 0$ (see fig.1.3),

$$G(t) = \frac{1}{2\pi i} \int_{-\varepsilon/2-i\infty}^{-\varepsilon/2+i\infty} d\lambda t^{-\lambda} G(s)\Gamma(\lambda) + G(s=0) + \sum_n c_n t^{-n+\varepsilon}. \tag{1.39}$$

If the theory is renormalizable in $d = 4$ dimensions then we can get rid of the divergences in λ by adding counterterms. We renormalize using the minimum subtraction to exactly cancel the $\lambda^{-n+\varepsilon}$ term, without any extra finite piece. After the renormalization we can take the limit $\lambda \to 0$. The net result for this particular graph is $G(s = 0)$ in $d = 4 - 2\varepsilon$ dimensions. In the limit $\varepsilon \to 0$ this might give a pole in ε which can be renormalized by an additional counterterm that subtracts the ε pole. This is always possible given the assumption that the theory is renormalizable. This may seem a very complicated way to renormalize the theory. However in practice we do need to bother with the various regularization and subtractions. We may work in $d = 4 - 2\varepsilon$ dimensions and calculate $G(s = 0)$ directly. Because the integrand is unchanged, for $s = 0$, most symmetries that do not depend on the dimension are preserved. Also the Euclidean "Lorentz" symmetry is preserved at each step.

Let us offer one last remark. As presented, the UV poles in ε correspond to the

logarithmic divergences, while higher order divergences are zero in dimensional regularization. There is actually a way of viewing this by extending the notion of integrable functions. Let us denote a function as homogeneous in a subset of momenta if the following holds for some s,

$$I(\lambda k_i, l_i) = \lambda^s I(k_i, l_i). \tag{1.40}$$

For the integral over all momenta we have

$$\begin{aligned}\int d^d k_1 \dots d^d l_1 \dots I(k_i, l_i) &= \int d\lambda^2 \int d^d k_1 \dots d^d l_1 \dots \delta(\lambda^2 - \sum_i k_i^2) I(k_i, l_i) \\ &= \int d\lambda^2 \int d^d u_1 \dots d^d u_n d^d l_1 \dots \lambda^{-dn} \delta\left(\lambda^2 - \lambda^2 \sum_i u_i^2\right) I(\lambda u_i, l_i) \\ &= \int \frac{d\lambda^2}{\lambda^2} \lambda^{s-dn} \int d^d u_1 \dots d^d u_n d^d l_1 \dots \delta(1 - \sum_i u_i^2) I(u_i, l_i). \end{aligned} \tag{1.41}$$

We see that this integral is always divergent due to the λ integral, no matter what s is. Therefore one can extend the notion of integrable functions by defining a function f to be integrable if it differs by a finite sum of homogeneous functions from a function g which is integrable in the usual sense. The integral of f is defined to be the integral of g. This extended definition of integrable function is consistent because it defines a proper equivalence relation, and any integrable equivalence class has exactly one representative that is integrable in the usual sense. With this definition of integration homogeneous integrals are zero. Also, integrals that are linearly divergent or worse can be made less divergent by subtracting appropriate homogeneous functions. This works only until a logarithmic divergence is present. For such a case, if one would try to improve the UV divergence one introduces an IR divergency. However the logarithmic divergency can be systematically regularized by the zeta function regularization or dimensional regularization. In QFT therefore only logarithmic divergences matter!

Note that because of the absence of linear (or higher) divergences the hierarchy problem of the Standard Model is more difficult to see within a renormalization scheme using dimensional regularization. But as the preceding analysis shows, that does not mean that within dimensional regularization there is no hierarchy problem. The higher divergences are implicitly renormalized through the regularization. One does see the hierarchy problem in dimensional regularization when one has a more complete theory which has the original theory as its low energy limit. The complete theory has some scale Λ and calculations in the complete theory of the corresponding divergences will give the appropriate power of Λ[3].

1.3.1 Dimensional regularization in massless theories

We remarked already that the real power of dimensional regularization for QCD is its ability to also regularize IR divergences. In the previous discussion we explicitly

assumed every propagator to be massive so as to remove any singularity of the integrand. In the limit where the masses go to zero the graphs might become singular, ie. $G(s=0)$ behaves as a negative power or logarithm of the mass. In this limit the precise power will depend on the dimension d and will become positive when d is large enough. If the massless theory makes physical sense, ie. if we can calculate finite cross sections or other physical observables, then these mass singularities must cancel. For such an observable we can take the limit $d \to 4$ and then $m \to 0$, but the precise order should not matter. One may first increase the dimension such that there are no mass singularities and then take the massless limit. The limit $d \to 0$ could become singular because UV poles in ε are not properly canceled anymore as setting the mass to zero eliminated some $1/\varepsilon$ terms. For example, for $\varepsilon < 0$

$$\frac{m^{-\varepsilon}}{\varepsilon} - \frac{1}{\varepsilon} \to -\frac{1}{\varepsilon}, \tag{1.42}$$

when the massless limit is taken. This seems like a dangerous source of ambiguity, but is not an undesirable feature because the divergences in ε are to be interpreted as IR divergences. The massless limit can be circumvented by setting the mass to be zero at the start. The absence of mass make some integrals homogeneous and thus equal to zero in dimensional regularization, as discussed before, however the UV counterterms are still needed. As for a physical UV cut-off, introducing masses may break symmetries and will make expressions much harder to evaluate. Dimensional regularization regulates the mass singularities without breaking the gauge invariance.

In the case the integral is linearly UV divergent or worse, it does not have an IR divergence. However because non-logarithmic divergences do not show up in dimensional regularization, they do not give rise to poles in ε. This is thus consistent with the vanishing of the integral. In the particular case of a scaleless integral which is logarithmic UV divergent then the integral is also IR divergent. Although the integral is still zero one must add the counterterm for the logarithmic UV divergence. After summing this diagram (which is zero) and the counterterm (proportional to $1/\varepsilon$) we are left with a $1/\varepsilon$ which is in fact the IR divergence. It is therefore important to not forget this counterterm. In case of a linear or higher UV divergence no UV counterterm is present and no IR $1/\varepsilon$ is generated.

1.3.2 Minkowski space-time

So far we have been working in Euclidean space, because its positive definite metric makes singularities easier to deal with. Space-time has Lorentz signature however. Whereas in Euclidean space the only possible singularities for massless propagators are at zero momentum, in Minkowski space even massive propagators can become singular when the momentum obeys the mass-shell condition,

$$\frac{1}{E^2 - \vec{p}^2 - m^2 + i\epsilon} \to \infty, \quad E^2 = \vec{p}^2 + m^2. \tag{1.43}$$

For massless propagators the situation becomes even worse when one considers momenta that are both on-shell and small. In fully massive theories one can always Wick

Figure 1.4: Collinear splitting of a line into two ($p \parallel k$ and light-like, $k^2 = p^2 = 0$). The propagator $1/(p+k)^2$ diverges in this case.

rotate the integrals to a singularity-free Euclidean setting. Therefore, no singularities are possible except for the UV singularities that we also have in the Euclidean theory. In theories with massless particles we have the IR singularities which also occur in the Euclidean theory, but there are additional collinear divergences. These divergences occur when several on-shell momenta of massless particles are oriented parallel, causing an internal line build up of parallel momenta to diverge (see the collinear splitting in fig.1.4).

A systematic study of these divergences requires the study of arbitrary Feynman integrals in Minkowski space. One needs to identify regions in the multi-dimensional space of loop momenta, over which one integrates, where the collinear divergences can occur, power count them to see if indeed they do occur, and then deal with the divergences such that finite scattering amplitudes are obtained. This leads to the concept of factorization, which we discuss in section 1.9.

The operator product expansion also becomes more troublesome in Minkowski space-time. When x^2 is zero then x need not be close to zero. This means that the use of the OPE when $x^2 \to 0$, which is the relevant limit for a number of physical processes, becomes questionable. The dimension of an operator is less relevant. The "twist" of an operator, which is the dimension minus number of Lorentz indices is actually the relevant quantity, since every Lorentz index μ must be contracted with a factor x^μ which need not be small. The OPE for Minkowski space has been used to calculate certain QCD cross sections, but factorization provides in general a more flexible framework for actual calculations.

Let us now explore the issue of IR divergences further, starting with models simpler than QCD.

1.4 A two-state model

We begin by analyzing a very simple 2-state system with Hamiltonian,

$$H = I + \alpha A, \quad A = \left(\begin{smallmatrix} 0 & 1 \\ 1 & 0 \end{smallmatrix}\right) \tag{1.44}$$

where I is the 2D identity matrix, α is the coupling constant and A the interaction Hamiltonian. The free Hamiltonian has a degenerate eigenspace $|1\rangle = (1,0)$ and $|2\rangle = (0,1)$. If we use perturbation theory to solve for the eigenvalues of, for example the 1-state, we obtain

$$E_1(\alpha) = 1 + \alpha^2 \frac{|\langle 1|A|2\rangle|^2}{E_1^{(0)} - E_2^{(0)}}. \tag{1.45}$$

We encounter a division by zero and thus a (IR) divergence. The solution is to diagonalize the interaction Hamiltonian A in the subspaces where the free Hamiltonian (I) is degenerate

$$H = I + \alpha\tilde{A}, \quad \tilde{A} = \left(\begin{smallmatrix} 1 & 0 \\ 0 & -1 \end{smallmatrix}\right). \tag{1.46}$$

We see that the origin of our divergence is just that we use perturbation theory around the wrong basis. This is the general feature of IR/COL divergences and should always be kept in mind. Although the solution to the above problem is rather trivial, in more complicated theories it might be not so easy to diagonalize the interaction Hamiltonian such that the IR divergences disappear. This is the case for QCD (and QED) so that we must resort to other methods to deal with these divergences. The first step is introducing an IR regulator to remove the divergences. In the present simple model we could replace I by a diagonal matrix with $(1+\varepsilon, 1)$ as elements along the diagonal. Here the regulator ε lifts the degeneracy and makes the perturbation theory finite, although it diverges upon taking the limit $\varepsilon \to 0$. We can then define a physical quantity which is the sum of the eigenvalues (i.e. the trace), calculate this in perturbation theory and notice that the infinities cancel; a well defined limit is obtained in the limit the regulator is removed. Such a quantity is called IR finite and are reliably calculated in perturbation theory, even in the presence of IR divergences.

1.5 A one-dimensional path integral model

Because IR divergences in QFT become more problematic when the dimension of space-time is being reduced, let us study IR divergences in ordinary quantum mechanics. This can be represented as a one-dimensional QFT, in which many technical difficulties are absent, so that further intuition may be developed.

Let us consider the Hamiltonian

$$H = \frac{1}{2}p^2 + \frac{1}{4!}x^4, \tag{1.47}$$

where $x(t)$ is the coordinate of a particle, and $p(t)$ its momentum. The Wick rotated path integral for this system is

$$Z = \int Dx(t) \exp\Big[- \int dt \left(\frac{1}{2}\dot{x}^2 + \frac{1}{4!}\lambda x^4 \right) \Big]. \tag{1.48}$$

To solve this Euclidean path integral and calculate correlation functions one would separate the action into a quadratic part and an interaction part and expand the interaction part in a perturbation series which may as usual be expressed in diagrams. However the "self-energy" diagram whose contribution is

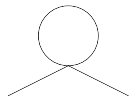

$$= \frac{1}{2}\lambda \int \frac{dp}{2\pi} \frac{1}{p^2}, \tag{1.49}$$

is clearly IR divergent at the lower integration range. This can be understood rather easily for this model. In perturbation theory the main assumption is that the interaction is somehow "small" and will perturb the spectrum only slightly. In this case, the spectrum of the unperturbed system is that of a free particle with any allowed momentum, while the spectrum of the perturbed system, no matter how small the perturbation is, is discrete (because the potential is infinite at infinity). Certainly for all non-zero values of λ the potential rises to infinity, which always produce a discrete spectrum with eigenfunctions that are bounded around the origin. Therefore the interaction cannot be thought of as 'small' at all and the perturbation theory is set up around the wrong set of states.

To solve the IR problem for this model we can write $S = S_0 + S_I$, where

$$S_0 = \frac{1}{2}\dot{x}^2 + \frac{1}{2}m^2x^2, \tag{1.50}$$

$$S_I = \frac{1}{4!}\lambda x^4 - \frac{1}{2}m^2x^2. \tag{1.51}$$

Here m^2 is an arbitrary non-zero parameter, which has no effect on the physics. The lowest order correction from the 'self-energy' diagram is now

$$-m^2 + \frac{1}{2}\lambda \int \frac{dp}{2\pi}\frac{1}{p^2+m^2} = -m^2 + \frac{\lambda}{4m}. \tag{1.52}$$

If we choose $m^2 = (\lambda/4)^{2/3}$, the above expression vanishes and the first order 'self-energy' diagrams can be ignored. We see that a mass has been generated and a well-defined perturbation theory is obtained.

We might also have introduced a regulator mass term $\frac{1}{2}\mu^2x^2$. In this case the Dyson-Schwinger equation for the two-point function gives us

$$m^2 = \mu^2 + \frac{1}{2}\lambda \int \frac{dp}{2\pi}\frac{1}{p^2+m^2} = \mu^2 + \frac{\lambda}{4m}, \tag{1.53}$$

where m^2 is defined here as the value of p^2 where the full propagator develops a pole. Removing the regulator by taking μ^2 to 0, we obtain the same equation for the mass as above. The non-zero value of m^2 indicates a spectrum close to a harmonic oscillator, which indeed has a discrete spectrum.

Two concepts are illustrated by this simple example. By introducing the mass m^2 we effectively made a different split between the free and interacting part of the Lagrangian. This split is purely our choice to make and is not in any way related to real physics. The self-consistency equation for the mass yields the value for which the perturbative correction to it is numerically the smallest. So, in a sense, the free Lagrangian is the best approximation for the full theory.

In the second solution we handled the infinities through regularization, which is the most common way. We removed the divergence by altering the physics with the intention to take the limit back to the physical system in the end, and in such a way that the final physical quantities are well-defined. In this simple example, once

corrections to all orders are included via the Dyson-Schwinger equation, we indeed get the same result, i.e. same mass. In modern QFT applications the problems are so complicated that it is in general unclear how to proceed in analogy to the first way, and we are left with the regularization route.

1.6 Two dimensional models

Our one-dimensional model does not fully reveal all intricacies of IR divergences that one encounters in perturbative QCD. We therefore study a more complicated and interesting field theory known as the non-linear SO(N) sigma model [5]. It is a two-dimensional field theory, where the field take values on the points of a $N-1$ dimensional sphere, known as target space. The target space has a natural SO(N) symmetry from the rotations of the sphere, and is a non-linear space (hence the name of the model). The action for this model is given by

$$S[\sigma] = \int d^2x \frac{1}{2} \langle \partial_i \sigma, \partial_i \sigma \rangle, \tag{1.54}$$

where σ is a map to the $N-1$ dimensional sphere, and the angled brackets represent the positive-definite inner product on the tangent space to the target space, which is simply $\mathbb{R}^{N-1}$. The path-integral for this model is then given by

$$Z = \int \mathcal{D}\sigma e^{-\frac{N}{g} S[\sigma]}, \tag{1.55}$$

with $\mathcal{D}\sigma$ some SO(N) invariant measure on the space of functions. We comment on g shortly. Because of the non-linear nature of the target space this representation is hard to work with. In our particular case it is convenient to represent the target space S_{N-1} as the space of unit vectors in $\mathbb{R}^N$. In this representation the action becomes

$$S[\sigma] = \int d^2x \frac{1}{2} \partial_i \sigma^a \partial_i \sigma^a = \int d^2x \frac{1}{2} \sigma^a (-\Delta) \sigma^a, \tag{1.56}$$

together with the constrain $\sigma^a \sigma^a = N/g$. In this theory g is a coupling constant. In the limit $g \to 0$ the radius of the constrain sphere becomes infinite, making the target space flat, and leaving the theory essentially non-interacting. For finite values of g the curvature of the sphere introduces interactions between fluctuations in different directions. The appearance of N in the constraint surface is such that a sensible large N limit is obtained. The full path-integral, including a source term, can be written as

$$\int \mathcal{D}\sigma \prod_x \delta \left(\frac{N}{g} - \sigma^a(x) \sigma^a(x) \right) e^{-S[\sigma] + \int d^2x J\sigma}, \tag{1.57}$$

introducing a Dirac delta function at every point in space to implement the constraint. The measure is now the usual measure on the linear space $\mathbb{R}^N$.

Classically, the ground state is simple, namely a constant field in an arbitrary direction with length $\sqrt{N/g}$. Using the SO(N) symmetry to choose the classical solution to be

$$\begin{aligned} \sigma^n &= 0 \quad n = 1 \dots N-1 \\ \sigma^N &= \sqrt{N/g}, \end{aligned} \tag{1.58}$$

we can rewrite the path-integral for small fluctuations around this classical solution. This results in

$$Z[J] = \int \mathcal{D}\sigma \prod_x \frac{1}{2\sqrt{\frac{N}{g} - \sigma^n \sigma^n}} e^{-\int d^2x \left[\frac{1}{2}\sigma^n(-\Delta)\sigma^n + V(\sigma) - J\sigma\right]}. \tag{1.59}$$

The ill-defined product arising from the Jacobian of the Dirac delta function clearly presents a nuisance. In lattice regularization this factor is well-defined and necessary to cancel certain perturbative infinities. In dimensional regularization both the factor $\prod_x \frac{1}{2}\sqrt{\frac{N}{g} - \sigma^n\sigma^n}^{-1}$ and the associated perturbative infinities are zero, drastically simplifying the calculations [5].

Inspection of the path-integral in eq. (1.59) shows that small perturbations around the classical ground state are approximated by massless particles. Thus in a perturbative treatment of this system we encounter integrals of the form

$$\int d^2p \frac{1}{p^2} \dots, \tag{1.60}$$

where the integration is over a loop momentum, and one propagator is made explicit. This integral is divergent in the region $p \to 0$, so that this theory is plagued by IR divergences, a result of the fact that we expand around the wrong vacuum. The Coleman-Mermin-Wagner theorem [6] tells us that in a two-dimensional QFT there can be no spontaneous symmetry breaking of a continuous symmetry, which means that our choice of the vacuum is wrong. Indeed one can solve this model non-perturbatively [7] in a large N expansion. One finds then a symmetric ground state with massive particle excitations. It is important to appreciate this fact. The original theory does not contain any manifest dimensionful parameter yet some mass scale is being generated dynamically. This is the well-known phenomenon of dimensional transmutation. The theory as it stands in eq. (1.59) is ill-defined and must be renormalized, bringing a dimensionful scale into the problem. The theory depend on the renormalization scale and its dependence can be calculated perturbatively.

The fact that the field theory contains only massive fundamental excitations makes it manifest that it is free IR divergences. The IR divergences encountered in the perturbative analysis of the path-integral (1.59) are therefore a result of choosing the wrong solution as a perturbative vacuum, not an essential problem of the theory.

In this theory we are fortunate to be able to solve the theory non-perturbatively due to the presence of an extra large parameter N. But if perturbation theory is all we have, can we still use perturbation theory to extract meaningful information about the

theory? The 2D non-linear sigma model presents us with an ideal situation to study this question. If we can make sense of the perturbative expansion we can compare the results to the non-perturbative solution. This would then bolster our confidence in using perturbation theory in cases with IR divergences where we don't have an exact solution.

The full path integral we want to study is

$$Z[J] = \int \mathcal{D}\sigma^a \prod_x \delta(\sigma^a\sigma^a(x) - N/g) \exp\left[-\frac{1}{\hbar}\int d^2 \frac{1}{2}\sigma^a(-\Delta)\sigma^a - J^a\sigma^a\right], \qquad (1.61)$$

where $\hbar$ is the perturbative (loop) expansion parameter. This expression needs regularization for it to be well-defined. Due to the non-linear nature of the target space lattice regularization would be the most natural and rigorous regularization method. In lattice regularization we have two cutoff parameters, the lattice spacing a and lattice size L, and one studies the theory in both the continuum limit $a \to 0$ and the infinite volume limit $L \to \infty$. We are allowed to renormalize the parameter g in the continuum limit, but the infinite volume limit should make sense. If one renormalizes g at a renormalization scale μ, one finds a running coupling that depends on the renormalization scale through

$$g(\mu) = \frac{4\pi}{\ln \frac{\mu^2}{m^2}}, \qquad (1.62)$$

where m is a dynamically generated mass scale. This mass is very physical as it is the mass of the particles in the spectrum of the theory. This is very analogous to QCD, in that asymptotic freedom is present and, a mass scale is dynamically generated.

The non-perturbative groundstate of this theory is actually a quantum superposition of long wavelength fields. As we already noted the theory is scale invariant at the classical level, but in the quantum setting a dynamical mass is generated. This could be viewed as a vacuum (ground state) effect: if the theory would be scale invariant, so will the vacuum be. That implies that quantum fluctuations in vacuum are of the same size independent of the scale. Given that the vacuum contains long wavelength fluctuations destroying the perturbative vacuum (see eq. (1.60)), scale invariance implies also strong short-wavelength fluctuations. But such fluctuations would increase the vacuum energy by a huge amount. Thus the true vacuum suppresses short wavelength fluctuations, thereby upsetting scale invariance. The dynamically generated mass m^2 sets the scale between long wavelength and short wavelength fluctuations.

We now expect that, if we calculate some short-distance effect much smaller then the fundamental scale, the background field could be taken as constant in an arbitrary direction. This is precisely the assumption of perturbation theory and thus we expect that for short-distance effects perturbation theory should be meaningful. In the discussion of the OPE, especially the non-perturbative discussion, we have seen that the OPE provides precisely such a setting. The coefficients are perturbative quantities that depend on the short-distance scale and are IR safe, while the operators provide the long distance behavior. This means that in the non-linear sigma model we should be able to calculate OPE's that match non-perturbative calculations.

Let us consider an example. Suppose we are interested in the Green's function

$$\langle \sigma^a(x)\sigma^a(0)\ldots\rangle, \tag{1.63}$$

where x is close to the origin, and the ellipses refer to any number of fields, far away from the origin. We wish to determine the x-dependence. The OPE can provide us with a solution, albeit somewhat involved. In the spirit of the discussion of the non-perturbative interpretation of the OPE, we assume a disc of a certain radius much larger than x but smaller than the inverse dynamical mass m around the origin. The vacuum fields are essentially constant within the disc and because $\sigma^a(x)\sigma^a(0)$ is SO(N) invariant it does not depend on the particular direction. So we may perform perturbation theory around the classical solution $\sigma^N = \sqrt{N/g}$. We then have

$$\sigma^a(x)\sigma^a(0) = \sigma^m(x)\sigma^m(0) + \frac{N}{g} - \frac{1}{2}\sigma^m(x)\sigma^m(x) - \frac{1}{2}\sigma^m(0)\sigma^m(0) + O(g), \qquad m = 1\ldots N-1, \tag{1.64}$$

where the RHS contains the dynamical fields and we used the constraint to solve σ^N component. Using the unrenormalized OPE up to terms vanishing as $x \to 0$, we obtain

$$\begin{aligned} \sigma^m(x)\sigma^m(0) &= (N-1)\int \frac{d^dp}{(2\pi)^d}\frac{e^{ipx}-1}{p^2+h^2} + \sigma^m(0)\sigma^m(0) + O(x), \\ \sigma^m(x)\sigma^m(x) &= \sigma^m(0)\sigma^m(0) + O(x). \end{aligned} \tag{1.65}$$

We found the coefficients of the operators by matching the LHS and RHS for appropriate Green's functions. We introduced a regulator mass h^2 which is not really necessary as we can trust dimensional regularization to regulate the IR divergences. However the regulator mass h^2 serves the purpose of disentangling different divergences. Adding it all up we get

$$\sigma^a(x)\sigma^a(0) = N\int \frac{d^dp}{(2\pi)^d}\frac{e^{ipx}-1}{p^2+h^2} + \sigma^a(0)\sigma^a(0), \tag{1.66}$$

where we neglected the difference between N and $N-1$. The last term is a peculiarity of this model because, $\sigma^a\sigma^a$ is constrained to be N/g. Now the integration still has a UV divergency which we add and subtract to obtain

$$\sigma^a(x)\sigma^a(0) = N\left(\int \frac{d^dp}{(2\pi)^d}\frac{e^{ipx}-1}{p^2+h^2} + \frac{\mu^{-2\varepsilon}}{4\pi\varepsilon}\right) + \left(\sigma^a(0)\sigma^a(0) - N\frac{\mu^{-2\varepsilon}}{4\pi\varepsilon}\right). \tag{1.67}$$

This form does not have UV divergences for the coefficient of the unit operator (the first term) and must be a proper renormalization for the operator. In this expression we can safely take the massless limit to finally obtain

$$\sigma^a(x)\sigma^a(0) = N\left(\int \frac{d^dp}{(2\pi)^d}\frac{e^{ipx}}{p^2} + \frac{\mu^{-2\varepsilon}}{4\pi\varepsilon}\right) + \left(\sigma^a(0)\sigma^a(0) - N\frac{\mu^{-2\varepsilon}}{4\pi\varepsilon}\right). \tag{1.68}$$

Now the ε pole we initially added to the coefficient of the unit operator to cancel the UV divergence now cancels its IR divergence (the large p behavior is fine due to the rapidly oscillating e^{ipx} factor). This change of guise can be confusing and is a general phenomenon when using dimensional regularization in theories with IR divergences.

We now check that the renormalization of the $\sigma^a\sigma^a$ term is correct. Using the constraint, we obtain that

$$\frac{1}{g} - \frac{\mu^{-2\varepsilon}}{4\pi\varepsilon} = \text{finite}. \tag{1.69}$$

Note that g is the bare coupling here, and we should really use the renormalized coupling. One way to define the renormalized coupling is

$$\frac{\mu^{-2\varepsilon}}{g(\mu)} = \frac{1}{g} - \frac{\mu^{-2\varepsilon}}{4\pi\varepsilon}. \tag{1.70}$$

To understand this, let us act with $\mu^{2+2\varepsilon}\frac{d}{d\mu^2}$ on both sides of the above equation. We find

$$-\varepsilon\frac{1}{g(\mu)} - \frac{1}{g(\mu)^2}\mu^2\frac{d}{d\mu^2}g(\mu) = \frac{1}{4\pi}, \tag{1.71}$$

which is the renormalization group (RG) equation for the running coupling constant, with solution

$$g(\mu) = \frac{4\pi}{\ln\frac{\mu^2}{m^2}}, \tag{1.72}$$

for some mass scale m^2. We now have precise agreement with the non-perturbative result of this theory (eq.(1.62)); all the essential information can be obtained from perturbation theory. Note that eq.(1.72) represents an asymptotically free coupling as it vanishes for increasing μ (large energies). Perturbation theory accurately predicts asymptotic freedom and the existence of a dynamical mass scale. Furthermore it correctly calculates the coefficients of operators in an operator product expansion. However the range of applicability is limited to the short distance regime and IR safe quantities. For instance the vacuum expectation values (vev's) of the operators themself cannot be calculated, but they can be determined in a computer simulation.

Let us summarize the results for the non-linear sigma model. We can make useful perturbative calculations within the context of the operator product expansion. When doing so we find an asymptotically free running coupling constant, together with a mass scale m. Predictions are precisely consistent with the non-perturbative calculations.

The above analysis motivates us to not give up on perturbation theory so easily, when infrared divergences and non-perturbative vacua are at play.

1.7 Quantum Chromodynamics

We have seen a number of illuminating examples of IR divergences in relative simple models, and now turn to QCD. Though a part of the Standard Model, QCD may

well be treated as a stand-alone theory. QCD is very different from quantum electrodynamics, mainly due to the behavior of the gauge particles. While photons do not interact with each other, because they are not charged, gluons do interact among themselves. The non-abelian nature of the gauge group is responsible for this interaction. The gluon fields transform non-trivially under the action of a gauge group symmetry transformation and are therefore charged themselves. This self-interaction has profound implications and it radically changes the spectrum of the theory. Both asymptotic freedom and confinement are a consequence of it.

The masslessness of gauge bosons leads to IR divergences in perturbation theory. In the case of QED[4] the absence of self-interaction of photons prevents the theory from generating such divergences and they do not pose a problem. This situation is completely different in QCD, where the interaction causes perturbation theory to diverge. This means that the vacuum structure of QCD is completely different from the perturbative ansatz. The situation is even more difficult than in the non-linear sigma model, because in order to do perturbation theory at all gauge fixing is needed. The well-known Faddeev-Popov [8] gauge fixing procedure, while powerful and sufficient for perturbative purposes is not without problems. Gribov copies in the gauge fixing and the absolute value of the determinant pose problems non-perturbatively. To define the path-integral non-perturbatively one does not need the Faddeev-Popov method, as lattice QCD has shown. However, we expect from the analogy to the non-linear sigma model that the QCD groundstate consist of strong long-distance fluctuations and small perturbative short distance fluctuations. The scale between the long and short wavelength fluctuations is a fundamental scale of the theory, this scale is called lambda QCD (Λ_{QCD}). If one studies QCD in some volume of space-time much smaller than fundamental scale, then one would expect the Faddeev-Popov method to work within this volume. So analogous to the case of the non-linear sigma model, one would expect that the coefficient functions in an OPE are perturbatively calculable. This is indeed true, the coefficients in an OPE are IR safe. The total cross-section of

$$e^+ + e^- \to \gamma^* \to \text{hadrons} \tag{1.73}$$

can be calculated in this way. This total cross-section is fully inclusive, there are no restraints on the final state. This cross-section is an example of an IR safe quantity, for which all the divergences cancel. Intuitively this can be understood as follow. The fundamental interaction is a hard-photon decaying into a quark/anti-quark pair. This happens on a very small distance scale and is perfectly calculable within perturbation theory. After the pair is produced long distance interactions produces the final state, a process we cannot calculate perturbatively. Nevertheless, the total probability that something happens after the quark/anti-quark pair has been produced is equal to one. So if we are not interested in any particular final state and thus sum over all final states, the total probability is just given by the fundamental hard interaction. This argument assumes the hard process and the long distance processes to be incoherent, so instead of adding amplitudes we can suffice with adding probabilities. This is very

[4] Without charged particles.

plausible when the hard scale and long distance scale is well-separated. In general one expects corrections to this picture of order $\Lambda^n_{\rm QCD}/Q^n$, where Q is the hard scale. These corrections are power corrections.

Thus far we discussed long distance IR divergences. In actual QCD calculations in real Minkowski space-time we also have collinear divergences. These present additional difficulties. Collinear divergences stem from the splitting of a massless particle into two massless particles going in the same direction. If this happens for a parton inside the proton it is a fluctuation that is part of the structure of the proton. In calculations of cross-sections with protons in the initial state, the divergent splitting of the initial parton should be part of the proton structure and not a QCD correction to the hard process. Collins, Soper and Sterman [9] and Bodwin [10] have proved that all the collinear divergences factorize and can be absorbed into a redefinition of the structure proton. In section 1.9 we discuss factorization in a little more detail and in chapter 5 factorization will be used in a calculation of a particular process (associated production of a top quark and a charged Higgs boson). We now discuss the cancellation of IR/COL divergences in suitably chosen cross-sections.

1.8 IR divergences cancellation and the KLN theorem

The Kinoshita, Lee, Nauenberg (KLN) theorem [11] establishes the fact that IR/COL divergences cancel in suitably defined transition rates. It is in fact an elementary theorem of quantum mechanics, not specifically of quantum field theory. Let us consider the following Hamiltonian

$$H = H_0 + gH_1, \tag{1.74}$$

where H_0 is the free and H_1 the interaction part of the Hamiltonian. We treat the spectrum of the full Hamiltonian H as a perturbation on the spectrum of free Hamiltonian H_0. Therefore we use the same label a for the two corresponding eigenstates of the two Hamiltonians. We encounter IR divergences in the perturbation series, when the spectra contain limit points, ie. when $(E-E')^{-1}$ diverges. We will prove the KLN theorem to first order in perturbation theory, but it is not difficult to do this to all orders in perturbation theory.

Let us denote $\{|a\rangle\}$ with $H_0|a\rangle = E_a|a\rangle$ as the set of eigenstates of H_0 and $U_\pm = U(0, \pm\infty)$ the unitary evolution operator of the full Hamiltonian. We can define the initial and final states

$$|a\rangle^i = U_-|a\rangle, \tag{1.75}$$

$$|a\rangle^f = U_+|a\rangle. \tag{1.76}$$

Then we have for the scattering matrix $S_{ba} = \langle b|^f a\rangle^i = \langle b|U_+^\dagger U_-|a\rangle$, and the consequent transition probability is given by

$$P_{ba} = |S_{ba}|^2 = \sum_{i,j} \Big[U^*_{+ib}U_{+jb}\Big]\Big[U^*_{-ja}U_{-ia}\Big]. \tag{1.77}$$

We can compute $U_{\mp}$ in perturbation theory, and find, to first order

$$(U_{\mp})_{ja} = \delta_{ja} + g\frac{1-\delta_{ja}}{E_a - E_j \pm i\epsilon}(H_1)_{ja} + O(g^2). \tag{1.78}$$

The IR divergences arise when $E_a = E_j$. We now introduce the set of states $D(E)$ which consists of all states that lie in some energy range Δ around E. We show that the following sum is finite

$$T^{\pm}(E)_{ij} = \sum_{a\in D(E)} \left[(U_{\pm})_{ia}(U_{\pm})^*_{ja}\right]. \tag{1.79}$$

This is easily proven by inserting the perturbation series into eq. (1.79). We find

$$T^{\pm}(E)_{ij} = \sum_{a\in D(E)} \left[\delta_{ia}\delta_{ja} + g\frac{\delta_{ia}(1-\delta_{ja})}{E_a - E_j \pm i\epsilon}(H_1)^*_{ja} + g\,\frac{\delta_{ja}(1-\delta_{ia})}{E_a - E_i \mp i\epsilon}(H_1)_{ia}\right]. \tag{1.80}$$

If both i, j are not in $D(E)$ the above expression is zero and thus finite. If $i \in D(E)$ and j is not, then the sum is also clearly finite. If both i, j are in $D(E)$ the two terms cancel because of the hermiticity of H_1. The finiteness of $T^{\pm}$ thus implies the finiteness of transition probability $p_{E'E}$ between these two energy regions,

$$p_{E'E} = \sum_{a\in D(E)}\sum_{b\in D(E')} P_{ba} = \mathrm{Tr}\, T^{+}(E')T^{-}(E). \tag{1.81}$$

The probability $p_{E'E}$ is a physical observable and is inclusive because we do not distinguish states with almost equal energies. The energy range Δ is a cut-off for the divergency and in the limit $\Delta \to 0$ the probabilities diverge. Typically there are terms which contain factors

$$\ln^n \frac{\Delta}{E}. \tag{1.82}$$

The intuitive explanation behind the KLN theorem is the fact that unitarity ensures the total probability for something to happen is 1. This means that IR/COL divergences have to cancel in inclusive processes. The IR/COL divergences indicate a strong mixing between states, so when evolving, these states are continuously rotated into each other and the notion of scattering is not appropriate. However if we sum over all these states we are not sensitive to this mixing, and scattering is the appropriate language.

1.9 Factorization

Experiments in particle colliders measure cross sections of processes in which hadrons are either produced in the final state, or constitute the colliding beams, or both. In order to make connection with these measurements we need to be able to calculate these hadronic cross-sections. Hadrons are bound states of the fundamental quark and gluonic degrees of freedom. Therefore, in principle, one would have to calculate

the bound state wave function in order to give a value for the cross-section from first principles. As confinement is not sufficiently well understood, this cannot be done with current methods, and we must resort to an alternative route to predict such cross sections.

The key idea was due to Feynman. In his parton model he viewed hadrons as a bunch of essentially free particles (partons) traveling together collinearly. Cross sections of hadron scattering are then given as a sum of parton cross sections, each weighted by the probability for a particular parton with a certain momentum to be found inside the hadron. Expressed in a formula this statement reads

$$d\sigma(p) = \sum_i \int_0^1 d\zeta d\sigma^i(\zeta p) f_i(\zeta), \tag{1.83}$$

where we sum over the parton species i, and integrate over the momentum fraction ζ of the partonic cross-section $d\sigma^i$, weighted with the parton distribution function (PDF) $f_i(\zeta)$. The latter are assumed, in this model, to be universal, and may be extracted from other processes.

The partonic cross section can be calculated using quarks and gluons rather than hadrons. The above formula works well enough at tree level , but once one tries to include loop effects one encounters divergences. However the same approach as in the OPE can be followed here and it has been proven [9] that one can factorize all remaining divergences into the parton distribution functions in a process independent way. The QCD improved parton model then has the following form

$$d\sigma(p) = \sum_i \int_0^1 \frac{d\zeta}{\zeta} d\sigma^i(\zeta p, \mu) f_i(\zeta, \mu) + \mathcal{O}\left(\frac{\Lambda^2_{\text{QCD}}}{Q^2}\right), \tag{1.84}$$

where Q^2 is the hard scale of the process. Compared to eq.(1.83), one notes the appearance of a factorization scale μ in both the factorized cross-section and the PDF, as well as the power correction $\mathcal{O}\left(\Lambda^2_{\text{QCD}}/Q^2\right)$. The generalization of the above formula to processes with two initial hadrons or with identified final state hadrons is straightforward. In case of more hadrons in the initial state every hadron gets a PDF and for every identified hadron in the final state one gets a so-called fragmentation function. The above formula is the key to predicting QCD cross sections at hadron colliders, and for every scattering process involving hadrons in the initial state we need to use the above formula to make systematic and accurate predictions. The research in this thesis in essence concerns a regime where the predictive power of the above formula is endangered by a badly behaved perturbative series.

To illustrate this breakdown, consider Drell-Yan (DY) scattering,

$$h_1(p_1) + h_2(p_2) \to l(k) + \bar{l}(k') + X, \tag{1.85}$$

such that a lepton-antilepton pair is produced through an intermediate vector boson in a hadron-hadron collision. The remainder of the final state is denoted by X. The hadron center-of-mass (CM) energy is $\sqrt{s}$ (where $s = (p_1 + p_2)^2$) and the energy of the

lepton pair is given by Q ($Q^2 = (k+k')^2$). The relevant kinematical parameter for this process is $\tau = Q^2/s$, which is the fraction of energy transferred to the leptons. The differential cross section at fixed τ is given by

$$d\sigma(\tau) = \sum_{ij} \int_0^1 \frac{d\zeta_1}{\zeta_1} \frac{d\zeta_2}{\zeta_2} d\sigma^{ij} \left(\frac{\tau}{\zeta_1 \zeta_2}, \mu \right) f_i^1(\zeta_1, \mu) f_j^2(\zeta_2, \mu). \tag{1.86}$$

In the limit $\tau \to 1$ all the energy of the incoming hadrons transfers to the leptons, so there is hardly energy available for other final state radiation: the final state radiation must be soft. The partonic cross section contains divergences corresponding to initial state collinear radiation, which are absorbed into the PDF's, and the IR divergences, which are canceled in the sum over all final states due to the KLN theorem. However, as the available energy for final state radiation is $(1-\tau)s$, we expect, by the KLN theorem (see eq. (1.82)), terms like

$$\left[\frac{\ln^k(1-z)}{1-z} \right]_+, \quad z = \frac{\tau}{\zeta_1 \zeta_2}. \tag{1.87}$$

Indeed such factors appear [12] and moreover at order n in perturbation theory the power k is $2n-1$ and lower. Effectively we have a perturbation theory in $\alpha \ln^2(1-z)$. These logarithms endanger the predictive power of the perturbation series. Their all-order resummation may rescue the predictive power. Let us form an impression of why this is so.

Resummation takes the simplest form in Mellin moment space, which diagonalizes the linear transformation eq. (1.86)

$$\tilde{d\sigma}(N) = \sum_{ij} \tilde{d\sigma}^{ij}(N, \mu) \tilde{f}_i^1(N, \mu) \tilde{f}_j^2(N, \mu). \tag{1.88}$$

The $z \to 1$ behavior is probed by the large N behavior in Mellin moment space. At order n in perturbation theory the most dominant term in the coefficient in the large z limit is $\left[\frac{\ln^{2n-1}(1-z)}{1-z} \right]_+$ which becomes $\ln^{2n}(N)$ in Mellin moment space. As we will see, these terms can be organized in the following schematic form

$$\tilde{d\sigma}^{ij}(N) = \exp\left[\alpha_S \ln^2 N \right] (1 + c_1 \alpha_S + \ldots). \tag{1.89}$$

The coefficients of the remaining perturbative series do not have terms proportional to $\ln^{2n}(N)$ at order n in perturbation theory, leaving the remaining series more rapidly convergent. The large logarithms have been brought under analytical control in the exponent. Also known as Sudakov exponentiation, it describes the all-order suppression of emission probabilities in the threshold region of phase space. To see how such an exponentiating structure comes about, we refer forward to the eikonal exponentiation in chapters 3 and 4. In the large N limit the eikonal approximation is valid, because all the gluons are soft, and can be applied to the cross section amplitudes. As

a result, the n-gluon amplitude, in a sense becomes the exponent of the 1-gluon amplitude. However the multi-gluon phase space is coupled due to a phase space delta function $\delta((1-\sqrt{z}) - \sum_i \frac{k_i^0}{\sqrt{s}})$ that ensures that the total radiated energy is fixed. So the phase space measure is

$$d\Phi_n = \left(\prod_i d^{4-2\varepsilon} k_i \delta_+(k_i^2)\right) \delta\left((1-\sqrt{z}) - \sum_i \frac{k_i^0}{\sqrt{s}}\right), \tag{1.90}$$

where i labels all the real gluons. If we put $z = e^{-\lambda}$ then the Mellin transform becomes a Laplace transform. We notice that $1-\sqrt{z} \approx \frac{1}{2}\lambda$ near threshold (large N) and the Laplace transformed phase space becomes

$$\int d\lambda e^{-\lambda N} d\Phi_n = \left(\prod d^{4-2\varepsilon} k_i \delta_+(k_i^2)\right) e^{-N\sum_i \frac{2k_i^0}{\sqrt{s}}}, \tag{1.91}$$

where N is the Laplace conjugate of λ. The phase space is now factorized and the final state gluons are independent of each other. The eikonal exponentiation tells us that in this case we have exponentiation of the series,

$$\exp\left[\text{real} + \text{virtual}\right]. \tag{1.92}$$

The diagrams in the exponent are called webs and are topological identified by the property that they cannot be separated into two parts by cutting a hard line twice. The simplest real and virtual webs are given by fig. 1.5, which is given by

$$\int d^{4-2\varepsilon} k\, \delta_+(k^2) e^{-N\frac{2k^0}{\sqrt{s}}} \frac{1}{k_+ k_-} = N^{2\varepsilon} s^{-\varepsilon} \left(\frac{A}{\varepsilon^2} + \frac{B}{\varepsilon} + \ldots\right), \tag{1.93}$$

where we leave the explicit expressions for A and B unspecified. The virtual diagrams give

$$\int d^{4-2\varepsilon} k \frac{1}{k_+ k_- k^2} = -\left(\frac{A}{\varepsilon^2} + \frac{B}{\varepsilon} + \ldots\right). \tag{1.94}$$

The poles cancel between the real and virtual graphs, resulting in

$$A \ln^2 N + 2B \ln N + 2A \frac{\ln N}{\varepsilon}. \tag{1.95}$$

The remaining pole is the initial state collinear singularity which is canceled through factorization, leaving the $\ln^2 N$ as predicted in the exponent of eq. 1.92. Further development [13, 14] leads to the resummation formula

$$\ln\left[d\sigma^{ij}(N,Q^2)\right] = \mathcal{F}_{\mathrm{DY}}\left(\alpha_s(Q^2)\right) + \int_0^1 dz\, z^{N-1} \left\{ \frac{1}{1-z} D\left[\alpha_s\left((1-z)^2 Q^2\right)\right] + 2\int_{Q^2}^{(1-z)^2 Q^2} \frac{dq^2}{q^2} A\Big[\alpha_s(q^2)\Big] \right\}_+, \tag{1.96}$$

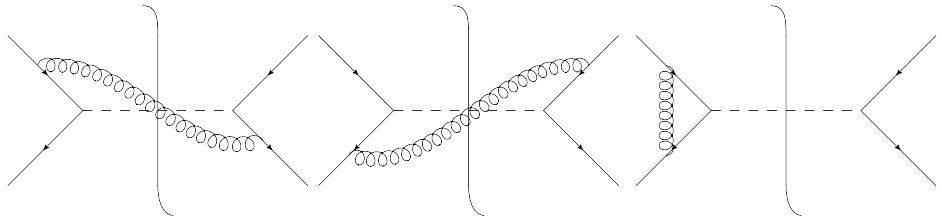

(a) Real emission webs. (b) Virtual correction web.

Figure 1.5: Basic DY webs.

which is the starting point of an improved resummation formula in chapter 2. This formula resums large perturbative contributions to all-orders in the exponent, A and D are universal functions that describe the large N behavior of the series. The remaining series for $\mathcal{F}_{\rm DY}$ has better convergence properties. From a theoretical point of view resummation is interesting because it makes all-order structure apparent. From a practical point of view it is crucial in order to reliably calculate cross sections in regions where a perturbative approach seemed hazardous.

A main component of this thesis will be the study of the resummation of next-to-eikonal corrections. The large logarithms which we resummed in the previous paragraph are the dominant eikonal logarithms and can be shown to be generated by the eikonal approximation. They are generated by soft radiation for which one can neglect the recoil of the particle that emits the radiation. One can show exponentiation of the contribution due to this soft radiation directly on the level of Feynman diagrams which goes under the name of eikonal exponentiation. A large part of this thesis is trying to capture the effects of the next-to-eikonal (when one include the effect of recoil) contributions into a resummation formula.

In chapter 2 we perform an "heuristic" study of resummation at the level of $\ln^k(N)/N$. Here we include well-motivated improvements of the resummation formulas to see how much of the next-to-eikonal structure we can capture. In chapters 3 and 4 we show that next-to-eikonal contributions to matrix elements, and in cases to cross sections, do exponentiate although that we have to include extra effective Feynman rules. The approach we use also simplifies, both technically and intuitively, the original proofs of eikonal exponentiation. Instead of a purely diagrammatic approach we use path integrals as much a possible. In this way many of the combinatorial technicalities disappear and a more physical picture of exponentiation emerges.

In chapter 5 we discuss single top plus charged Higgs production. We constructed a computer program, a Monte Carlo generator, that generates fully exclusive events for this process. We describe the calculations and the framework for creating such a program, and using this program we discuss the physics of this process.

Chapter 2

Next-to-eikonal resummation in Drell-Yan and Deep Inelastic Scattering

2.1 Introduction

Sudakov resummations are established in perturbative QCD for all logarithmic contributions, to leading power in the total momentum fraction carried by soft gluons. To illustrate this fact, consider as an example threshold resummation for the Drell-Yan process, or for a similar electroweak annihilation cross section at the hard scale Q. In this case, large logarithms arise in the hard partonic cross section when the total available center-of-mass energy, $\hat{s}$, is only slightly larger than the mass Q^2 of the selected electroweak final state. Gluon radiation into the final state is then forced to be soft, as gluons carry (at most) a total energy $(1-z)\hat{s}$, with $z \equiv Q^2/\hat{s}$. As a consequence, perturbative contributions at order α_s^n are enhanced by large logarithms in the form of 'plus' distributions, up to $\left[\ln^{2n-1}(1-z)/(1-z)\right]_+$. Upon taking a Mellin transform, these distributions turn into powers of logarithms of the Mellin variable N, conjugate to z, up to $\ln^{2n} N$. All these contributions can be resummed [13, 14], and they display a nontrivial pattern of exponentiation: the logarithm of the cross section in Mellin space, in fact, is enhanced only by single logarithms, up to $\ln^{n+1} N$ at order α_s^n.

It has been understood since the early days of QCD [15] that at least some non-logarithmic contributions (terms independent of N, which are Mellin conjugate to virtual corrections proportional to $\delta(1-z)$) also exponentiate. In fact, Ref. [16] later proved, at least for electroweak annihilation and DIS, that all such contributions can be organized in exponential form. One may naturally wonder to what extent this pattern of exponentiation can be extended beyond leading power in the Mellin variable N, or in the soft gluon energy fraction $1-z$.

There are several problems in attempting to extend the resummation formalism beyond leading power in N, or $1-z$. Indeed, resummation can be understood to be a consequence of Sudakov factorization, as discussed in [17]. To leading power in N, it can be shown that the Mellin moments of the cross section factorize into distinct functions responsible for infrared and collinear enhancements, times a hard remainder which is free of logarithms. Exponentiation follows from evolution equations that are dictated by this factorization. To date, no proof of such a Sudakov factorization is available beyond leading power in N. Part of this issue is the fact that, in order the achieve exponentiation, the phase space specific to the observable at hand, in the threshold limit, must itself factorize; this is achieved at leading power by taking the Mellin transform, thanks to the fact that the observable (essentially $1-z$ for the inclusive Drell-Yan cross section) is linear in soft gluon energies to leading power in $1-z$. Again, this simple property is lost beyond leading power.

Not withstanding these obstacles, there is intriguing, if scattered, evidence that some of the mechanisms that lead to the resummation of leading power logarithms are still operating at next-to-leading power. Theoretically, evidence in this direction is provided by the Low-Burnett-Kroll theorem [18, 19], which states that (in QED) cross sections involving soft photons can be expressed in terms of radiation-less amplitudes not only at leading power in soft gluon energies (which corresponds to the bremsstrahlung spectrum and to the eikonal approximation), but also at next-to-leading power. For such cross sections radiation is simply related to classical fields, and one expects some form of soft photon exponentiation to hold. In QCD, direct application of Low's theorem is complicated by the presence of collinear divergences [20], but one may still expect it to be relevant for soft emissions.

At a more practical level, one may observe that resummed cross sections are expressed in terms of integrals of certain anomalous dimensions, with integration limits dictated by the phase space available for soft radiation, and with the running coupling evaluated at the typical transverse momentum of the first gluon emission. These kinematical quantities are evaluated in the threshold limit, and one may expect that correcting their values in order to make them accurate at next-to-leading power in the soft momentum should lead to a physically meaningful improvement of the resummation.

This kind of reasoning has led to attempts to include certain sub-eikonal effects in practical implementations of Sudakov resummations, mostly in view of gauging the theoretical uncertainty of the resummation [21]. Typically, this involves including subleading terms in the collinear evolution kernel into the resummation, which is particularly appealing for Drell-Yan and related cross sections, where the entire singularity structure is determined by initial state soft and collinear radiation. This was applied in the case of Higgs production in Refs. [21, 22, 23, 24], and for prompt photon production in Ref. [25].

More recently, following the evaluation of collinear evolution kernels at three loops [26], a bold suggestion has been put forward by Dokshitzer, Marchesini and Salam (DMS) [27], who proposed a modified evolution equation for parton distributions, based on the idea that the proper ordering variable in the collinear shower should be the lifetime

of parton fluctuations rather than the gluon transverse momentum. This modified evolution has remarkable consequences: it explains a previously mysterious numerical coincidence observed by [26], and it connects eikonal and sub-eikonal terms in the splitting function in a nontrivial way, consistent with the idea that all evolution effects which are non-vanishing as $z \to 1$ should be determined at one loop, with an appropriate definition of the coupling. The DMS proposal has later been refined by Basso and Korchemsky [28], who traced the recursive relation which determines the collinear anomalous dimension to the conformal invariance of the classical theory, and its breaking by the β function. The relations connecting eikonal and next-to-eikonal terms for parton evolution are then generalized to higher twist operators as well.

In this chapter, we begin to develop a systematic approach for the inclusion of next-to-eikonal terms in the resummation, inspired by the results of [27] and by the earlier work of [21]. We begin, in Section 2.2, by briefly reviewing the DMS approach, and describing how we intend to implement it in the context of Sudakov resummation. There, we also introduce some simple tools and definitions to evaluate the integrals that appear in resummed exponents to the desired accuracy. Then, in Section 2.3, we propose an ansatz to include in the resummation all next-to-eikonal effects that can be argued to be under theoretical control. We do this for the Drell-Yan cross section and for the Deep Inelastic structure function F_2. It is clear from the outset that our ansatz controls only a subset of all next-to-eikonal terms in the cross section: indeed, it may well be that not all such terms can be organized in exponential form. We believe however that the terms we include are physically well motivated, so we expect our ansatz to reproduce with reasonable accuracy higher order perturbative results, based on the evaluation of the exponent at lower orders. We proceed to test this expectation by comparing the results of expanding our proposed resummed expressions with the known exact results at two loops for the Drell-Yan cross section [29], and at two and three loops for DIS [30, 31].

As we will outline in our discussion, in Section 2.4, the results of this comparison are consistent with the assumption that at least leading next-to-eikonal logarithms do exponentiate, for all color structures. Furthermore, the implementation of the DMS approach reproduces with considerable accuracy (though not exactly) certain classes of subleading next-to-eikonal logarithms which could not have been generated by the standard resummation. We believe that these results are encouraging regarding the possibility that next-to-eikonal logarithms could be understood and organized to all orders, an effort which will ultimately require a full analysis of soft gluon effects beyond the eikonal approximation.

2.2 Tools for next-to-eikonal resummation

The task of probing the extension of the resummation formalism beyond the eikonal approximation requires both conceptual and practical tools. In this section we describe briefly the main conceptual progress that we are going to employ, which is the idea, put forward by DMS, that all NE terms in collinear evolution trace their origin to

one loop effects, phase space, and the choice of an appropriate, physically motivated coupling. We present the DMS equation, and we show how it can be solved in exponential form, just like ordinary collinear evolution, to NE accuracy. Next, making use of a technique developed in [32], which we generalize to NE level, we present some simple results for the generic integrals that may appear in NE resummed cross section to any perturbative order.

2.2.1 The DMS evolution equation and its solution

Consider first the familiar collinear evolution equation for the non-singlet quark density

$$\mu^2 \frac{\partial}{\partial \mu^2} q(x,\mu^2) = \int_x^1 \frac{dz}{z}\, q\left(\frac{x}{z},\mu^2\right)\, P_{qq}\left(z,\alpha_s(\mu^2)\right)\,. \tag{2.1}$$

As is well known, this simple convolution can be turned into a product by taking a Mellin transform,

$$\mu^2 \frac{\partial}{\partial \mu^2} \tilde{q}(N,\mu^2) = \gamma_N\left(\alpha_s(\mu^2)\right)\, \tilde{q}(N,\mu^2)\,, \tag{2.2}$$

which leads to an exponential solution for the Mellin moments of the quark distribution,

$$\tilde{q}(N,\mu^2) = \exp\left[\int_{\mu_0^2}^{\mu^2} \frac{d\mu'^2}{\mu'^2} \gamma_N\left(\alpha_s(\mu'^2)\right)\right]\, \tilde{q}(N,\mu_0^2)\,. \tag{2.3}$$

Note that here we express the solution in terms of a generic initial condition at some reference scale, as appropriate for the evolution of physical, measured parton distributions. When one instead considers parton-in-parton distributions, defined in QCD in terms of matrix elements of bilocal operators, one can use dimensional regularization to express the solution as a pure exponential (with no prefactor), using the fact that the dimensionally regularized coupling vanishes with the scale [17, 33]. Within the framework of dimensional regularization and in a minimal subtraction scheme, the structure of the anomalous dimension $\gamma_N(\alpha_s)$ at large values of N (corresponding to the $z \to 1$ limit) is known [34] to be single-logarithmic. It is of the form

$$\gamma_N\left(\alpha_s\right) = -A\left(\alpha_s\right) \ln \bar{N} + B_\delta\left(\alpha_s\right) - C_\gamma\left(\alpha_s\right)\, \frac{\ln \bar{N}}{N} + D_\gamma\left(\alpha_s\right)\, \frac{1}{N} + \mathcal{O}\left(\frac{1}{N^2}\right) \tag{2.4}$$

where the function $A(\alpha_s)$ is one half of the cusp anomalous dimension $\gamma_K(\alpha_s)$, and $\bar{N} = N\, \mathrm{e}^{\gamma_E}$. The DMS proposal is that the functions $C_\gamma(\alpha_s)$ and $D_\gamma(\alpha_s)$ are not genuinely independent, but they can be derived from the knowledge of $A(\alpha_s)$. In turn, $A(\alpha_s)$ can be interpreted as a definition of the coupling in a suitable scheme, which has been variously described as 'physical', or 'bremsstrahlung', or 'Monte Carlo' scheme [35]. In order to implement this idea, DMS propose to replace Eq. (2.1) with

$$\mu^2 \frac{\partial}{\partial \mu^2} \psi(x,\mu^2) = \int_x^1 \frac{dz}{z}\, \psi\left(\frac{x}{z}, z^\sigma \mu^2\right)\, \mathcal{P}\left(z, \alpha_s\left(\frac{\mu^2}{z}\right)\right)\,. \tag{2.5}$$

Here we have denoted by $\psi(x,\mu^2)$ a distribution which can be understood either as a fragmentation function or as a parton distribution; the parameter $\sigma = \pm 1$ serves to distinguish the two cases: $\sigma = +1$ for the space-like evolution of parton distributions, while $\sigma = -1$ for the time-like evolution of fragmentation functions. DMS argue (and verify at two loops) that with Eq. (2.5) the evolution kernel is the same for both kinematics. Furthermore, at least up to second order in α_s, the kernel $\mathcal{P}$ has no contributions at order $(1-z)^0$, so that it can be written as

$$\mathcal{P}\left(z,\alpha_s\right) = \frac{A\left(\alpha_s\right)}{(1-z)_+} + B_\delta\left(\alpha_s\right)\delta(1-z) + \mathcal{O}\left((1-z)\right) . \tag{2.6}$$

If one now chooses the cusp anomalous dimension (divided by the Casimir invariant of the appropriate representation, in this case C_F) as the definition of the coupling, setting $A\left(\alpha_s(\mu^2)\right) = C_F\,\alpha_{\rm PH}(\mu^2)$, one may conclude that all contributions to the evolution kernel that do not vanish as $z \to 1$ appear at the first non-trivial order in this scheme.

In the physical scheme, writing $\mathcal{P}(z,\alpha_{\rm PH}) = \mathcal{P}_1(z)\,\alpha_{\rm PH}/\pi + \mathcal{O}(\alpha_{\rm PH}^2)$, it is easy to construct an exponential solution, analogous to Eq. (2.3) but valid to NE order, for the distribution D. Indeed one may write

$$\mu^2\frac{\partial}{\partial\mu^2}\,\psi(N,\mu^2) = \int_0^1 dz\, z^{N-1}\,\mathcal{P}_1(z)\,\alpha_{\rm PH}\left(\frac{\mu^2}{z}\right)\psi(N,z^\sigma\mu^2) . \tag{2.7}$$

The scale of the coupling can be shifted by using the β function, as

$$\begin{aligned}\mu^2\frac{\partial}{\partial\mu^2}\,\psi(N,\mu^2) \;&=\; \int_0^1 dz\, z^{N-1}\,\mathcal{P}_1(z)\left[\frac{\alpha_{\rm PH}}{\pi}\right. \\ &\qquad \left. + (1-z)\left(\beta(\alpha_{\rm PH}) - \sigma\,\frac{\alpha_{\rm PH}}{\pi}\,\mu^2\,\frac{\partial}{\partial\mu^2}\right)\right]\psi(N,\mu^2) .\end{aligned} \tag{2.8}$$

One can now perform a Mellin transform, and introduce the anomalous dimensions

$$\widehat{\gamma}_1(N) = \int_0^1 dz\, z^{N-1}\,\mathcal{P}_1(z) , \qquad \widehat{\gamma}_1\,'(N) = \int_0^1 dz\, z^{N-1}(1-z)\,\mathcal{P}_1(z) , \tag{2.9}$$

which clearly obey $\widehat{\gamma}\,'(N) = \widehat{\gamma}(N) - \widehat{\gamma}(N+1)$. One finds then

$$\psi(N,\mu^2) = \exp\left[\int_{\mu_0^2}^{\mu^2}\frac{d\mu^2}{\mu^2}\,\frac{\widehat{\gamma}_1(N)\;\left(\alpha_{\rm PH}(\mu^2)/\pi\right) + \widehat{\gamma}_1\,'(N)\,\beta(\alpha_{\rm PH}(\mu^2))}{1+\sigma\,\widehat{\gamma}\,'(N)\;\left(\alpha_{\rm PH}(\mu^2)/\pi\right)}\right]\psi(N,\mu_0^2) , \tag{2.10}$$

which is valid up to corrections vanishing as $z \to 1$.

2.2.2 Moment integrals to $\mathcal{O}(1/N)$

Let us now turn to the practical issue of evaluating the generic integrals appearing in the exponents of threshold resummations, to our required accuracy, *i.e.* including all

correction of order $1/N$. To this accuracy threshold-resummed partonic cross sections can be written as

$$\ln\left[\hat{\sigma}(N)\right] - H = \int_0^1 dz\, \frac{z^{N-1}-1}{1-z}\, f_1\big[\ln(1-z)\big] + \int_0^1 dz\, z^{N-1} f_2\big[\ln(1-z)\big]\,, \quad (2.11)$$

where H represents N-independent terms. Expanding the functions f_i in powers of their argument, as

$$f_i\big[\ln(1-z)\big] = \sum_{p=0}^{\infty} f_i^{(p)} \ln^p(1-z)\,, \quad (2.12)$$

we can write

$$\ln\left[\hat{\sigma}(N)\right] - H = \sum_{p=0}^{\infty} \left[f_1^{(p)}\, \mathcal{D}_p(N) + f_2^{(p)}\, \mathcal{J}_p(N) \right]\,, \quad (2.13)$$

in terms of the basic integrals

$$\mathcal{D}_p(N) = \int_0^1 dz\, \frac{z^{N-1}-1}{1-z}\, \ln^p(1-z)\,, \qquad \mathcal{J}_p(N) = \int_0^1 dz\, z^{N-1}\, \ln^p(1-z)\,. \quad (2.14)$$

In order to evaluate the integrals in Eq. (2.14), we follow [32] and introduce two generating functions, defined by

$$G_{\mathcal{D}}(\lambda, N) \equiv \int_0^1 (z^{N-1}-1)(1-z)^{\lambda-1} = \frac{\Gamma(N)\Gamma(\lambda)}{\Gamma(N+\lambda)} - \frac{1}{\lambda}\,, \quad (2.15)$$

and by

$$G_{\mathcal{J}}(\lambda, N) \equiv \int_0^1 z^{N-1}\,(1-z)^{\lambda} = \frac{\Gamma(N)\Gamma(\lambda+1)}{\Gamma(N+\lambda+1)} = \frac{1}{N+\lambda}\left[\lambda\, G_{\mathcal{D}}(\lambda, N) + 1\right]\,, \quad (2.16)$$

>From these definitions, one sees that the integrals in Eq. (2.14) are given by

$$\mathcal{D}_p(N) = \frac{\partial^p}{\partial \lambda^p}\, G_{\mathcal{D}}(\lambda, N)\bigg|_{\lambda=0}\,, \qquad \mathcal{J}_p(N) = \frac{\partial^p}{\partial \lambda^p}\, G_{\mathcal{J}}(\lambda, N)\bigg|_{\lambda=0}\,. \quad (2.17)$$

In order to evaluate the integrals explicitly to $1/N$ accuracy, we only need the first correction to Stirling's formula for the $\mathcal{D}$-type integrals,

$$\Gamma(z) = \mathrm{e}^{-z}\, z^{z-1/2}\, \sqrt{2\pi} \left(1 + \frac{1}{12z}\right) \left(1 + \mathcal{O}\left(\frac{1}{z^2}\right)\right)\,, \quad (2.18)$$

leading to

$$G_{\mathcal{D}}(\lambda, N) = \frac{1}{\lambda}\left[\frac{\Gamma(1+\lambda)}{N^{\lambda}} \left(1 + \frac{\lambda(1-\lambda)}{2N}\right) - 1\right]\,, \quad (2.19)$$

while for the $\mathcal{J}$-type integrals it suffices to take

$$G_{\mathcal{J}}(\lambda, N) = \frac{\Gamma(1+\lambda)}{N^{1+\lambda}}\,. \quad (2.20)$$

We note in passing that, to $1/N$ accuracy, there is a simple relation between the $\mathcal{J}$ and the $\mathcal{D}$ integrals; in fact

$$\mathcal{J}_p(N) = -\frac{d}{dN}\mathcal{D}_p(N) + \mathcal{O}\left(\frac{1}{N^2}\right), \tag{2.21}$$

which follows from an identical relation between the generating functions,

$$G_{\mathcal{J}}(\lambda, N) = -\frac{d}{dN}G_{\mathcal{D}}(\lambda, N) + \mathcal{O}\left(\frac{1}{N^2}\right). \tag{2.22}$$

A useful way to evaluate both sets of integrals in the large N limit is to map them into simpler integrals, where the dependence on N has been moved from the integrand to the upper limit of integration. This technique is well known [14, 32], and we extend it here to $1/N$ accuracy. Let the generating function of cutoff integrals be

$$G_L(\lambda, N) \equiv \int_0^{1-1/N} dz\,(1-z)^{\lambda-1} = \frac{1-N^{-\lambda}}{\lambda}. \tag{2.23}$$

It is then easy to relate this function to the functions $G_{\mathcal{D}}$ and $G_{\mathcal{J}}$. Expanding Eq. (2.19) in powers of λ one finds

$$G_{\mathcal{D}}(\lambda, N) = -G_L(\lambda, N) + \sum_{k=1}^{\infty} \frac{\Gamma_k(N)}{k!}\,\lambda^{k-1}\,\frac{1}{N^{\lambda}}, \tag{2.24}$$

where

$$\Gamma_k(N) = \frac{d^k}{d\lambda^k}\left[\Gamma(1+\lambda)\left(1+\frac{\lambda(1-\lambda)}{2N}\right)\right]_{\lambda=0}. \tag{2.25}$$

This can be rewritten as

$$G_{\mathcal{D}}(\lambda, N) = \sum_{k=0}^{\infty} \frac{\Gamma_k(N)}{k!}(-1)^{k-1}\frac{\partial^k}{\partial(\ln N)^k}G_L(\lambda, N). \tag{2.26}$$

Using Eq. (2.22) one then immediately finds

$$G_{\mathcal{J}}(\lambda, N) = \frac{1}{N}\sum_{k=0}^{\infty} \frac{\Gamma_k(N)}{k!}(-1)^{k}\frac{\partial^{k+1}}{\partial(\ln N)^{k+1}}G_L(\lambda, N). \tag{2.27}$$

eqs. (2.26) and (2.27) can be used to evaluate directly the $\mathcal{D}$ and $\mathcal{J}$ integrals to the desired accuracy, and indeed we will make use of this explicit evaluation in Section 2.3. One finds

$$\begin{aligned}
\mathcal{D}_p &= \frac{1}{p+1}\sum_{k=0}^{p+1}\Gamma_k(N)\binom{p+1}{k}(-\ln N)^{p+1-k} + \mathcal{O}\left(\frac{\ln^m N}{N^2}\right), \\
\mathcal{J}_p &= \frac{1}{N}\sum_{k=0}^{p}\Gamma^{(k)}(1)\binom{p}{k}(-\ln N)^{p-k} + \mathcal{O}\left(\frac{\ln^m N}{N^2}\right),
\end{aligned} \tag{2.28}$$

where $\Gamma^{(k)}$ is the k'th derivative of the Euler gamma function. On the other hand, one can use eqs. (2.26) and (2.27) to directly relate the logarithm of the cross section to a cutoff integral of the same functions f_1 and f_2 appearing in Eq. (2.11). This is useful when one needs to correctly account for running coupling effects to all orders, as done in [14, 32]. To the present accuracy one can write

$$\begin{aligned}\ln\left[\hat{\sigma}(N)\right] - H \;&=\; \sum_{k=0}^{\infty} \frac{\Gamma_k(N)}{k!}(-1)^{k-1}\frac{\partial^k}{\partial(\ln N)^k}\int_0^{1-1/N} dz\;\frac{f_1\big[\ln(1-z)\big]}{1-z} \\ &-\; \frac{1}{N}\sum_{k=0}^{\infty}\frac{\Gamma^{(k)}(1)}{k!}(-1)^{k-1}\frac{\partial^{k+1}}{\partial(\ln N)^{k+1}}\int_0^{1-1/N} dz\;\frac{f_2\big[\ln(1-z)\big]}{1-z}\,.\end{aligned} \tag{2.29}$$

We now move on to applying these tools to the concrete example of threshold resummation for the Drell-Yan and DIS cross sections.

2.3 An ansatz for next-to-eikonal logarithms

In order to include NE effects in threshold resummation formulas we propose to modify the exponents in three ways. First of all, following DMS, we include subleading corrections in the argument of the running coupling. Second, we change the boundary of phase space accordingly. Third, and most relevant, we interpret the leading-logarithm function $A(\alpha_s)$ as arising from collinear evolution, and thus replace it with a NE generalization dictated by the DMS equation. This is done in the following way. While Eq. (2.5) cannot be diagonalized by means of a simple Mellin transform, it is however possible, as pointed out by DMS, to map the kernel $\mathcal{P}(z,\alpha_s)$ in Eq. (2.6) back to the conventional evolution kernel, order by order in perturbation theory, if one explicitly performs the shifts in the arguments of Eq. (2.5) by the action of differential operators. Indeed, one may rewrite Eq. (2.5) as

$$\mu^2\frac{\partial}{\partial\mu^2}\,\psi(x,\mu^2) = \int_x^1 \frac{dz}{z}\,\mathrm{e}^{-\ln z\left(\beta(\alpha_s)\frac{\partial}{\partial\alpha_s}-\sigma\frac{\partial}{\partial\ln\mu^2}\right)}\,\psi\left(\frac{x}{z},\mu^2\right)\,\mathcal{P}\left(z,\alpha_s(\mu^2)\right)\,, \tag{2.30}$$

where one should note that dependence on the coupling is only through the kernel $\mathcal{P}$, while explicit scale dependence arises only in the distribution ψ. Expanding the exponential and the kernel $\mathcal{P}$ in perturbation theory one is led to an equation which can be diagonalized order by order. When solved in this way, the DMS equation can be understood as a framework to generate classes of higher-order contributions to collinear anomalous dimensions using low-order information. In this spirit, we will write conventional resummation formulas, but we will generalize the collinear evolution function $A(\alpha_s)$ by including all terms that are generated by the DMS equation. As we will see, this will lead to slightly different implementations for space-like and time-like kinematics. Let us now consider our two examples in turn.

2.3.1 The Drell-Yan cross section

We first consider the Drell-Yan hard partonic cross section in the $\overline{\rm MS}$ factorization scheme, denoted $\widehat{\omega}(N)$. We propose to generalize the exponentiation of threshold corrections (see eq.(1.96)) in the following way.

$$\begin{aligned}\ln\Big[\widehat{\omega}(N)\Big] &= \mathcal{F}_{\rm DY}\left(\alpha_s(Q^2)\right) + \int_0^1 dz\, z^{N-1}\left\{\frac{1}{1-z}\,D\left[\alpha_s\left(\frac{(1-z)^2Q^2}{z}\right)\right]\right. \\ &+ \left. 2\int_{Q^2}^{(1-z)^2Q^2/z}\frac{dq^2}{q^2}\,P_s\Big[z,\alpha_s(q^2)\Big]\right\}_+ , \end{aligned} \tag{2.31}$$

where for simplicity we have set the factorization scale $\mu_F^2 = Q^2$. Here and below we adopt the convention that the 'plus' prescription applies only to singular terms in the expansion of the relevant functions in powers of $1-z$. In other words, for a singular function $f(z)$ with Laurent expansion $f(z) = \sum_{n=-1}^{\infty} f_n\,(1-z)^n$, and for any smooth function $g(z)$, regular as $z \to 1$, we define

$$\int_0^1 dz\, g(z)\Big[f(z)\Big]_+ \equiv f_{-1}\int_0^1 dz\,\frac{g(z)-g(1)}{1-z} + \int_0^1 dz\, g(z)\left(f(z) - \frac{f_{-1}}{1-z}\right) . \tag{2.32}$$

In Eq. (2.31), $\mathcal{F}_{\rm DY}(\alpha_s)$ is responsible for the exponentiation of N-independent terms, in accordance with [16]. It comprises purely virtual contributions given in terms the quark form factor, and real emission terms, which were denoted by $F_{\overline{\rm MS}}\,(\alpha_s)$ in [16]. The single-logarithm function $D(\alpha_s)$ can also be related to form factor data, and to the virtual part of the collinear evolution kernel $B_\delta(\alpha_s)$, as was done in [36], according to

$$D(\alpha_s) = 4\,B_\delta(\alpha_s) - 2\,\widetilde{G}(\alpha_s) + \beta(\alpha_s)\,\frac{d}{d\alpha_s}F_{\overline{\rm MS}}\,(\alpha_s)\,, \tag{2.33}$$

where $\widetilde{G}$ is constructed from single pole contributions to the quark form factor, as described in [16]. Finally, the DMS-improved space-like collinear evolution kernel $P_s(z,\alpha_s)$ is given in perturbation theory by $P_s(z,\alpha_s) = \sum_{n=1}^{\infty} P_s^{(n)}(z)\,(\alpha_s/\pi)^n$, where

$$P_s^{(n)}(z) = \frac{z}{1-z}A^{(n)} + C_\gamma^{(n)}\ln(1-z) + \overline{D}_\gamma^{(n)}\,. \tag{2.34}$$

Here $A^{(n)}$ and $C_\gamma^{(n)}$ are the perturbative coefficients of the functions appearing in Eq. (2.4), while $\overline{D}_\gamma^{(n)}$ is related to the perturbative coefficients of $D_\gamma(\alpha_s)$ by the simple shift $\overline{D}_\gamma^{(n)} = D_\gamma^{(n)} + A^{(n)}$; this takes into account the explicit factor of z multiplying $A(\alpha_s)$ in Eq. (2.34), which in turn is responsible for the inclusion of NE terms in the ordinary evolution kernel. In our normalization, $A^{(1)} = C_F$, $C_\gamma^{(1)} = \overline{D}_\gamma^{(1)} = 0$, while at two loops

$$\begin{aligned} A^{(2)} &= \frac{1}{2}\left[\left(\frac{67}{18} - \zeta(2)\right)C_A C_F - \frac{5}{9}n_f C_F\right], \qquad C_\gamma^{(2)} = C_F^2\,, \\ \overline{D}^{(2)} &= \frac{3}{4}C_F^2 - \frac{11}{12}C_A C_F + \frac{1}{6}n_f C_F\,. \end{aligned} \tag{2.35}$$

Notice in particular that the DMS procedure has brought into the resummation exponent abelian-like terms proportional to C_F^2 at two loops. As we will see, these terms do indeed find a match in the finite order expansion of $\widehat{\omega}(N)$. The ansatz (2.31) can be written in form of eq. (2.11), and evaluated using the methods of Section 2.2. In Section 2.4, we will compare the perturbative expansion of Eq. (2.31), with the coefficients given in Eq. (2.35), to the exact results of [29]. In both cases, one may write the expansion

$$\widehat{\omega}(N) = \sum_{i=0}^{\infty} \left(\frac{\alpha_s}{\pi}\right)^n \left[\sum_{m=0}^{2n} a_{nm} \ln^m \bar{N} + \sum_{m=0}^{2n-1} b_{nm} \frac{\ln^m \bar{N}}{N} \right] + \mathcal{O}\left(\frac{\ln^p N}{N^2}\right) , \qquad (2.36)$$

and then compare the expressions for the coefficients a_{nm} and b_{nm} arising from the resummation to the exact ones.

2.3.2 DIS structure functions

We consider next the resummation for the DIS structure function $\widehat{F}_2(N)$, in the $\overline{\rm MS}$ factorization scheme. Phase space and kinematics in this case are somewhat more complicated, since one has to deal with the final state jet, which is approximately massless near threshold, as well as with initial state soft and collinear radiation. We propose to generalize the conventional resummation formula as

$$\ln\left[\widehat{F}_2(N)\right] = \mathcal{F}_{\rm DIS}\left(\alpha_s(Q^2)\right) + \int_0^1 dz\, z^{N-1} \left\{ \frac{1}{1-z} B\left[\alpha_s\left(\frac{(1-z)Q^2}{z}\right)\right] + \int_{Q^2}^{(1-z)Q^2/z} \frac{dq^2}{q^2} P_s\Big[z, \alpha_s(q^2)\Big] + \int_{(1-z)^2Q^2/z}^{(1-z)Q^2/z} \frac{dq^2}{q^2}\, \delta P\Big[z, \alpha_s(q^2)\Big] \right\}_+ . \qquad (2.37)$$

Here, as above, $\mathcal{F}_{\rm DIS}(\alpha_s)$ is responsible for the exponentiation of N-independent terms. The case of the DIS cross section in the $\overline{\rm MS}$ factorization scheme was not explicitly treated in Ref. [16], but it is easy to work out the relevant contributions from the information collected there. Indeed, one can reconstruct the structure function $\widehat{F}_2(N)$ from the moment space ratio of the Drell-Yan cross section computed in the $\overline{\rm MS}$ scheme to that computed in the DIS scheme, both given in [16], as $\widehat{F}_2^{(\overline{\rm MS})}(N) = \sqrt{\widehat{\omega}^{(\overline{\rm MS})}(N)/\widehat{\omega}^{(\rm DIS)}(N)}$. One then easily verifies that $\mathcal{F}_{\rm DIS}(\alpha_s)$ comprises a virtual part, given by the finite terms in the modulus squared of the space-like quark form factor, plus a combination of real emission contributions, which can be written as $\left(F_{\overline{\rm MS}}\left(\alpha_s\right) - F_{\rm DIS}(\alpha_s)\right)/2$ in the notation of [16]. The single-logarithm function $B(\alpha_s)$ can be associated with the evolution of the final state jet. It is interesting to note here that $B(\alpha_s)$ can also be expressed in terms of form factor data, plus virtual corrections to the collinear evolution kernel, plus a total derivative of lower order contributions, just like the function $D(\alpha_s)$ in Eq. (2.33). Indeed, one verifies that existing results up

to three loops are consistent with

$$B(\alpha_s) = B_\delta(\alpha_s) - \widetilde{G}(\alpha_s) + \beta(\alpha_s)\,\frac{d}{d\alpha_s} F_{\rm B}(\alpha_s)\,, \tag{2.38}$$

with easily computed perturbative coefficients for the function $F_{\rm B}(\alpha_s)$. Eq. (2.38) is in keeping with the general results of Ref. [37], where it was shown, at the amplitude level, that all IR and collinear singularities in massless gauge theories can be constructed from combinations of eikonal functions with the virtual collinear function $B_\delta(\alpha_s)$, up to total derivatives with respect to the scale. Finally, we turn to the second line of Eq. (2.37). There, we have used the fact that the integration over the scale q^2 has a range that can be split into two intervals, which correspond to different physical sources of radiation. Scales between the factorization scale Q^2 and the soft scale $(1-z)^2Q^2$ correspond to Drell-Yan-like initial state radiation, while scales between the soft scale and the jet scale, $(1-z)Q^2$, correspond to the evolution of the final state jet. Accordingly, in the first range we use the same space-like evolution kernel $P_s(z,\alpha_s)$ that was employed in Eq. (2.31), while in the second range we use the time-like fragmentation kernel $P_t(z,\alpha_s)$. One may then define $\delta P(z,\alpha_s) \equiv P_t(z,\alpha_s) - P_s(z,\alpha_s)$, and thus get to Eq. (2.37). The function $\delta P(z,\alpha_s)$ begins at two loops, where it is given by [38]

$$\delta P^{(2)}(z) = -\frac{1}{2}\,C_F^2\,\left(4\ln(1-z)+3\right) + \mathcal{O}(1-z)\,. \tag{2.39}$$

Once again, using the methods of Section 2.2, we can expand both the resummed and the exact results for $\widehat{F}_2(N)$ in powers of logarithms of $\overline{N}$, and in inverse powers of N, as

$$\widehat{F}_2(N) = \sum_{i=0}^{\infty}\left(\frac{\alpha_s}{\pi}\right)^n \left[\sum_{m=0}^{2n} c_{nm}\ln^m \bar{N} + \sum_{m=0}^{2n-1} d_{nm}\frac{\ln^m \bar{N}}{N}\right] + \mathcal{O}\left(\frac{\ln^p N}{N^2}\right)\,. \tag{2.40}$$

We can then compare the resummed and exact values of the coefficients c_{nm} and d_{nm}, up to two and three loops, using the results of [30, 31].

2.4 Discussion

We begin by checking the behavior of our ansatz at the one loop level. This is not trivial, since we have not added new coefficients in the exponent at one loop, and the only sources of $1/N$ terms are the expansions of the $\mathcal{D}_p$ integrals, and the simple modifications of phase space. Using the one loop results for the functions $A(\alpha_s)$ and $D(\alpha_s)$, we find that for the Drell-Yan cross section the one-loop exact result is recovered, including all corrections down to $\mathcal{O}(1/N)$. Specifically, expanding Eq. (2.31), we find $b_{11} = 2C_F$ and $b_{10} = 0$, which is exact. Note that b_{10} vanishes as a consequence of a cancellation between subleading terms in the expansion of the $\mathcal{D}_p$ integrals and the modified phase space boundary. For DIS, including the one-loop value of the function $B(\alpha_s)$, we find that $d_{11} = C_F/2$ is correctly reproduced, while the non-logarithmic

term at $\mathcal{O}(1/N)$ is underestimated: Eq. (2.37) yields $d_{10} = C_F/8$, while the exact result is $d_{10} = 21/8\, C_F$. We take this as evidence (to be reinforced below) that our treatment of phase space for the final state jet is sufficiently precise to reproduce single NE logarithms, but not enough to fix NE constants (of course at this level non-factorizing effects for the observable, leading to a failure of exponentiation, at least in the form of Eq. (2.37), may also be a source of the discrepancy).

	C_F^2		$C_A C_F$		$n_f C_F$	
b_{23}	4	4	0	0	0	0
b_{22}	$\frac{7}{2}$	$\mathbf{4}$	$\frac{11}{6}$	$\frac{11}{6}$	$-\frac{1}{3}$	$-\frac{1}{3}$
b_{21}	$8\zeta_2 - \frac{43}{4}$	$8\zeta_2 - 11$	$-\zeta_2 + \frac{239}{36}$	$-\zeta_2 + \frac{133}{18}$	$-\frac{11}{9}$	$-\frac{11}{9}$
b_{20}	$-\frac{1}{2}\zeta_2 - \frac{3}{4}$	$4\zeta_2$	$-\frac{7}{4}\zeta_3 + \frac{275}{216}$	$\frac{7}{4}\zeta_3 + \frac{11}{3}\zeta_2 - \frac{101}{54}$	$-\frac{19}{27}$	$-\frac{2}{3}\zeta_2 + \frac{7}{27}$

Table 2.1: Comparison of exact and resummed 2-loop coefficients for the Drell-Yan cross section. For each color structure, the left column contains the exact results, the right column contains the prediction from resummation.

At the two-loop level, we proceed as follows. Since our aim is to verify our ability to reproduce NE terms, suppressed by a power of N, we include in the exponent all terms that are required to reproduce ordinary Sudakov logarithms, *i.e.* the two-loop values of the functions $A(\alpha_s)$ and $D(\alpha_s)$ for the Drell-Yan cross section, and of the function $B(\alpha_s)$ for DIS. We include the two-loop DMS-induced contributions $C_\gamma^{(2)}$ $\overline{D}_\gamma^{(2)}$ and $\delta P^{(2)}(z)$ as well, since they are responsible for effects that originate at two loops, and can only be reproduced by their inclusion. Our results are summarized in Tables 1 (for the Drell-Yan cross section) and in Table 2 (for the DIS structure function). We observe the following.

- The leading non-vanishing NE logarithms ($\ln^3 \bar{N}/N$ for the 'abelian' terms proportional to C_F^2, and $\ln^2 \bar{N}/N$ for non-abelian terms) are correctly reproduced by the exponentiation, both for DY and for DIS, and separately for each color structure.

- Next-to-leading NE logarithms ($\ln^2 \bar{N}/N$ for terms proportional to C_F^2, and $\ln \bar{N}/N$ for non-abelian terms) are reproduced with remarkable accuracy for the Drell-Yan process (in fact exactly for the $n_f C_F$ color structure), and reasonably well for the DIS process.

- The remaining NE logarithms, *i.e.* single logarithmic terms proportional to C_F^2, are well reproduced by exponentiation for the Drell-Yan process, but only roughly approximated for DIS. Non-logarithmic NE corrections are not well approximated by the exponentiation.

- More specifically, we note that for the Drell-Yan process the only source of terms proportional to $C_F^2 \ln^2 \bar{N}/N$ is the DMS-induced coefficient $C_\gamma^{(2)}$; indeed, the fact

that $b_{10} = 0$ ensures that no such term can arise from the square of the one-loop contribution. This contribution, yielding $b_{22} = 4$, is an excellent approximation to the exact result, $b_{22} = 7/2$. For DIS, as might be expected, the situation is somewhat more intricate; indeed d_{22} receives contributions from three sources: the square of the one-loop exponent, $C_\gamma^{(2)}$, and $\delta P^{(2)}(z)$; also here, however, the final result, $d_{22} = 55/16$, is a fair approximation of the exact answer, $d_{22} = 39/16$.

	C_F^2		$C_A C_F$		$n_f C_F$	
d_{23}	$\frac{1}{4}$	$\frac{1}{4}$	0	0	0	0
d_{22}	$\frac{39}{16}$	$\frac{55}{16}$	$\frac{11}{48}$	$\frac{11}{48}$	$-\frac{1}{24}$	$-\frac{1}{24}$
d_{21}	$\frac{7}{4}\zeta_2 - \frac{49}{32}$	$-\frac{1}{4}\zeta_2 - \frac{105}{32}$	$-\frac{5}{4}\zeta_2 + \frac{1333}{288}$	$-\frac{1}{4}\zeta_2 + \frac{565}{288}$	$-\frac{107}{144}$	$-\frac{47}{144}$
d_{20}	$\frac{15}{4}\zeta_3 - \frac{47}{16}\zeta_2 - \frac{431}{64}$	$-\frac{3}{4}\zeta_3 + \frac{53}{16}\zeta_2 - \frac{21}{64}$	$-\frac{11}{4}\zeta_3 + \frac{13}{48}\zeta_2 - \frac{17579}{1728}$	$\frac{5}{4}\zeta_3 + \frac{7}{16}\zeta_2 - \frac{953}{1728}$	$\frac{1}{24}\zeta_2 - \frac{1699}{864}$	$-\frac{1}{8}\zeta_2 + \frac{73}{864}$

Table 2.2: Comparison of exact and resummed 2-loop coefficients for the DIS structure function. For each color structure, the left column contains the exact results, the right column contains the prediction from resummation.

Clearly, since some of the DMS modifications enter the stage at two-loops, our results verify that these contributions improve the approximation, but do not really test exponentiation. We can put at least our DIS ansatz to a more stringent test by comparing to the complete three-loop calculation performed by Moch, Vermaseren and Vogt [31]. In this case, since our aim is to test exponentiation at NE level, we have included the three-loop value of the function $B(\alpha_s)$, contributing to single Sudakov logarithms, but we have not included three-loop DMS-induced contributions such as $C_\gamma^{(3)}$ and $\delta P^{(3)}(z)$. We can then expect reasonable agreement only for a limited set of NE logarithms. Since at three loops one finds six independent color structures, up to five powers of NE logarithms, and transcendentals up to ζ_5, we do not include here the lengthy tables of coefficients, but we give the most relevant results.

The three-loop analysis confirms that leading non-vanishing NE logarithms (in this case $\ln^5 \bar{N}/N$ for the color structure C_F^3, $\ln^4 \bar{N}/N$ for the color structures $C_A C_F^2$ and $n_f C_F^2$, and $\ln^3 \bar{N}/N$ for the color structures $C_A^2 C_F$, $n_f^2 C_F$ and $n_f C_A C_F$) are exactly reproduced by our resummation ansatz. Next-to-leading NE logarithms are reasonably well reproduced: specifically, for all color structures and separately for each degree of transcendentality the approximate results from the resummation have the same sign and similar numerical values to the corresponding exact results. In particular, this applies to the coefficient d_{34}, whose exact value is $57/64$, while the approximate result is $109/64$. Since d_{34} arises in part from interference between the NE coefficient $C_\gamma^{(2)}$ and the leading one-loop Sudakov logarithms in the exponent, we take this as mild evidence in favor of the exponentiation of DMS-induced corrections.

To summarize, we have provided an ansatz to include in threshold resummation a set of next-to-eikonal corrections, allowing for subleading phase-space effects, and including the modified collinear evolution proposed by Dokshitzer, Marchesini and

Salam. It is understood that these modifications of conventional threshold resummation do not exhaust all possible sources of NE threshold logarithms, and indeed it may be expected that some such corrections might break Sudakov factorization and fail to exponentiate. By comparing our ansatz to finite order perturbative results for the Drell-Yan and DIS cross sections, up to three loops, we have however provided evidence that at least the leading non-vanishing NE logarithms do indeed exponentiate according to our proposal. We have furthermore provided evidence that the DMS equation induces a definite improvement for resummation at NE level: for example, abelian-like next-to-leading NE terms that conventional resummation completely fails to generate are accurately approximated when DMS evolution is implemented. In general, it is clear that our ansatz gives better results for the Drell-Yan process, presumably thanks to its simple phase space and kinematics. The presence of the final state jet in DIS, and the related constraints on phase space, may require a more detailed factorization analysis in order to collect all sources of NE terms, and indeed may well induce a breakdown of simple Sudakov factorization at NE level. To aid this preliminary exploration of NE exponentiation, we have provided here some practical tools that will be useful in future extensions of this work, and we have taken the opportunity to note a connection, given in Eq. (2.38), between the jet function $B(\alpha_s)$ and the virtual collinear function $B_\delta(\alpha_s)$, as was previously done for the soft function $D(\alpha_s)$ in the Drell-Yan cross section [36]. We believe that this work provides further motivation both to include leading NE correction in phenomenological resummation studies, and to pursue the corresponding theoretical work. Indeed, a full understanding of NE threshold logarithms requires a more thorough analysis of soft gluon radiation beyond the eikonal approximation in the non-abelian theory, and specifically an adequate implementation of Low's theorem, mapping its boundaries of applicability in the case of massless QCD. In the next chapter we begin and develop tools for such an analysis.

Chapter 3

A path-integral approach to next-to-eikonal exponentiation

3.1 Introduction

Higher order corrections arising from soft gauge bosons in perturbative gauge theory, be they real or virtual, have been the subject of many investigations. Such radiation generically leads to series of perturbative contributions to differential cross-sections of the form $\alpha^n \log^m(\xi)/\xi$, where α is the coupling constant of the gauge theory, and ξ is related to the energy carried away by the soft particles. In the soft limit $\xi \to 0$ (in which the eikonal approximation may be taken), it becomes necessary to resum these terms to all orders in perturbation theory, as has been achieved by a variety of methods [13, 14, 39, 40, 41, 17, 32, 42]. Central to resummation is the exponentiation of eikonalized soft gauge boson corrections and it has been shown for both abelian and non-abelian gauge theory that this indeed occurs [43, 44, 45, 46].

To form an exponential series for a cross-section, both the matrix element and the phase space must exhibit an appropriate factorized structure. The statement for the matrix elements rests upon a thorough analysis of the general structure of higher order diagrams. The result for an amplitude $\mathcal{A}$ in abelian gauge theory is simply expressed in the eikonal approximation as

$$\mathcal{A} = \mathcal{A}_0 \exp\left[\sum G_c\right], \tag{3.1}$$

where $\mathcal{A}$ is the amplitude without soft radiation containing a number of hard outgoing *external lines*, and the sum in the exponent is over connected diagrams G_c between the external lines, with the Born contribution $\mathcal{A}_0$ factored out. Examples are shown for the case of hard production of a particle-antiparticle pair in figure 3.1. The non-abelian case is complicated by the nontrivial color structure of the Feynman diagrams at successive orders in perturbation theory. Nevertheless, in the case of two external

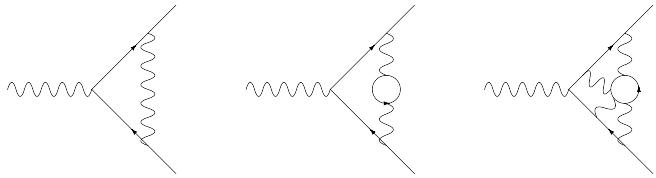

Figure 3.1: Examples of connected diagrams G_c of soft emissions between hard outgoing particle legs in abelian perturbation theory.

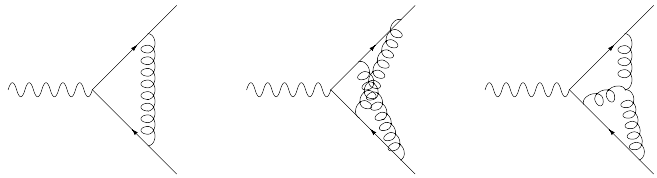

Figure 3.2: Examples of webs of soft emissions between external lines in non-abelian perturbation theory.

lines[1], exponentiation still holds provided one generalizes eq. (3.1) to

$$\mathcal{A} = \mathcal{A}_0 \exp\left[\sum \bar{C}_W W\right]. \tag{3.2}$$

Here W are so-called *webs*, and are diagrams which are two-eikonal irreducible. That is, one cannot partition a web into webs of lower order by cutting both external lines exactly once [44, 45, 46][2]. Examples are shown in figure 3.2. Each web has an associated color factor $\bar{C}_W$ which is not the same as the normal color factor C_W associated with the web graph. The color factors $\bar{C}_W$ are given in terms of C_W by an iterative relation to all orders in perturbation theory.

The nature of eq.(3.1) in terms of disconnected diagrams is reminiscent of another well-known property of quantum field theory, namely the exponentiation of disconnected Feynman diagrams in terms of connected ones. This latter property most naturally emerges using path integral methods (see appendix 3.A for a brief proof), and thus the suggestion arises of whether it is possible to relate the exponentiation of soft radiative corrections to the gauge theory path integral. The aim in this chapter is to show that this is indeed the case, and the result is important for a number of reasons. Firstly, it provides a new perspective on exponentiation. Secondly, it allows one to straightforwardly explore which properties of exponentiation survive at next-to-eikonal limit and beyond (i.e. corresponding to subleading terms in ξ

[1] In the case of more than two external lines, the structure is more complicated.

[2] See [47] for a pedagogical exposition.

above)[3]. Although at next-to-eikonal order fermion emissions also contribute (leading to flavor-changing effects), we restrict ourselves here to gluon emissions.

The essential idea of our approach is as follows. One first relates the field theory path integral for a particle interacting with a gauge field to a first-quantized path integral with respect to the particle. That is, the external lines become worldlines of particles in quantum mechanics (rather than quantum field theory). Here we utilize the techniques of [48, 49, 50] which have originally been applied in a different context (that of constructing string theoretical analogues of fixed order field theory amplitudes [51, 52]). A first-quantized approach to Sudakov resummation has also appeared in [53]. We will see explicitly that in this representation the eikonal limit corresponds to the radiating particles moving classically, and next-to-eikonal terms originate from fluctuations around the classical path. The soft radiation emission vertices can then be interpreted as interactions of the gauge field with a source, such that individual emission vertices form disconnected diagrams. Then exponentiation of eikonal corrections follows naturally from usual combinatoric properties of the path integral.

In the non-abelian case, exponentiation is complicated by the fact that vertices for the emissions of gluons do not commute. However, one can rephrase the problem using the *replica trick* of statistical physics (see e.g. [54]), such that a subset of diagrams arises which exponentiate. These are then precisely the webs of [44, 45]. Furthermore, we provide an explicit closed form solution for the modified color factors, given in terms of normal (rather than modified) color weights.

Our formalism allows one to straightforwardly consider subleading effects with respect to the eikonal limit, and we classify the possible next-to-eikonal corrections. This can be divided into a subset which exponentiate (involving NE generalizations of the webs discussed above), and a set of remainder terms which do not formally exponentiate, but have an iterative structure in that each order of the perturbation expansion is sufficient to generate the next order.

Earlier attempts to include certain sub-eikonal effects were done in practical implementations of Sudakov resummation, mostly in view of gauging the theoretical uncertainty of the resummation [21]. Typically, this involved including subleading terms in the collinear evolution kernel in the resummation, which is particularly appealing for Drell-Yan, Higgs production and related cross sections [21, 22, 23, 24, 55, 25]. In the previous chapter we performed a study based on a proposal in Ref. [27].

In the rest of this introduction we review the derivation of the path-integral representation of propagators in quantum field theory, for both scalar and spinor particles and in the presence and absence of an abelian gauge field. These results will be used in section 2 to demonstrate the exponentiation of soft radiative corrections in the presence of an abelian gauge field. We also consider generalization of the results to beyond the eikonal limit, and classify the resulting corrections into a subset which exponentiate and a remainder term which mixes with these at next-to-eikonal order. In section 3 we consider the extension to non-abelian gauge fields, recovering the properties of

[3]We only consider matrix elements in this chapter. Exponentiation in differential cross-sections also depends upon factorization of the multiple particle phase space, and is deferred for further study.

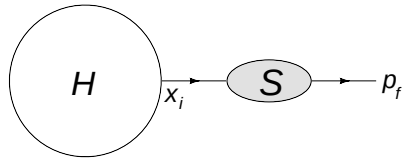

Figure 3.3: Anatomy of an external line, considered throughout this chapter as emerging from a hard interaction at 4-position x_i at time $t = 0$, and having momentum p_f at final time T. The propagator for the external line contains the effects of soft radiation.

webs and again examining corrections to the eikonal limit. We conclude in section 4, and some technical details are presented in the appendices.

3.1.1 Propagators as first quantized path integrals

Throughout this chapter we will be concerned with *external lines*, namely hard external particles susceptible to soft radiation emission. A given external line is created from a hard interaction process at time $t = 0$ at space-time point x_i, and and has a momentum p_f at some final time $T \to \infty$ (see figure 3.3). Soft radiation corrections enter the two-point function for the emitting particle i.e. the propagator for the external line. In the following subsections, we review the representation of field theory propagators in terms of first quantized path integrals [48, 49, 50], which will later on be used in the derivation of matrix element exponentiation at eikonal order and beyond. We begin with the simplest case, that of a free scalar particle.

Free scalar particle

The propagator for a free scalar particle between 4-positions x and y is the Green's function for the Klein-Gordon equation

$$i(S - i\varepsilon)\Delta_F(x, y) = \delta^{(d)}(x, y), \qquad S = (-\Box_x + m^2), \tag{3.3}$$

where S, Δ_F are Hermitian operators working on the Hilbert space $\mathcal{H}$ of square integrable functions of space-time, and we adopt the standard Feynman $i\varepsilon$ prescription. Note that we are using the metric $(-,+,+,+)$. Schematically the propagator may be written as

$$\Delta_F = [i\,(S - i\varepsilon)]^{-1}, \tag{3.4}$$

where the inverse operator can be defined via an inverse Fourier transform from momentum space. The usual representation then reads

$$\Delta_F(x, y) = -i \int \frac{d^d p}{(2\pi)^d} \frac{e^{ip\cdot(y-x)}}{p^2 + m^2 - i\varepsilon}\,. \tag{3.5}$$

To derive this expression using a first-quantized path integral, let us first write the inverse Klein-Gordon operator using the Schwinger representation

$$-i(S-i\varepsilon)^{-1} = \frac{1}{2}\int_0^\infty dT e^{-i\frac{1}{2}(S-i\varepsilon)T} \tag{3.6}$$

where the $i\varepsilon$ now ensures the convergence of the integral. The integrand contains the exponential $U(T) = e^{-i\frac{1}{2}ST}$, which is a unitary operator acting on the Hilbert space $\mathcal{H}$ and satisfying the Schrödinger equation

$$i\frac{d}{dT}U(T) = \hat{H}U(T), \quad U(0) = I, \quad \hat{H} = \frac{1}{2}S. \tag{3.7}$$

We can therefore interpret $\hat{H}$ as the Hamiltonian operator of a quantum system, with internal time coordinate T. Given we are considering external lines as shown in figure 3.3, we must calculate the expectation value of the evolution operator U between a state of definite position (at time $t = 0$) and definite momentum (at time $t = T$). To do this we introduce states $|x\rangle$ and $|p\rangle$ in the Hilbert space $\mathcal{H}$, and write the Hamiltonian as

$$\hat{H}(\hat{x},\hat{p}) = \sum_{n=0}^{\infty} \hat{p}_{\mu_1}\dots\hat{p}_{\mu_n}\, H^{\mu_1\dots\mu_n}_{\nu_1\dots\nu_n}\, \hat{x}^{\nu_1\dots\nu_n}, \tag{3.8}$$

where $\hat{x}$ and $\hat{p}$ are the position and momentum operators whose continuous eigenstates are $|x\rangle$ and $|p\rangle$ respectively. Note we have expressed $\hat{H}$ in Weyl ordered form, with all momentum operators to the left of position operators. One then finds, for small time separations Δt

$$\langle p|e^{-iH\Delta t}|x\rangle = e^{-iH(p,x)\Delta t + O[(\Delta t)^2]}\langle p|x\rangle, \tag{3.9}$$

where $H(p,x)$ is the c-number obtained by replacing the operators on the right-hand-side of eq. (3.8) with their corresponding variables. Slicing the time variable into N steps of duration Δt and inserting a complete set of both position and momentum states at each step, eq. (3.9) becomes

$$\int dx_1\dots dx_N \int dp_0\dots dp_{N-1} \exp\left[-i\sum_{k=0}^{N-1} H(p_k,x_k)\Delta t\right] \prod_{k=0}^{N}\langle p_k|x_k\rangle \prod_{k=0}^{N-1}\langle x_{k+1}|p_k\rangle. \tag{3.10}$$

Using the normalization of the basis states

$$\langle x|p\rangle = \frac{e^{ixp}}{(2\pi)^d}, \tag{3.11}$$

where d is the number of space-time dimensions, the continuum limit of eq.(3.10) is

$$\langle p_f|U(T)|x_i\rangle = \int_{x(0)=x_i}^{p(T)=p_f} \mathcal{D}p\mathcal{D}x \exp\left[-ip(T)x(T) + i\int_0^T dt(p\dot{x} - H(p,x))\right]. \tag{3.12}$$

We have absorbed factors of 2π into the measure, and made the boundary conditions explicit. This is the well-known path-integral result for the evolution operator sandwiched between initial and final position states, with an additional term in the exponent involving $p(T)x(T)$ arising from considering a final state of given momentum, rather than position.

For the present case of a free massive scalar, the Hamiltonian function is given by

$$H(p) = \frac{1}{2}\left(p^2 + m^2\right). \tag{3.13}$$

We can perform the path integrations over $p(t)$ and $x(t)$ by expanding around the classical solution of the equations of motion, given by

$$p(t) = p_f + p'(t), \quad x(t) = x_i + p_f t + x'(t). \tag{3.14}$$

The boundary conditions imply $p'(T) = 0$ and $x'(0) = 0$, and without confusion we can drop the primed notation from now on. Substituting eq. (3.14) into eq. (3.12) gives

$$\langle p_f|U(T)|x_i\rangle = e^{-ip_f x_i - i\frac{1}{2}(p_f^2+m^2)T} \int_{x(0)=0}^{p(T)=0} \mathcal{D}p\mathcal{D}x\, e^{i\int_0^T dt(p\dot{x}-\frac{1}{2}p^2)}. \tag{3.15}$$

One can now perform the path integral as the continuum limit of a product of Gaussian integrals in the intermediate position and momentum variables. The measure is such that this gives unity, and one therefore finds

$$\langle p_f|U(T)|x_i\rangle = e^{-ip_f x_i - \frac{1}{2}i(p_f^2+m^2)T}. \tag{3.16}$$

The momentum space propagator $\tilde{\Delta}_F$ is found by substituting eq. (3.16) into eq. (3.6), and one finds

$$\tilde{\Delta}_F(p_f^2) = \frac{1}{2}\int_0^\infty dT \frac{\langle p_f|U(T)|x_i\rangle}{\langle p_f|x_i\rangle} = -\frac{i}{p_f^2 + m^2 - i\varepsilon}, \tag{3.17}$$

in agreement with eq. (3.5). Having reviewed the relationship between propagators and path integrals in a simple case, we now consider the extension to a scalar particle interacting with a gauge field.

3.1.2 Scalar particle in an abelian background gauge field

We consider a charged scalar particle in an abelian background gauge field. Such a system is described by the generating functional

$$Z[J^*, J] = \int \mathcal{D}\phi^*\mathcal{D}\phi\, \exp\left[i\int d^dx \left(\phi^*(D_\mu D^\mu - m^2 + i\varepsilon)\phi + J^*\phi + \phi^* J\right)\right], \tag{3.18}$$

where J, J^* are sources for the complex scalar field, and $D_\mu = \partial_\mu - iA_\mu$. By completing the square and defining $S = (-D_\mu D^\mu + m^2)$ we can write this as

$$Z[J^*, J] = \int \mathcal{D}\phi^*\mathcal{D}\phi\, \exp\left[i\int d^dx \left(-\phi^*(S - i\varepsilon)\phi - J^*(S - i\varepsilon)^{-1}J\right)\right]. \tag{3.19}$$

The propagator is given by the inverse of operator quadratic in ϕ, ϕ^*, which gives eq. (3.4) as before. Using the fact that $p_\mu = -i\partial_\mu$, we can write the operator S in normal form (i.e. with all momenta operators on the left-hand-side) as

$$S = (p-A)^2+m^2 = p^2-p\cdot A-A\cdot p+A^2+m^2 = p^2-2p\cdot A-i(\partial\cdot A)+A^2+m^2. \quad (3.20)$$

Now defining the Hamiltonian operator $H = \frac{1}{2}S$ as before, one may carry out the manipulations of the previous section to obtain the first-quantized path integral representation of the evolution operator sandwiched between the external line position and momentum states

$$\langle p_f|U(T)|x_i\rangle = \int_{x(0)=x_i}^{p(T)=p_f} \mathcal{D}p\mathcal{D}x \exp\Big[-ip(T)x(T)+i\int_0^T dt(p\dot{x}-\frac{1}{2}(p^2+m^2)+p\cdot A + \frac{i}{2}\partial\cdot A-\frac{1}{2}A^2)\Big]. \quad (3.21)$$

This differs from the free particle case due to the presence of the gauge field in the exponent. When the strength of the gauge field is weak, the classical path of the emitting particle is well approximated by the free particle solution of eq. (3.14)[4]. One then finds

$$\langle p_f|U(T)|x_i\rangle = e^{-ip_fx_i-i\frac{1}{2}(p_f^2+m^2)T}f(T), \quad (3.22)$$

where

$$f(T) = \int_{x(0)=0}^{p(T)=0} \mathcal{D}p\mathcal{D}x\ \exp\Big[i\int_0^T dt(p\dot{x}-\frac{1}{2}p^2+(p_f+p)\cdot A(x_i+p_ft+x) + \frac{i}{2}\partial\cdot A(x_i+p_ft+x)-A^2(x_i+p_ft+x))\Big]. \quad (3.23)$$

Again the boundary conditions have again been made explicit, and we have dropped the primes on the quantities defined in eq. (3.14).

3.1.3 Spinor particle

We now consider the case of an emitting fermion in the presence of a background gauge field. The system is described by the generating functional

$$Z[\eta,\bar{\eta}] = \int \mathcal{D}\bar{\psi}\mathcal{D}\psi \exp\left[i\int d^dx\left(\bar{\psi}\left(\not{D}-m\right)\psi+\bar{\eta}\psi+\bar{\psi}\eta\right)\right], \quad (3.24)$$

where $\bar{\eta}$, η are Grassmann-valued source fields[5]. The momentum space propagator is then given by

$$\Delta_F = \frac{1}{-i(\not{D}-m)} = (\not{D}+m)\frac{1}{i[(-i\not{D})^2+m^2]}. \quad (3.25)$$

[4]We will formalize this statement in section 3.2.2 when we discuss next-to-eikonal exponentiation.

[5]Recall we use the metric $(-,+,+,+)$ throughout.

Now we define $S = (-i\not{D})^2 + m^2$, by analogy with the scalar case. Using the standard trick

$$\gamma^\mu\gamma^\nu = \frac{1}{2}\{\gamma^\mu, \gamma^\nu\} + \frac{1}{2}[\gamma^\mu, \gamma^\nu], \tag{3.26}$$

we can rewrite

$$(-i\not{D})^2 + m^2 = p^2 - 2p\cdot A - i\partial\cdot A + A^2 + m^2 - \sigma^{\mu\nu}F_{\mu\nu}, \tag{3.27}$$

where $\sigma^{\mu\nu} = -\frac{i}{4}[\gamma^\mu, \gamma^\nu]$ are the generators of the Lorentz group, and $F_{\mu\nu}$ is the field strength tensor for the gauge field. Carrying out the path integral manipulations as in the scalar case yields

$$\langle p_f|U(T)|x_i\rangle = \int_{x(0)=x_i}^{p(T)=p_f} \mathcal{D}p\mathcal{D}xP \exp\Big[-ip(T)x(T) + i\int_0^T dt(p\dot{x} - \frac{1}{2}(p^2+m^2) + p\cdot A + \frac{i}{2}\partial\cdot A - \frac{1}{2}A^2) + \frac{1}{2}\sigma^{\mu\nu}F_{\mu\nu}\Big], \tag{3.28}$$

The representation (3.28) is almost identical to the case of a scalar eikonal line, apart from the coupling to the field strength tensor. This is not surprising, as it is well known [48, 56] that one can cast fermion actions into a second-order form that gives rise to scalar-like vertices supplemented by additional seagull vertices involving couplings to the field strength (see e.g. [57, 58]). The latter correspond physically to the magnetic moment of the spinning emitting particle, and thus have no analogue in the scalar case.

In this introduction, we have reviewed the representation of particle propagators, including the possible presence of an abelian background gauge field, as first-quantized path integrals. The phase space variables x and p correspond to the position and momentum of the emitting particle, and the classical path is interpreted as an eikonal line. In the following section we formalize these statements, and show how the above representations can be used to derive the exponentiation of soft radiative corrections.

3.2 Soft emissions in scattering processes

We now turn to the description of soft radiation from external lines, considering Green's functions having the form shown schematically in figure 3.4, and consisting of a *hard interaction* $H(x_1, \ldots, x_n)$ with external lines emerging at positions $\{x_i\}$. This is a sum of subdiagrams containing gauge boson modes of as yet unspecified momentum. Each external line has a propagator associated with it summing the effect of soft gauge boson emission, and we call such diagrams *eikonally factorized*.

This is based upon the general analysis of [13], which characterizes the regions of infrared sensitivity in Feynman diagrams in a number of scattering processes. The proof that soft radiation contributions exponentiate now amounts to showing two things. Firstly, that for the eikonally factorized diagrams defined above (and shown

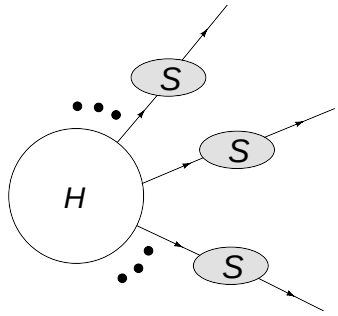

Figure 3.4: The factorized form of the Green's functions of eq. (3.33), where H is a hard interaction with n outgoing external lines, and S is a propagator for the eikonal particle in the presence of the background soft gauge field which, after the path integral over A_s^μ, generates connections between the external lines.

in Fig. 3.4), the contributions from soft radiation on the outgoing external lines exponentiates. Secondly, that all leading soft radiation terms originate from diagrams having this factorized structure. In this chapter, we prove the first property and assume that the second indeed holds, as has been shown to be the case elsewhere at eikonal level. We return to the issue of corrections to the above factorized form (at NE level) in Sec. 3.2.4.

To make these statements more direct, we begin by separating the path integral over the gauge boson field into a product of integrals over hard and soft modes

$$\int \mathcal{D}A^\mu \equiv \int \mathcal{D}A_s^\mu \mathcal{D}A_h^\mu \tag{3.29}$$

The precise definition of A_s^μ and A_h^μ amounts to specifying a surface in the multi-boson momentum space that separates it into two distinct regions corresponding to soft and hard modes. Such a surface is, in general, very complicated [13]. Its precise definition does not concern us in what follows, where we characterize soft radiation by the fact that one may neglect the recoil of the eikonal particles[6]. However, the fact that such a surface exists allows us to introduce the factorization of eq. (3.29), given that the path integral is a product of integrals over gauge fields of definite momentum.

The above separation is not gauge invariant, which can be easily seen as follows. Consider a given soft gauge field A_s^μ, whose momentum modes live only in the soft region of momentum space. A general gauge transformation has the form

$$A_s^\mu(x) \to A_s^\mu(x) + \partial^\mu \xi(x), \tag{3.30}$$

for some function $\xi(x)$. Transforming to momentum space, $\xi(x)$ may well have momentum modes defined in the hard region of momentum space, and thus the trans-

[6]We will consider corrections to this idea when discussing next-to-eikonal exponentiation in section 3.2.2.

formed gauge field will have in general both soft and hard components. Instead, both the soft and hard gauge fields obey a restricted gauge invariance given by the momentum space analogue of eq. (3.30)

$$A^{\mu}_{s,h}(k) \to A^{\mu}_{s,h}(k) + k^{\mu}\xi'(k). \tag{3.31}$$

Here $\xi'(k)$ is non-zero only if k is in the soft and hard regions for A^{μ}_{s} and A^{μ}_{h} respectively.

We now formally define the hard interaction as

$$H(x_1,\ldots,x_n) = \int \mathcal{D}A^{\mu}_{h}\,\mathcal{D}\phi\,\mathcal{D}\phi^{*}\,\frac{1}{i^n}\frac{\delta}{\delta J(y_1)}\cdots\frac{\delta}{\delta J(y_n)}\langle y_1|S-i\epsilon|x_1\rangle\ldots\langle y_n|S-i\epsilon|x_n\rangle$$
$$\times\exp\Big[iS[\phi,\phi^{*},A^{\mu}] + i\int d^{d}x\big(J(x)\phi^{*}(x)+J(x)\phi^{*}(x)\big)\Big]. \tag{3.32}$$

This is analogous to the expression for a Green's function, except for the fact that the path integral over soft gauge field modes A^{μ}_{s} has yet to be performed. Also, the factors $\langle y_i|S-i\epsilon|x_i\rangle$ (i.e. inverse propagators for the particle in the background of the soft gauge field) truncate the external legs of the Green's function.

We now define the further quantity

$$G(p_1,\ldots,p_n) = \int \mathcal{D}A^{\mu}_{s}\,H(x_1,\ldots,x_n)\langle p_1|(S-i\varepsilon)^{-1}|x_1\rangle\ldots\langle p_n|(S-i\varepsilon)^{-1}|x_n\rangle, \tag{3.33}$$

where a propagator factor has been associated with each external line, and the path integral over A^{μ}_{s} inserted. This latter integral does two things. Firstly, it generates all possible subgraphs within the hard interaction H (i.e. such that there are n external lines emerging at 4-positions $\{x_i\}$), containing both soft and hard gauge boson modes. Secondly, it produces soft radiation, both real and virtual, from the external lines. This is shown schematically in figure 3.4, where real and soft radiation is included in the soft blobs attached to each external line. One thus sees that G is a full Green's function of the theory, written in eikonally factorized form. Note that the propagator for the emitting particle in the presence of the background soft gauge field is removed in eq.(3.32), and replaced in eq.(3.33) with the propagator sandwiched between states of given initial position and final momentum.

To obtain the contribution to the scattering amplitude from the function $G(p_1,\ldots,p_n)$, one must truncate each external propagator. That is, for external leg i one multiplies by a factor $p_i^2+m^2$ to take account of the fact that the line is external and thus has no (free) propagator attached. In principle one must also divide by the residue of the scalar propagator, arising from renormalization of the scalar field. However, this residue is unity due to the absence of self-interactions for the eikonal particle, and also the fact that the gauge field is treated as a background. As is clear from eq. (3.33), one may treat each external line separately. Using the representation (3.21), one can

rewrite each external line contribution as

$$\begin{aligned} i(p_f^2+m^2)\langle p_f| - i(S-i\varepsilon)^{-1}|x_i\rangle &= i(p_f^2+m^2)\frac{1}{2}\int_0^\infty dT e^{-ip_f x_i - i\frac{1}{2}(p_f^2+m^2-i\varepsilon)T} f(T) \\ &= -e^{-ip_f x_i}\int_0^\infty dT \left(\frac{d}{dT}e^{-i\frac{1}{2}(p_f^2+m^2)T}\right)\left(e^{-\frac{1}{2}\varepsilon T} f(T)\right) \\ &= -e^{-ip_f x_i}\left(-f(0) - \int_0^\infty dT e^{-i\frac{1}{2}(p_f^2+m^2)T}\left(\frac{d}{dT}e^{-\frac{1}{2}\varepsilon T} f(T)\right)\right) \\ &= -e^{-ip_f x_i}\left(-f(0) - \int_0^\infty dT e^{-i\frac{1}{2}(p_f^2+m^2)T}\frac{d}{dT} f(T)\right). \end{aligned} \tag{3.34}$$

In the last step we have taken the limit $\varepsilon \to 0$. At this point one can let p_f approach its mass shell and obtain the simple result

$$i(p_f^2+m^2)\langle p_f| - i(S-i\varepsilon)^{-1}|x_i\rangle = e^{-ip_f x_i} f(\infty). \tag{3.35}$$

The limit $T \to \infty$ of $f(T)$ in eq. (3.35) allows us to simplify the expression for f in eq. (3.22) by performing the Gaussian integral over p. After shifting the integration variable $p \to p + A$ the result is a path integral over x only

$$f(\infty) = \int_{x(0)=0} \mathcal{D}x\, e^{i\int_0^\infty dt\left(\frac{1}{2}\dot{x}^2 + (p_f+\dot{x})\cdot A(x_i+p_f t+x(t)) + \frac{i}{2}\partial\cdot A(x_i+p_f t+x)\right)}. \tag{3.36}$$

Thus, the eikonally factorized contribution to the scattering amplitude for a charged scalar in an abelian background field takes the form

$$S(p_1,\ldots,p_n) = \int \mathcal{D}A_s^\mu H(x_1,\ldots,x_n)\, e^{-ip_1 x_1} f_1(\infty)\ldots e^{-ip_n x_n} f_n(\infty)\, e^{iS[A_s]}. \tag{3.37}$$

with $f(\infty)$ given by eq. (3.36), and the label of each $f(\infty)$ indicates the particular external line. Also we have explicitly factored out the action for the soft gauge field, which remains after the path integrals over the particle and hard gauge fields. This form (3.37) will now enable us to find all-order expressions for these amplitudes.

As a simple one-dimensional path integral, it can be further manipulated using simple classical methods. The strictest approximation is to neglect the fluctuations $x(t)$ and $p(t)$. This is equivalent to the eikonal approximation in Feynman diagrams, and one sets $x = 0,\ \dot{x} = 0,\ p = 0$ and as well as neglecting the $\partial\cdot A$ and A^2 terms in eq. (3.21). One then finds an Aharanov-Bohm-like phase factor for the straight line trajectory

$$f(\infty) \propto e^{i\int dx\cdot A(x)}. \tag{3.38}$$

Inserting this result into the path integral (3.37) where we integrate over soft gauge field fluctuations the Wilson lines, being linear in the soft gauge field A_s^μ, act as a collection of classical source terms for the soft A-field, distributed along the classical trajectory.

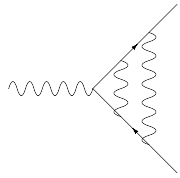

Figure 3.5: Example of a disconnected subdiagram between two outgoing external lines, to be compared with the connected subdiagrams of figure 3.1.

3.2.1 Eikonal exponentiation

Now that we have established that in the eikonal approximation the soft radiation is described by a Wilson line we can analyze what happens in perturbation theory. Let us consider, without loss of generality, an external line created at $x_i = 0$ and in direction $n^\mu \equiv p_f^\mu$. Then eq. (3.38) becomes

$$\exp\left[i\int_0^\infty dt n^\mu A_\mu(nt)\right]. \tag{3.39}$$

This can be written, after a Fourier transform to momentum space, as

$$i\int_0^\infty dt\, n^\mu A_\mu(nt) = -\int \frac{d^dk}{(2\pi)^d}\frac{n^\mu \tilde{A}_\mu(k)}{n\cdot k}. \tag{3.40}$$

Note that this is invariant under rescalings of the eikonal momentum n^μ. As seen above, this acts as a source term for the soft gauge field when the path integral over A_s^μ is performed. It can be represented as a 1-photon vertex with the momentum space Feynman rule

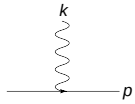

$$-\frac{n^\mu}{n\cdot k}, \tag{3.41}$$

where momentum k flows into the vertex. The path integral over the soft gauge field generates all possible diagrams connecting numbers of source vertices. By the usual rules of quantum field theory, one finds connected and disconnected diagrams, which in this case connect the external lines given that the source vertices lie along the latter. The collection of all diagrams exponentiates in terms of connected diagrams.

To illustrate this further, consider the case of a hard interaction with two outgoing eikonal lines, an example of which is shown in figure 3.1. There one sees a number of connected subdiagrams connecting the external lines. One also finds disconnected diagrams, such as that shown in figure 3.5. However, given the usual property of exponentiation of disconnected diagrams in quantum field theory, one has:

$$\sum G = \exp\left[\sum G_c\right]. \tag{3.42}$$

The sum on the left is over all subdiagrams G, while the sum on the right is over all connected diagrams G_c.

We have thus succeeded in showing that the exponentiation of soft radiative corrections in the eikonal limit can be related to the exponentiation of disconnected diagrams. We now consider what happens when next-to-eikonal corrections are considered.

3.2.2 Next-to-eikonal exponentiation

The analysis of the previous section relied on the fact that the factors $f(\infty)$ describing soft radiation from the external lines are written as path integrals in x. This allowed the straightforward interpretation of the eikonal limit as the limit in which the emitting particle follows a classical free path. However, this identification also allows one to go easily beyond the eikonal approximation. If the emitted radiation is soft but with non-negligible momentum, the classical path is still a good approximation to the equations of motion for the eikonal particle, and one can examine deviations from the straight-line path in a systematic expansion. Given that this does not affect the interpretation of gauge boson emission vertices in terms of disconnected subdiagrams, one still expects such corrections to exponentiate.

To formalize this argument, we reconsider the external line given by eq. (3.14), where again we take $x_i = 0$ without loss of generality. Given that the external eikonal particles have light-like momenta, one may write $p_j = \lambda n_j$, where $n_j^2 = 0$. Then eq. (3.36) becomes

$$f(\infty) = \int_{x(0)=0} \mathcal{D}x \, \exp\Big[i \int_0^\infty dt \Big(\frac{1}{2}\dot{x}^2 + (\lambda n + \dot{x}) \cdot A(\lambda n t + x) + \frac{i}{2} \partial \cdot A(\lambda n t + x) \Big) \Big]. \tag{3.43}$$

One now clearly sees that in the limit $\lambda \to \infty$, one may neglect all terms involving x, $\dot{x}$ and $\partial \cdot A$, leaving precisely the eikonal approximation discussed in the previous section. That is, fluctuations about the classical free path are suppressed by inverse powers of λ. By expanding in λ, one keeps the first subleading corrections to the eikonal approximation, i.e. corresponding to the next-to-eikonal (NE) limit.

For subsequent purposes it is more convenient to rescale the time variable $t \to t/\lambda$, so that eq. (3.43) becomes

$$f(\infty) = \int_{x(0)=0} \mathcal{D}x \, \exp\Big[i \int_0^\infty dt \Big(\frac{\lambda}{2}\dot{x}^2 + (n + \dot{x}) \cdot A(n t + x) + \frac{i}{2\lambda} \partial \cdot A(n t + x) \Big) \Big]. \tag{3.44}$$

The first term in the exponent is now $\sim \mathcal{O}(\lambda)$, but gives rise to a propagator for $x(t)$ which is $\mathcal{O}(\lambda^{-1})$ by virtue of being the inverse of the quadratic operator in $x(t)$. The remaining terms generate effective vertices for soft gauge boson emission in the NE limit, which one can again interpret as source terms for the soft gauge field. Thus,

following the reasoning in the previous section, one finds that these NE corrections exponentiate as before, i.e. one has:

$$f(\infty) = \exp\left[\sum G_c^x\right] , \tag{3.45}$$

where G_c^x are connected (through x propagators) diagrams along external lines, and located on the latter by vertices derived by a systematic expansion of eq.(3.44) in λ^{-1}. At LO, one recovers the eikonal approximation of the previous section. To obtain the NE approximation one must gather all terms $\sim \mathcal{O}(\lambda^{-1})$, which can be described as follows.

Firstly, NE graphs must have at most one propagator for the emitting particle $x(t)$, due to its being $\mathcal{O}(\lambda^{-1})$ as remarked above. There is also a NE vertex originating from the term in $\partial \cdot A$, and a given NE graph containing such a vertex must then contain no propagator factors for $x(t)$. We examine in detail the NE Feynman rules that result from eq. (3.44) in appendix 3.B, and show that they agree with the results one obtains in standard perturbation theory after expanding to NE order. The advantage of the above representation, however, is that exponentiation of these corrections is manifest.

3.2.3 Exponentiation for spinor particles

We have so far only considered the case of a scalar eikonal particle. For emitting fermions (with a similar expression for combinations of fermions and antifermions etc.), we write the definition of the hard interaction as

$$H(x_1,\dots,x_n) = \int \mathcal{D}A_h^\mu\, \mathcal{D}\psi\, \mathcal{D}\bar\psi \frac{1}{i^n} \frac{\delta}{\delta\bar\eta(y_1)} \dots \frac{\delta}{\delta\bar\eta(y_n)} \langle y_1|S_0 - i\epsilon|x_1\rangle \dots \langle y_n|S_0 - i\epsilon|x_n\rangle$$
$$\times \exp\Big[iS[\psi,\bar\psi,A^\mu] + i\int d^dx\big(\bar\eta(x)\psi(x) + \bar\psi\eta(x)\big)\Big], \tag{3.46}$$

where $S_0 - i\epsilon$ is the free fermion inverse propagator. The eikonally factorized Green's function has the same form as before (eq. (3.33)), where the propagator in the presence of the background gauge field is given by eqs. (3.28). Truncating the external lines of the full Green's function[7], one finds that the eikonally factorized scattering amplitudes are given by the same expression eq. (3.37), but where the external line factor is now:

$$f(\infty) = \int_{x(0)=0} \mathcal{D}x\, \exp\Big[i\int_0^\infty dt\Big(\frac{\lambda}{2}\dot x^2 + (n+\dot x)\cdot A(nt+x)$$
$$+ \frac{i}{2\lambda}\partial\cdot A(nt+x) + \frac{1}{2\lambda}\sigma^{\mu\nu}F_{\mu\nu}\Big)\Big], \tag{3.47}$$

and we have rescaled the time variable $t \to t/\lambda$ as before. The proof of exponentiation up to NE order proceeds directly as in the scalar case, except for the additional

[7] In the spinor case we defined the evolution operator $U(T)$ as involving only the denominator of eq. (3.25). The leftover factor in the numerator indeed combines correctly with the inverse free propagator to give a factor $p_f^2 + m^2$ as in the scalar case of eq. (3.34).

magnetic moment vertex which, although absent in the scalar case, does nothing to invalidate the proof. Note that, due to suppression by λ, the additional vertex is indeed of NE order, as expected given that in the strict eikonal limit, radiation is insensitive to the spin of the emitting particle.

One may worry about ordering of Dirac matrices when the exponential of eq. (3.47) is expanded. However, this is not an issue due to the fact that the magnetic moment vertex is NE and thus occurs in each diagram only once at this order.

The preceding analysis has shown that in eikonally factorized Green's functions, soft gauge boson corrections exponentiate up to NE order. This is not yet a proof that such corrections exponentiate in matrix elements themselves, which include Green's functions not having an eikonally factorized structure. At strictly eikonal level (as is well known), one may in fact ignore contributions from diagrams which are not eikonally factorized. At NE order, however, contributions arise from diagrams in which a soft emission connects an external line with the hard interaction. This is the subject of the following section.

3.2.4 Low's theorem

In the previous section we have demonstrated exponentiation for next-to-eikonal photon emissions from external lines. That is, the exponentiation holds for scattering amplitudes having the eikonally factorized form of figure 3.4. However, at NE order there are also corrections to the exponentiation arising from soft gluon emissions which land on an external line, having originated from inside the hard interaction. A given matrix element then has the schematic form (up to next-to-eikonal level):

$$\mathcal{M} = \exp\left[\mathcal{M}^{\mathrm{E}} + \mathcal{M}^{\mathrm{NE}}\right](1 + \mathcal{M}_r). \tag{3.48}$$

Here $\mathcal{M}^{\mathrm{E,NE}}$ collect the eikonal and next-to-eikonal diagrams from eikonally factorized Green's functions respectively, and $\mathcal{M}_r$ is a remainder term which does not exponentiate, and contains NE contributions from diagrams such as that shown in figure 3.6. In what follows, we refer to emissions from within the hard interaction as *internal emissions*, and those originating from external lines as *external*. Diagrams with internal emissions have been studied before in the literature. It has been shown for a fixed number of scalar external lines that, up to NE order, the sum of diagrams containing a soft emission (internal or external) can be related to the scattering amplitude with no emissions [18]. This result is known as *Low's theorem*, and was generalized to the case of spinor external lines in [19], an extension known as the *Low-Burnett-Kroll theorem*. Generalization to higher orders was considered in [20]. The fact that graphs with an extra emission can be related simply to those without an emission means that, although the remainder term does not have a formal exponential structure, it has an iterative form to all orders in perturbation theory. In this section we discuss these properties in the path integral formalism adopted in this chapter, in order to complete our discussion of NE exponentiation. This also allows for a generalization of the ideas presented in [18, 19, 20].

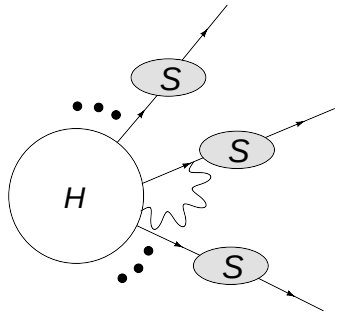

Figure 3.6: An example of a diagram which contributes to the remainder factor $\mathcal{M}_r$ of eq. (3.48). Such contributions are formed by taking an eikonally factorized Green's function, and adding a soft gluon emission which lands on an external line, but originates from inside the hard interaction.

Our starting point is the expression for the n-particle scattering amplitude (see also eq. (3.37))

$$S(p_1,\dots,p_n) = \int \mathcal{D}A_s H(x_1,\dots,x_n;A_s) e^{-ip_1x_1} f(x_1,p_1;A_s)\dots \\ \times e^{-ip_nx_n} f(x_1,p_1;A_s) e^{iS[A_s]}\,, \quad (3.49)$$

where we have explicitly indicated the dependence of the external leg factors (eq. (3.44)) on the soft gauge field. We also now consider the fact that the external lines are produced at 4-positions $x_i \neq 0$ i.e.

$$f(x_i,p_f,A_s) = \int_{x(0)=x_i}^{p(\infty)=p_f} \mathcal{D}x\, \exp\Big[i\int_0^\infty dt\Big(\frac{\lambda}{2}\dot{x}^2 + q_i\,(n+\dot{x})\cdot A(x_i+nt+x) \\ + \frac{i}{2\lambda} q_i\,\partial\cdot A(x_i+pt+x)\Big)\Big]. \quad (3.50)$$

We have also indicated the dependence of the hard part on the soft photon field A_s and rescaled this field so as to explicitly display the dependence on the eikonal particle's electric charge q_i. Furthermore, we drop the subscript s on the gauge field in what follows, and leave implicit the path integrals over the external line 4-positions x_i.

Both H and the f's depend on the soft gauge field A. As discussed in section 3.2, the separation between soft and hard gauge modes leaves a residual gauge invariance, given by the usual form of eq. (3.30), but where the function $\Lambda(x)$ has only soft modes when transformed to momentum space. It is implicitly assumed that this in the case in the following. Under such a transformation, the external line factors transform as

$$f(x_i,p_f;A) \to f(x_i,p_f;A+\partial\Lambda) = e^{-iq\Lambda(x_i)} f(x_i,p_f;A), \quad (3.51)$$

which follows from the definition of eq. (3.35).

In order for the path integral to remain invariant under the family of gauge transformations given by eq. (3.30), the hard function H must transform as

$$H(x_1,\ldots,x_n;A) \to H(x_1,\ldots,x_n;A+\partial\Lambda) = H(x_1,\ldots,x_n;A)e^{iq_1\Lambda(x_1)+\ldots+iq_n\Lambda(x_n)}. \tag{3.52}$$

We can now use the gauge invariance to relate diagrams with soft emissions from inside the hard interaction to similar diagrams with no emission, as follows. First, one may expand both sides of eq. (3.52) to first order in A and in Λ, which gives

$$\begin{aligned} H(x_1,\ldots,x_n) + \int d^dx\, H^\mu(x_1,\ldots,x_n;x)(A_\mu(x)+\partial_\mu\Lambda(x)) = \\ H(x_1,\ldots,x_n) + \int d^dx\, H^\mu(x_1,\ldots,x_n;x)A_\mu(x) \\ + i\int d^dx \left(H(x_1,\ldots,x_n)\sum_j^n q_j\delta(x-x_j)\right)\Lambda(x). \end{aligned} \tag{3.53}$$

When the path integral over the soft gauge field is performed, $H^\mu(x_1,\ldots,x_n;x)$ generates hard interactions which a single soft photon emission (with Lorentz index μ). Because $\Lambda(x)$ is arbitrary we infer

$$-\partial_\mu H^\mu(x_1,\ldots,x_n;x) = iH(x_1,\ldots,x_n)\sum_j^n q_j\delta(x-x_j), \tag{3.54}$$

where we have integrated by parts on the left hand side of eq. (3.53). In momentum space this becomes

$$-k_\mu H^\mu(p_1,\ldots,p_n;k) = \sum_j^n q_j H(p_1,\ldots,p_j+k,\ldots,p_n). \tag{3.55}$$

One can expand this up to first order in k to obtain

$$-k_\mu H^\mu(p_1,\ldots,p_n;k) = \sum_j^n q_j k_\mu \frac{\partial}{\partial p_{j\,\mu}} H(p_1,\ldots,p_n)\,, \tag{3.56}$$

where the zeroth order term on the right hand side vanishes due to charge conservation $\sum_j q_j = 0$. Now, because k^μ is an arbitrary soft momentum, one may write

$$H^\mu(p_1,\ldots,p_n;k) = -\sum_j^n q_j \frac{\partial}{\partial p_{j\,\mu}} H(p_1,\ldots,p_n)\,. \tag{3.57}$$

This simply relates internal emission from the hard interaction with the same hard interaction but with no emission. For a simple example of how this works using more traditional methods, we refer the reader to appendix 3.C.

In section 3.2 we ignored the fact that the external lines emerge at positions x_i which are integrated over and thus in general non-zero. Taking this into account also leads to corrections of NE order (and beyond), which enter the above remainder term $\mathcal{M}_r$. To see this, we write the eikonal one-photon source term as:

$$-q\int\frac{d^dk}{(2\pi)^d}\frac{n\cdot A(k)}{n\cdot k}e^{ix\cdot k}. \tag{3.58}$$

This can be expanded as

$$-q\int\frac{d^dk}{(2\pi)^d}\,(1+ix\cdot k)\,\frac{n\cdot A(k)}{n\cdot k}, \tag{3.59}$$

where the first bracketed term corresponds to the eikonal approximation, and the second term (involving the factor $x\cdot k$) is suppressed by one power of momentum and is thus a NE correction. We now combine these terms with the factors of eq. (3.57), and up to NE order the scattering amplitude is given by a sum over all such corrections, where each NE factor occurs at most once. One then finds

$$\begin{aligned}S(p_1,\dots,p_n)=\int\mathcal{D}A\Bigg[\Big(-\sum_j^n q_j\frac{\partial}{\partial {p_j}_\mu}H(p_1,\dots,p_n)\Big)\int\frac{d^dk}{(2\pi)^d}\,A_\mu(k)+\\ \int dx_1^d\dots dx_n^d\,H(x_1,\dots,x_n)\Big(\sum_j q_j\int\frac{d^dk}{(2\pi)^d}(-ix_j\cdot k)\frac{n\cdot A(k)}{n\cdot k}\Big)e^{-ix_1\cdot p_1-\dots-ix_n\cdot p_n}\Bigg]\\ f(0,p_1;A)\dots f(0,p_n;A)\,,\end{aligned} \tag{3.60}$$

where we have explicitly instated the integrals over the initial positions of the external lines $\{x_i\}$. Performing these integrals, the scattering amplitude is given by

$$\begin{aligned}S(p_1,\dots,p_n)=\int\mathcal{D}A\Bigg[\int\frac{d^dk}{(2\pi)^d}\sum_j^n q_j\Big(\frac{n_j^\mu}{n_j\cdot k}k_\nu\frac{\partial}{\partial {p_j}_\nu}-\frac{\partial}{\partial {p_j}_\mu}\Big)\\ \times H(p_1,\dots,p_n)A_\mu(k)\Bigg]f(0,p_1;A)\dots f(0,p_n;A)\,.\end{aligned} \tag{3.61}$$

Some comments are in order regarding the form and interpretation of this result. The external line factors $f(0,p_i;A)$ contain exponentiated eikonal and NE terms, as discussed previously. Corrections to the NE exponentiation then arise due to the bracketed prefactor in eq. (3.61), which contains a sum over different possible NE corrections. Such corrections contribute to the remainder term $\mathcal{M}_r$ in eq. (3.48), and do not exponentiate. However, eq. (3.61) shows that they can be obtained as derivatives of the hard interaction with no soft emissions. Thus, the remainder term has an iterative structure to all orders in perturbation theory.

For scattering amplitudes, one may summarize this as follows. Leading eikonal logarithms arising from soft gluon emission exponentiate. NE logarithms do not exponentiate, but can be separated into the sum of a series which does exponentiate,

and a remainder sum which does not exponentiate, but is obtainable in principle to all orders in the coupling constant.

To further clarify the above formulae, it is instructive to consider the case where the hard interaction H is a scalar. Then it can only depend on Lorentz invariant products of momenta. The derivatives with respect to the 4-momenta in eq. (3.61) can be reexpressed in terms of derivatives with respect to products of 4-vectors (corresponding to Mandelstam invariants in the hard scattering process). One may verify that derivatives w.r.t. p_i^2 vanish, and in the case of two external lines ($n = 2$) there is only one scalar $p_1 \cdot p_2$. eq. (3.61) then becomes

$$S(p_1, \ldots, p_n) = \int \mathcal{D}A \Bigg[\int \frac{d^d k}{(2\pi)^d} \Big(\frac{n_1^\mu (k \cdot n_2 - k \cdot n_1)}{n_1 \cdot k} + \frac{n_2^\mu (k \cdot n_1 - k \cdot n_2)}{n_2 \cdot k} \Big) \times \frac{\partial}{\partial (p_1 \cdot p_2)} H(p_1, \ldots, p_n) A_\mu(k) \Bigg] f(0, p_1; A) \ldots f(0, p_n; A) \,. \quad (3.62)$$

This is precisely the form one expects based on a conventional Feynman diagram treatment (see appendix 3.C), and one may interpret the bracketed factor in eq. (3.62) as an extra vertex describing soft emission from within the hard interaction.

3.3 Non-abelian gauge theory

So far we have considered an abelian background gauge field. In the case where the gauge field is non-abelian, the derivation of the scattering amplitude for eikonally factorized diagrams proceeds similarly to Sec. 3.2. Here we consider the simple case of a hard interaction with two outgoing external lines. That is, the analogue of eq. (3.37) can be written

$$S(p_1, p_2) = \int \mathcal{D}A_s^\mu \, H^{i_1 i_2}(x_1, x_2) e^{-ip_1 x_1} f_1^{i_1 j_1}(\infty) e^{-ip_2 x_2} f_2^{i_2 j_2}(\infty) e^{iS[A_s]}. \quad (3.63)$$

Here $\{i_k\}$ and $\{j_k\}$ are indices in the fundamental representation of the gauge group, such that the outgoing particles have indices $\{j_k\}$ and summation over repeated color indices is implied. The external line factors $f^{i_k j_k}(\infty)$ have the form

$$f^{i_1 j_1}(\infty) = \left[\int_{x(0)=x_i} \mathcal{D}x \, \mathcal{P} e^{i \int_0^\infty dt \left(\frac{1}{2}\dot{x}^2 + (p_f + \dot{x}) \cdot A(x_i + p_f t + x(t)) + \frac{i}{2} \partial \cdot A(x_i + p_f t + x) \right)} \right]^{i_1 j_1}, \quad (3.64)$$

i.e. similar to before[8], but matrix-valued in color space due to the exponent being linear in the non-abelian gauge field $A^\mu = A_A^\mu t^A$, where t^A is a generator of the gauge group. Furthermore, there is a path ordering of the color matrices along the external

[8] One might be concerned about performing the Gaussian p integral by completing the square in eq.(3.23). However one could also use perturbation theory directly in eq.(3.23), without first integrating over p, giving the same end result.

line. As before, the external line factors act as source terms for the soft gauge field when the path integral over A_s^μ is performed. However, it is no longer immediately clear that the soft corrections exponentiate. In the abelian case, the exponentiation of soft gauge boson corrections was identified with the exponentiation of disconnected diagrams between sources. Crucial to the combinatorics of this result is the fact that in the abelian case, the source terms commute with each other. This is no longer true in the non-abelian case, due to the matrix valued nature of the source terms, and also the path ordering of the exponential in eq. (3.64). We will see, however, that it is still possible to address exponentiation in the non-abelian case, by rephrasing the problem using the *replica trick* of statistical physics (see appendix 3.A for another application i.e. the proof of the exponentiation of disconnected diagrams in field theory). One can then write the scattering amplitude in a form such that extra structure emerges in the exponent, whereby the contraction of soft gluon emissions between eikonal lines gives rise to a exponentiating subset of diagrams. These can then be identified with the *webs* of [45, 44].

To simplify the discussion, we first restrict ourselves to the strict eikonal limit. Furthermore, we consider the case of a hard interaction with the color singlet structure

$$H^{i_1 i_2}(x_1, x_2) = H(x_1, x_2)\, \delta^{i_1 i_2}, \tag{3.65}$$

where $\delta^{i_1 i_2}$ is the Kronecker symbol. Such a structure arises in interactions where e.g. an incoming color singlet particle gives rise to the pair production of two hard final charged scalars (the scalar analogue of e^+e^- pair production by a virtual photon), as shown in figure 3.2. Given that, up to the NE corrections discussed in section 3.2.4, one may consider the external lines as being created at $x = 0$, one may take the hard interaction outside the path integral over A_s in eq. (3.63) to obtain (in this case)

$$S(p_1, p_2) = H(p_1, p_2) \int \mathcal{D}A_s^\mu\, f_1^{ij_1}(\infty)\, f_2^{ij_2}(\infty)\, e^{iS[A_s]}. \tag{3.66}$$

Here $S[A_s]$ is the action for the soft gauge field which is independent of the emitting particles. The product of external line factors, suppressing momentarily the color indices, is given by

$$f_1(\infty) f_2(\infty) = \left[\mathcal{P} e^{i\int dx_1 \cdot A(x_1)}\right] \left[\mathcal{P} e^{i\int dx_2 \cdot A(x_2)}\right]. \tag{3.67}$$

The first factor is a Wilson line parameterized by $x_1(s)$, where $s = -t$ increases along the direction of the charge flow, with $-\infty < s < 0$. The second factor is a Wilson line parameterized by $x_2(s)$, with $s = t$ and $0 < s < \infty$. One may combine these into a single curve given by

$$x(s) = \begin{cases} x_1(s), & -\infty < s < 0; \\ x_2(s), & 0 \le s < \infty. \end{cases} \tag{3.68}$$

Due to the path ordering in the definition of the Wilson line, one has the property

$$\left[\mathcal{P} e^{i\int dx_1 \cdot A(x_1)}\right] \left[\mathcal{P} e^{i\int dx_2 \cdot A(x_2)}\right] = \mathcal{P} e^{i\int dx \cdot A(x)}, \tag{3.69}$$

so that, for the simple interaction considered here, one may combine the two external line factors into the single factor

$$f(\infty) = f_1(\infty) f_2(\infty) = \mathcal{P} e^{i \int dx \cdot A(x)}. \tag{3.70}$$

The scattering amplitude of eq. (3.66) is now given by:

$$S(p_1, p_2) = H(p_1, p_2)\, \mathcal{F}, \tag{3.71}$$

where

$$\mathcal{F} = \int \mathcal{D}A_s^\mu f(\infty) e^{iS[A_s]}. \tag{3.72}$$

We now consider the quantity

$$\mathcal{F}^N = \left[\int \mathcal{D}A_1^\mu f^{(1)}(\infty) e^{iS[A_1]} \right] \dots \left[\int \mathcal{D}A_N^\mu f^{(N)}(\infty) e^{iS[A_N]} \right]. \tag{3.73}$$

Here $\{A_i^\mu\}$ are N replicas of the soft gauge field (we have dropped the subscript s for brevity), and $S[A_i]$ the action for the i^{th} replica. One has a different external line factor $f^{(i)}$ for each replica field. Combining the path integrals using $\mathcal{D}A^\mu \equiv \prod_i \mathcal{D}A_i^\mu$, one can rewrite eq. (3.73) as

$$\mathcal{F}^N = \int \mathcal{D}A^\mu f^{(1)}(\infty) \dots f^{(N)}(\infty) e^{iS[A_1] + \dots + iS[A_N]}. \tag{3.74}$$

The physical interpretation of this quantity is as follows. The external line factors, as in the abelian case, contain sources for the gauge field. In this case, they generate diagrams containing any mixture of the N replica gauge fields, which span the external lines of the hard interaction (which in this case have become a single external line). Each of the vertices for the emission of a gauge field replica has a non-trivial color structure, such that neither the external factors $f^{(i)}$ nor the vertices they give rise to commute. However, by definition one has:

$$\mathcal{F}^N = 1 + N \log(\mathcal{F}) + \mathcal{O}(N^2). \tag{3.75}$$

It follows that, if one can extract a term in eq. (3.74) that is linear in the number N of replica fields, one has

$$\mathcal{F} = \exp\left[\sum W \right], \tag{3.76}$$

where the sum is over all diagrams W that contribute at $\mathcal{O}(N)$. Crucially, we will find that not all diagrams in the theory have terms of $\mathcal{O}(N)$, so one recovers the property of exponentiation of soft radiative corrections in terms of a subset of diagrams with certain properties. The diagrams in this case will still contain replica fields. However, given that the gauge group of the replicated theory is the same as that in the standard theory, it must be true that the color structures of the subdiagrams which exponentiate are the same in the two theories.

We now describe how to isolate the term linear in N in eq. (3.74). The product of external line factors has the form:

$$f^{(1)}(\infty)\dots f^{(N)}(\infty) = \mathcal{P}\exp\left[\int dx\cdot A_1(x)\right]\dots\mathcal{P}\exp\left[\int dx\cdot A_N(x)\right]. \tag{3.77}$$

Ideally we want to write this as a single path-ordered exponential, so that one can identify the usual rules of perturbation theory. This can be achieved by writing eq. (3.77) in the following form:

$$\prod_{i=1}^{N}\mathcal{P}\exp\left[\int dx\cdot A_i(x)\right] = \mathcal{R}\mathcal{P}\exp\left[\sum_{i=1}^{N}\int dx\cdot A_i(x)\right], \tag{3.78}$$

where we have introduced the *replica ordering* operator $\mathcal{R}$, defined such that

$$\mathcal{R}[A_i(x)A_j(y)] = \begin{cases} A_i(x)A_j(y), & i\le j \\ A_j(y)A_i(x), & i>j \end{cases}, \tag{3.79}$$

with obvious generalization to higher numbers of operators. That is, $\mathcal{R}$ orders any product of matrix-valued fields into a sequence of increasing replica number. Note that the resulting product is no longer strictly time ordered, although the matrix fields of any given replica number remain time ordered.

As before (and by analogy with conventional Feynman perturbation theory for non-Abelian gauge fields), the single exponent in eq. (3.79) acts as a collection of sources for the soft gauge field. The path integration over the soft gauge field generates diagrams containing multiple replica emissions along the eikonal line, where the replica numbers are not necessarily ordered along the line (see figure 3.7). However, the expression for a given diagram, as dictated by the source terms arising from eq. (3.78), involves replica ordered products of operators, each of which involves a color matrix. Thus, the color structure associated with each diagram is not the same as that which would result from conventional perturbation theory, but rather that associated with the given replica-ordered product of matrix-valued fields. The subset of diagrams which exponentiates then has a modified color structure, as is known to be the case for webs [44, 45, 46]. To see which diagrams W actually contribute in eq. (3.76), one must consider contracting gluons emitted from two or more vertices. Given that the gauge field replicas do not interact with each other (i.e. are only tangled through color structure), one can clearly only contract gluons which have the same replica number i and adjoint color index A. Here we consider this up to $\mathcal{O}(A_\mu^4)$ in the scattering amplitude (i.e. up to two gluon lines). Firstly, we need only consider contributions from vertices on different segments of the combined Wilson line $x(t)$, as those on the same segment ultimately give contributions proportional to (at least in covariant gauges) $p_1^2 = 0$ or $p_2^2 = 0$. Also, each diagram has a multitude of similar diagrams obtained by permuting the replica labels. The operator $\mathcal{R}$ for each diagram orders the color matrices in the form

$$[t_1^{A_1}\dots t_1^{A_{n_1}}]\dots[t_N^{B_1}\dots t_N^{B_{n_N}}] \tag{3.80}$$

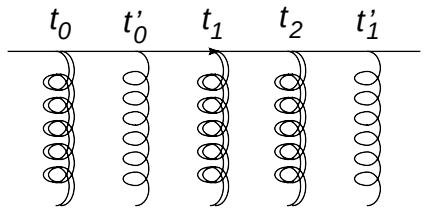

Figure 3.7: Example of an radiative corrections generated by the source terms of eq. (3.79), where two gauge boson replicas are shown. Each set of replica emissions is time ordered, such that (in this case) $t_2 > t_1 > t_0$ and $t_1' > t_0'$.

i.e. a product of strings of color matrices, with one string for each replica (if present), and n_i matrices for replica i. Given that the replicas do not interact with each other, the color indices of each string in eq. (3.80) are contracted independently of the other strings. That is, the color factor for each diagram has the form

$$\prod_{i=1}^{N} K_i^{A_1 \ldots A_{n_i}} [t_1^{A_1} \ldots t_1^{A_{n_i}}], \tag{3.81}$$

where $K_i^{A_1 \ldots A_{n_i}}$ is a combination of factors involving f^{ABC} and δ^{AB} which implements the color contractions for replica i in the diagram being considered. Each of the strings of color matrices corresponding to a given replica number in eq. (3.81) has two color indices in the fundamental representation, thus by Schur's Lemma must be proportional to the identity. Hence, the color factor of a complete diagram in the replica ordered perturbation theory is the product of the individual color factors associated with the subdiagrams formed from each replica separately. Furthermore, the ordering of the factors in eq. (3.80) is unimportant, so that the color factors associated with the set of diagrams obtained from a given diagram merely by permuting replica numbers are the same. There are ${}_N P_m = N!/(N-m)!$ such permutations, where m is the number of different replica species present in the diagram.

For one gluon emission, there is only one possible diagram, shown in figure 3.8(a). There is a sum over the replica number of the exchanged gluon, so that this diagram is clearly proportional to N, denoting a color structure that exponentiates. The color factor of this diagram is

$$t^A t^A = C_F, \tag{3.82}$$

where t^A is a generator in the fundamental representation of the gauge group, and C_F the relevant Casimir invariant. Note that this is the same as the color factor in conventional perturbation theory, although things become more complicated when more than one gluon is involved.

For two gluon emission, one has the two diagrams shown in Fig. 3.8(b,c). For each of these, one must consider separately the cases where $i = j$ and $i \neq j$, because of the fact that the replica ordering operator $\mathcal{R}$ acts differently in the two cases.

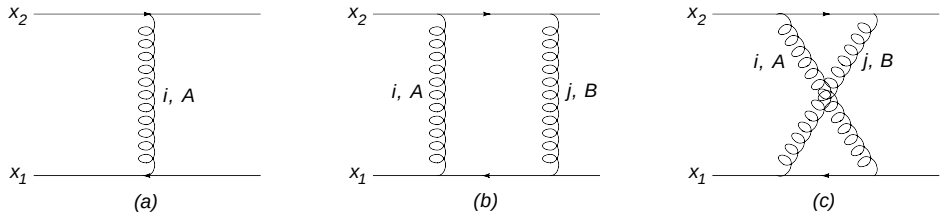

Figure 3.8: Diagrams that potentially contribute to the exponentiated contribution to the scattering amplitude in the case of two external lines connected by a color singlet structure, for one and two gluon emissions. In fact, only (a) and (c) contribute as discussed in the text.

For Fig. 3.8(b), in the case where $i = j$ one has a color factor

$$t_j^B \, t_i^A \, t_i^A \, t_j^B = C_F^2, \tag{3.83}$$

where we have explicitly indicated which color matrix is associated with each replica. When $i \neq j$, the color matrices in eq. (3.84) get reordered by the $\mathcal{R}$ operator i.e. one has

$$t_i^A \, t_i^A \, t_j^B \, t_j^B = C_F^2 \tag{3.84}$$

for $i < j$, with a similar expression for $i > j$ (but where i and j are interchanged). The color factors of these diagrams are the same, and thus one may combine the results for $i = j$ and $i \neq j$. Then one sees that the contribution from Fig. (3.8)(b) is $\mathcal{O}(N^2)$.

For Fig. 3.8(c), the $i = j$ case has the color factor

$$t_i^A \, t_j^B \, t_i^A \, t_j^B = C_F^2 - \frac{C_F C_A}{2}. \tag{3.85}$$

When $i \neq j$ one has

$$t_i^A \, t_i^A \, t_j^B \, t_j^B = C_F^2. \tag{3.86}$$

Note that the color factors for $i = j$ and $i \neq j$ are now different, such that the two cases do not combine to give a term $\mathcal{O}(N^2)$. There are N diagrams where $i = j$, and ${}_N P_2 = N(N-1)$ diagrams where $i \neq j$. Thus the term linear in N has a color factor:

$$N \left(C_F^2 - \frac{C_F C_A}{2} \right) + (-N) C_F^2 = N \left(-\frac{C_F C_A}{2} \right). \tag{3.87}$$

The above discussion can be summarized as follows. Up to two gluon emissions, a subset of diagrams exponentiates. Namely, the one gluon emission diagram of Fig. 3.8(a), and the crossed gluon diagram of Fig. 3.8(c). Fig. 3.8(b) does not contribute due to being $\mathcal{O}(N^2)$, and Fig. 3.8(c) has a color factor which differs from that of conventional perturbation theory, and indeed is precisely the modified color factor associated with the known webs of [44, 45, 46].

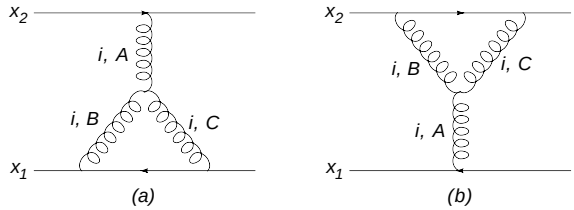

Figure 3.9: Diagrams contributing to the exponentiated scattering amplitude at $\mathcal{O}(\alpha_S^4)$, and involving the 3-gluon vertex.

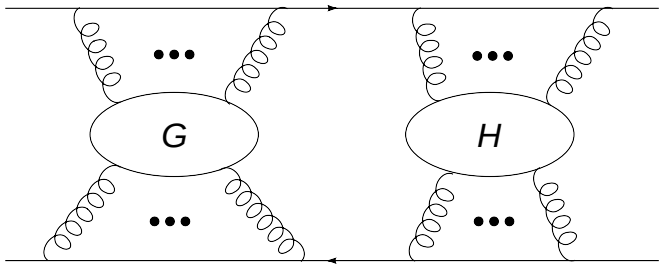

Figure 3.10: A two-eikonal reducible diagram, in the simplest case of two disconnected components with respect to the external lines.

Note at this order in α_S one also has diagrams containing gluon self-interactions, of which there are two possibilities, shown in Fig. 3.9. There are N such diagrams in each case, so that they also exponentiate (i.e. are webs) with a color factor equal to the ordinary one.

We now consider the generalization of the above remarks to higher orders in perturbation theory. The subdiagrams which exponentiate can be characterized by the fact that they are two-eikonal irreducible. That is, one cannot disconnect each diagram by cutting eikonal lines in two places. This property is well-known [45, 44], but we prove it in the following using the methods outlined above.

Consider the general two-eikonal reducible diagram shown in Fig. 3.10 (where each of the subdiagrams could itself be reducible). We focus on a given gauge boson replica i in subdiagram H in Fig. 3.10, and consider first the case where subdiagram G contains no gauge bosons with replica number i. According to the Feynman rules of the replica-ordered perturbation theory described above, the diagram of Fig. 3.10 then gives a color factor

$$K_i^{A_1 \dots A_n \, B_1 \dots B_m} \left[t_H^{A_1} \dots t_H^{A_n} \right] \left[t_H^{B_m} \dots t_H^{B_1} \right] \times \prod_{j \neq i} C(j), \tag{3.88}$$

where $C(j)$ is the color factor associated with replica j, and $K_i^{A_1 \dots A_n \, B_1 \dots B_m}$ is the

color contraction factor for replica i introduced above. That is, $\prod C(j)$ contains the results of all contractions in G as well as those of H that do not involve replica number i. The indices $\{A_k\}$ and $\{B_k\}$ denote emissions from the lower and upper eikonal lines respectively. Now consider the case where G as well as H contains emissions with replica number i. Then (due to the reducible structure) one can write K_i as a product of factors S_{G_i}, S_{H_i} for each subdiagram, so that the color factor associated with Fig. 3.10 is

$$K_{G_i}^{A_{n_H+1}\dots A_n\, B_{m_H+1}\dots B_m} S_{H_i}^{A_1\dots A_{n_H}\, B_1\dots B_{m_H}} \left[t_H^{A_1}\dots t_H^{A_{n_H}}\right] \times \left[t_G^{A_{n_H+1}}\dots t_G^{A_n}\right]\left[t_G^{A_m}\dots t_G^{A_{m_H+1}}\right]\left[t_H^{B_{m_H}}\dots t_H^{B_1}\right] \times \prod_{j\neq i} C(j). \tag{3.89}$$

We may use the fact that

$$K_{G_i}^{A_{n_H+1}\dots A_n\, B_{m_H+1}\dots B_m}\left[t_G^{A_{n_H+1}}\dots t_G^{A_n}\right]\left[t_G^{A_m}\dots t_G^{A_{m_H+1}}\right] \propto I, \tag{3.90}$$

where I is the identity in color space. This follows given that the contribution in color space from a given replica in a disconnected subdiagram G has two indices in the fundamental representation. By Schur's Lemma, this must be proportional to the identity i.e. the only possible two-index invariant tensor. We may then rewrite eq. (3.89) as

$$K_{G_i}^{A_{n_H+1}\dots A_n\, B_{m_H+1}\dots B_m} K_{H_i}^{A_1\dots A_{n_H}\, B_1\dots B_{m_H}} \left[t_H^{A_1}\dots t_H^{A_{n_H}}\right] \times \left[t_H^{B_{m_H}}\dots t_H^{B_1}\right]\left[t_G^{A_{n_H+1}}\dots t_G^{A_n}\right]\left[t_G^{A_m}\dots t_G^{A_{m_H+1}}\right] \times \prod_{j\neq i} C(j). \tag{3.91}$$

This has the same color structure as would arise if one were considering a different replica number in G than has been considered in H. I.e. one can absorb all G-dependent factors into the product $\prod C(j)$, such that eq. (3.91) is then the same as eq. (3.88). The color structures of the subdiagrams are thus independent, and it follows that the number of ways of forming the total diagram in Fig 3.10 is the product of the number of ways of forming the individual subdiagrams. For each subdiagram this is at least $\propto N$, such that the contribution from diagrams which are two-eikonal reducible is at least $\propto N^2$ (in general, $\propto N^M$, where M is the number of disconnected subdiagrams). Thus, two-eikonal reducible diagrams do not exponentiate.

In fact, one can proceed further and obtain a general solution for the color factors of the diagrams to all orders. Consider a given diagram consisting of n_c connected pieces (i.e. gluons connected by self interactions or fermion bubbles). For each such diagram, we then consider the set $\{P\}$ of *partitions*. These are sets containing a number $n(P)$ of subgraphs g, each of which contains only one replica (see Fig. 3.11). Permuting the replica numbers (but keeping the subgraphs g intact) corresponds to the same partition (see Fig. 3.12), such that there are ${}_N P_{n(P)}$ distinct diagrams in each partition, each of which has the same color factor

$$\prod_{g\in P} C(g), \tag{3.92}$$

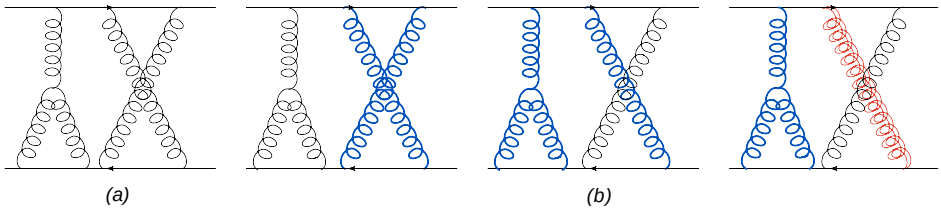

Figure 3.11: Examples of (a) a diagram containing 3 connected pieces; (b) three possible partitions generated by this diagram, where colors represent distinct replica numbers. Permuting colors gives the same partition.

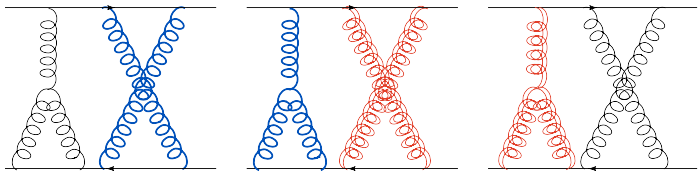

Figure 3.12: Examples of diagrams in the same partition, where colors represent distinct replica numbers.

where $C(g)$ is the color factor associated with subgraph g. The total color factor of the complete diagram is now given by

$$\sum_P {}_N P_{n(P)} \prod_{g \in P} C(g) \tag{3.93}$$

i.e. one sums over all possible partitions, each of which has a color factor given by eq. (3.92), and weighted by the number of diagrams represented by each partition. The only dependence on the replica number resides in the factor ${}_N P_{n(P)}$, which has the form

$${}_N P_{n(P)} = (-1)^{n(P)-1}(n(P)-1)!N + \mathcal{O}(N^2). \tag{3.94}$$

The contribution from a given complete diagram G which is linear in N is thus given by

$$\bar{C}(G) = \sum_P (-1)^{n(P)-1}(n(P)-1)! \prod_{g \in P} C(g). \tag{3.95}$$

The bar on the left hand side denotes the fact that this is the modified color factor associated with G, rather than the color factor one would obtain in conventional perturbation theory (i.e. without the $\mathcal{R}$ operator). The color factors on the right hand side, $C(g)$, are the ordinary color factors associated with each replica subgraph g. eq. (3.95) is a closed form solution for the modified color factor associated with any

given diagram, in that modified color factors only appear on the left-hand side. It has the property, as it must do from the above considerations, of being zero if G is not a web. As a simple example (already encountered above), consider the diagram of Fig. 3.8(c). There are two possible partitions. Either the two gluons have the same replica number, i.e. one subgraph with color factor $C(\,)$, or they have different color factors i.e. two subgraphs with total color factor $C(\,)C(\,)$. Then eq. (3.95) gives a total modified color factor

$$\bar{C}(\,) = C(\,) - C(\,)C(\,), \tag{3.96}$$

which gives $-\frac{1}{2}C_F C_A$ as required.

To further clarify the discussion, we consider here a pair of three loop examples. We consider first the diagram represented in the above shorthand notation by . From eq. (3.95), one has schematically

$$\begin{aligned}\bar{C}(\,) &= C(\,) - 2C(\,)C(\,) - C(\,)C(\,) + 2C(\,)^3 \\ &= C(\,) - 2\bar{C}(\,)\bar{C}(\,) - \bar{C}(\,)^3,\end{aligned} \tag{3.97}$$

where in the second line we have used the fact that $\bar{C}(\,) = C(\,)$ and $\bar{C}(\,) = C(\,) - C(\,)^2$. The second line then agrees with the modified color factor given in [44, 45].

Our second example is , for which one has

$$\bar{C}(\,) = C(\,) - C(\,)C(\,). \tag{3.98}$$

Reducibility implies $C(\,) = C(\,)C(\,)$, and thus $\bar{C}(\,) = 0$, as expected for a non-web.

To summarize, the above replica trick has allowed us to determine the subset of diagrams which exponentiate in non-abelian theory i.e. the diagrams which exponentiate are those which have a term linear in the number of replicas N. This is related to the original gauge theory (with no replicas) as follows. Firstly, the replica gluons all have the same self-interactions and scalar-gluon interactions, but do not interact with each other. Thus in any diagram one can replace replica gluons with original gluons to yield the same kinematic result. Then the color weights of the exponentiating diagrams are precisely those found above i.e. modified with respect to the original theory. The structure of two-eikonal irreducible diagrams with modified color factors is precisely that of web exponentiation, described in [45, 47].

The above discussion proceeds similarly in the case of fermionic emitting particles, given that the gauge boson emission vertices which distinguish scalar from fermion emitters only appear at NE order. We discuss subleading corrections in the next section.

3.3.1 Non-abelian exponentiation at NE order

The significance of the above derivation of web exponentiation in terms of the path integral method is that one may then easily extend the analysis to NE order, using the λ-scaling technique discussed in section 3.2.2. We have already shown that a subset

of NE corrections exponentiate in the abelian case, and that eikonal corrections in the non-abelian case exponentiate. Thus, it is not surprising that a subset of non-abelian NE terms exponentiates.

In this section we again consider the simple case of two external lines emerging from a hard interaction which has a color singlet structure. Then the scattering amplitude factorizes as in eq. (3.72), but where the external line factor is given by

$$f(\infty) = \int_{x(0)=0} \mathcal{D}x\, \mathcal{P} \exp\Big[i \int_0^\infty dt \Big(\frac{\lambda}{2}\dot{x}^2 + (n+\dot{x})\cdot A(nt+x) + \frac{i}{2\lambda}\partial \cdot A(nt+x) - \frac{1}{2\lambda}\sigma^{\mu\nu}F_{\mu\nu}\Big)\Big], \quad (3.99)$$

One next performs the path integral in x (as detailed for the abelian case in appendix 3.B), which gives

$$\begin{aligned} f(\infty) =& \mathcal{P} \exp\Big[i \int_0^\infty dt\, n\cdot A(nt) - \frac{1}{2\lambda}\int_0^\infty dt\, \partial \cdot A(nt) \\ & - \frac{1}{2}\int_0^\infty dt \int_0^\infty dt' \langle \dot{x}^\mu(t)\dot{x}^\nu(t')\rangle A_\mu(nt) A_\nu(nt') \\ & - \int_0^\infty dt \int_0^\infty dt'\, \langle \dot{x}^\mu(t) x^\alpha(t')\rangle n^\nu A_\mu(nt)\partial_\alpha A_\nu(nt') \\ & - \frac{1}{2}\int_0^\infty dt \int_0^\infty dt'\, \langle x^\alpha(t) x^\beta(t')\rangle n^\mu n^\nu \partial_\alpha A_\mu(nt)\partial_\beta A_\nu(nt') \\ & + \frac{i}{2}\int_0^\infty dt\, n^\mu \langle x^\nu(t) x^\alpha(t)\rangle \partial_\nu\partial_\alpha A_\mu(nt)\Big]. \end{aligned} \quad (3.100)$$

For reasons that will become clear, we have stayed in position space in the exponent. Inserting the correlators of the x fields (see eqs. (3.135)), eq. (3.100) becomes:

$$\begin{aligned} f(\infty) =& \mathcal{P} \exp\Big[i \int_0^\infty dt\, n\cdot A^A(nt)\, t^A - \frac{1}{2\lambda}\int_0^\infty dt\, \partial \cdot A^A(nt) t^A \\ & - \frac{i}{2\lambda}\int_0^\infty dt\, \eta^{\mu\nu} A^A_\mu(nt)\, A^B_\nu(nt) \frac{1}{2}\{t^A, t^B\} - \frac{1}{2\lambda}\int_0^\infty dt\, n^\mu \partial^\nu \partial_\nu A^A_\mu(nt)\, t^A \\ & - \frac{i}{\lambda}\int_0^\infty dt \int_t^\infty dt'\, \eta^{\mu\alpha} n^\nu A^A_\mu(nt)\partial_\alpha\, A^B_\nu(nt')\, t^B\, t^A \\ & - \frac{i}{\lambda}\int_0^\infty dt \int_t^\infty dt'\, t' n^\mu n^\nu \partial_\alpha A^A_\mu(nt)\, \partial^\alpha\, A^B_\nu(nt')\, t^B\, t^A\Big]. \end{aligned} \quad (3.101)$$

Here we have explicitly factored out color matrices from the non-abelian gauge fields. Note that path ordering (i.e. time ordering in this case) has appeared in some of the terms in the exponent, due to the Θ function occurring in the correlators of eq. (3.135). There are two types of vertex occurring in eq. (3.101) - those that depend on a single time (in the first two lines), and those that depend on two different times (in the third and fourth lines). Of the former type, there are one gluon vertices and a two gluon

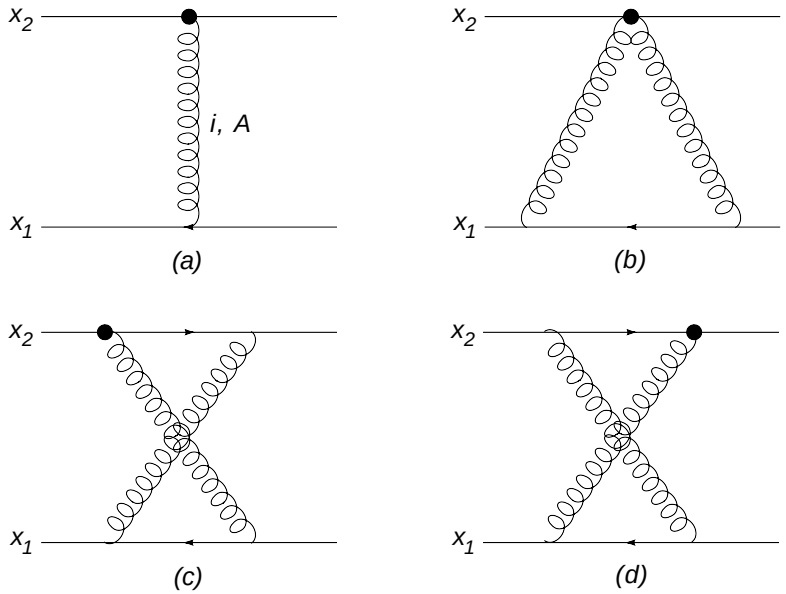

Figure 3.13: Webs involving local vertices occurring at NE order, where • represents a vertex of NE order. Additional diagrams arise by reflecting each diagram shown about the horizontal axis.

vertex. For these vertices, the arguments of the previous section (involving the replica trick) carry forward with minimal modification, and one has eikonal exponentiation up to NE webs, where each NE vertex must occur only once per diagram. The additional webs that appear at two gluon order are shown in figure 3.13. At higher orders, the NE webs again have the property of being two-external-line irreducible. The time ordered vertices in the third line of eq. (3.101) generate diagrams such as those shown in figure 3.14, which involve correlated emissions from different positions on the external line, but where additional eikonal emissions may occur in between. One must then sum over all possible correlations (pairs of gluons). There are two types of such diagrams. Firstly, diagrams whose structure is such that they form a web at eikonal level (i.e. are two-eikonal irreducible in that case). The time ordered vertices then implement correlations between pairs of gluons in the same web. Secondly, one has diagrams that would be two-eikonal reducible at eikonal level (i.e. are a product of webs), but which become irreducible at NE level due to correlations between gluons in separate webs (e.g. Fig. 3.14). The sum over all such diagrams then enters the exponent of eq. (3.76). To summarize, the set of NE corrections resulting from non-abelian gauge boson emission outside of the hard interaction exponentiate. The exponent involves a subset of diagrams, NE webs, some of which are more complicated in structure than their eikonal equivalents. However, they still share the property of being

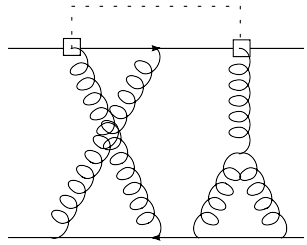

Figure 3.14: Example of a web involving the NE vertex (denoted here by □), which correlates gluons emitted from different positions on the external line. As shown here, further eikonal emissions may occur between the correlated NE emissions.

two-external-line irreducible.

In the case of a spinor emitting particle, the additional vertex

$$\frac{i}{2\lambda}\int_0^\infty \sigma^{\mu\nu}F_{\mu\nu} \tag{3.102}$$

appears in the exponent of eq. (3.99) i.e. the non-abelian analogue of eq. (3.146). This gives rise to both a one- and a two-gluon vertex, derived from the position space expressions

$$\frac{i}{\lambda}\int_0^\infty \partial_\mu A^A_\nu(t)\,\sigma^{\mu\nu}\,t^A; \tag{3.103}$$

$$\frac{1}{2}\int_0^\infty \sigma^{\mu\nu}A^A_\mu(t)\,A^b_\nu\,[t^A,t^B](t). \tag{3.104}$$

Both of these vertices depend on a single time, and thus are handled similarly to those occurring in eq. (3.101). Note that the two-gluon vertex eq. (3.104) has no abelian analogue, which can be seen from the fact that the commutator $[t^A,t^B]$ vanishes for an abelian gauge field.

Some comments are in order regarding the color factors associated with the NE webs. We note that the derivation of the formula for modified color factors in the eikonal case (eq. (3.95)) is independent of the eikonal approximation. Thus, it also applies also in the NE case, where the color factors $C(j)$ associated with each subgraph involving replica number j are the normal color factors one obtains using the NE Feynman rules.

The above discussion shows that, for the simple hard interaction considered above, a subset of corrections exponentiates up to NE order i.e. those associated with soft gauge boson emission outside the hard interaction. As in the abelian case, one still has to worry about corrections due to eikonal emissions from within the hard interaction (which give rise to the remainder term in eq. (3.48)). This is the subject of the next section.

3.3.2 Internal emissions of non-abelian gauge fields

In the abelian case, we identified a subset of NE corrections which exponentiate (i.e. those arising from soft gauge boson emissions outside of the hard interaction). There were then remainder terms, which did not have an exponential structure but could be obtained iteratively to all orders in the perturbation expansion. Here we briefly discuss how this structure can be generalized to the case of a non-abelian gauge field. As in the previous section, we consider the case where the matrix element for the hard interaction with no internal emissions has a color singlet structure, with two outgoing eikonal lines.

We begin with the non-abelian analogue of the abelian gauge transformation law of eq. (3.52), which is

$$f(x_i, p_f; A_\mu) \to f(x_i, p_f, UA_\mu U^{-1} - iU\partial_\mu U^{-1}) = U(x_i) f(x_i, p_f; A_\mu) \tag{3.105}$$

for an external particle, and

$$f(x_i, p_f; A_\mu) \to f(x_i, p_f, UA_\mu U^{-1} - iU\partial_\mu U^{-1}) = f(x_i, p_f; A_\mu) U^{-1}(x_i) \tag{3.106}$$

for an external antiparticle, where $U(x) = \exp(i\theta^A(x)t^A)$, and the coupling constant g of the non-abelian gauge field has been absorbed in A. The hard interaction (in the two eikonal line, color singlet case considered in the previous sections) then transforms as

$$H(x_1, x_2, A) \to H(x_1, x_2, UA_\mu U^{-1} - iU\partial_\mu U^{-1}) = U(x_2) H(x_1, x_2) U^{-1}(x_1). \tag{3.107}$$

Expanding this to first order in A and $\theta^a(x)$, and using the fact that the latter is arbitrary gives the analogue of eq. (3.54)

$$-\partial_\mu H^\mu(x_1, x_2; x) t^A = iH(x_1, x_2) \sum_j g_j \delta(x - x_j) t^A, \tag{3.108}$$

where $g_j = +1$ for an eikonal particle, and -1 for an antiparticle. This has the same interpretation as in the abelian case i.e. the amplitude for an internal emission is related to the amplitude with no such emission. In the non-abelian case, the amplitude for internal emission is proportional to the color matrix t^A, as indeed it must be from group theory considerations (the quantity H^μ has one adjoint index and two fundamental indices).

As in the abelian case, eq. (3.108) can be interpreted as an extra vertex for soft gluon emission. This vertex is located on the Wilson line at $t = 0$ i.e. where the eikonal segments x_1 and x_2 meet. There are terms (also by analogy with the abelian case of Sec. 3.2.4) which correct for the fact that the external lines do not originate from $x = 0$. However, these also take the form of an additional vertex localized at $t = 0$. The diagrams containing these additional vertices do not necessarily exponentiate (as before), and form a remainder term analogously to that of eq. (3.48).

Thus, the all-order structure of matrix elements up to NE order is conceptually equivalent to the abelian case. One has a subset of NE corrections which exponentiate (i.e. NE webs), and a set of corrections which form a remainder term which mixes

with the exponentiated NE corrections. The remainder term does not necessarily have a simple structure, but at least has an iterative structure due to the fact that diagrams with no internal emission are sufficient to generate higher order diagrams involving an internal emission.

3.4 Discussion

In this chapter, we have considered the issue of soft gauge boson corrections for matrix elements in abelian and non-abelian gauge theories from a path integral point of view. This involves considering factorized diagrams involving hard interactions with a given number of external lines, each of which emits further soft radiation. The propagator for each external line can then be cast into a first quantized path integral representation, where the integral is a sum over paths for the emitting particle. This path integral can be performed by expanding about the classical straight line path for the emitter, which corresponds to systematic corrections to the eikonal approximation. The scattering amplitude then factorizes into a hard interaction plus factors for each external line which act as source terms for the soft gauge field A_s^μ, where the sources are placed along the external lines. In the abelian case, exponentiation of eikonal corrections then follows from the usual exponentiation of disconnected diagrams in quantum field theory. Furthermore, a subset of next-to-eikonal corrections can also be shown to exponentiate, and a set of effective Feynman rules for radiation in the NE limit is obtained.

The case of a non-abelian gauge field is more complicated, but can be analyzed using the replica trick, in which one considers an ensemble of N gauge fields. Diagrams which have a term linear in N then exponentiate, and crucially only a subset of diagrams in the theory have such a property. We considered the simple case of two external lines, connected by a hard interaction with color singlet structure. Then the diagrams which exponentiate contain sources arising from the replica ordered perturbation theory arising from eq. (3.78). Those which contribute at $\mathcal{O}(N)$ have the property of being two-external line irreducible, and also have (in general) color factors which differ from those of the corresponding diagrams in the original theory. These diagrams are then precisely the webs of [45, 47]. As in the abelian case, a subset of NE corrections also exponentiates, and the exponent contains a sum of webs up to NE level.

In both the abelian and non-abelian cases, there are NE corrections which do not exponentiate, and which form a remainder term such that the total matrix element (up to NE order) has the form shown in eq. (3.48). These terms are associated with Low's theorem, and the relevant diagrams involve contractions between eikonal photons or gluons on the external lines, and a NE vertex localized at the cusp at which the outgoing eikonal lines meet. Furthermore, these terms have an iterative structure in perturbation theory, in that the extra vertices that contribute can be related to diagrams at a lower order in the perturbation expansion.

A comment is in order regarding the nature of NE exponentiation. Up to NE order,

eq. (3.48) can be expanded to give

$$\mathcal{M} = \exp\left[\mathcal{M}^{\mathrm{E}}\right]\left(1 + \mathcal{M}_r + \mathcal{M}^{\mathrm{NE}}\right) \tag{3.109}$$

i.e. one may either consider the NE terms arising from eikonally factorized diagrams as being in the exponent, or kept to linear order. This masks the fact that the terms in $\mathcal{M}^{\mathrm{NE}}$ genuinely do exponentiate, whereas the remainder terms in $\mathcal{M}_r$ do not. However, it is true that the exponentiated NE terms lead to NNE, NNNE etc. contributions which would then mix with higher order (in the eikonal expansion) remainder terms. The exponentiated form of eq. (3.109) is particularly useful if the contribution from $\mathcal{M}^{\mathrm{NE}}$ (when exponentiated) gives the dominant contribution to higher order terms in the eikonal expansion. Whether or not this is the case is presumably process dependent.

The proof of exponentiation in the abelian case, as presented here, clearly generalizes to higher numbers of eikonal lines. However, in the non-abelian case we considered only the simplest possible hard interaction, namely that with two external lines with a color singlet structure. This could be easily related to a single Wilson line with a cusp. The general case of higher numbers of external lines is more complicated due to the color structures involved. Nevertheless, the methods introduced in this chapter may provide a useful starting point in addressing NE corrections in these situations.

We have only considered matrix elements in this chapter. Thus, any exponentiation of NE corrections pertains only before any integration over the phase space of the final state gauge bosons has been performed. In the strict eikonal approximation, the phase space factorizes into a product of single particle phase spaces (i.e. conservation of energy is a subleading effect), thus exponentiation in the matrix element implies exponentiation of soft logarithms in differential (but partially integrated) cross-sections. This is not necessarily the case beyond the eikonal approximation, where one expects NE corrections resulting from the eikonal matrix element with integration over the full phase space. Naïvely, one expects a given differential cross-section (e.g. in some variable ξ related to the total energy fraction carried by soft gluons) to have the form

$$\frac{d\sigma}{d\xi} = \int d\mathrm{PS}^{(\mathrm{E})}\,|\mathcal{M}^{(\mathrm{E})}|^2 + \left[\int d\mathrm{PS}^{(\mathrm{E})}\,|\mathcal{M}^{(\mathrm{NE})}|^2 + \int d\mathrm{PS}^{(\mathrm{NE})}\,|\mathcal{M}^{(\mathrm{E})}|^2\right] + \mathcal{O}(\mathrm{NNE}). \tag{3.110}$$

Here $\mathcal{M}^{(\mathrm{E,\,NE})}$ denote the eikonal and next-to-eikonal matrix elements respectively, and $d\mathrm{PS}^{(\mathrm{E})}$ the eikonal phase space, consisting of a factorized product of one-particle phase spaces. The first term in eq.(3.110) is then of eikonal order, and the bracketed term is NE, where $d\mathrm{PS}^{(\mathrm{NE})}$ represents that part of the multi-gluon phase space which implements next-to-eikonal corrections (i.e. subleading terms in ξ). The precise nature of this latter term is unclear, and an investigation of its effect is deferred to a future publication. Nevertheless, all of the ingredients for the first bracketed term in eq. (3.110) are contained in this chapter.

To conclude, the path integral methods used in this chapter provide a new viewpoint for the exponentiation of soft radiative corrections to matrix elements, in both abelian and non-abelian gauge theories. In particular, the discussion of webs is rephrased

such that a closed form solution for the modified color factors can be given. Furthermore, the approach naturally encompasses the exponentiation of classes of next-to-eikonal corrections. This approach should prove fruitful in the further investigation of soft radiative corrections to all orders in perturbation theory. In the following chapter we examine the same classes of terms from a diagrammatic point of view and begin to validate our findings by comparing to the exact calculations.

3.A Exponentiation of disconnected diagrams

Here we briefly prove the exponentiation of disconnected diagrams in quantum field theory, using the *replica trick* of statistical physics. Although we consider a single self-interacting scalar field ϕ, the proof generalizes easily to other systems.

The Green's functions of a given quantum field theory are described by the generating functional

$$Z[J] = \int \mathcal{D}\phi e^{iS[\phi]+i\int J\phi}, \tag{3.111}$$

where J is a source for the field ϕ, and S is the classical action. Now consider defining N replicas of the theory, involving fields ϕ_i ($i \in \{1,\dots,n\}$). This has generating functional

$$Z_N[J] = \int \mathcal{D}\phi_1 \dots \mathcal{D}\phi_N e^{iS[\phi_1]+i\int J\phi_1} \dots e^{iS[\phi_N]+i\int J\phi_N}, \tag{3.112}$$

which clearly satisfies

$$Z_N[J] = (Z[J])^N. \tag{3.113}$$

The Feynman rules for each field are similar, and there are no interactions between the fields. Thus, there can be no more than one field in each connected Feynman diagram, and connected diagrams therefore have N copies. By the same reasoning, disconnected diagrams containing $n \geq 2$ constituent parts have N^n copies. It follows that

$$\sum G_c \propto N, \tag{3.114}$$

where G_c denotes a connected diagram. Furthermore, no disconnected diagrams contribute terms proportional to N. From eq. (3.113) one has

$$Z_N[J] = 1 + N\log(Z[J]) + \mathcal{O}(N^2), \tag{3.115}$$

and comparing eqs. (3.114, 3.115) gives

$$\sum G_c = \log(Z[J]). \tag{3.116}$$

Finally, one writes this as:

$$Z[J] = \exp\left[\sum G_c\right] \tag{3.117}$$

and sets $N = 1$. This is the statement that disconnected diagrams exponentiate, as required.

The above proof shortcuts the nontrivial combinatoric fact that the symmetry factor associated with a disconnected Feynman graph is the product of the symmetry factors of each of the constituent connected graphs. The results of this chapter demonstrate that the same combinatoric reasoning applies to the exponentiation of soft radiative corrections from fast-moving external particles.

3.B Next-to-eikonal Feynman rules

In this appendix, we show how to derive effective Feynman rules for the eikonal and next-to-eikonal approximations in the path integral approach discussed in section 3.2.2, and show explicitly that these agree with the rules one obtains by starting from exact perturbation theory before taking the NE limit.

We begin with the conventional perturbative approach, and consider the case of a charged scalar interacting with a background gauge field. The theory and its Green functions are defined via the generating functional

$$Z[J,J^*] = \int \mathcal{D}\phi\mathcal{D}\phi^* \, \exp\left[i \int d^dx \left[-(D_\mu\phi)^* D^\mu\phi - m^2\phi^*\phi + J\phi^* + J^*\phi \right] \right]. \quad (3.118)$$

where $D_\mu = \partial_\mu - iA_\mu$. From this functional one derives the Feynman rules

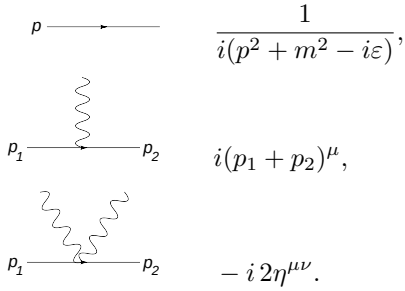

$$\frac{1}{i(p^2+m^2-i\varepsilon)}, \qquad i(p_1+p_2)^\mu, \qquad -i\,2\eta^{\mu\nu}. \quad (3.119)$$

Note the symmetry factor in the seagull vertex. With these rules one can describe emissions from a charged scalar line, and from them we can derive Feynman rules for the eikonal and NE approximation. To do so, we shall take $m = 0$ and use λ-scaling as discussed in section 3.2. That is, we consider an external particle of 4-momentum $p = \lambda n$, and consider the limit $\lambda \to \infty$. As discussed in section 3.2, this corresponds to the eikonal approximation, with the first subleading corrections in λ representing the NE approximation.

We first consider the propagator-vertex combination for one-photon emission. The diagram and corresponding expression is

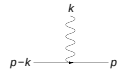

$$\frac{1}{i(p-k)^2} i(2p-k)^\mu\,, \quad (3.120)$$

where we have taken this diagram to represent the combined vertex and propagator factors (to the left of the vertex). Setting $p = \lambda n$ and expanding eq. (3.120) to $\mathcal{O}(1/\lambda)$ yields

$$-\frac{n^\mu}{n\cdot k}+\frac{1}{\lambda}\left(\frac{k^\mu}{2n\cdot k}-k^2\frac{n^\mu}{2(n\cdot k)^2}\right). \tag{3.121}$$

We recognize the first term as the eikonal approximation, and the remainder as the NE contribution. Each term in eq. (3.121) is to be contracted with a background gauge field, so that we can treat each as a one-photon source. We represent these sources graphically as

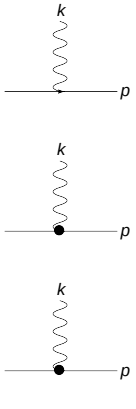

$$\begin{aligned} &(1) && -\frac{p^\mu}{p\cdot k},\\ &(2a) && \frac{k^\mu}{2p\cdot k},\\ &(2b) && -k^2\frac{p^\mu}{2(p\cdot k)^2}. \end{aligned} \tag{3.122}$$

Note that here and in following graphs, we replace $n \to p/\lambda$ so that the Feynman rules are given in terms of the physical momenta. We now consider possible two-photon sources. Starting with the seagull term, we take the following propagator-vertex combination:

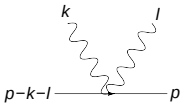

$$\frac{1}{i(p-k-l)^2}(-i2\eta^{\mu\nu}). \tag{3.123}$$

Scaling p and gathering terms up to $\mathcal{O}(1/\lambda)$ yields

$$\frac{1}{\lambda}\frac{\eta^{\mu\nu}}{n\cdot(k+l)}. \tag{3.124}$$

Evidently, at the eikonal level the seagull term is absent. One expects this given that there is no such seagull vertex in the exact Feynman rules for a fermionic emitting particle, and, as is well known, in the eikonal approximation the emitted radiation is insensitive to the particle's spin.

We next examine the contribution of two individual photon emissions, as shown in Fig. 3.15. At eikonal level these diagrams give a contribution

$$\left(-\frac{n^\nu}{n\cdot(k+l)}\right)\left(-\frac{n^\mu}{n\cdot k}\right)+\left(-\frac{n^\nu}{n\cdot(k+l)}\right)\left(-\frac{n^\mu}{n\cdot(l)}\right), \tag{3.125}$$

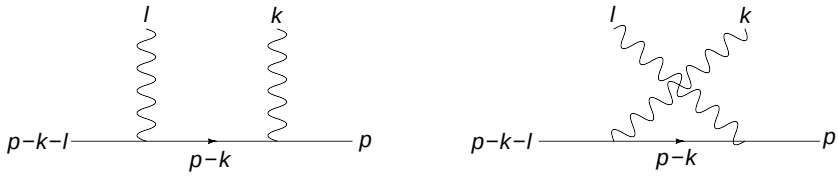

Figure 3.15: Diagrams contributing to two photon emission. At NE level, one must sum over all possible insertions of a NE one-photon emission vertex, as given in eq. (3.122).

which one may rearrange to give:

$$\left(-\frac{n^\nu}{p\cdot k}\right)\left(-\frac{n^\mu}{p\cdot l}\right). \tag{3.126}$$

The contribution from the soft emissions explicitly factorizes into a product of uncorrelated emissions, as is well-known.

At $\mathcal{O}(1/\lambda)$, corresponding to the NE limit, one must sum over all possible insertions of a NE one-photon emission vertex in Fig. (3.15). There are possible vertices, as given in eq. (3.122). The vertex (2a) yields an expression

$$\left(-\frac{n^\nu}{n\cdot(k+l)}\right)\left(\frac{k^\mu}{2n\cdot k}\right)+\left(\frac{(2k+l)^\nu}{2n\cdot(k+l)}\right)\left(-\frac{n^\mu}{n\cdot k}\right)+ \\ \left(-\frac{n^\mu}{n\cdot(k+l)}\right)\left(\frac{l^\nu}{2n\cdot l}\right)+\left(\frac{(k+2l)^\mu}{2n\cdot(k+l)}\right)\left(-\frac{n^\nu}{n\cdot l}\right). \tag{3.127}$$

which can be rearranged to give

$$\left(-\frac{n^\nu}{n\cdot l}\right)\left(\frac{k^\mu}{2n\cdot k}\right)+\left(-\frac{n^\mu}{n\cdot k}\right)\left(\frac{l^\nu}{2n\cdot l}\right)-\frac{l^\mu n^\nu n\cdot k+k^\nu n^\mu n\cdot l}{n\cdot(k+l)n\cdot k n\cdot l}. \tag{3.128}$$

Notice that the first two terms correspond to two uncorrelated NE emissions, while the last term represents a correlated two-photon emission (i.e. is non-factorizable into terms dependent on a single photon momentum). The NE vertex (2b) gives a contribution

$$\left(-\frac{n^\nu}{n\cdot(k+l)}\right)\left(-k^2\frac{n^\mu}{2(n\cdot k)^2}\right)+\left(-(k+l)^2\frac{n^\nu}{2(n\cdot(k+l))^2}\right)\left(-\frac{n^\mu}{n\cdot k}\right)+ \\ \left(-\frac{n^\mu}{n\cdot(k+l)}\right)\left(-l^2\frac{n^\nu}{2(n\cdot l)^2}\right)+\left(-(k+l)^2\frac{n^\mu}{2(n\cdot(k+l))^2}\right)\left(-\frac{n^\nu}{n\cdot l}\right), \tag{3.129}$$

which can be rewritten as

$$\left(-\frac{n^\nu}{n\cdot l}\right)\left(-k^2\frac{n^\mu}{2(n\cdot k)^2}\right)+\left(-\frac{n^\mu}{n\cdot k}\right)\left(-l^2\frac{n^\nu}{2(n\cdot l)^2}\right)+\frac{n^\mu n^\nu k\cdot l}{n\cdot(k+l)n\cdot k n\cdot l}. \tag{3.130}$$

Again this is the sum of an uncorrelated part, and a term implementing correlated photon emission. The various correlated contributions given in eqs. (3.124), (3.128) and (3.130) can be represented as new two-photon vertices, and are given respectively by

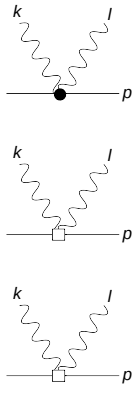

$$\begin{aligned} &\text{(3)} && + \frac{\eta^{\mu\nu}}{p\cdot(k+l)}, \\ &\text{(4a)} && - \frac{l^\mu p^\nu p\cdot k + k^\nu p^\mu p\cdot l}{p\cdot(k+l)p\cdot k p\cdot l}, \\ &\text{(4b)} && + \frac{p^\mu p^\nu k\cdot l}{p\cdot(k+l)p\cdot k p\cdot l}. \end{aligned} \tag{3.131}$$

We have shown that these vertices apply when two photons are emitted next to the on-shell eikonal line. From our analysis in this appendix, it does not necessarily follow that these vertices apply to emissions anywhere on the external line, at all orders of perturbation theory. That this is indeed the case is clear when one rederives these vertices using the path integral methods described in this chapter, and we defer a full proof within conventional perturbation theory to chapter 4. Here we will only demonstrate that these terms are precisely reproduced in our path-integral formalism. The path integral representation of a charged scalar coupled to a background gauge field is given by eq. (3.44) as

$$f(\infty) = \int_{x(0)=0} \mathcal{D}x \, \exp\left[i \int_0^\infty dt \left(\frac{\lambda}{2}\dot{x}^2 + (n+\dot{x})\cdot A(x_i + nt + x) \right.\right. \\ \left.\left. + \frac{i}{2\lambda}\partial\cdot A(x_i + p_f t + x) \right) \right]. \tag{3.132}$$

Our task is to derive the photon source terms from this expression. To this end we need to determine the propagator and vertices for the x field, and their scaling with λ.

The x kinetic term is given by

$$-\int_0^\infty dt \frac{1}{2} x(t) \left(i\lambda \frac{\partial^2}{\partial t^2} \right) x(t)\,, \tag{3.133}$$

The propagator for x is given by the inverse of the quadratic operator in eq. (3.133), which is found to be

$$G(t,t') = \frac{i}{\lambda}\min(t,t')\,. \tag{3.134}$$

Note that it is symmetric, proportional to $1/\lambda$ (thus is of NE order), and satisfies the condition $G(0,t')=0$. Other two-point correlators of x and $\dot{x}$, which we need below, are

$$\begin{aligned}\langle x(t)x(t')\rangle &= G(t,t') = \frac{i}{\lambda}\min(t,t'),\\ \langle \dot{x}(t)x(t')\rangle &= \frac{\partial G(t,t')}{\partial t} = \frac{i}{\lambda}\theta(t'-t),\\ \langle \dot{x}(t)\dot{x}(t')\rangle &= \frac{\partial^2 G(t,t')}{\partial t\partial t'} = \frac{i}{\lambda}\delta(t'-t)\,.\end{aligned} \tag{3.135}$$

We will also need the properties of the equal time correlator $\langle \dot{x}(t)x(t)\rangle$. Using the discretization of space-time adopted throughout this chapter, the derivative $\dot{x}(t)$ is given by

$$\lim_{\epsilon\downarrow 0}\epsilon\frac{x(t+\epsilon)-x(t)}{\epsilon} \tag{3.136}$$

and thus one has

$$\langle \dot{x}(t)x(t)\rangle = \frac{i}{\lambda}\lim_{\epsilon\downarrow 0}\frac{\min(t+\epsilon,t)-\min(t,t)}{\epsilon} = 0. \tag{3.137}$$

The vertices involving the x field can be obtained by Taylor expansion of the other terms in eq. (3.132). Due to the subleading nature of the x propagator in the eikonal limit, we shall need them to second order in x or $\dot{x}$ only for a NE analysis. The terms without a power of x are

$$\begin{aligned} i\int_0^\infty dt n\cdot A(nt) &= -\int\frac{d^dk}{(2\pi)^d}\frac{n^\mu}{n\cdot k}\tilde{A}_\mu(k),\\ -\frac{1}{2\lambda}\int_0^\infty dt\partial\cdot A(nt) &= \frac{1}{2\lambda}\int\frac{d^dk}{(2\pi)^d}\frac{k^\mu}{n\cdot k}\tilde{A}_\mu(k),\end{aligned} \tag{3.138}$$

where we have also represented the terms in momentum space. Note that these A source terms correspond to the vertex in eq. (3.122) (2a). Terms with one power of x are

$$\begin{aligned} i\int_0^\infty dt\dot{x}^\mu A_\mu(nt) &= \int\frac{d^dk}{(2\pi)^d}\tilde{A}_\mu(k)\int_0^\infty dt\, i\dot{x}^\mu(t)e^{i(n\cdot k)t} \quad \clubsuit\\ i\int_0^\infty dt n^\mu\partial_\nu A_\mu(nt)x^\nu(t) &= -\int\frac{d^dk}{(2\pi)^d}n^\mu\tilde{A}_\mu(k)k_\nu\int_0^\infty dt\, x^\nu(t)e^{i(n\cdot k)t} \quad \diamondsuit\end{aligned} \tag{3.139}$$

To distinguish the vertices in our discussion below, we have labeled them with sym-

bols. Terms with two powers of x are

$$i\int_0^\infty dt\dot{x}^\mu\partial_\nu A_\mu(nt)x^\nu = -\int\frac{d^dk}{(2\pi)^d}\tilde{A}_\mu(k)k_\nu\int_0^\infty dt\dot{x}^\mu(t)x^\nu(t)e^{i(n\cdot k)t} \quad \heartsuit$$

$$\frac{i}{2}\int_0^\infty dtn^\mu\partial_\nu\partial_\kappa A_\mu(nt)x^\nu(t)x^\kappa(t) = -\frac{i}{2}\int\frac{d^dk}{(2\pi)^d}n^\mu\tilde{A}_\mu(k)k_\nu k_\kappa \times\int_0^\infty dtx^\nu(t)x^\kappa(t)e^{i(n\cdot k)t}\,. \quad \spadesuit$$

The term $\spadesuit$ is quadratic in x, and thus the factor of $1/2$ does not appear in the resulting vertex.

The next step is to carry out the x path-integral. This amounts to using the Feynman rules in eqs. (3.134 - 3.140), keeping terms to $\mathcal{O}(1/\lambda)$

$$\int_{x(0)=0}\mathcal{D}x\,\exp\left[i\int_0^\infty dt\Big(\frac{\lambda}{2}\dot{x}^2+(n+\dot{x})\cdot A(x_i+nt+x)+\frac{i}{2\lambda}\partial\cdot A(x_i+p_ft+x)\Big)\right] =$$

$$\exp\left[-\int\frac{d^dk}{(2\pi)^d}\frac{n^\mu}{n\cdot k}\tilde{A}_\mu(k)+\frac{1}{2\lambda}\int\frac{d^dk}{(2\pi)^d}\frac{k^\mu}{n\cdot k}\tilde{A}_\mu(k)+\sum\cdot\!\!-\!\!\cdot+\sum\cdot\!\!\bigcirc\right]. \quad (3.140)$$

We have written the result as the exponent of connected diagrams, where terms beyond $\mathcal{O}(1/\lambda)$ are neglected. The first two terms (3.138) are the vertices (1) and (2a) of (3.122). The third and fourth terms represent tree and loop graphs, with a sum over all possible insertions of the vertices denoted above by $\clubsuit$, $\diamondsuit$, $\heartsuit$ and $\spadesuit$. In the tree graph, there are three different combinations of one-x vertices from (3.139). The $\clubsuit-\clubsuit$ combination together with a two-x correlator gives

$$\frac{1}{2}\int\frac{d^dk}{(2\pi)^d}\frac{d^dl}{(2\pi)^d}\tilde{A}_\mu(k)\tilde{A}_\nu(l)\int_0^\infty dt\,dt'\,\frac{-i}{\lambda}\delta(t-t')\eta^{\mu\nu}e^{i(n\cdot kt+n\cdot lt')} = \frac{1}{2}\int\frac{d^dk}{(2\pi)^d}\frac{d^dk}{(2\pi)^d}\tilde{A}_\mu(k)\tilde{A}_\nu(l)\frac{\eta^{\mu\nu}}{\lambda n\cdot(k+l)}. \quad (3.141)$$

This precisely reproduces source term (3) of eq. (3.131). The $\clubsuit-\diamondsuit$ combination gives

$$\int\frac{d^dk}{(2\pi)^d}\frac{d^dl}{(2\pi)^d}\tilde{A}_\mu(k)\tilde{A}_\nu(l)n^\nu(-k_\kappa)\int_0^\infty dt\,dt'\,i\left(\frac{i}{\lambda}\delta(t-t')\right)\eta^{\mu\kappa}\frac{e^{i(n\cdot kt+n\cdot lt')}}{-in\cdot l} = \int\frac{d^dk}{(2\pi)^d}\frac{d^dk}{(2\pi)^d}\tilde{A}_\mu(k)\tilde{A}_\mu(l)\frac{-n^\nu l^\mu}{\lambda n\cdot ln\cdot(k+l)}\,, \quad (3.142)$$

which can be rewritten as

$$\frac{1}{2}\int\frac{d^dk}{(2\pi)^d}\frac{d^dl}{(2\pi)^d}\tilde{A}_\mu(k)\tilde{A}_\nu(l)\left(-\frac{n^\nu l^\mu n\cdot k+n^\mu k^\nu n\cdot l}{\lambda n\cdot ln\cdot kn\cdot(k+l)}\right). \quad (3.143)$$

This is source term (4a) of (3.131). The $\diamondsuit - \diamondsuit$ combination gives

$$\frac{1}{2}\int \frac{d^dk}{(2\pi)^d}\frac{d^dl}{(2\pi)^d}\tilde{A}_\mu(k)\tilde{A}_\nu(l)n^\mu\, n^\nu\, k_\rho\, l_\sigma \times \int_0^\infty dt\, dt'\, \left(\frac{i}{\lambda}\delta(t-t')\right)\eta^{\rho\sigma}\frac{e^{i(n\cdot kt+n\cdot lt')}}{(-in\cdot k)(-in\cdot l)} = \frac{1}{2}\int \frac{d^dk}{(2\pi)^d}\frac{d^dk}{(2\pi)^d}\tilde{A}_\mu(k)\tilde{A}_\mu(l)n^\mu n^\nu \frac{k\cdot l}{\lambda n\cdot l n\cdot k n\cdot (k+l)}\,. \quad (3.144)$$

which produces term (4b) of (3.131).

The loop graph in eq. (3.140) has in principle two possible choices of vertex from (3.140). However, the $\heartsuit$ vertex does not actually contribute, as it involves the equal time correlator $\langle \dot{x}(t)x(t)\rangle$, which was shown above to be zero. The $\spadesuit$ vertex, however, does contribute and gives

$$-\frac{1}{2}i\int \frac{d^dk}{(2\pi)^d}\tilde{A}_\mu(k)k_\rho k_\sigma \int dt\,\frac{i}{\lambda}\,t\,e^{in\cdot kt} = -\frac{1}{2}\int \frac{d^dk}{(2\pi)^d}\tilde{A}_\mu(k)\frac{k^2}{(n\cdot k)^2}. \quad (3.145)$$

This finally yields source term (2b) of (3.122).

We conclude that, to next-to-eikonal order, the one- and two-photon source terms found by approximations in standard perturbation theory are precisely reproduced in our first-quantized path-integral approach. The considerations of section 3.2 then show that NE corrections from eikonally factorized diagrams exponentiate to all orders.

We have considered the case of scalar emitting particles in the above discussion. However, things proceed similarly for the spinor case, with the only modification arising due to the presence of an additional term in the exponent of eq. (3.132)

$$\frac{i}{2\lambda}\int_0^\infty \sigma^{\mu\nu}F_{\mu\nu} = -\frac{1}{\lambda}\int \frac{d^dk}{(2\pi)^d}k_\nu\,[\gamma^\nu,\gamma^\mu]\,\tilde{A}_\mu(k), \quad (3.146)$$

where the right-hand-side corresponds to the momentum space vertex

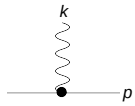

$$-k_\nu\,[\gamma^\nu,\gamma^\mu]. \quad (3.147)$$

This is $\mathcal{O}(1/\lambda)$, as expected from the fact that a magnetic moment vertex only contributes for particles having non-zero spin, and radiation in the strictly eikonal limit is insensitive to the spin of the emitting particle.

The above discussion assumes an abelian gauge field. The non-abelian generalization is discussed in Sec. 3.3.

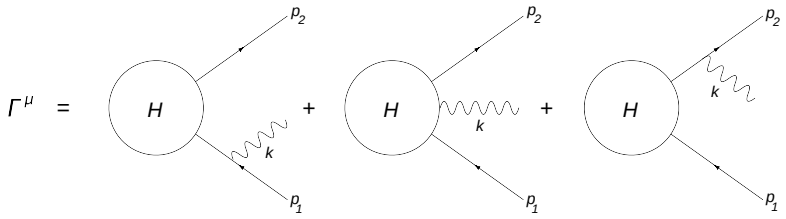

Figure 3.16: Amplitude Γ^μ corresponding to all possible soft emissions from a graph containing a given hard interaction, in the simple case of two outgoing scalar particles. The Lorentz index corresponds to the emitted photon.

3.C Matrix elements with internal emissions

In section 3.2.4, we show from our path integral representation of the scattering amplitude how NE corrections arising from soft photon emissions from within the hard interaction can be related to the hard interaction with no emissions, which is part of the content of the Low-Burnett-Kroll theorem [18, 19] (see also [20]). To clarify this discussion, we here present how one would obtain a similar result using traditional Feynman diagram methods, in the case of two scalar lines. Our presentation follows that of e.g. [59].

We consider the momentum-space amplitude Γ^μ shown pictorially in Fig. 3.16, and corresponding to a single gluon emission emitted from a graph containing a given hard interaction with two external scalar particles. We first define $\Gamma \equiv \Gamma(p_1^2, p_2^2, p_1 \cdot p_2)$ to be the hard interaction amplitude with no photon emission. Then using the normal Feynman rules for scalar electrodynamics, one may write Γ^μ as

$$\Gamma^\mu = \frac{(2p_1 - k)^\mu}{-2p_1 \cdot k}\Gamma[(p_1 - k)^2, p_2^2, (p_1 - k) \cdot p_2] + \frac{(2p_2 + k)^\mu}{2p_2 \cdot k}\Gamma[p_1^2, (p_2 + k)^2, p_1 \cdot (p_2 + k)] + \Gamma^\mu_{int}, \quad (3.148)$$

where we have assumed light-like external particles, and Γ^μ_{int} is the amplitude for emission from within the hard interaction, as represented by the second diagram on the right-hand-side in figure 3.16. Also, we have neglected coupling constants for brevity. In the limit where k is soft, one may Taylor expand eq. (3.148) to next-to-leading order in k (corresponding to the NE approximation) to obtain

$$\Gamma^\mu = \frac{2p_1^\mu}{-2p_1 \cdot k}\left[\Gamma - 2p_1 \cdot k\frac{\partial\Gamma}{\partial p_1^2} - p_2 \cdot k\frac{\partial\Gamma}{\partial p_1 \cdot p_2}\right] + k^\mu\left(\frac{1}{2p_1 \cdot k} + \frac{1}{2p_2 \cdot k}\right) + \frac{2p_2^\mu}{2p_2 \cdot k}\left[\Gamma + 2p_2 \cdot k\frac{\partial\Gamma}{\partial p_2^2} + p_1 \cdot k\frac{\partial\Gamma}{\partial p_1 \cdot p_2}\right] + \Gamma^\mu_{int}. \quad (3.149)$$

The gauge invariance condition $k_\mu \Gamma^\mu = 0$ implies

$$k_\mu \Gamma^\mu_{int} = -2p_2 \cdot k \frac{\partial \Gamma}{\partial p_2^2} - 2p_1 \cdot k \frac{\partial \Gamma}{\partial p_1^2} - k \cdot (p_1 + p_2) \frac{\partial \Gamma}{\partial p_1 \cdot p_2}. \tag{3.150}$$

This must be true for arbitrary k, so that one may remove factors of k^μ in eq. (3.150). Then one may substitute the resulting form of Γ^μ back into eq. (3.16) to obtain

$$\begin{aligned}\Gamma^\mu = &\left[\frac{(2p_1 - k)^\mu}{-2p_1 \cdot k} + \frac{(2p_2 + k)^\mu}{2p_2 \cdot k} \right] \Gamma \\ &+ \left[\frac{p_1^\mu (k \cdot p_2 - k \cdot p_1)}{p_1 \cdot k} + \frac{p_2^\mu (k \cdot p_1 - k \cdot p_2)}{p_2 \cdot k} \right] \frac{\partial \Gamma}{\partial p_1 \cdot p_2}. \end{aligned} \tag{3.151}$$

Identifying $p_i = n_i$ in the notation of section 3.2.4, one sees that the first term of eq. (3.151) is the contribution one expects from the effective Feynman rules for soft emission up to NE order. Also, the second term in eq. (3.151) is precisely the contribution contained in eq. (3.62). Furthermore, when $p_1^2 = p_2^2 = 0$, one may simplify eq. (3.150) so that one obtains

$$\Gamma^\mu_{int} = -p_1^\mu \frac{\partial \Gamma}{\partial p_1 \cdot p_2} - p_2^\mu \frac{\partial \Gamma}{\partial p_1 \cdot p_2}. \tag{3.152}$$

Rewriting

$$p_i^\mu \frac{\partial}{\partial p_i \cdot p_j} = \frac{\partial}{\partial p_{i\mu}}, \tag{3.153}$$

one finds

$$\Gamma^\mu_{int} = -\sum_i \frac{\partial \Gamma}{\partial p_{i\mu}}, \tag{3.154}$$

which is indeed a special case of eq. (3.57).

Chapter 4

A perturbative approach to exponentiation at next-to-eikonal order

4.1 Introduction

It has long been known that soft gauge boson emission give rise to large corrections to cross-sections. Generically, if ξ is a dimensionless variable related to the energy carried by soft gauge bosons in a given process, the differential cross-section receives contributions of the form

$$\frac{d\sigma}{d\xi} = \sum_{m,n} \alpha^n \left[a_{nm} \frac{\ln^m(\xi)}{\xi} + b_{nm} \ln^m(\xi) + \dots \right] \tag{4.1}$$

where α is the coupling constant, and the ellipsis denotes terms suppressed by successive powers of ξ. When ξ is small, the convergence of the perturbation expansion breaks down and resummation becomes necessary i.e. one must calculate successively the coefficients $\{a_{nm}\}$, $\{b_{nm}\}$ etc. for all values of n. The leading logarithms in eq. (4.1) originate from the *eikonal* approximation, in which the momenta k_i of all outgoing gluons satisfy $k_i \to 0$. The first set of subleading logarithms corresponds to the *next-to-eikonal* (NE) approximation in which $k_i \to 0$ for all but one gluon, whose momentum is kept to linear order in the total scattering amplitude.

Resummation of eikonal logarithms has been understood in abelian theories since the early 1960s [43]. Crucial to the resummation is the result that soft photon corrections exponentiate. That is, an amplitude $\mathcal{A}$ with many soft photon emissions may be written in the schematic form

$$\mathcal{A} = \mathcal{A}_0 \exp\left[\sum G_c\right], \tag{4.2}$$

where $\mathcal{A}_0$ is the Born amplitude, and the sum in the exponent is over connected subdiagrams. Exponentiation was also shown to hold in non-abelian theories in the early 1980s [44, 45, 46], although the ensuing structure is more complicated due to the non-trivial color structure. The non-abelian analogue of eq.(4.2) is

$$\mathcal{A} = \mathcal{A}_0 \exp\left[\sum \bar{C}_W W\right], \tag{4.3}$$

where the sum in the exponent involves diagrams W which are two-particle irreducible with respect to the hard emitting particles, and are named *webs* in the literature. The factors $\bar{C}_W$ are modified color factors, which differ from the conventional color factors C_W associated with each diagram using the standard Feynman rules.

Since then, soft gluon resummation has been widely investigated using a variety of techniques [13, 14, 39, 40, 41, 17, 32, 42], and phenomenological applications of resummation have been successfully achieved in many scattering processes. It is then natural to consider the complete extension of the resummation program to next-to-eikonal logarithms.

There are sound phenomenological reasons for doing so, given that NE contributions are formally divergent as $\xi \to 0$, (albeit via an integrable singularity), such that one expects such terms to have a sizeable practical impact in cross-sections. Indeed, sub-eikonal effects have already been considered in [21, 22, 23, 24, 55, 25], based upon the inclusion of subleading terms in the collinear evolution kernel for the resummation. Another interesting proposal was presented in [27] (see [60] for a phenomenological application). However, a complete classification of the properties of next-to-eikonal logarithms has not yet appeared.

A step in this direction was presented in chapter 3. In that paper, the problem of soft gluon resummation was recast using path integral methods. A factorised form was assumed for Green's functions with a number of hard outgoing particles which emit any number of soft gluons. By recasting the propagators for the external particles (in the background of a soft gauge field) in terms of first-quantized path integrals, a field theory was found for the soft gauge field with source vertices localized along the external lines. Exponentiation of soft photon contributions (i.e. in abelian field theory) was shown to be straightforwardly related to the exponentiation of disconnected diagrams in quantum field theory, a well-known textbook result. Furthermore, the physical interpretation offered by the path integral technique allowed straightforward generalization of exponentiation to next-to-eikonal order. In the non-abelian case, the field theory for the soft gauge field was more complicated due to the fact that the source terms are matrix-valued in color space and, thus, non-commuting. However, it was possible to ascertain that a subset of diagrams exponentiate, and these were found to be precisely the webs of [45]. As in the abelian case, the extension to NE order was straightforward.

The final result of the previous chapter was a classification of the next-to-eikonal contributions to matrix elements, which have the schematic form (in both the abelian and non-abelian cases)

$$\mathcal{M} = \mathcal{M}_0 \exp\left[\mathcal{M}^{\mathrm{E}} + \mathcal{M}^{\mathrm{NE}}\right](1 + \mathcal{M}_r) + \mathcal{O}(NNE). \tag{4.4}$$

Here $\mathcal{M}_0$ is the Born contribution, and $\mathcal{M}^{\mathrm{E,NE}}$ collect the contributions due to emissions external to the hard interaction (eikonal and next-to-eikonal webs in the non-abelian case, and connected subdiagrams in the abelian case). The remainder term $\mathcal{M}_r$, also of NE order, arises from internal emission graphs i.e. those where an eikonal gauge boson from an external line lands inside the hard interaction. This contribution does not formally exponentiate, but has an iterative structure to all orders in perturbation theory. A derivation was presented in chapter 3, although this was essentially a rederivation of the Low-Burnett-Kroll theorem [18, 19].

The aim of this chapter is to show how the results of chapter 3 can also be obtained using a traditional Feynman diagram analysis. We use iterative methods to derive a set of effective Feynman rules for next-to-eikonal emissions, which agree with the results obtained using the path integral method. Armed with these modified Feynman rules, one may then show that a subset of soft gauge boson diagrams exponentiates, which are precisely the NE webs considered in [61]. This strengthens the validity of the conclusions reached by the path integral method.

Next-to-eikonal corrections were considered in only at the matrix element level. In order to predict soft logarithms in differential cross-sections, one must consider the phase space of the emitted soft gauge bosons. At eikonal level, exponentiation at cross-section level follows straightforwardly from the result for matrix elements, as the phase space for multiple photon or gluon emission can be written as a product of uncorrelated single boson phase spaces. At NE level this is no longer true, and in this paper we consider the appropriate generalization.

The structure of this chapter is as follows. In section 4.2 we review the derivation of exponentiation of soft corrections in the abelian and non-abelian cases using an iterative Feynman diagram method. In section 4.3 we derive effective Feynman rules for NE emissions. Crucial to this result is the fact that the sum over all NE diagrams has a factorisable form. These results will demonstrate exponentiation of a class of NE contributions (see eq.(4.123)), and we compare our conclusions with those obtained using the path integral method of the previous chapter. In section 4.4 we discuss subleading corrections to the eikonal form of the multi-boson phase space. In section 4.6 we apply the ideas derived in this paper to a simple phenomenological example, namely Drell-Yan production of a vector boson. Our aim here is not to conduct a thorough analysis of NE logarithms to all orders, but rather to clarify the somewhat technical discussion which precedes this application. Finally, in section 4.7 we discuss our results and conclude.

4.2 Introduction to eikonal exponentiation

Exponentiation of soft gauge boson corrections at the eikonal level was first shown for abelian theories in [43], and later generalized to non-abelian theories in [44, 45, 46]. Here we review the derivation of this result using Feynman diagram methods (see also [47] for a pedagogical exposition), both in order to make this chapter reasonably self-contained and also in order to introduce methods and notation that will prove

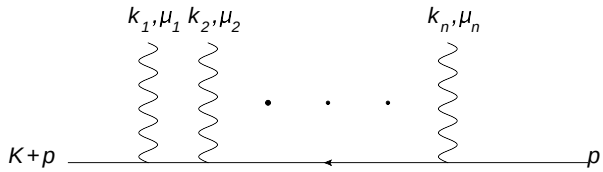

Figure 4.1: The basic eikonal line.

useful when generalizing to NE order.

The proof of exponentiation is two-fold. Firstly, one establishes a set of effective Feynman rules in the eikonal approximation (i.e. one must show that rules derived from lower order diagrams indeed hold to all orders in perturbation theory). Secondly, one uses these effective Feynman rules to classify a subset of diagrams which exponentiates. We first consider the simpler case of an abelian theory.

4.2.1 Abelian eikonal exponentiation

In order to derive the eikonal Feynman rules it is sufficient to consider a single hard external line of final off-shell momentum p, originating from some unspecified hard interaction. This may emit a number n of soft photons of momentum k_i, as depicted in figure 4.1, where k_1 lies closest to the hard interaction. In the case where the emitting particle is a scalar, such an external line contributes the following contribution to the scattering amplitude:

$$\frac{1}{(p+K_1)^2}(2p+K_2+K_1)^{\mu_1}\dots\frac{1}{(p+K_n)^2}(2p+K_n)^{\mu_n}, \tag{4.5}$$

where we have introduced quantities $\{K_i\}$ denoting the partial sum of gluon emissions starting from the on-shell end of the external line:

$$K_i=\sum_{m=i}^{n}k_m. \tag{4.6}$$

In the eikonal approximation in which $k_i\to 0$ for all photons i, eq. (4.5) becomes

$$\frac{1}{2pK_1}2p^{\mu_1}\dots\frac{1}{2pK_n}2p^{\mu_n}. \tag{4.7}$$

The analogue of eq. (4.5) for a fermionic emittor is

$$\frac{\not{p}+\not{K}_1}{(p+K_1)^2}\gamma^{\mu_1}\dots\frac{\not{p}+\not{K}_n}{(p+K_n)^2}\gamma^{\mu_n}u(p), \tag{4.8}$$

where $u(p)$ is the spinor associated with the final state on-shell particle. In the eikonal approximation, this reduces to

$$\frac{\not{p}}{2pK_1}\gamma^{\mu_1}\dots\frac{\not{p}}{2pK_n}\gamma^{\mu_n}u(p). \tag{4.9}$$

This is more complicated than the scalar case due to the non-trivial spinor structure. However, one may use the anticommutation property of the Dirac matrices

$$\{\not{p},\gamma^{\mu_i}\}=2p^{\mu}, \tag{4.10}$$

as well as the (massless) Dirac equation

$$\not{p}u(p)=0 \tag{4.11}$$

to move all factors of $\not{p}$ in equation (4.9) to the right-hand-side, leaving the result:

$$\frac{1}{2pK_1}2p^{\mu_1}\dots\frac{1}{2pK_n}2p^{\mu_n}u(p). \tag{4.12}$$

Note that the prefactor is the same expression as in the scalar case, which is the well-known result that in the eikonal approximation, emitted gauge bosons are insensitive to the spin of the emitting particle[1]. This factor can be further decomposed in a factorised form, which decouples each of the photon momenta. To do this, one first uses the fact that the above factor will be contracted with some quantity $I_{\mu_1\dots\mu_n}$ denoting the rest of the diagram, such that the squared amplitude has the form

$$|\mathcal{A}|^2=\left(\prod_i\frac{p^{\mu_i}}{p\cdot K_i}\right)I_{\mu_1\dots\mu_n}(k_1,\dots,k_n). \tag{4.13}$$

Here $I_{\mu_1\dots\mu_n}$ includes the phase space integration over the emitted soft photons, which in the eikonal approximation is a decoupled product of n one-photon phase space factors. Furthermore, $I_{\mu_1\dots\mu_n}$ may include a symmetric phase space condition leading to a differential cross-section. Given that individual photon emissions on the eikonal line also decouple from each other, it follows that one interchange momenta on the eikonal line to obtain a diagram yielding the same result (as can be seen by relabeling momenta). Then one may rewrite eq. (4.7) as

$$\frac{1}{2pK_1}2p^{\mu_1}\dots\frac{1}{2pK_n}2p^{\mu_n}=\frac{1}{n!}\sum_{\pi}\frac{1}{p\cdot k_{\pi_1}}\frac{1}{p\cdot(k_{\pi_1}+k_{\pi_2})}\dots\frac{1}{p\cdot(k_{\pi_1}+k_{\pi_2}+\dots k_{\pi_n})}, \tag{4.14}$$

where the sum π is over all permutations of the photon momenta, and k_{π_i} is the i^{th} momentum in a given permutation. There are $n!$ permutations, and each gives the

[1] In non-Abelian gauge theories the same is also true if the emitting particle is itself a (hard) gluon. However, there is a different color factor associated with the three-gluon vertex.

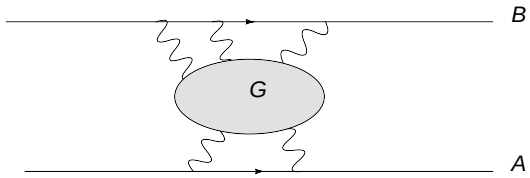

Figure 4.2: A process involving two eikonal lines A, B that interact through a soft blob.

same result, as follows from relabeling of the momenta and the fact that the multi-photon phase space is symmetric under interchange of any two photons. This can be simplified using the *eikonal identity*

$$\sum_{\pi} \frac{1}{p\cdot k_{\pi_1}} \frac{1}{p\cdot (k_{\pi_1}+k_{\pi_2})} \cdots \frac{1}{p\cdot (k_{\pi_1}+k_{\pi_2}+\ldots k_{\pi_n})} = \prod_i \frac{1}{p\cdot k_i}. \tag{4.15}$$

The simplest example of this identity occurs for the special case of two photon momenta, which gives

$$\frac{1}{p\cdot k_1}\frac{1}{p\cdot (k_1+k_2)} + \frac{1}{p\cdot k_2}\frac{1}{p\cdot (k_2+k_1)} = \frac{1}{p\cdot k_1}\frac{1}{p\cdot k_2}. \tag{4.16}$$

Using eq. (4.15), the factor eq. (4.7) arising from n soft emissions on an external line becomes

$$\prod_i \frac{p^\mu}{p\cdot k_i}. \tag{4.17}$$

That is, each eikonal emission is given by the effective Feynman rule

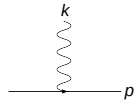

$$\frac{p^{\mu_i}}{p\cdot k}. \tag{4.18}$$

Having constructed the effective Feynman rule, one may proceed to demonstrate the exponentiation of soft photon corrections as follows. As an example, we consider the amplitude shown in figure 4.2, at a given order in the perturbation expansion. This consists of two eikonal lines, labeled A and B in the figure, each of which emits a number of soft photons. In general, one may then distinguish the subdiagram G consisting of soft photons and fermion loops. Photons from either eikonal line must land on the other eikonal line, or on a fermion loop in the sub-diagram G[2]. A photon cannot land on the same eikonal line, as the eikonal Feynman rules dictate that there

[2]that we take figure 4.2 to represent the squared amplitude. Real emissions then result from all possible additions of final state cuts.

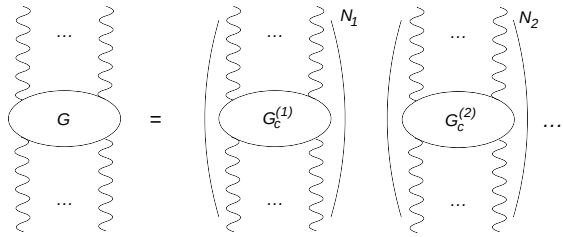

Figure 4.3: Decomposition of a soft photon subgraph into connected diagrams $G_c^{(i)}$, each of which occurs N_i times.

is a resulting factor $p^\mu p_\mu$, which is zero. Although we consider only two eikonal lines here, the following analysis generalizes to any number of emitting particles.

Using the effective eikonal Feynman rules, the expression for the squared amplitude resulting from figure 4.2 has the form

$$|\mathcal{A}|^2 = |\mathcal{A}_0|^2 \sum_G \left[\prod_i \frac{p_A^{\mu_i}}{p_A \cdot k_i}\right] \left[\prod_j \frac{p_B^{\nu_j}}{p_B \cdot l_j}\right] G_{\mu_1 \dots \mu_n;\nu_1 \dots \nu_m}, \tag{4.19}$$

where $|\mathcal{A}_0|^2$ is the squared amplitude without soft emissions, and k_i, l_j are the momenta of the photons emitted from lines A and B respectively, where $i \in \{1 \dots n\}$ and $j \in \{1 \dots m\}$. Given that we have already summed over permutations in order to obtain the eikonal Feynman rules, each subdiagram G has a unique decomposition in terms of connected subdiagrams, as indicated schematically in figure 4.3, where each possible connected subdiagram $G_c^{(i)}$ occurs N_i terms. According to the standard rules of perturbation theory, the subdiagram G has a symmetry factor corresponding to the number of permutations of internal lines and external lines which leave the diagram invariant[3]. This is given by

$$S_G = \prod_i (S_i)^{N_i} \, (N_i)!, \tag{4.20}$$

where S_i is the symmetry factor associated with each connected subdiagram G, and the factorial factors account for permutations of identical connected subdiagrams. Contracting the Lorentz indices in eq. (4.19), this may be written as

$$|\mathcal{A}|^2 = |\mathcal{A}_0|^2 \sum_{\{N_i\}} \prod_i \frac{1}{N_i!} [G_c^{(i)}]^{N_i} = |\mathcal{A}_0|^2 \prod_i \sum_{N_i} \frac{1}{N_i!} [G_c^{(i)}]^{N_i}, \tag{4.21}$$

where

$$G_c^{(i)} = \frac{1}{S_i} \left(\prod_k \frac{p_A^\mu}{p_A \cdot k}\right) \left(\prod_l \frac{p_B^\nu}{p_B \cdot l}\right) G^{(i)}_{\{\mu\},\{\nu\}} \tag{4.22}$$

[3]We consider the external lines of $G_{\mu_1 \dots \mu_n;\nu_1 \dots \nu_m}$ to be internal as they are internal in the full diagram.

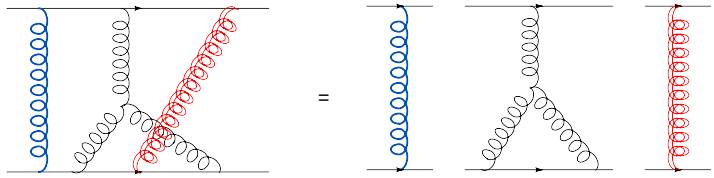

Figure 4.4: Decomposition of a higher order non-Abelian subgraph in terms of webs.

is the expression for each connected subdiagram (including its corresponding symmetry factor), with μ, ν the Lorentz indices of all associated photons. Recognizing eq. (4.21) as an exponential series, it follows that

$$|\mathcal{A}|^2 = |\mathcal{A}_0|^2 \exp\left[\sum_i G_c^{(i)}\right]. \tag{4.23}$$

That is, photon corrections exponentiate in the eikonal approximation, where the exponent contains connected subdiagrams. The same result was rederived in chapter 3 using path integral methods to relate this exponentiation to the known exponentiation of disconnected diagrams in quantum field theory.

4.2.2 Non-Abelian eikonal exponentiation

We now consider the generalization of exponentiation to non-abelian theories. The aim here is not to present a complete derivation (including explicit results for modified color factors etc.), but to introduce methods and notation that will prove useful in the extension to next-to-eikonal order. We will examine the simple case of two outgoing emitting particles connected by a color-singlet hard interaction, as happens in e.g. Drell-Yan production.

The proof of the abelian result relies crucially on the application of the eikonal identity after performing sums over the permutations of all gluon momenta on each eikonal line. In the non-abelian case, one is not able to apply this identity due to the presence of the noncommutating color matrices associated with each emission. However, exponentiation is still possible, but with a somewhat more complicated structure.

First we introduce the concepts of webs and groups. A *web* is a two-eikonal irreducible subdiagram i.e. a subgraph of the subdiagram G that cannot be disconnected by cutting the two eikonal lines. Higher order subdiagrams can be *decomposed* into sums of products of webs. An example is illustrated in figure 4.4, which shows a particular fourth order diagram which is not a web, and its subsequent decomposition into webs. Webs were introduced by [44, 45, 47].

Here we introduce a *group* as the projection of a web onto a single eikonal line [47]. That is, gluon emissions from an eikonal line belong to the same group if they belong

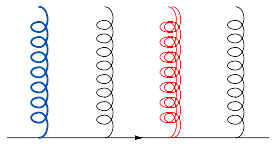

Figure 4.5: Gluon groups obtained from the lower eikonal line of figure 4.4, where the color identifications are the same as in that figure.

to the same web. This is illustrated in figure 4.5, where we depict the groups that result on the lower eikonal line of figure 4.4. Members of the same group have been given the same color.

Having introduced the concept of a group, one can also define a generalization of the eikonal identity [45, 47]. Let $\tilde{\pi}$ be a permutation of the gluons (with momenta $\{k_i\}$) on a given eikonal line of momentum p, but such that the ordering of the gluons in each group g is held fixed, so that not all permutations are allowed. Then one may write:

$$\sum_{\tilde{\pi}} \frac{1}{2p\cdot k_{\tilde{\pi}_1}} \frac{1}{2p\cdot(k_{\tilde{\pi}_1}+k_{\tilde{\pi}_2})} \cdots \frac{1}{p\cdot(k_{\tilde{\pi}_1}+\ldots+k_{\tilde{\pi}_n})} = \prod_g \frac{1}{2p\cdot k_{g_1}} \frac{1}{2p\cdot(k_{g_1}+k_{g_2})} \cdots \frac{1}{2p\cdot(k_{g_1}+\ldots+k_{g_m})}. \tag{4.24}$$

Here $k_{\tilde{\pi}_i}$ and k_{g_i} are the momentum of the i^{th} gluon in permutation $\tilde{\pi}$ and group g respectively, where g contains, say, m gluons. As an example of this result, consider an eikonal line with 3 gluon emissions, where gluons 1 and 2 are in one group, and gluon 3 in another. Then equation (4.24) amounts to the statement

$$\frac{1}{2p\cdot(k_1+k_2+k_3)} \frac{1}{2p\cdot(k_2+k_3)} \frac{1}{2p\cdot k_3} + \frac{1}{2p\cdot(k_1+k_3+k_2)} \frac{1}{2p\cdot(k_3+k_2)} \frac{1}{2p\cdot k_2} + \frac{1}{2p\cdot(k_3+k_1+k_2)} \frac{1}{2p\cdot(k_1+k_2)} \frac{1}{2p\cdot k_2} = \left(\frac{1}{2p\cdot(k_1+k_2)} \frac{1}{2p\cdot k_2}\right) \frac{1}{2p\cdot k_3}. \tag{4.25}$$

On the RHS one explicitly sees the factorization of gluons from different groups. From now on all permutations of gluon momenta, unless otherwise stated, involve fixed ordering of the gluons in each group. Thus we drop the tilde on the permutation symbols $\tilde{\pi}$ for brevity.

Next we examine contractions of soft gluons emanating from two emitting lines connected by a color singlet hard interaction. A given subdiagram spanning the external lines then has two color indices in the fundamental representation of the non-abelian gauge group (i.e. one from each eikonal line). By Schur's lemma, it follows

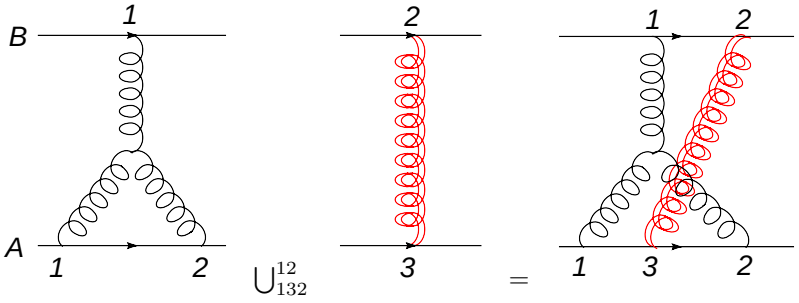

Figure 4.6: Illustration of the merging product $\cup_{\pi_A}^{\pi_B}$ between two eikonal graphs, where π_A and π_B are permutations of the gluons on eikonal lines A and B such that ordering within each group is held fixed.

that the color structure of a given subdiagram is proportional to the identity δ_{ij} in color space, where i and j are fundamental indices.

Consider two soft gluon subdiagrams H_1 and H_2 connecting the same two eikonal lines A and B. We denote by $E(G)$ the (eikonal) amplitude arising from subdiagram G, not including color matrices. That is, $E(G)$ encodes the momentum information carried by a particular subdiagram, but not its color structure, such that the form for a given subdiagram is

$$c_G \delta_{ij} E(G), \tag{4.26}$$

where c_G is the color factor associated with G. One may then apply the generalized eikonal identity, eq. (4.24), in reverse to write the product of two eikonal diagrams as follows:

$$E(H_1)E(H_2) = \sum_{\pi_A} \sum_{\pi_B} E(H_1 \cup_{\pi_A}^{\pi_B} H_2), \tag{4.27}$$

where $H_1 \cup_{\pi_A}^{\pi_B} H_2$ is the particular *merging* that results from combining H_1 and H_2 i.e. such that the gluon permutations on the eikonal lines are given by π_A and π_B. Note that there may be a different number of gluons on each external line. An example of this is shown in figure 4.6.

The merging of H_1 and H_2 can give some new diagrams G. The same diagram could result from different mergings, so that

$$E(H_1)E(H_2) = \sum_G E(G) N_{G|H_1 H_2}, \tag{4.28}$$

where the multiplicity $N_{G|H_1 H_2}$ denotes the number of ways that diagram G can result from mergings of H_1 and H_2. This generalizes immediately to the product of any

number of eikonal subdiagrams:

$$E(H_1)^{s_1}E(H_2)^{s_2}\dots E(H_n)^{s_n} = \sum_G E(G)N_{G|H_1^{s_1}H_2^{s_2}\dots H_n^{s_n}}, \tag{4.29}$$

where each diagram H_i occurs s_i times in the product. Suppose we expand

$$\exp\left\{\sum_H \bar{c}_H E(H)\right\}, \tag{4.30}$$

where the sum is over all subdiagrams H, each with an accompanying constant $\bar{c}_H$ whose interpretation will become clear in what follows. Note that these may be decomposable in terms of products of smaller subdiagrams. Using eq.(4.29) one finds

$$\exp\left\{\sum_H \bar{c}_H E(H)\right\} = \prod_H \left(\sum_n \frac{1}{n!}[\bar{c}_H E(H)]^n\right) = \sum_G c_G E(G), \tag{4.31}$$

where the sum on the right-hand side is again over all possible subdiagrams G (i.e. we use a different label on the left- and right-hand sides), and $\{c_G\}$ are constants that are undetermined at this point, but will become the usual color factors belonging to G (see eq. (4.26)). Expanding out the various terms in the exponential, one generates all possible products of subdiagrams. Each such product leads, after mergings, to a sum of subdiagrams (by eq. (4.29)), and thus contributes to various terms on the right-hand side of eq. (4.31). Each subdiagram H in the exponent thus appears on the right-hand side of eq. (4.31) in two ways. Either as itself (i.e. contributing only to the term where G is equal to H, so that indeed all terms one expects on the right-hand side are present), or as a merging ingredient for a larger subdiagrams G. Linear independence[4] of the subdiagrams then allows one to equate coefficients on the left- and right- hand sides of eq. (4.31), so that the choice of constants $\{c_G\}$ uniquely fixes, at least in principle, the constants $\{\bar{c}_H\}$. One now fixes these constants by requiring that the $\{c_G\}$ are the usual color factors of perturbation theory on the right-hand side. It can now be shown that the constants $\{\bar{c}_H\}$ are zero except for a subset of diagrams H which have the property of being two-eikonal line irreducible (i.e. the webs of [44, 45] and referred to above).

One proceeds as follows. First one notes that each subdiagram G has a set of decompositions into smaller subdiagrams H. This includes the case where G cannot be decomposed into smaller parts, and thus has only the trivial decomposition consisting of a single subdiagram H which is equal to G. A simple example is shown in figure 4.7. Each decomposition can be uniquely labeled by a set of numbers $\{m_H\}$ which specify how many times each subdiagram H occurs in the decomposition of G. In the simple example shown in figure 4.7, there are two decompositions labeled by $\{m_|, m_X\} = \{2, 0\}$ and $\{0, 1\}$, where the meaning of the notation $m_{|,X}$ is clear from the figure. In perfect analogy to (4.21), the expansion of the exponential in eq. (4.31) can be written

[4]The formal sum of all subdiagrams forms a vector space endowed with a product (see eq. (4.29). Any element in this vector space, e.g. a result of a merging, can be uniquely written as such a formal sum. This we exploit.

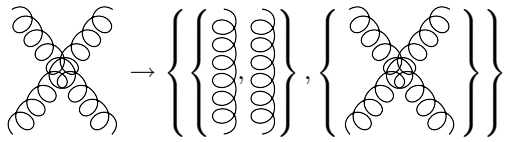

Figure 4.7: A diagram and its set of decompositions. The first decomposition has $m_| = 2$ and $m_X = 0$, the second decomposition has $m_| = 0$ and $m_X = 1$.

$$\prod_H \left(\sum_n \frac{1}{n!} [\bar{c}_H E(H)]^n \right) = \sum_{\{m_H\}} \prod_H \frac{1}{m_H!} [\bar{c}_H E(H)]^{m_H}. \tag{4.32}$$

Some explanatory remarks are in order. The sum on the right-hand side is over all sets of numbers $\{m_H\}$, which thus corresponds to summing over all possible decompositions. Each decomposition comes with a product of inverse factorials, stemming from the expansion of the exponential, and corresponding to the number of times each subdiagram appears in the decomposition. Inserting eq. (4.29) into eq. (4.32), the latter can be rewritten as

$$\sum_G E(G) \sum_{m_H} N_{G|\{H^{\{m_H\}}\}} \left(\prod_H \frac{1}{m_H!} (\bar{c}_H)^{m_H} \right). \tag{4.33}$$

Here $N_{G|\{H^{m_H}\}}$ is the number of ways that the diagram G can be formed out of the given decomposition specified by $\{m_H\}$. The expression now has the form of a single sum over all subdiagrams G (weighted by non-trivial coefficients) which can be matched to the right-hand side of eq. (4.31). One thus finds

$$c_G = \sum_{\{m_H\}} N_{G|\{H^{m_H}\}} \left(\prod_H \frac{1}{m_H!} (\bar{c}_H)^{m_H} \right). \tag{4.34}$$

This equation relates the coefficients $\bar{c}_H^{m_H}$ to the color factors $\{c_G\}$. A similar relation was given in [47], and the solution (in which the $\{\bar{c}_H\}$ are given explicitly in terms of the $\{c_G\}$) was derived in chapter 3. One may interpret the coefficients $\{\bar{c}_H\}$ as modified color factors for the diagrams appearing in the exponent of eq. (4.31). At present this equation appears to contain no information, as the full set of subdiagrams appears in both the exponent and on the right-hand side. Crucially however, the modified color factors are zero except for a subclass of subdiagrams, which are two-eikonal line irreducible, as we now show.

The proof proceeds inductively, where the first step is to separate the sum over decompositions $\{m_H\}$ on the right-hand side of eq. (4.34) into those terms involving a trivial decomposition, and those involving proper decompositions i.e. where G genuinely reduces to a product of smaller subdiagrams. That is, one may write eq. (4.34) as

$$c_G = \bar{c}_G + \sum_{\{m'_H\}} N_{G|\{H^{m'_H}\}} \left(\prod_H \frac{1}{m'_H!} (\bar{c}_H)^{m'_H} \right), \tag{4.35}$$

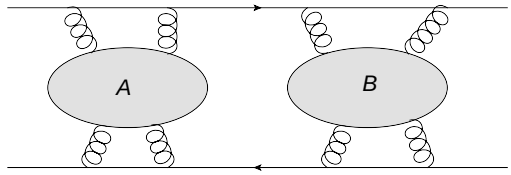

Figure 4.8: General form of a subdiagram which is two-eikonal line reducible.

where the prime denotes a proper decomposition, and the first term has come from the trivial decompositions. One now assumes that the fact that the modified color factors are zero for two-eikonal line irreducible subdiagrams has already been shown up to some given order, such that for the diagrams H appearing on the right-hand side can be taken to have this property. This will then be used to show that two eikonal-line irreducibility is there for G in (4.35) and therefore persists, by induction, to higher orders.

We consider a general two-eikonal line reducible diagram, shown in figure 4.8. The normal color factor for such a diagram is given by

$$c_{AB} = c_A \, c_B, \tag{4.36}$$

which follows from the fact that each reducible component of the subdiagram AB is proportional to the identity matrix in color space from Schur's lemma, as discussed earlier. The sum over proper decompositions for the diagram AB has the form (from eq. (4.35))

$$\sum_{\{m'_H\}} N_{AB|\{H^{m'_H}\}} \left(\prod_H \frac{1}{m'_H!} \bar{c}_H^{m'_H} \right), \tag{4.37}$$

where according to the above remarks each subdiagram H is two eikonal-line irreducible. This allows the multiplicity factor $N_{AB|\{H^{m'_H}\}}$ to be factorised. Each proper decomposition $\{m_H\}$ can be split into two parts denoted by $\{m_H^A\}$ and $\{m_H^B\}$, where the subdiagrams in each case contribute solely to A or B respectively. That no subdiagram H contributes to both A and B follows from the two-eikonal line irreducibility of the former. For each subdiagram H, one then has

$$m'_H = m_H^A + m_H^B, \tag{4.38}$$

which allows one to rewrite eq.(4.37) as follows:

$$\sum_{\{m_H^A\}} \sum_{\{m_H^B\}} N_{A|\{H^{m_H^A}\}} N_{B|\{H^{m_H^B}\}} \left(\prod_H \frac{1}{m'_H!} \mathbf{C}(m'_H, m_H^A) \bar{c}_H^{m'_H} \right), \tag{4.39}$$

where the combination function

$$\mathbf{C}(m'_H, m_H^A) = \frac{m'_H!}{(m_H^A)! \, (m_H^B)!} \tag{4.40}$$

has arisen from the number of ways in which the proper decomposition $\{m'_H\}$ can be partitioned. Eq. (4.39) can now be written as a product of sums depending separately on A and B i.e.

$$\left\{\sum_{\{m_H^A\}} N_{A|\{H^{m_H^A}\}}\left(\prod_H \frac{1}{(m_H^A)!}\bar{c}_H^{m_H^A}\right)\right\}\left\{\sum_{\{m_H^B\}} N_{B|\{H^{m_H^B}\}}\left(\prod_H \frac{1}{(m_H^B)!}\bar{c}_H^{m_H^B}\right)\right\}. \quad (4.41)$$

By eq. (4.34), this is equal to $c_A c_B$, i.e. the products of the color factors of the subdiagrams A and B. Combining this with eqs. (4.35,4.36) yields $\bar{c}_{AB} = 0$, i.e. the modified color factor for two eikonal-line reducible graph is zero, which is the desired result. The fact that the lowest order diagrams are two-eikonal irreducible completes the inductive proof.

In this section we have derived the exponentiation of soft gluon corrections for two eikonal lines coupled by a color singlet hard interaction, and in doing so have introduced methods and notation that will be useful in what follows. The non-abelian eikonal exponentiation may then be summarized as follows:

> *The amplitude from all diagrams involving soft-gluon emission from two eikonal lines exponentiates, where the exponent contains only a subset of diagrams (webs) $\{H_i\}$ with modified color factors $\{\bar{c}_i\}$.*

In the rest of this chapter, we consider the extension of this result to next-to-eikonal order.

4.3 Effective Feynman Rules at NE Order

In the previous section we reviewed the exponentiation of eikonal contributions to the scattering amplitude. The proof of this result involves the use of effective Feynman rules in the eikonal approximation i.e. when all emitted gluon momenta $k_i \to 0$. Armed with these Feynman rules, one may classify the subdiagrams involved in the exponentiation.

The proof of the existence of effective Feynman rules in the eikonal approximation relies crucially on the factorization of contributions from individual gluons (in the abelian case) and different gluon groups (in the non-abelian case).

In extending eikonal exponentiation to next-to-eikonal order (subleading by one power of gluon momentum), we also seek to identify effective Feynman rules which can be applied in calculating diagrams with at most one next-to-eikonal gluon insertion. We will see that it is indeed possible to obtain effective rules, and that this result again relies on the factorization of contributions from different gluon groups. The method used here is analogous to that used in the previous section, although we will also be able to compare our results with the Feynman rules obtained using the path integral approach in the previous chapter.

It will be shown that the effective Feynman rules for NE emission include vertices which couple gluon pairs to the emitting particles. This is perhaps to be ex-

pected, given that it is only at eikonal order that individual gluon contributions completely factorize. Similar considerations apply to the NE phase space considered in section 4.4.

The ensuing discussion will apply to both abelian and non-abelian gauge theories. We will again adopt the concept of *groups* of gluons, as defined in section 4.2. Recall that these take into account the fact that, in a non-Abelian gauge theory, gluon emissions from one of the external lines may be part of the same web (see figures 4.4 and 4.5).

The emission of gluons from fermions is complicated somewhat by the non-trivial structure in spinor space, as it is no longer true beyond the eikonal approximation that soft gauge boson emissions are insensitive to the spin of the emitting particle. Thus, we consider first the simpler case of a spinless emittor.

4.3.1 NE Emission from a spinless particle

Considering the expression for multiple gluon emission from an eikonal line (equation (4.5)), the most divergent contribution to the scattering amplitude is given by the eikonal approximation of equation (4.7), as noted previously. The NE contribution receives contributions from three sources

1. Subleading corrections to the gluon emission vertex, in which one of the emission vertices in the eikonal approximation is replaced as follows
$$2p^{\mu_i} \to (K_{i+1} + K_i)^{\mu_i}. \tag{4.42}$$
2. Taylor expansion of a propagator factor, which leads to a replacement of an eikonal propagator
$$\frac{1}{2p \cdot K_i} \to -\frac{K_i^2}{(2p \cdot K_i)^2}. \tag{4.43}$$
3. For a scalar emitting particle, there is a two-gluon vertex from the Lagrangian, as shown in figure 4.9. A diagram with one 2-gluon vertex has one eikonal propagator less then the corresponding diagram with the two gluons attached via two 1-gluon vertices and thus such a diagram contributes at NE order.

The full NE amplitude consists of a sum over all possible insertions of the above replacements on each of the external lines. The 2-gluon vertex has no analogue in the exact Feynman rules for emission from a fermion. We will see, however, that a 2-gluon vertex of this form arises in the effective Feynman rules for NE emissions from a fermion line, and consider such a case in the following subsection.

In what follows, it will be convenient to rewrite the NE emission vertex. Using $K_i + K_{i+1} = 2K_i - k_i$, one may rewrite eq. (4.42) as
$$2p^{\mu_i} \to 2K_i^{\mu_i} - k_i^{\mu_i}. \tag{4.44}$$
This decomposes the vertex into a part which depends only on a single gluon momentum, and a part that depends on a single partial sum of gluon momenta. Any

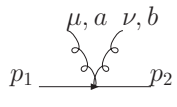

$$= g^{\mu\nu}\{T^a, T^b\}$$

Figure 4.9: The 2 gluon vertex arising in scalar field theories, which is absent for fermionic emitting particles.

vertex which explicitly depends only on local gluon momenta can be immediately interpreted as an effective Feynman rule, as the other gluon emissions will factorise upon application of the eikonal identity, as in section 4.2. The part of the vertex which still depends on a sum over many gluon momenta will be reconsidered in section 4.3.3.

4.3.2 NE Emission from a spin-$\frac{1}{2}$ particle

The analogue of equation (4.5) for emission from a fermion is given in equation (4.8), and the eikonal limit is given in equation (4.9). The spinor structure is reduced by anticommuting the factors of $\not{p}$ and using the Dirac equation, and one recovers the eikonal approximation of equation (4.7). From now on, we omit the on-shell spinor $u(p)$ from our equations for convenience.

At NE order, there are once again two types of contribution, arising from corrections to the vertex and to the propagators respectively. Taylor expansion of the propagators proceeds exactly as in the scalar case. Given that the numerator of the resulting expression is the same as in the eikonal approximation, the total propagator correction is the same as in the spinless case.

The vertex correction is more complicated, owing to the non-trivial spinor structure. The sum of all such corrections gives the following numerator:

$$\sum_{i=1}^{n} \not{p}\gamma^{\mu_1} \dots \not{K}_i \gamma^{\mu_i} \dots = \sum_{i=1}^{n} \not{p}\gamma^{\mu_1} \dots (2K_i^{\mu_i} - \gamma^{\mu_i}\not{K}_i) \dots , \tag{4.45}$$

where factors of $\not{p}$ to the right of the NE vertex insertion can be simplified using anticommutation and the Dirac equation (as in the eikonal case). Note that in the non-abelian case there is also a product of color matrices $T^{a_1} \dots T^{a_n}$ associated with the multiple emissions. We can omit these in subsequent equations, given that the order of gluon emissions is held fixed. Note that we have interchanged the order of $\not{K}_i^{\mu_i}$ and γ^{μ_i} on the right-hand side of equation (4.45), such that the sum over all NE gluon insertions can be written as two sums. The first is over terms having no spinor structure, thus one may anticommute all factors of $\not{p}$ through to the right-hand side, as in

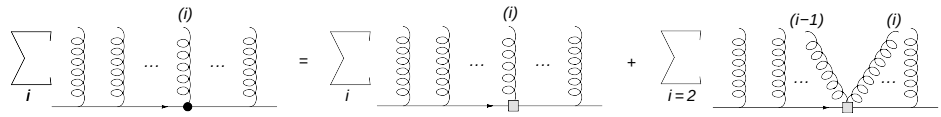

Figure 4.10: Schematic representation of the theorem given in equation (4.47). Here • denotes a vertex which depends upon a sum of gluon momenta, and □ a vertex depending only upon the momenta entering the vertex.

the eikonal case. One may then rewrite this sum using $2K_i = K_i + K_{i+1} + k_i$ as

$$\sum_{i=1}^{n}(2p^{\mu_1})\dots 2K_i^{\mu_i}\dots = \left[\sum_{i=1}^{n}(2p^{\mu_1})\dots(K_i+K_{i+1})^{\mu_i}\dots\right] + \sum_{i=1}^{n}(2p^{\mu_1})\dots k_i^{\mu_i}\dots. \tag{4.46}$$

The first summation on the right-hand side is the same as the sum over NE vertex corrections in the spinless case (section 4.3.1). The second summation is over terms which only depend upon a single gluon momentum.

For the second series of terms in equation (4.45), which still have a spinor structure, we will prove the following theorem

$$\sum_i \not{p}\gamma^{\mu_1}\dots\gamma^{\mu_i}\not{K}_i\dots = \sum_i 2p^{\mu_1}\dots\gamma^{\mu_i}\not{k}_i\dots + \sum_{i=2} 2p^{\mu_1}\dots 2pK_i\gamma^{\mu_{i-1}}\gamma^{\mu_i}\dots. \tag{4.47}$$

This theorem expresses the fact that the LHS of eq. (4.47) can be expressed via two sums. The first implements 1-gluon vertex corrections, each depending on the momentum of a single gluon. The second sum implements a new 2-gluon vertex, as can be seen from the fact that the factor $2p\cdot K_i$ in equation (4.47) is precisely such as to cancel the eikonal propagator connecting the two neighboring gluons i and $i-1$. We show this schematically in figure 4.10. We prove equation (4.47) by induction. First, we note that the theorem is obviously true for $n=1$ i.e. one gluon. Next, we must establish the validity of the theorem for n emissions, assuming its validity for $n-1$ emissions. To do this, one may rewrite the left-hand side of equation (4.47) so as to isolate the first gluon (i.e. furthest from the on-shell fermion)

$$\sum_i \not{p}\gamma^{\mu_1}\dots\gamma^{\mu_i}\not{K}_i\dots = \gamma^{\mu_1}\not{K}_1(2p^{\mu_2})\dots(2p^{\mu_n}) + \not{p}\gamma^{\mu_1}\sum_{i=2}^{n}\not{p}\gamma^{\mu_2}\dots\gamma^{\mu_i}\not{K}_i\dots. \tag{4.48}$$

Here we have used the fact that either the first gluon is eikonal (the first term on the RHS) or it is next-to-eikonal (the second term). For the sum in the second term, one may substitute the theorem for $n-1$ gluons to obtain

$$\begin{aligned}\sum_i \not{p}\gamma^{\mu_1}\dots\gamma^{\mu_i}\not{K}_i\dots = \gamma^{\mu_1}\not{K}_1 2p^{\mu_2}\dots + \not{p}\gamma^{\mu_1}\sum_{i=2}2p^{\mu_2}\dots\gamma^{\mu_i}\not{k}_i\dots + \\ \not{p}\gamma^{\mu_1}\sum_{i=3}2p^{\mu_2}\dots(2p\cdot K_i)\gamma^{\mu_{i-1}}\gamma^{\mu_i}\dots.\end{aligned} \tag{4.49}$$

In the second and third terms of equation (4.49), one may remove the factors of $\not{p}$ using anticommutation and the Dirac equation for the on-shell fermion. This can be achieved using the following commutators (acting implicitly on $u(p)$)

$$[\not{p}\gamma^\mu, \gamma^\nu \not{k}] = 2pk\gamma^\mu\gamma^\nu - \gamma^\mu \not{k} 2p^\nu, \tag{4.50}$$

$$[\not{p}\gamma^\rho, \gamma^\mu\gamma^\nu] = \gamma^\rho\gamma^\mu 2p^\nu - \gamma^\rho 2p^\mu\gamma^\nu. \tag{4.51}$$

One may use the first of these to rewrite equation (4.49)

$$\sum_i \not{p}\gamma^{\mu_1}\dots\gamma^{\mu_i}\not{K}_i\dots = \sum_{i=1}^n (2p^{\mu_1})\dots\gamma^{\mu_i}\not{k}_i\dots(2p^{\mu_n}) + \sum_{i=2}^n (2p^{\mu_2})\dots(2p\cdot k_i)\gamma^{\mu_1}\gamma^{\mu_i}\dots$$
$$+ \not{p}\gamma^{\mu_1}\sum_{i=3}^n (2p^{\mu_2})\dots(2p\cdot K_i)\gamma^{\mu_{i-1}}\gamma^{\mu_i}\dots. \tag{4.52}$$

The third sum on the RHS can be rewritten using equation (4.51) to give

$$\not{p}\gamma^{\mu_1}\sum_{i=3}^n \dots(2p\cdot K_i)\gamma^{\mu_{i-1}}\gamma^{\mu_i}\dots =$$
$$\sum_{i=3}\left[(2p^{\mu_1})\dots\gamma^{\mu_{i-1}}(2p\cdot K_i)\gamma^{\mu_i}\dots - \gamma^{\mu_1}\dots(2p\cdot K_i)\gamma^{\mu_i}\dots\right]$$
$$+\gamma^{\mu_1}(2p\cdot K_3)\gamma^{\mu_2}\dots + \sum_{i=3}^{n-1}\gamma^{\mu_1}\dots(2p\cdot K_{i+1})\gamma^{\mu_i}\dots, \tag{4.53}$$

where in the last line we have relabeled $i \to (i+1)$ in the summation, and explicitly brought out the $i=2$ term. Using $K_i - K_{i+1} = k_i$, and substituting back into equation (4.52), one finds

$$\sum_i \not{p}\gamma^{\mu_1}\dots\gamma^{\mu_i}\not{K}_i\dots = \sum_{i=1}(2p^{\mu_1})\dots\gamma^{\mu_i}\not{k}_i + \sum_{i=3}^n (2p^{\mu_1})\dots 2p\cdot K_i\gamma^{\mu_{i-1}}\gamma^{\mu_i}\dots \tag{4.54}$$
$$+\gamma^{\mu_1}\gamma^{\mu_2}(2p^{\mu_3})\dots(2p^{\mu_n})[2p\cdot K_3 + 2p\cdot k_2]. \tag{4.55}$$

Finally, the last line combines with the second sum on the RHS to give equation (4.47), which completes the proof of the latter.

Combining eqs. (4.46) and (4.47), one sees that the sum over all NE insertions on a fermion line leads to a sum of contributions where single and double NE emissions factorise (i.e. can be written in terms of a vertex which only depends on at most two gluon momenta), and a series of terms which still depends on sums of gluon momenta along the eikonal line. The latter, given by the first set of terms on the right-hand-side of eq. (4.46) together with the corrections from Taylor expansion of the propagators, are the same in case of a fermionic emitting particle as in the scalar case (eqs. (4.42) and (4.43)). The factors involving up to two gluon momenta can immediately be interpreted as effective NE Feynman rules. Firstly, there is a one gluon

vertex resulting from the second set of terms in eq. (4.46) and the first set of terms in eq. (4.47), which has the form

$$(k^\mu - \gamma^\mu \not{k})T^a. \tag{4.56}$$

Secondly, there is a two gluon emission vertex arising from the second set of terms in eq.(4.47), which has the form

$$\gamma^\mu \gamma^\nu T^a T^b \tag{4.57}$$

for correlated emission of two gluons. We have explicitly reinstated the color factors associated with each emission in the case of a non-abelian theory. For abelian theories these factors are absent. These contributions only depend upon the momenta emanating from the vertices, thus ultimately lead to a factorised expression for the amplitude after applying the eikonal identity as in the strictly eikonal case. This is not yet true, however, for the spin zero contributions to the 1-gluon emission vertex. We will see in the next section that the sum of these contribution can indeed be expressed in a factorised form, up to a remainder term expressing correlations between gluons in different groups.

First, it is interesting to note some properties of the above emission vertices. Using:

$$\gamma^\mu \not{k} = \frac{1}{2}\left([\gamma^\mu, \not{k}] + \{\gamma^\mu, \not{k}\}\right), \tag{4.58}$$

equation (4.56) may be rewritten as

$$\frac{k_\nu}{2}[\gamma^\mu, \gamma^\nu]T^a = 2ik_\nu \sigma^{\mu\nu} T^a, \tag{4.59}$$

where we have recognized the generators of the Lorentz group $\sigma^{\mu\nu} = -\frac{i}{4}[\gamma^\mu, \gamma^\nu]$. The physical interpretation of this vertex, which does not occur for scalar emitting particles, is now clear i.e. it is a magnetic moment vertex (chromo-magnetic in the non-abelian case) associated with the interaction between the spin of the emitting particle, and the emitted soft boson. That this occurs for the first time at NE order is consistent with the fact that, in the eikonal approximation, emitted radiation is insensitive to the spin of the emittor.

One may rewrite equation (4.57) as

$$g^{\mu\nu} T^a T^b + \frac{1}{2}[\gamma^\mu, \gamma^\nu]T^a T^b. \tag{4.60}$$

In any given diagram, one sums over both orderings π of the gluon momenta entering the vertex. Then one has

$$\sum_\pi \gamma^\mu \gamma^\nu T^a T^b = g^{\mu\nu}\{T^a, T^b\} + \frac{1}{2}[\gamma^\mu, \gamma^\nu][T^a, T^b]. \tag{4.61}$$

The first term has the same form as the spin 0 gluon vertex, and the second term again involves the Lorentz generators $\sigma^{\mu\nu}$. The latter term vanishes in abelian gauge theories (i.e. when $[T^a, T^b] = 0$), thus contributes a non-abelian component of the

chromo-magnetic moment. As in the scalar case, it will be convenient to rewrite the NE vertex for one gluon emission, such that this is left as $2K_i$ in eq. (4.45). Then the part of the emission vertex which still depends on sums of momenta involves only a single partial sum, which simplifies the analysis in the following sections.

In this section we have demonstrated the existence of a set of effective Feynman rules describing next-to-eikonal emissions. Some of these rely on individual momenta ((4.59) and (4.60)), whereas others ((4.42) and (4.43)) rely still upon partial sums of gluon momenta. This is analogous to the eikonal case, in which the eikonal Feynman rule having the form of eq. (4.18) is applied using partial momentum sums. Crucial to the eventual exponentiation of soft gauge boson corrections is the factorization of gluon or photon emissions. In the abelian case, this results from the application of the eikonal identity which ultimately factorises all individual photon emissions. In the non-abelian case, the generalized eikonal identity is applied. Individual gluon emissions do not completely factorise, but the contribution of each *group* (as defined in section 4.2.2) does. This latter property ensures the exponentiation of soft gluon effects, as shown also in that section.

We now consider the extension of these same methods to NE order. Having derived effective Feynman rules, the next step is to show that contributions from different gluon groups factorise. As in the eikonal case, one may factor off the color structure of subdiagrams (c.f. eq. (4.26), and then show factorization of the momentum structure arising from the NE Feynman rules. This factorization procedure is more complicated than at eikonal order (i.e. one lacks the relatively simple form of the generalized eikonal identity), and in fact introduces extra effective Feynman rules which correlate the emissions of pairs of gluons from different groups. This is the subject of the following subsection.

4.3.3 factorization of next-to-eikonal diagrams

In the previous section we have seen that there are two classes of effective Feynman rule at NE order. Firstly, there are those depending on the specific momentum associated with a particular gluon emission. Secondly, there are those that still rely on partial sums of gluon momenta. The first type of rule lead simply to the factorization of NE contributions from different gluon groups, using the same generalized eikonal identity as in the eikonal approximation. More work is needed to show that the contribution from the second type of Feynman rule indeed leads to factorization of the contributions from different groups. We will see in this section that such a factorization does indeed occur, up to a remainder term which implements correlations between pairs of gluon emissions from different groups. However, the resulting structure is still sufficient to achieve exponentiation of NE effects in terms of a subset of diagrams, as shown later.

There are two Feynman rules which depend on partial momentum sums, arising from propagator or vertex corrections. As discussed in the previous section, the prop-

agator correction has the form

$$\frac{K^2}{(2p\cdot K)^2}2p^{\mu_l}, \tag{4.62}$$

and the vertex correction has the form

$$\frac{2K^{\mu_l}}{2p\cdot K}, \tag{4.63}$$

i.e. where K here potentially represents a partial momentum sum rather than a single momentum. Given that each diagram at NE order has either a vertex or a propagator correction (but not both), we can consider these two types of correction separately in what follows.

First we introduce some convenient notation. As in the eikonal case, we partition the n emitted gluons in figure 4.1 into groups g. That is, gluons in the same group belong to the same two-eikonal irreducible subgraph (web). Gluons are labeled along a given eikonal line as in figure 4.1 i.e. from 1 to n, where the index increases away from the hard interaction. Then we sum over permutations such that the order of gluons in each group is held fixed, and denote such a permutation by π. The order of gluons along the line in any given permutation is then given by $\pi_1 \dots \pi_n$, where π_i labels the i^{th} insertion away from the hard interaction in permutation π.

Furthermore, we introduce a label l denoting those gluons which are the first gluon of a group. The group which contains this gluon we label by $g(l)$. The notation G_k denotes the partial momentum sum of gluons in group g, from gluon k up to gluon m (where g contains m gluons), and we shorten G_1 to G (i.e. the sum of all momenta in group g). We also define

$$\tilde{g} = \begin{cases} g, & g \neq g_l \\ g\backslash\{l\}, & g = g_l \end{cases}, \tag{4.64}$$

i.e. a tilde over a group denotes that group without the first gluon (if indeed it contains gluon l).

To clarify the above definitions, we consider the simple case of two gluon groups depicted in figure 4.11, where we label the various gluon emissions by upper and lower case letters corresponding to each group. Figure 4.11(a) shows a given eikonal line with two gluon groups $g = \{A, B, C\}$ and $h = \{a, b\}$. In this permutation, one has $\pi = (A, a, B, C, b\}$. Figure 4.11(b) corresponds to a different permutation, i.e. $\pi = (A, B, a, b, C)$, where the order of gluons in each group is not changed.

Also in fig. 4.11, the label l takes the values $\{A, a\}$, where $g(A) = g$ and $g(a) = h$. The partial momentum sums G and H in each case are given by $G = k_A + k_B + k_C$ and $H = k_a + k_b$. Finally, if $l = A$ then one has $\tilde{g} = \{B, C\}$ and $\tilde{h} = \{a, b\}$; alternatively, if $l = a$ then one has $\tilde{g} = \{A, B, C\}$ and $\tilde{h} = \{b\}$.

We define the combined eikonal vertex and propagator

$$\mathrm{E}^{\mu}(k) = \frac{2p^{\mu}}{2p\cdot k}, \tag{4.65}$$

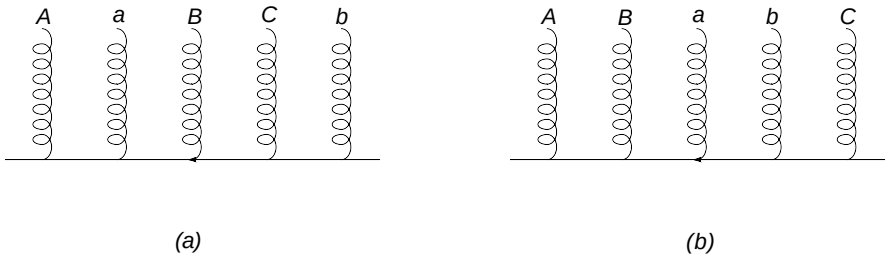

Figure 4.11: Simple example of two groups of gluon emissions on a single eikonal line. See the discussion in the text.

and also NE^{μ} to be the NE correction from either the propagator (eq. (4.62)) or vertex (eq. (4.63)) correction. Furthermore, we write

$$\begin{aligned}
\mathrm{NE}(\pi) &= \sum_{i=1}^{n} \mathrm{E}^{\mu_{\pi_1}}(K_1^{\pi}) \ldots \mathrm{NE}^{\mu_{\pi_i}}(K_i^{\pi}) \ldots, \\
\mathrm{NE}'(\pi) &= \sum_{i=2}^{n} \mathrm{E}^{\mu_{\pi_1}}(K_1^{\pi}) \ldots \mathrm{NE}^{\mu_{\pi_i}}(K_i^{\pi}) \ldots, \\
\mathrm{NE}_1(\pi) &= \mathrm{NE}^{\mu_{\pi_1}}(K_1^{\pi}) \mathrm{E}^{\mu_{\pi_2}}(K_2^{\pi}) \ldots,
\end{aligned} \tag{4.66}$$

which will be convenient in the following proof. Here $\mathrm{NE}(\pi)$ is the sum over all possible NE insertions, for a given permutation π (with obvious extension of this notation to groups g). For a given permutation, K_i^{π} is the partial momentum sum from gluon i (defined w.r.t. the hard interaction) up to gluon n (furthest from the hard interaction). I.e. this is the analogue of the partial momentum sum K_i introduced in eq. (4.6). Also in eq. (4.66), $\mathrm{NE}'(\pi)$ is a sum over all insertions, where the first gluon is restricted to be eikonal; $\mathrm{NE}_1(\pi)$ is the term resulting when the first gluon in permutation π (i.e. furthest from the on-shell fermion) is NE. Thus one has

$$\mathrm{NE}(\pi) = \mathrm{NE}'(\pi) + \mathrm{NE}_1(\pi). \tag{4.67}$$

We can now state the theorem

$$\sum_{\pi} \mathrm{NE}(\pi) = \sum_{h} \mathrm{NE}(h) \prod_{g \neq h} E(g) + \ldots, \tag{4.68}$$

where h and g are groups, and the ellipsis denotes a remainder term whose discussion we postpone until section 4.3.4. This can be summarized as follows

> *Up to a remainder term involving two gluon correlations between different groups, the sum of all possible NE diagrams is a sum of terms in which the groups are factorised. Each term contains a NE gluon insertion in a given group.*

This is the NE extension of the factorization of groups in the eikonal case, which was expressed by the generalized eikonal identity, and will result in exponentiation (eq.(4.123)).

The proof is by induction. First, we note that the theorem is true for a single gluon. Next, we separate out the first gluon (i.e. next to the hard interaction) from the sum over permutations. This gluon, being the first along the line, will also be the first gluon of a group. Thus, it will be labeled by l, and belong to the group $g(l)$. Furthermore, it will either be eikonal or NE. Thus, using the notation introduced above, one may write

$$\sum_{\pi} \mathrm{NE}(\pi) = \sum_{l} \mathrm{NE}^{\mu_l}(K) \sum_{\tilde{\pi}} \mathrm{E}(\tilde{\pi}) + \sum_{l} \mathrm{E}^{\mu_l}(K) \sum_{\tilde{\pi}} \mathrm{NE}(\tilde{\pi}), \tag{4.69}$$

where $K = \sum_i k_i$ is the sum of all emitted gluon momenta. As is perhaps clear from the above definitions, $\tilde{\pi}$ represents a permutation of all but gluon l, where the order in each group is held fixed. In the first term, one may use the eikonal identity for all but the first gluon

$$\sum_{\tilde{\pi}} E(\tilde{\pi}) = \prod_{g} E(\tilde{g}). \tag{4.70}$$

In the second term, one may use the validity of the conjecture (4.68) for $n-1$ gluons to obtain

$$\sum_{\pi} \mathrm{NE}(\pi) = \sum_{l} \mathrm{NE}^{\mu_l}(K) \prod_{g} \mathrm{E}(\tilde{g}) + \sum_{l} \mathrm{E}^{\mu_l}(K) \sum_{h} \mathrm{NE}(\tilde{h}) \prod_{g \neq h} \mathrm{E}(\tilde{g}) + \dots. \tag{4.71}$$

Here we have ignored the remainder term - we return to this point in section 4.3.4. The next two subsections consider separately the cases where NE^{μ_l} represents the propagator and vertex corrections of eqs. (4.62, 4.63), and prove that for both of these eq. (4.71) is indeed equal to (4.68), up to a remainder.

The NE propagator

In this subsection we have explicitly

$$\mathrm{NE}^{\mu_l}(k) = \frac{k^2}{(2p\cdot k)^2} 2p^{\mu_l}, \tag{4.72}$$

i.e. the NE contribution contains the Taylor-expanded propagator, as well as the eikonal vertex factor. Let us first consider the first term of equation (4.71). Here one may write

$$\mathrm{NE}^{\mu_l}(K) = \frac{K^2}{(2p\cdot K)^2} 2p\cdot G_l \mathrm{E}^{\mu_l}(G_l), \tag{4.73}$$

where the factor $2p\cdot G_l$ cancels the eikonal propagator in $\mathrm{E}^{\mu_l}(G_l)$. Substituting this into the first term of equation (4.71) and using

$$\mathrm{E}^{\mu_l}(G_l) \prod_{g} \mathrm{E}(\tilde{g}) = \prod_{g} \mathrm{E}(g), \tag{4.74}$$

one has

$$\sum_l \mathrm{NE}^{\mu_l}(K)\prod_g \mathrm{E}(\tilde{g}) = \left(\prod_g \mathrm{E}(g)\right)\frac{K^2}{(2pK)^2}\sum_l 2pG_l. \tag{4.75}$$

Now we may use the fact that $\sum_l G_l = K$ (i.e. the sum of all partial momenta in every group is the same as the sum of all momenta along the line) to write this as

$$\sum_l \mathrm{NE}^{\mu_l}(K)\prod_g \mathrm{E}(\tilde{g}) = \frac{K^2}{(2p\cdot K)}\prod_g \mathrm{E}(g). \tag{4.76}$$

We now use the fact that

$$K^2 = \sum_l G_l^2 + \sum_l\sum_{r\neq l} G_l\cdot G_r. \tag{4.77}$$

The cross-terms involve correlated emissions of gluons in different groups, and thus enter the remainder term, to be discussed later. For the G_l^2 terms, and noting

$$\mathrm{NE}_1(g_l) = \frac{G_l^2 2p^{\mu_l}}{(2p\cdot G_l)^2}\mathrm{E}(\tilde{g}_l) = \frac{G_l^2}{2p\cdot G_l}\mathrm{E}(g_l), \tag{4.78}$$

(where we have absorbed an eikonal numerator and denominator in $E(g_l)$) one obtains

$$\sum_l \mathrm{NE}^{\mu_l}(K)\prod_g \mathrm{E}(\tilde{g}) = \sum_l \frac{2p\cdot G_l}{2p\cdot K}\mathrm{NE}_1(g_l)\prod_{g\neq g_l}\mathrm{E}(g). \tag{4.79}$$

Next, we consider the second term in equation (4.71). In this term, either $h = g_l$ or $h \neq g_l$. Thus one may write

$$\begin{aligned}\sum_l \mathrm{E}^{\mu_l}(K)\sum_h \mathrm{NE}(\tilde{h})\prod_{g\neq h}\mathrm{E}(\tilde{g}) = &\sum_l \mathrm{E}^{\mu_l}(K)\mathrm{NE}(\tilde{g}_l)\prod_{g\neq g_l}\mathrm{E}(g)\\ &+\sum_l \mathrm{E}^{\mu_l}(K)\sum_{h\neq g_l}\mathrm{NE}(h)\prod_{g\neq h}\mathrm{E}(\tilde{g}),\end{aligned} \tag{4.80}$$

where in the second term one may use the fact that h does not contain gluon l to replace $\tilde{h}\to h$. Using the fact that

$$\mathrm{E}^{\mu_l}(K) = \frac{2p\cdot G_l}{2p\cdot K}\mathrm{E}^{\mu_l}(G_l), \tag{4.81}$$

one finds

$$\begin{aligned}\sum_l \mathrm{E}^{\mu_l}(K)\sum_h \mathrm{NE}(\tilde{h})\prod_{g\neq h}\mathrm{E}(\tilde{g}) = &\sum_l \frac{2p\cdot G_l}{2p\cdot K}\mathrm{NE}'(g_l)\prod_{g\neq g_l}\mathrm{E}(g)\\ &+\sum_l\sum_{h\neq g_l}\frac{2p\cdot G_l}{2p\cdot K}\mathrm{NE}(h)\prod_{g\neq h}\mathrm{E}(g).\end{aligned} \tag{4.82}$$

In the first term on the right-hand side, we have used the definition (4.66) for $\mathrm{NE}'(g_l)$ to recognize

$$\mathrm{NE}'(g_l) = \mathrm{E}^{\mu_l}(G_l)\mathrm{NE}(\tilde{g}_l). \tag{4.83}$$

In the second term on the right-hand side of eq. (4.82) we have used the fact that

$$\mathrm{E}^{\mu_l}(G_l)\prod_{g\neq h}\mathrm{E}(\tilde{g}) = \prod_{g\neq h}\mathrm{E}(g). \tag{4.84}$$

We may now recombine eq. (4.82) with eq. (4.80). In doing so, the first term on the right-hand side of eq. (4.82) combines with the right-hand side of eq. (4.80) using eq. (4.67) and one finds

$$\begin{aligned}\sum_{\pi}\mathrm{NE}(\pi) &= \sum_l \frac{2p\cdot G_l}{2p\cdot K}\mathrm{NE}(g_l)\prod_{g\neq g_l}\mathrm{E}(g) + \sum_l\sum_{h\neq g_l}\frac{2p\cdot G_l}{2p\cdot K}\mathrm{NE}(h)\prod_{g\neq h}\mathrm{E}(g) + \dots \\ &= \sum_l \frac{2p\cdot G_l}{2p\cdot K}\sum_h \mathrm{NE}(h)\prod_{g\neq h}\mathrm{E}(g) + \dots,\end{aligned} \tag{4.85}$$

where the ellipsis again denotes the remainder term. in the second line, we have used

$$\sum_h = \sum_{h=g_l} + \sum_{h\neq g_l}. \tag{4.86}$$

Using $\sum G_l = K$, this indeed gives the right-hand side of eq. (4.68), which is the desired result.

The NE vertex

In this subsection we have

$$\mathrm{NE}^{\mu_l}(k) = \frac{2k^{\mu_l}}{2p\cdot k}, \tag{4.87}$$

where we recall that we rewrote the NE emission vertex in both sections 4.3.1 and 4.3.2 to involve only one partial momentum sum rather than $K_i + K_{i+1}$. Using

$$K^{\mu_l} = G_l^{\mu_l} + \sum_{k\neq l} G_k^{\mu_k}, \tag{4.88}$$

the first term of equation (4.71) can be written

$$\begin{aligned}\sum_l \mathrm{NE}^{\mu_l}(K)\prod_{\tilde{g}}\mathrm{E}(\tilde{g}) = &\sum_l \frac{2p\cdot G_l}{2p\cdot K}\mathrm{NE}_1(g_l)\prod_{g\neq g_l}\mathrm{E}(g) \\ &+ \sum_l\sum_{k\neq l}\frac{2G_k^{\mu_l}}{2p\cdot K}\prod_{\tilde{g}}\mathrm{E}(\tilde{g}),\end{aligned} \tag{4.89}$$

where we have used the fact that

$$NE_1(g_l) = \frac{2G_l^{\mu_l}}{2p \cdot G_l} E(\tilde{g}_l). \tag{4.90}$$

The second term in eq. (4.89) involves correlations between gluons in different groups, and enters the remainder term to be discussed later. The first term has the same form as the analogous result for the propagator correction (eq. (4.79)).

For the second term in equation (4.71) one proceeds similarly as in section 4.3.3. eqs. (4.80)-(4.82) apply also in the case of the vertex correction, given that the form of $\mathrm{NE}(g)$ is not explicitly specified there. Given the forms of eq. (4.79) and the first term of eq. (4.89) are the same, combining the latter with eq. (4.82) leads (as in the previous subsection) to the right-hand side of eq. (4.68), which is the desired result.

4.3.4 The remainder term

In the preceding subsections, we have proved the form of equation (4.68), expressing the fact that the total NE matrix element is a sum of terms where the groups are factorised. As stated above, this holds true up to a remainder term expressing the correlated emission of pairs of gluons in different groups, which can be seen to arise from neglected contributions in the derivation of section 4.3.3. We will see that the exact formulation of equation (4.68) can be written as

$$\sum_{\pi} \mathrm{NE}(\pi) = \sum_{h} \mathrm{NE}(h) \prod_{g \neq h} \mathrm{E}(g) + \sum_{g \neq h} R(g,h) \prod_{f \neq \{g,h\}} \mathrm{E}(f), \tag{4.91}$$

where the term $R(g,h)$ receives separate contributions from the propagator and vertex corrections of eqs. (4.62,4.63). Again, given that each NE diagram has only one of these types of correction, we may consider the two types separately and write

$$R(g,h) = R^p(g,h) + R^v(g,h) \tag{4.92}$$

i.e. the sum of the propagator and vertex contributions respectively.

The strategy for obtaining the remainder is as follows. One repeats the inductive step in the proof of the preceding subsections, to obtain

$$\begin{aligned} \sum_{\pi} \mathrm{NE}(\pi) = &\sum_{l} \mathrm{NE}^{\mu_l}(K) \prod_{g} \mathrm{E}(\tilde{g}) + \sum_{l} \mathrm{E}^{\mu_l}(K) \sum_{h} \mathrm{NE}(\tilde{h}) \prod_{g \neq h} \mathrm{E}(\tilde{g}) \\ &+ \sum_{l} \mathrm{E}^{\mu_l}(K) \sum_{g \neq h} R(\tilde{g}, \tilde{h}) \prod_{f \neq \{g,h\}} E(\tilde{f}). \end{aligned} \tag{4.93}$$

In our derivation in section 4.3.3 we ignored the remainder. In particular we ignored the cross terms in eqs. (4.77)) and (4.88). Including these terms now in eq. (4.85),

we find

$$\sum_{\pi}\mathrm{NE}(\pi)=\sum_{h}\mathrm{NE}(h)\prod_{g\neq h}E(g)+\sum_{l}\mathrm{E}^{\mu_l}(K)\sum_{g\neq h}R(\tilde{g},\tilde{h})\prod_{f\neq\{g,h\}}E(\tilde{f})$$
$$+\sum_{l\neq r}\frac{G_l\cdot G_r}{2p\cdot K}\prod_{g}E(g)+\sum_{r\neq l}\frac{2G_r^{\mu_l}}{2p\cdot K}\prod_{g}E(\tilde{g}). \tag{4.94}$$

Implementing the separation of eq. (4.92), the first term in the last line contributes, by definition, to R^p, whereas the second term contributes to R^v. Equating eqs. (4.94) and (4.91) yields the relations

$$\sum_{g\neq h}R^p(g,h)\prod_{f\neq\{g,h\}}E(f)=\sum_{l}\mathrm{E}^{\mu_l}(K)\sum_{g\neq h}R^p(\tilde{g},\tilde{h})\prod_{f\neq\{g,h\}}E(\tilde{f})$$
$$+\sum_{g\neq h}\frac{G\cdot H}{2p\cdot K}\mathrm{E}(g)\mathrm{E}(h)\prod_{f\neq g,h}\mathrm{E}(g); \tag{4.95}$$
$$\sum_{g\neq h}R^v(g,h)\prod_{f\neq\{g,h\}}E(f)=\sum_{l}\mathrm{E}^{\mu_l}(K)\sum_{g\neq h}R^v(\tilde{g},\tilde{h})\prod_{f\neq\{g,h\}}E(\tilde{f})$$
$$+\sum_{g\neq h}\frac{2H^{\mu_{g_1}}}{2p\cdot K}\mathrm{E}(\bar{g})\mathrm{E}(h)\prod_{f\neq g,h}\mathrm{E}(f). \tag{4.96}$$

which may be solved for the remainder terms $R^{p,v}$. Note that we have relabeled the sum in the penultimate term on the right-hand side in eq. (4.94):

$$\sum_{l\neq r}\equiv\sum_{g\neq h}, \tag{4.97}$$

i.e. the sum over all first gluons is equivalent to a sum over all groups, with $g=g_l$ and $h=h_r$. We have also introduced G and H as the sum of all momenta in groups g and h respectively. Here we will just write down these solutions, and show they indeed satisfy eqs.(4.95) and (4.96).

Firstly, the solution to equation (4.96) is

$$R^v(g,h)=\sum_{\pi}^{(g,h)}\sum_{i,\pi_i\in g}\sum_{j>i,\pi_j\in h}(2h_j^{\mu_{g_i}})E(\pi). \tag{4.98}$$

Some explanatory remarks are in order. In the first sum π is a given permutation of the gluons in groups g and h, such that the order of gluons in each group is held fixed in the merging of the two. A given term in the remaining sums then picks out pairs of gluons (one from each group), such that the gluon from h is further from the hard interaction than the gluon from g. For each such pair of gluons, the NE vertex correction is applied, where $h_j^{\mu_{g_i}}$ is the momentum of the gluon from h (i.e. rather than a partial momentum sum).

The proof of eq. (4.98) is obtained by substituting the solution into eq. (4.96) to obtain

$$\sum_{g\neq h} R^v(g,h) \prod_{f\neq g,h} \mathrm{E}(f) = \sum_{g\neq h} \frac{2H^{\mu_{g_1}}}{2p\cdot(G+H)} \frac{2p(G+H)}{2p\cdot K} \mathrm{E}(\bar{g})\mathrm{E}(h) \prod_{f\neq g,h} \mathrm{E}(f) + \sum_l \mathrm{E}^{\mu_l}(K) \sum_{g\neq h} R^v(\tilde{g},\tilde{h}) \prod_f \mathrm{E}(\tilde{f}), \tag{4.99}$$

In the second term one may distinguish the cases in which the gluon l is not in g or h ($l \notin \{g,h\}$) from those in which $l \in g$ and $l \in h$. Then the term in the lower line of eq.(4.99) can be split into three separate terms corresponding to each of these cases, and one gets

$$\begin{aligned}\sum_{g\neq h} R^v(g,h) \prod_{f\neq g,h} \mathrm{E}(f) = &\sum_{g\neq h} \frac{2H^{\mu_{g_1}}}{2p\cdot(G+H)} \frac{2p(G+H)}{2p\cdot K} \mathrm{E}(\bar{g})\mathrm{E}(h) \prod_{f\neq g,h} \mathrm{E}(f) \\ &+ \sum_{g\neq h} R^v(g,h) \sum_{l\notin\{g,h\}} \frac{2p\cdot G_l}{2p\cdot K} \prod_f \mathrm{E}(f) \\ &+ \sum_{g\neq h} \frac{2p\cdot(G+H)}{2p\cdot K} \mathrm{E}^{\mu_{g_1}}(G+H) R^v(\bar{g},h) \prod_f \mathrm{E}(f) \\ &+ \sum_{g\neq h} \frac{2p\cdot(G+H)}{2p\cdot K} \mathrm{E}^{\mu_{h_1}}(G+H) R^v(g,\bar{h}) \prod_f \mathrm{E}(f)\end{aligned} \tag{4.100}$$

Note that we have again used eq. (4.81) to rewrite $E^{\mu_l}(K)$ in terms of group partial momentum sums. Also, we have introduced the notation $\bar{g}$, which designates the group g without its first gluon (i.e. $\tilde{g} = \bar{g}$ if $l \in g$). The fourth line contains all mergings of g and h such that the first gluon along the line (i.e. next to the hard interaction) comes from the group h. This gluon does not couple to any of the gluons in g (due to the restriction $i < j$ from eq.(4.98)). The third line contains all mergings such that the first gluon along the line is a gluon from g, and does not couple to any of the gluons in h. In the first line, the generalized eikonal identity implies

$$E(\bar{g})E(h) = \sum_{\pi}^{(\bar{g},h)} E(\pi), \tag{4.101}$$

i.e. the right-hand side contains a sum over all mergings of $\bar{g}$ and h. The validity of eq. (4.98) can be demonstrated (after some straightforward but tedious algebra) as follows. After substituting eq. (4.98) into eq. (4.100), the first and third lines combine to give all contributions where the first gluon along the line comes from the group g. This then combines with the fourth line to give the sum over all possible mergings, with a prefactor in the sum of $2p\cdot(G+H)/2p\cdot K$. Finally, this combines with the

second term to give a total prefactor

$$\frac{2p\cdot(G+H)}{2p\cdot K}+\sum_{l\notin\{g,h\}}\frac{2p\cdot G_l}{2p\cdot K}=1. \tag{4.102}$$

Equating the result to the left-hand-side of eq. (4.100), one finds after careful accounting that $R^v(g,h)$ is given by eq. (4.98), i.e. that this is indeed the solution to eq. (4.96).

The solution to the relation (4.95) for the propagator correction is given by

$$R^p(g,h)=\sum_{\pi(g,h)}\sum_{i,\pi_i\in g}\sum_{j>i,\pi_j\in h}\frac{G_i\cdot h_j}{2p(G_i+H_j)}E(\pi), \tag{4.103}$$

where G_i (H_j) is the partial momentum sum of gluon π_i (π_j) in group g (h) respectively. The structure of the sums is the same as in the vertex case. That is, one applies the correlation between pairs of gluons (one from each group), where the gluon from the second group is further from the hard interaction than that from the first. The proof is directly analogous to the vertex case. One first rewrites eq. (4.103) as follows:

$$\begin{aligned}\sum_{g\neq h}R^p(g,h)\prod_{f\neq g,h}E(f)=&\sum_{g\neq h}\frac{G\cdot H}{2p\cdot(G+H)}\frac{2p\cdot(G+H)}{2p\cdot K}E(g)E(h)\prod_{f\neq g,h}E(f)\\&+\sum_l \mathrm{E}^{\mu_l}(K)\sum_{g\neq h}R^p(\tilde{g},\tilde{h})\prod_f E(\tilde{f}),\end{aligned} \tag{4.104}$$

One again considers the separate cases in which $l\in\{g,h\}$, $l\in g$ and $l\in h$, which allows one to separate the second line of eq. (4.104) into three sums. Carrying out similar manipulations to those in eq. (4.100), one finds after substituting (4.103) and combining terms that R^p on the left-hand side of eq. (4.104) is indeed given by eq. (4.103). We do not show this algebra explicitly here, but the reader may verify the above results using the methods outlined in this section.

In this section, we have shown that the sum over all possible NE gluon insertions factorises into contributions arising from distinct groups. In showing this factorization, a two-gluon vertex arises which correlates gluons at different positions along the line (i.e. non-adjacent gluons in general). This two-gluon vertex may either correlate pairs of gluons within the same group (in which case this remains a group), or it may correlate gluons in different groups (in which case the merging of g and h becomes a single group). This completes the proof that there exists a set of effective Feynman rules for NE emissions. Such Feynman rules were also derived using path integral methods in the previous chapter. In the following section we collect and present the effective Feynman rules obtained in this paper, and discuss the relationship with the path integral approach, finding that the two analyses are completely equivalent.

4.3.5 The next-to-eikonal Feynman rules

In the preceding sections we established the theorem expressed in eq. (4.91), which states that the sum over all NE gluon insertions on a given external line can be writ-

ten in a form where contributions from different groups factorise. There is then a remainder term which correlates gluon emissions from different groups.

This implies the existence of a set of effective Feynman rules, which generalise those used in the eikonal approximation. In this section, we write the explicit forms for these Feynman rules, and compare them with the results obtained using the path integral approach. We restrict ourselves to the case of a scalar eikonal line; the spinor case is very similar (as we discuss later).

Firstly, there is a one-gluon vertex that comes from combining the vertex factor in the previous section with the second term on the right-hand side of eq. (4.44). The result is

$$\frac{2K_i - k_i}{2p \cdot K_i} \equiv \frac{K_i + K_{i+1}}{2p \cdot K_i}. \tag{4.105}$$

One recognizes the right-hand side as having the same form as the corresponding factors in our original expression for the contribution of an external line (eq. 4.5)[5].

Note that both the numerator and denominator of eq. (4.105) involve partial sums of gluon momenta. This is also true for the denominator in eikonal perturbation theory. It is somewhat strange that the numerator in the NE case involves a partial momentum sum rather than a single gluon momentum. After all, numerators arise from vertices and denominators arise from propagators. One expects sums of momenta to occur in propagators, but that vertices will only depend upon the momentum associated with the given gluon emission. Indeed, writing

$$K_i + K_{i+1} = k_i^{\mu_i} + \sum_{j>i} 2k_j^{\mu_i}, \tag{4.106}$$

one may rewrite the rule of eq. (4.105) as follows:

$$\frac{k_i^{\mu_i}}{2p \cdot K_i} + \sum_{j>i} \frac{2k_j^{\mu_i}}{2p \cdot K_i}. \tag{4.107}$$

The first term involves only the momentum (and Lorentz index) of gluon i, together with the corresponding eikonal propagator. The other terms involve momenta of different gluons, but carrying the Lorentz index of gluon i (and having the same eikonal propagator). An example of the former is shown in figure 4.12(a), and an example of the latter in figure 4.12(b).

Further effective rules arise from the propagator contribution. This has the form

$$-\frac{K_i^2 2p^{\mu_i}}{(2p \cdot K_i)^2}, \tag{4.108}$$

which again has a partial momentum sum in the numerator (as indeed results from Taylor expanding a denominator). One may also interpret this as being a mixture of terms depending on information from more than one gluon emission, and a term

[5]We have since shown, however, that the sum over all such vertex insertions gives an expression which factorises into contributions from distinct groups.

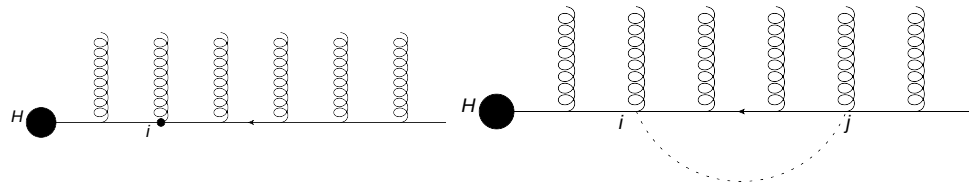

(a) One gluon vertex with numerator $k_i^{\mu_i}$. (b) Two gluon vertex with numerator $2k_j^{\mu_i}2p^{\mu_j}$.

Figure 4.12: Next-to-eikonal one and two gluon vertices.

which only involves the single gluon momentum in the numerator which corresponds to the squared eikonal propagator. To see this, one writes

$$K_i^2 = \sum_{j\geq i} k_j^2 + 2\sum_{i\leq j<l} k_j \cdot k_l, \tag{4.109}$$

so that eq. (4.108) becomes

$$-\frac{k_i^2 2p^{\mu_i}}{(2p\cdot K_i)^2} - \sum_{j>i}\frac{k_j^2 2p^{\mu_i}}{(2p\cdot K_i)^2} - 2\sum_{i\leq j<l}\frac{k_j\cdot k_l 2p^{\mu_i}}{(2p\cdot K_i)^2}. \tag{4.110}$$

The first sum involves the single momentum of gluon j, but the squared eikonal propagator of gluon i. The second sum involves information from three gluons i.e. the dot product of momenta from gluons j and l, but (again) the squared eikonal propagator of gluon i. This structure will later prove useful in showing the equivalence with the path integral framework of the previous chapter. Writing the NE contributions in this way makes the remainder term more transparent. The NE contributions contain correlations between two different gluons (the last terms of eqs.(4.107) and (4.110)). Such a correlation can be depicted as in fig.4.12(b). Consider the eikonal webs of section 4.2.2. Using the extra two-gluon correlation vertex of fig.4.12(b) we can join two webs (see fig.4.13). Such a joined pair of webs was not part of the original exponentiation in webs, but is part in the full exponentiation. Looking at the structure of the remainder term one sees that it precisely gives joined webs.

Although the NE vertex corrections consists of perfect one and two-gluon vertices, the NE propagator correction of eq.(4.110) has a sum over two and three indices respectively, seemingly involving three-gluon vertices. How does this agrees with the results from chapter 3, where only two-gluon vertices are present? We will now show the correspondence between these two approaches. The effective Feynman rules of chapter 3 are stated in position space, while we work here in momentum space. Because of the time ordering necessary in the non-abelian setting, care must be taken upon integrating over the positions of the gluons along the eikonal line. The position space Feynman rules corresponding to the rules in eq.(4.110) are (see eq. (3.100))

$$\frac{1}{2}n^\mu k^2 \int_0^\infty dt\, t e^{-i(n\cdot k)t} T^a(t), \tag{4.111}$$

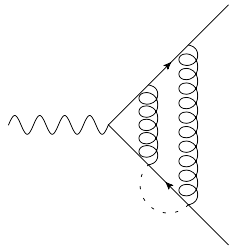

Figure 4.13: Example of a new joined web not present in the original exponentiation.

and

$$n^\mu n^\nu k\cdot l\int_0^\infty dtdt' i\min(t,t')e^{-i(n\cdot k)t-i(n\cdot l)t'}T^a(t)T^b(t'). \tag{4.112}$$

These vertices describe a one gluon (k,μ,a) vertex and a two gluon $(k,\mu,a),(l,\nu,b)$ vertex coupled to the eikonal line. The color matrices have a formal time dependence, because we need to keep track of time ordering. The time ordering procedure results in the following structure of the time integrals

$$\int_0^\infty idt_1 e^{-i(n\cdot k_1)t_1}\int_{t_1}^\infty idt_2 e^{-i(n\cdot k_2)t_2}\dots\int_{t_{n-1}}^\infty idt_n e^{-i(n\cdot k_n)t_n}, \tag{4.113}$$

which produce the partial momentum sums in the denominator of the eikonal propagators. Now, in case one of the next-to-eikonal vertices is present we obtain an extra t_i in the time integrations[6]. The i^{th} integral becomes

$$\int_0^\infty idt_1 e^{-i(n\cdot k_1)t_1}\int_{t_1}^\infty idt_2 e^{-i(n\cdot k_2)t_2}\dots\int_{t_{i-1}}^\infty dt_i e^{-i(n\cdot K_i)t_i}t_i, \tag{4.114}$$

where the presence of K_i in the last factor indicates that all subsequent integrals have been carried out. Upon integrating by (4.114) parts becomes

$$\int_0^\infty idt_1 e^{-i(n\cdot k_1)t_1}\int_{t_1}^\infty idt_2 e^{-i(n\cdot k_2)t_2}\dots \times\int_{t_{i-2}}^\infty idt_{i-1}e^{-i(n\cdot K_{i-1})t_{i-1}}\left(\frac{t_{i-1}}{in\cdot K_i}-\frac{1}{(n\cdot K_i)^2}\right). \tag{4.115}$$

The second term gives the first term in eq.(4.110), but the first term is exactly equivalent to the original integral but with t_{i-1} instead of t_i. Iteratively integrating by parts, one generates the complete sum in the second term in eq.(4.110). Similarly the third term in eq.(4.110) is generated by the vertex (4.112). This provides a complete consistency check of the two approaches on next-to-eikonal contributions.

[6]The time ordering fits nicely with the $\min(t,t')$ prescription of eq.(4.112).

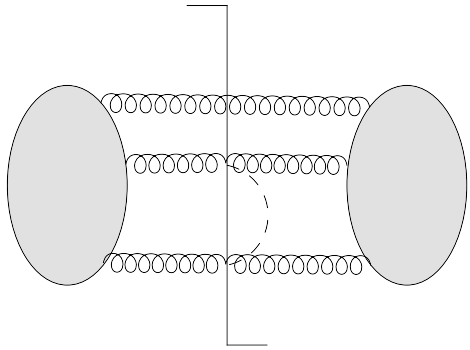

Figure 4.14: A cut-diagram with two gluons, through the final state cut, coupled.

This also presents us with a interpretation of the remainder term. In the path integral formalism we have a natural exponentiation in webs, including the next-to-eikonal vertices. Summing over all the two-gluon correlations gives back the normal next-to-eikonal rules for the propagator and vertex. However in case one has a diagram that consists of two separate webs connected by two gluon vertex between the two webs this diagram is present in the exponent, whereas the same diagram with the two-gluon vertex between gluons of the same web is absent in the exponent. Therefore we cannot perform the sum and we are left with precisely the remainder terms of eqs.(4.103) and (4.98).

After completing the factorization proof we find exponentiation to next-to-eikonal order (see section 4.2.2 and [61]), which become particularly simple in the abelian case. In electrodynamics each photon is its own group and factorize completely, except for a two photon vertex. Therefore one finds exponentiation into connected graphs including a two photon vertex.

4.4 Phase space factorization

In order to achieve useful exponentiation for cross sections we need to address phase space. Let us do so in the context of Drell-Yan. As discussed in the introduction (eq.(1.91)), at the eikonal level phase space factorizes in N-space[7]. Here we extend this to next-to-eikonal accuracy. Indeed, we shall find that the n-gluon phase space factorizes into a product of one-gluon phase spaces, where in addition now two gluons can get coupled. This can be visualized as a connection of two gluons through the final state cut (see fig. 4.14). This correlated phase space factorizes sufficiently such that, when combined with the eikonal amplitudes, exponentiation to order $1/N$ results.

To show factorization, we start with the full n-gluon phase space measure, and

[7] Recall that N is the Mellin/Laplace moment in our DY discussion of section 1.9.

immediately perform the Laplace transform to N-space

$$d\Phi_n(N) = \int d\lambda\, e^{-N\lambda} \left(\prod_i d^{4-2\varepsilon} k_i \delta_+(k_i^2) \right) \delta\left(z - \frac{Q^2}{s} \right), \quad z = e^{-\lambda}, \tag{4.116}$$

where $Q = (\sqrt{s} - K_0, -\vec{K})$ is the momentum of the produced vector boson and K is the sum of all final state momenta k_i. Substituting $\psi = N\lambda$ results in

$$d\Phi_n(N) = \int \frac{d\psi}{N} e^{-\psi} \left(\prod_i d^{4-2\varepsilon} k_i \delta_+(k_i^2) \right) \delta\left(e^{-\frac{\psi}{N}} - 1 + \left(\frac{2K_0}{\sqrt{s}} - \frac{K^2}{s} \right) \right). \tag{4.117}$$

Because of the exponential suppression by $\exp[-\psi]$, the dominant contribution comes from the region $\psi = \mathcal{O}(1)$, implying that one can approximate the argument of the delta function, in the large N limit, by a Taylor expansion in ψ. Thus we obtain, to next-to-eikonal order

$$d\Phi_n(N) = \int \frac{d\psi}{N} e^{-\psi} \left(\prod_i d^{4-2\varepsilon} k_i \delta_+(k_i^2) \right) N\delta\left(\psi - \frac{1}{2}\frac{\psi^2}{N} - \left(\frac{2NK_0}{\sqrt{s}} - \frac{NK^2}{s} \right) \right), \tag{4.118}$$

where we have also extracted a factor N from the delta function. To the order at which we are working, we can integrate over the delta function, and find

$$\psi = \frac{2NK_0}{\sqrt{s}} + \frac{N(K_0^2 + \vec{K}^2)}{s}. \tag{4.119}$$

It clear that $K = \mathcal{O}(1/N)$, so up to this order we obtain for the phase space (including the Jacobian of the delta-function)

$$d\Phi_n(N) = e^{-N\frac{2K_0}{\sqrt{s}}} \left(\prod_i d^{4-2\varepsilon} k_i \delta_+(k_i^2) \right) \left(1 - \frac{N(K_0^2 + \vec{K}^2)}{s} + \frac{2K_0}{\sqrt{s}} \right). \tag{4.120}$$

The last two terms make the phase space correct to NE order. They involve adjustments for either a single final state gluon or two final state gluons,

$$d\Phi_n(N) = e^{-N\frac{2K_0}{\sqrt{s}}} \left(\prod_i d^{4-2\varepsilon} k_i \delta_+(k_i^2) \right) \left(1 + \sum_i \left(\frac{2k_{i0}}{\sqrt{s}} - \frac{N(k_{i0}^2 + \vec{k}_i^2)}{s} \right) - \sum_{i \neq j} \frac{N(k_{i0}k_{j0} + \vec{k}_i \cdot \vec{k}_j)}{s} \right). \tag{4.121}$$

Three-gluon correlations obviously do not appear. This demonstrates factorization of phase space to next-to-eikonal order. The basic structure of the cross section to next-to-eikonal order is then, schematically,

$$d\sigma(N) = \sum_n \left[\int d\Phi_n^{\mathrm{E}}(N) |\mathcal{M}^{\mathrm{E}}|^2 + \int d\Phi_n^{\mathrm{NE}}(N) |\mathcal{M}^{\mathrm{E}}|^2 + \int d\Phi_n^{\mathrm{E}}(N) |\mathcal{M}^{\mathrm{NE}}|^2 \right]. \tag{4.122}$$

Here $\mathcal{M}^{\mathrm{E,\,NE}}$ are the strictly eikonal and next-to-eikonal matrix elements respectively. In the next section we shall see an extra source of next-to-eikonal terms, which we ignore here for the moment. The result, then, including phase space, takes the form

$$d\sigma(N) = \exp\left[\sum_G G + \sum_H H\right], \tag{4.123}$$

where the first sum over is over all webs (G) including the next-to-eikonal vertices, and the second sum is over all webs (H) where the phase space of one or two gluons is next-to-eikonal.

4.5 Power counting for next-to-eikonal webs in Drell-Yan

To study DY at order $1/N$ we first write down the full formula for a particular DY Feynman graph,

$$\int d\Phi_n(N) \int \prod_j \frac{d^d l_j}{(2\pi)^d} I(\{l_j\}, \{k_i\}, p, \bar{p}). \tag{4.124}$$

In here k labels the momenta of the final state gluons (see eq.(4.121)), l the momenta of the virtual gluons and $p, \bar{p}$ are the incoming momenta. If we look at the measure for the k momenta we see that all components are suppressed by a factor $1/N$ (with respect to $\sqrt{s}$). The virtual momenta are unbounded integrals which therefore cannot be assumed to be either small or large. We separate the domain of integration of the virtual integrals into a soft regime, with all components $\mathcal{O}(\sqrt{s}/N)$, and a hard regime. Contracting all hard momenta into the hard vertex, which is the gist of factorization, we obtain

$$\int d\Phi_n(N) \int_{\text{soft}} \prod_j \frac{d^d l_j}{(2\pi)^d} I'(\{l_j\}, \{k_i\}, p, \bar{p}), \tag{4.125}$$

where we integrate l over the soft regime and the prime on I indicates that all hard integrations are already performed. The graphical representation of I looks like the original DY diagram, with two differences: the hard vertex is the effective result of carrying out all the hard integrals and there are soft lines directly coming from the hard vertex (see also section 3.2.4). Now we rescale each soft momentum by $1/N$ to find

$$\int d\Phi_n(1) \int_{\text{soft}} \prod_j \frac{d^d l_j}{(2\pi)^d} N^{-(d-2)n-dm} I'\left(\left\{\frac{l_j}{N}\right\}, \left\{\frac{k_i}{N}\right\}, p, \bar{p}\right), \tag{4.126}$$

where m is the number of soft virtual momenta. We can now analyze the large N limit of I' to next-to-eikonal order. Schematically to this order I' can be written as

$$I'\left(\left\{\frac{l_j}{N}\right\}, \left\{\frac{k_i}{N}\right\}, p, \bar{p}\right) = H^{(0)}\left(p + \frac{K}{N}, \bar{p} + \frac{\bar{K}}{N}\right) E(\{k_i\}, \{l_j\}, p, \bar{p}), \tag{4.127}$$

where the E indicates the two outgoing hard lines from where the soft emissions take place. $H^{(0)}$ is the effective hard vertex from which no soft radiation is emitted. This is the case when no soft line comes directly out of the hard vertex. When there is a soft line emitted from the hard vertex we have

$$I'\left(\left\{\frac{l_j}{N}\right\},\left\{\frac{k_i}{N}\right\},p,\bar{p}\right)=H^{(1)}(p+K,\bar{p}+\bar{K},l_j)E(\{k_i\},\{l_j\},p,\bar{p})\,. \tag{4.128}$$

Of course there can be more soft lines coming from the hard vertex but these are suppressed beyond our accuracy. Note that $H^{(1)}$ can contain soft emissions from a hard collinear loop that has ended up in H (in contrast to the usual analysis of [9]). The next-to-eikonal matrix elements can be separated into three classes: namely the next-to-eikonal coming from the hard lines $E(\ldots)$ in eq.(4.127), the first order Taylor expansion of $H^{(0)}$ in eq.(4.127) or from eq.(4.128). The second and third class combine by *Low's theorem* [18, 19] (see 3.2.4) and we disregard them here (we discuss them in the conclusion). For the first class of corrections we rescale $p,\bar{p}$ by N and find for eq.(4.126)

$$\int d\Phi_n(1)\int_s\prod_j\frac{d^dl_j}{(2\pi)^d}N^{2\varepsilon(n+m)}H(p,\bar{p})E\left(\{l_j\},\{k_i\},Np,N\bar{p}\right). \tag{4.129}$$

By powercounting the overall N dependence cancels in $d=4$ dimensions. Observe that the large N limit is precisely the limit that gives (4.42) and (4.43) (see also eq. (3.43)). This means that for calculating terms up to $1/N$ it is sufficient to use the NE Feynman rules of section 4.3.

By inspecting eq.(4.129) it is clear that logarithms $\ln N$ are produced by IR and COL $1/\varepsilon$ poles in dimensional regularization. If we focus on the leading logarithm at a given order n in perturbation theory, we know that all radiation must be soft, and collinear to one of the two lines. In the large N limit we see, from the rescaling argument of the previous paragraph, that we can use the eikonal approximation because all radiation becomes soft. We have seen that non-abelian eikonal exponentiation says that the large N limit implies an exponential structure at leading logarithmic order [44]. It is known that each web has only one overall IR and one overall COL divergence, giving the logarithmic structure $A\ln^2 N+B\ln N$ [47]. The double logarithm is generated from the region in phase space where the gluons are both collinear and soft. Analyzing this logarithmic structure, it is easy to see that the leading logarithmic contributions at order α_S^n are given by

$$\frac{1}{n!}\alpha_S^2A^n\ln^{2n}N, \tag{4.130}$$

where A is given by the lowest order single gluon graphs. Of course, subleading logarithms at this order can receive contributions in multiple ways, and require more calculations to predict. Let us extend this analysis to next-to-eikonal accuracy. Because the basic structure of the exponentiating graphs is not altered, i.e. there is still an exponentiation into graphs that cannot be disconnected by cutting two eikonal lines,

much of the analysis carries over. The difference is that the next-to-eikonal webs do not have an overall IR divergence. The extra power of momentum in the numerator makes the diagram IR finite, without subdivergences. Therefore the leading logarithm for α_S^n at next-to-eikonal order $(1/N)$ is

$$\frac{1}{(n-1)!}A^{n-1}C\frac{\ln^{2n-1}N}{N}, \tag{4.131}$$

coming from the lowest order contribution

$$\alpha_S\left(A\ln^2 N + B\ln N + C\frac{\ln N}{N}\right), \tag{4.132}$$

in the exponent. Here C is seen to be equal to A in chapter 2 (and $B = 0$ for Drell-Yan). This shows the exponentiation of the leading logarithm at $1/N$, a result long noted in the literature [21]. We continue now by working out the DY cross section using the NE Feynman rules in order to verify the results.

4.6 Illustrative example - Drell-Yan Production

In the previous sections, we have used iterative Feynman diagram methods to analyse the structure of soft gauge boson corrections up to NE order. The result is a classification of NE contributions to matrix elements in terms of both external and internal emission graphs. The former contain effective Feynman rules up to NE order, which have been shown to agree with those obtained using the path integral methods, whilst the latter are given by the Low-Burnett-Kroll theorem (see section 3.2.4).

In order to clarify the meaning of the results obtained in the previous sections, we consider in this section a simple illustrative example - that of Drell-Yan production of a virtual photon at NE order. We will consider the soft gluon corrections contributing to the C_F^2 color structure up to NNLO, and show how these arise from the techniques introduced above. The NLO corrections to the DY process have been calculated in [62], and NNLO results in [29] (eikonal NNLO results were first presented in [63, 64]).

The LO Drell-Yan process [65] is shown in figure 4.15, and corresponds to

$$\mathcal{Q}(p) + \bar{\mathcal{Q}}(\bar{p}) \to \gamma^*(q), \tag{4.133}$$

where $\mathcal{Q}$ denotes a quark, and q is the momentum of the off-shell photon. It is conventional to normalize the NLO (and higher order) cross-sections to the Born result, i.e. one defines the K-factor

$$K^{(i)}(z) = \frac{1}{\sigma^{(0)}}\frac{d\sigma^{(i)}}{dz}, \tag{4.134}$$

where $\sigma^{(0)}$ is the integrated LO cross-section, and $\sigma^{(i)}$ the cross-section at $\mathcal{O}(\alpha_s^i)$. Here we calculate the Born cross-section for completeness. The amplitude from figure 4.15 is given by

$$\mathcal{A}^{(0)\alpha} = \bar{u}(p)\gamma^\alpha v(\bar{p}), \tag{4.135}$$

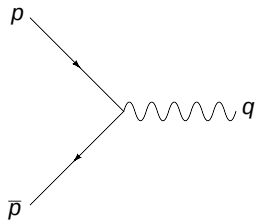

Figure 4.15: Born level diagram for DY production of a photon.

where we neglect coupling factors and spin averaging, as these will ultimately cancel upon taking ratios in the NLO case. After squaring and multiplying by the polarization tensor of the photon, one may integrate over the phase space of the photon to give the cross-section

$$\sigma^{(0)} = 4\pi(2+\epsilon)\delta(1-z), \tag{4.136}$$

where $z = Q^2/s$ is the fraction of the final state energy carried by the virtual photon (i.e. at LO this is fixed to be $z = 1$).

4.6.1 NLO contributions at NE order

We now consider NLO corrections to the DY process of eq. (4.135), and show how the eikonal and next-to-eikonal terms arise from the Feynman rules derived in section 4.3. Given that the aim of this section is merely to clarify the results of the preceding sections, we will simplify matters and consider corrections to the $q\bar{q}$ initial state only, and focus solely on the C_F color structure. This then corresponds to two incoming eikonal lines, coupled by a color-singlet hard interaction. Furthermore, for these terms the non-abelian structure of QCD is not relevant. Thus, this is in a sense the simplest example with which to demonstrate application of the NE Feynman rules.

In this and the following section, instead of working with the phase space rules found in 4.4, we simply integrate over the exact multigluon phase space in z-space. We do this to make easy connection with the full result in the literature.

First we calculate the eikonal contributions to the NLO K-factor. The effective Feynman rule for one gluon emission of momentum k^μ from an eikonal line p is:

$$ig_S \frac{2p^\mu}{2p\cdot k} T^a \tag{4.137}$$

Then the squared amplitude coming from the effective eikonal Feynman rules is:

$$\mathcal{A}_\alpha^{(1)E}\mathcal{A}^{(1)E\dagger\alpha} = 2g_s^2 C_F \frac{p\cdot\bar{p}}{(p\cdot k)(\bar{p}\cdot k)}\mathrm{Tr}[\not{p}\gamma^\alpha\not{\bar{p}}\gamma_\alpha], \tag{4.138}$$

where the factor of 2 in the first line comes from combining the diagrams shown in figure 4.16. Integrating eq.(4.138) over phase space one finds [66]:

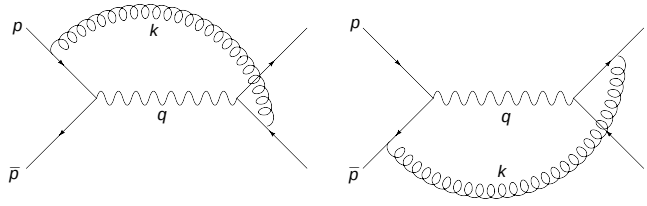

Figure 4.16: Squared matrix elements contributing at NLO in the eikonal limit.

$$K^{(1)E}(z) = \frac{\alpha_S C_F}{4\pi}\Bigg\{\frac{16\mathcal{D}_0}{\epsilon} + 16\mathcal{D}_1 - \frac{8\ln(z)}{1-z} + \epsilon\left[8\mathcal{D}_2 - 6\zeta_2\mathcal{D}_0 - \frac{8\ln z\ln(1-z)}{(1-z)} + \frac{2\ln^2(z)}{1-z}\right]\Bigg\}, \quad (4.139)$$

where we use the notation

$$\mathcal{D}_i = \left[\frac{\ln^{i-1}(1-z)}{1-z}\right]_+ \quad (4.140)$$

to denote plus-distributions. Such terms arise from the eikonal matrix element integrated with eikonal phase space, and subleading (when $z \to 1$) corrections in eq. (4.139) arise from including subleading corrections to the phase space. Note that we removed have removed any term proportional to $\delta(1-z)$.

Next we consider NE corrections. According to the results of section 4.3, the effective Feynman rules for single gluon emission at NE order is

$$ig_s\left(\frac{\gamma^\mu \not{k}}{2p\cdot k} - k^2\frac{2p^\mu}{(2p\cdot k)^2}\right)T^a, \quad (4.141)$$

indicated by a black dot in fig.4.17. Given that k corresponds to a real emission, the second term in equation (4.141) vanishes due to the gluon being on-shell. The diagrams contributing at NE level are shown in figure 4.17, and consist of all possible NE vertex insertions in the eikonal diagrams of figure 4.16. They lead to

$$\mathcal{A}^{(1)NE}_\alpha \mathcal{A}^{E(1)\dagger\alpha} + \mathcal{A}^{(1)E}_\alpha \mathcal{A}^{NE(1)\dagger\alpha} = g_S^2 C_F \frac{2\bar{p}_\mu}{2\bar{p}\cdot k}\frac{\mathrm{Tr}[\not{p}\gamma^\mu \not{k}\gamma^\alpha \not{\bar{p}}\gamma_\alpha]}{2p\cdot k} + \frac{2p_\mu}{2p\cdot k}\frac{\mathrm{Tr}[\not{p}\gamma^\alpha \not{\bar{p}}\gamma^\mu \not{k}\gamma_\alpha]}{2\bar{p}\cdot k} \quad (4.142)$$

Carrying out the phase space integration and dividing by the Born normalization leads to the NE K-factor contribution:

$$K^{(1)NE}(z) = \frac{\alpha_S C_F}{4\pi}\Big\{-\frac{16}{\epsilon} - 16\ln(1-z) + 8\ln(z) + \epsilon\left[-8\ln^2(1-z) + 8\ln(z)\ln(1-z) - 2\ln^2(z) + 6\zeta_2\right]\Big\}. \quad (4.143)$$

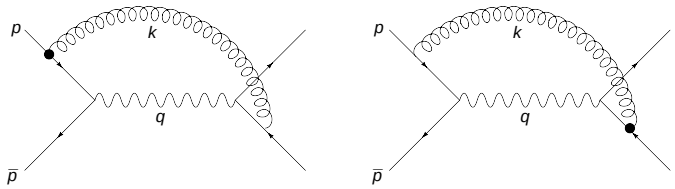

Figure 4.17: Diagrams contributing to the squared amplitude for NLO real emissions. Two additional diagrams, arising from complex conjugation, are not shown.

Combining eqs. (4.139,4.143), and keeping only logarithmic terms up to NE order, one has

$$K^{(1)}(z) = \frac{\alpha_S C_F}{4\pi}\Big\{\frac{16\mathcal{D}_0 - 16}{\epsilon} + 16\mathcal{D}_1 - 16\ln(1-z) + \epsilon\left[8\mathcal{D}_2 - 6\zeta_2\mathcal{D}_0 - 8\ln^2(1-z) + 8\ln(1-z)\right]\Big\}. \tag{4.144}$$

In obtaining this result we have expanded about $z = 1$, i.e. this includes the replacement

$$\ln(z) \to (z-1) + \mathcal{O}[(z-1)^2]. \tag{4.145}$$

One may compare this result with the corresponding result including full z dependence, which is [62]

$$K^{(1)}(z) = \frac{\alpha_S C_F}{4\pi}\left[\frac{8(1+z^2)}{1-z}\frac{1}{\epsilon} + \frac{8(1+z^2)\ln(1-z) - 4(1+z^2)\ln(z)}{1-z} - \frac{\epsilon}{2}\left(\frac{(1+z^2)[-8\ln^2(1-z) + 6\zeta_2 - 2\ln(z) + 8\ln(z)\ln(1-z)] - 4(1-z)^2}{1-z}\right)\right], \tag{4.146}$$

It is easily verified that expanding this expression about $z = 1$ gives the same terms, up to NE order, as eq. (4.144). Thus, the effective Feynman rules derived above do indeed reproduce correct structure of the NLO K factor. Having described the simplest example, we consider the NNLO K-factor in the following section.

4.6.2 NNLO contributions at NE order

Here we consider the C_F^2 contribution to the NNLO K-factor for DY production of a virtual photon, and as in the previous section restrict our attention to the $q\bar{q}$ initial state. In reproducing the soft logarithms, one may divide the NNLO diagrams into two gauge-invariant classes. Firstly, there are diagrams involving two real gluon emissions. Secondly, there are interference diagrams between the one loop virtual correction, and diagrams involving one real emission. We consider the former diagrams

in this thesis, as they all involve external emission corrections to a point-like hard interaction and so have a simpler structure at NE order. The one loop diagrams (as we will see) involve internal emissions from hard graphs [66], which we will ignore here.

Double real emission graphs

The structure of NE corrections found in the preceding sections implies that the amplitude for the two real emission graphs is given by the relevant term in

$$\mathcal{A} = \mathcal{A}^{(0)} \exp\left[\bar{\mathcal{A}}^{(1)\mathrm{E}} + \bar{\mathcal{A}}^{(1)\mathrm{NE}} + \bar{\mathcal{A}}^{(2)\mathrm{NE}}\right], \tag{4.147}$$

where $\mathcal{A}^{(0)} \propto \mathrm{Tr}\left[\not{p}\gamma^{\alpha}\not{\bar{p}}\gamma_{\alpha}\right]$, and the bar over an amplitude represents the expression for that amplitude with the Born result factored out. Note there is no $\mathcal{O}(\alpha_S^2)$ eikonal amplitude in the exponent. This is because we are not considering non-abelian interactions, and so the exponent must contain connected subdiagrams. There is no connected subdiagram involving two eikonal emissions, hence the absence of such a term.

Expanding the exponential in eq. (4.147) one has an $\mathcal{O}(\alpha_S^2)$ contribution

$$\mathcal{A}^{(0)}\left[|\bar{\mathcal{A}}^{(1)\mathrm{E}}|^2 + \bar{\mathcal{A}}^{(1)\mathrm{E}}\bar{\mathcal{A}}^{(1)\mathrm{NE}\dagger} + \bar{\mathcal{A}}^{(1)\mathrm{E}\dagger}\bar{\mathcal{A}}^{(1)\mathrm{NE}} + |\bar{\mathcal{A}}^{(2)\mathrm{NE}}|^2\right]. \tag{4.148}$$

The first term is the exponentiated eikonal result eikonal, and has the explicit expression

$$\mathcal{A}^{(0)}|\bar{\mathcal{A}}^{(1)\mathrm{E}}|^2 = \frac{2p\cdot\bar{p}}{p\cdot k_1\, p\cdot k_2\, \bar{p}\cdot k_1\, \bar{p}\cdot k_2}\mathrm{Tr}\left[\not{p}\gamma^{\alpha}\not{\bar{p}}\gamma_{\alpha}\right], \tag{4.149}$$

where we have neglected overall coupling and color / spin averaging factors for brevity. After integrating over phase space the final result from the eikonal term is [66]

$$\left(\frac{\alpha_S C_F}{4\pi}\right)^2\left[\frac{1024\mathcal{D}_3}{3} + 640\ln^2(1-z) + 32 + \frac{512\mathcal{D}_2 + 640\ln(1-z)}{\epsilon} + \frac{512\mathcal{D}_1 + 320}{\epsilon^2} + \frac{256\mathcal{D}_0}{\epsilon^3}\right]. \tag{4.150}$$

Note that in this result that we have omitted logarithmic terms which are proportional to transcendental constants (ζ_2) to simplify the result somewhat. After all, our aim is merely to illustrate that the same structure of logarithmic terms arises from both the NE Feynman rule approach and a full calculation truncated to NE order.

Next, one has the contribution arising from the second and third terms in eq. (4.148), which (using the results derived in the previous section) is given by

$$\bar{\mathcal{A}}^{(1)\mathrm{E}}\bar{\mathcal{A}}^{(1)\mathrm{NE}\dagger} + \bar{\mathcal{A}}^{(1)\mathrm{E}\dagger}\bar{\mathcal{A}}^{(1)\mathrm{NE}} = \frac{-2s}{p\cdot k_1\, \bar{p}\cdot k_1}\left(\frac{1}{p\cdot k_2} + \frac{1}{\bar{p}\cdot k_2}\right)\mathrm{Tr}\left[\not{p}\gamma^{\alpha}\not{\bar{p}}\gamma_{\alpha}\right]. \tag{4.151}$$

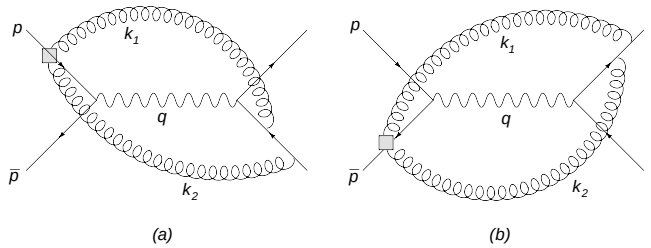

Figure 4.18: Squared Feynman diagrams involving the next-to-eikonal remainder term $R^{\mu\nu}$. One must also include the complex conjugates.

The integration over phase space can be carried out as for the eikonal term, and one finds a contribution to the K-factor

$$\left(\frac{\alpha_S C_F}{4\pi}\right)^2 \left[\frac{-1024\ln^3(1-z)}{3} - \frac{512\ln^2(1-z)}{\epsilon} - \frac{512\ln(1-z)}{\epsilon^2} - \frac{256}{\epsilon^3}\right]. \tag{4.152}$$

Finally, one has the contribution given by the final term in eq. (4.148), which involves the NE contributions from correlated two-gluon emission. That is, one must consider the two gluon vertex discussed in section 4.3, and having the form (for emission momenta k_1, k_2)

$$R^{\mu\nu}(p;k_1,k_2) = \frac{2(p\cdot k_2)2p^\mu k_1^\nu + 2(p\cdot k_1)k_2^\mu 2p^\nu - 2(k_1\cdot k_2)2p^\mu 2p^\nu}{(2p\cdot k_1)(2p\cdot k_2)(2p\cdot(k_1+k_2))} - \frac{g^{\mu\nu}}{2p\cdot(k_1+k_2)}, \tag{4.153}$$

It is easily checked that this gives zero if either of the gluons lands on the same eikonal line that it was emitted from. Thus, the only possible contributions come from diagrams such as those shown in figure 4.18. In fact, these diagrams are also zero as can be seen from the following argument. Considering e.g. the diagram in figure 4.18(a), this involves the factor

$$\frac{R^{\mu\nu}\bar{p}_\mu\bar{p}_\nu}{(\bar{p}\cdot k_1)(\bar{p}\cdot k_2)(p\cdot k_1)(p\cdot k_2)} = \frac{2p\cdot\bar{p}}{(p\cdot(k_1+k_2))(\bar{p}\cdot k_1)(\bar{p}\cdot k_2)(p\cdot k_1)(p\cdot k_2)} \times\left[(p\cdot k_2)(\bar{p}\cdot k_1) + (\bar{p}\cdot k_2)(p\cdot k_1) - (k_1\cdot k_2)(p\cdot\bar{p})\right], \tag{4.154}$$

where the term involving $g_{\mu\nu}$ has already vanished as a consequence of the on-shellness of $\bar{p}$. Now one may parameterize the fermion momenta as

$$p = \sqrt{\frac{s}{2}}n, \quad \bar{p} = \sqrt{\frac{s}{2}}\bar{n}, \tag{4.155}$$

where

$$n = \sqrt{\frac{1}{2}}(1, 0, \dots 1), \quad \bar{n} = \sqrt{\frac{1}{2}}(1, 0, \dots -1) \tag{4.156}$$

are constant light-like vectors. Introducing the light-like coordinates

$$k^{\pm} = \sqrt{\frac{1}{2}}(k^0 \pm k^3), \tag{4.157}$$

one has

$$n \cdot k = k^-, \quad \bar{n} \cdot k^+, \quad k_1 \cdot k_2 = k_1^+ k_2^- + k_1^- k_2^+ - k_1^T \cdot k_2^T, \tag{4.158}$$

where k_i^T is transverse to both n and $\bar{n}$. Then the bracketed term in eq. (4.154) becomes

$$p \cdot k_2 \bar{p} \cdot k_1 + \bar{p} \cdot k_2 p \cdot k_1 - k_1 \cdot k_2 p \cdot \bar{p} = -\frac{s}{2} k_1^T \cdot k_2^T. \tag{4.159}$$

The prefactor of this term depends only on longitudinal momentum components. Thus the diagram involving the two-gluon vertex, whilst locally present in phase space, vanishes upon integration over the transverse momenta.

Putting things together, the NE contribution to the NNLO K-factor is given by the sum of eqs. (4.150) and (4.152), which is

$$\begin{aligned} K^{(2)NE} = \left(\frac{\alpha_S C_F}{4\pi}\right)^2 \Bigg[& \frac{1024\mathcal{D}_3}{3} - \frac{1024\ln^3(1-z)}{3} + 640\ln^2(1-z) \\ & + \frac{512\mathcal{D}_2 - 512\ln^2(1-z) + 640\ln(1-z)}{\epsilon} + \frac{512\mathcal{D}_1 - 512\ln(1-z)}{\epsilon^2} \\ & + \frac{256\mathcal{D}_0 - 256}{\epsilon^3} \Bigg]. \end{aligned} \tag{4.160}$$

Note we have only included terms which are logarithmic (apart from the constant term in the ϵ^3 pole, which is indeed the leading NE contribution at this order). This indeed agrees with the same result obtained from a full calculation of the two real emission contributions, which is then expanded to NE order [66].

We have thus succeeded in demonstrating that the NE terms in the two-real emission contribution to the DY K-factor (for the simple case considered) arise from the NE Feynman rules derived in section 4.3.

4.7 Conclusion

In this chapter we have shown the exponentiation of next-to-eikonal contributions to soft radiation in non-abelian gauge theory. We derived the next-to-eikonal Feynman rules and showed that these factorize, up to well-understood remainder, in cross sections. The non-factorized part could be described by new effective Feynman rules, which makes exact exponentiation possible. These extra effective vertices can be interpreted as a correlated emission of two gluons, which is to be expected when one

interprets the next-to-eikonal effect as a back-reaction. After the first emission the next emission can notice that the hard particle is slightly disturbed, introducing an effective coupling between those two gluons. Furthermore, we studied phase space and showed that it exhibits a factorized structure with a possible two gluon correlation. This corresponds to the two gluon correlation structure of the matrix elements.

These next-to-eikonal factorization properties imply exponentiation of the Drell-Yan cross section at this order. By powercounting the divergences of the diagrams entering the exponent, we derived the exponentiation of the leading next-to-eikonal logarithms. As shown in chapter 3 there is one more source of $1/N$ contributions, which is given by the hard interaction: due to the radiation from the eikonal line, the momenta entering the hard interaction are not the final momenta of the eikonal lines, but are instead shifted by the total momenta of the radiation. Furthermore, there could also be a soft particle emitted by the hard interaction directly. *Low's theorem*[18, 19] combines these two contributions into a contribution solely dependent on the elastic form factor of the hard interaction. This contribution can thus be consistently included, without having to include diagrams that violate the separation between hard and soft physics.

Chapter 5

NLO top plus charged higgs production

In this chapter, we examine a topic somewhat different from those in earlier chapters, and consider QCD corrections to charged Higgs boson production. In order to obtain accurate predictions for cross-sections at hadron colliders, next-to-leading order (NLO) calculations are often required. An even better description may be obtained if one in addition interfaces the resulting matrix elements with *parton shower algorithms*, that simulate the effect of extra QCD radiation. Parton showers form a quite accurate approximation for soft and collinear radiation, so that the subject of this chapter fits with the theme of this thesis.

We first motivate the need to understand charged Higgs production, before describing the details of how to calculate this process at NLO in QCD. Then, we briefly describe how the calculation can be interfaced to a parton shower algorithm for implementation in a Monte Carlo event generator for fully exclusive final states.

One of the least understood parts of the Standard Model is the Higgs sector. The hierarchy problem indicates a fine-tuning of the Higgs mass, which is ultimately related to the quadratic nature of self-energy divergences for a scalar particle. A more natural solution to this problem can be given if new physics occurs at just above the energy scale of electro-weak symmetry breaking. Given that the mass of the top quark is of the same order as the electroweak scale, it follows that the top quark sector provides a potentially sensitive probe of new physics. Of the various top quark production channels, single top production is especially interesting, because it is governed solely by the weak interaction in the Standard Model.

At leading order the possible single top production modes are given by

$$\begin{aligned} &b + u \to t + d \quad \text{(t-channel } W \text{ exchange, fig. 5.1(b))} \\ &u + \bar{d} \to W^+ \to t + \bar{b} \quad \text{(s-channel } W^+ \text{ mediation, fig. 5.1(b))}, \end{aligned} \tag{5.1}$$

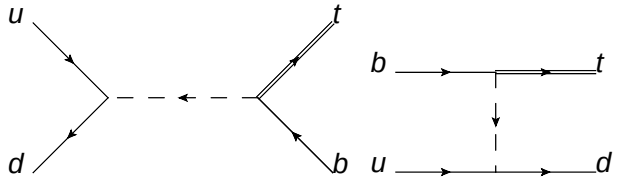

(a) Single top s-channel. (b) Single top t-channel.

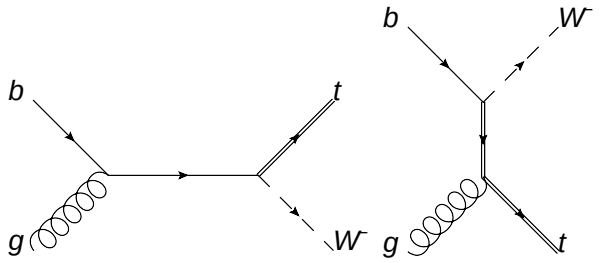

(c) Single top plus W^+ born graphs.

Figure 5.1: Leading order graphs for single top processes within the Standard Model.

as studied in [67, 68, 69, 70], and by

$$b + g \to t + W^- \quad (Wt \text{ associated production, fig. fig. 5.1(c)}), \tag{5.2}$$

which has been calculated up to NLO in [71, 72].

In the Standard Model the electro-weak symmetry breaking is implemented in the minimal way. A Higgs-doublet field receives a vacuum expectation value (VEV), which gives the $W^{\pm}, Z$ and all fundamental matter particles their mass. The particle corresponding to the Higgs field is called the Higgs boson and is an electrically neutral fundamental scalar. A number of possible extensions of the Standard Model, such as the Minimal Supersymmetric Standard Model (MSSM) or two-Higgs doublet models (2HDM) include more Higgs fields, which can result in charged Higgs bosons. In the presence of a charged Higgs boson another single top production channel is possible

$$g + b \to H^- + t. \tag{5.3}$$

This channel is important to determine the presence of a charged Higgs boson in a quite general way, which would give impetus to the study of beyond the Standard Model physics. At the advent of the LHC era we want to be prepared for this possibility. Therefore we need to understand the signal of top plus charged Higgs production well, and preferably in a fully exclusive context. To produce fully exclusive cross sections we need computer programs to generate simulated events. These computer programs are called Monte Carlo event generators, and use the underlying cross section for charged Higgs production to generate simulated events that hopefully give a statistically faithful representation of the events that would be detected at the LHC.

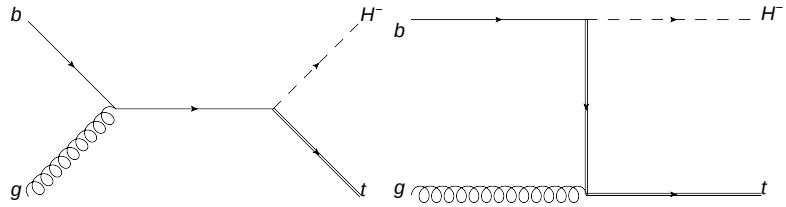

Figure 5.2: The s and t-channel born graphs for charged Higgs production.

One can calculate the cross section for this process at leading order and built it into standard Monte Carlo generators to study charged Higgs plus single top production. However, QCD corrections are important and NLO corrections are potentially needed for quantitative agreement between theory and measurement. Therefore our aim is to construct a Monte Carlo generator for this process that is accurate to NLO precision. We discuss such a procedure for the case of charged Higgs production in section 5.3. Here we first outline the NLO calculation of this process.

The first step is to calculate the Born amplitude, which fixes the conventions for all the coupling constants and overall normalization. After that we have to calculate all the virtual one loop corrections to the Born cross sections. The virtual integrals involve integrations over the loop momenta, where in general these have powers of loop momenta in the numerators as well as the denominators. Each such integral can be reduced to a sum of terms involving a set of scalar integrals only i.e. having no tensor structure in the numerators. A systematic algorithm for this is given by the Passarino-Veltman reduction [73] procedure. These standard integrals are known analytically and contain poles in ε, which correspond to both UV and IR/COL divergences. After renormalizing the UV divergences through the appropriate counterterms, the IR/COL divergences that are left consist of kinematic coefficients (containing poles in ε) multiplying the Born cross-section in d dimensions. The initial COL singularities (which are the only COL singularities present) are factorized into the PDFs. The remaining IR singularities must cancel against the real emissions contributions. As we will see, it is convenient to analytically cancel the real and virtual singularities before implementing the cross-section in an NLO code. To this end we adopt the FKS subtraction formalism of [74], which we discuss in more detail in section 5.2. Let us now first discuss the Born calculation.

5.1 Next-to-leading order calculation

Extended Higgs sectors are a fairly generic feature of many theories beyond the Standard Model. The charged Higgs boson couples an up-type quark to a down-type quark, and in what follows we take these to be the top and bottom quarks without loss of generality (i.e. we are ultimately interested in charged Higgs production in

association with a top quark). Then we define the coupling of the charged Higgs via

$$V_{tb}\bar{\psi}_t(a+b\gamma_5)H\psi_b + \text{cc.}, \tag{5.4}$$

where we have explicitly factored out the CKM matrix element V_{tb}, and a and b are separate coupling constants with (beyond LO) an associated renormalisation scale. Note that in order to be general we have allowed both a scalar and a pseudo-scalar coupling. The Born cross-section potentially involves a contribution containing a Levi-Cevita epsilon tensor, due to the presence of the γ_5 matrix. This does not appear in the final result, however, due to the fact that there are only four external momenta. Given that these are linearly dependent, any Lorentz invariant combination of these momenta with the epsilon tensor vanishes. Consequently, the result for the Born cross section is proportional to

$$|V_{t\bar{b}}|^2\left(|a|^2+|b|^2\right). \tag{5.5}$$

The result for the Born amplitude is

$$|\mathcal{A}^{(0)}|^2 = -4\frac{N_C C_F}{st_1^2}\big(2t_1(m_H^2+m_t^2)^2 - 2t_1^2(m_H^2-m_t^2) + t_1^3 - 2st(m_H^2-m_t^2) + s^2t_1 + 2st_1^2\big), \tag{5.6}$$

where we introduced $t_1 = t - m^2$ and $u_1 = u - m^2$. We summed over all initial and final spin polarizations, therefore the differential cross section is given by

$$\begin{aligned} d\sigma^{(0)} &= \mathcal{M}^{(0)}d\Phi_2, \\ \mathcal{M}^{(0)} &= \frac{1}{2s}\frac{1}{4}\frac{1}{N_C(N_C^2-1)}g_s^2(|a|^2+|b|^2)|\mathcal{A}^{(0)}|^2. \end{aligned} \tag{5.7}$$

In this equation $d\Phi_2$ is the two-body phase space measure. The factor $1/4$ is from averaging over the spin states of the quark and gluon, and the factors $1/N_C$ and $1/(N_C^2-1)$ from averaging over the color states of the quark and gluon.

At NLO one has virtual corrections (fig. 5.3 and 5.4) to (5.3) and real emission diagrams (5.5). We first describe the virtual corrections.

5.1.1 Virtual diagrams

The relevant virtual diagrams for this process are shown in figs.5.3 and 5.4. We have calculated these using FORM [75]. The mass of the bottom quark is much less than the typical hard momentum scale of the process and therefore it is set to zero. We have to factorize the associated mass singularities (see section 1.9), which are treated (as are the other massless particles) through dimensional regularization. We will work in the $\overline{\text{MS}}$ renormalization scheme, except that we use an on-shell scheme for the top mass renormalization [76]. The relevant counterterms in the Lagrangian are then found to be

$$\mathcal{L}_{\text{ct}} = \delta Z\bar{\psi}(i\partial\!\!\!/ - m)\psi - \delta m\bar{\psi}\psi - i\delta g\bar{\psi}A\!\!\!/\psi + \delta y\bar{\psi}H\psi, \tag{5.8}$$

where ψ represents the top quark (or bottom in which $m = 0$), A represents the gluon and H represents the Higgs particle. The LSZ reduction formula states that the scattering amplitude is given by

$$\mathcal{A}^{(1)} = \sqrt{\tilde{Z}_t}\sqrt{\tilde{Z}_b}\sqrt{\tilde{Z}_A}G_{\text{amp}}, \tag{5.9}$$

where the $\tilde{Z}$-factors are the on-shell residues of the Dyson-summed propagators for the corresponding fields. Because we work at NLO only in the QCD coupling, which does not affect the Higgs, there is no Z-factor for the Higgs particle. The amputated Green's function G_{amp} is given by the sum of all graphs without self-energy insertions in external legs.

After we calculate all one-loop diagrams we have to renormalize the UV poles. The UV divergences of the self-energy diagrams fig. 5.3(d) and 5.4(d) are cancelled by the following counterterms

$$\begin{aligned} \delta Z &= -\alpha_S \frac{C_F}{4\pi\bar{\varepsilon}} \\ \delta m &= -\alpha_S \frac{mC_F}{4\pi}\left(\frac{3}{\bar{\varepsilon}} + 4 + 3\ln\left(\frac{\mu^2}{m^2}\right)\right), \end{aligned} \tag{5.10}$$

where we defined $1/\bar{\varepsilon} = 1/\varepsilon - \gamma_E + \ln 4\pi$ as conventional in $\overline{\text{MS}}$. Note the choice of on-shell scheme for δm. For the bottom quark $m = 0$ and so there is no mass renormalization counterterm present. The QCD vertex corrections of fig. 5.3(a) and 5.4(a) are renormalized through

$$\delta g = -\alpha_S \frac{C_A + C_F}{4\pi\bar{\varepsilon}}. \tag{5.11}$$

Note that this is not proportional to the well-known QCD beta function, because we do not include the wave function corrections of the legs. The Higgs vertex (fig. 5.3(b) and 5.4(b)) correction is renormalized by the Yukawa coupling countertem

$$\delta y = -\frac{4C_F}{4\pi\bar{\varepsilon}}\alpha_S. \tag{5.12}$$

Next we have to calculate the UV finite $\tilde{Z}$-factors of the LHZ reduction formula. The self-energy graph for the massless bottom is zero because it is scaleless (see section 1.3). The UV finite $\tilde{Z}_b$ factor for the bottom is thus

$$\tilde{Z}_b = 1 + 0 - \frac{C_F}{4\pi\bar{\varepsilon}}\alpha_S, \tag{5.13}$$

where the zero indicates the contribution from the self-energy graph and the last term comes from δZ in eq. (5.10). Although $\tilde{Z}_b$ is clearly divergent, its divergence is an IR divergence because the massless bottom can split into a collinear bottom-gluon pair. For the top quark the $\tilde{Z}_t$ factor is indeed truly finite. The gluon self-energy has

contributions from the massless particles (which give zero) and from the top quark, which gives a non-zero contribution. Therefore $\tilde{Z}_A$ has an IR divergence from the massless particles, plus a finite piece due to the top quark.

In this renormalization procedure all the Green's functions are UV finite, because we have explicitly cancelled all the UV divergences through counterterms. For scattering processes this is not the most convenient approach (wave function renormalization is ultimately irrelevant in S-matrix elements). Therefore we resum the Dyson series of all the wavefunction counterterms to obtain, e.g. for the top quark propagator,

$$\sum_{n=0}^{\infty} \frac{i}{\not{p}-m}\left(i\delta Z(\not{p}-m)\frac{i}{\not{p}-m}\right)^n = \frac{1}{1+\delta Z}\frac{i}{\not{p}-m} \tag{5.14}$$

which is equivalent to a wavefunction renormalization. Each propagator carries this factor, such that one may choose to absorb the square root of this factor in each of the endpoints. The vertices acquire a factor $(1+\delta Z)^{-1/2}$ from each leg. Then the counterterms become

$$\begin{aligned}\delta Z_g &= -\frac{\frac{11}{6}C_A - \frac{2}{3}N_F}{4\pi\bar{\varepsilon}}\alpha_S \\ \delta Z_y &= -\frac{3C_F}{4\pi\bar{\varepsilon}}\alpha_S\end{aligned} \tag{5.15}$$

and the LSZ formula gives

$$\begin{aligned}\mathcal{A}^{(1)} &= \sqrt{\tilde{Z}_t}\sqrt{\tilde{Z}_b}\sqrt{\tilde{Z}_g}(1+\delta Z)(1+\delta Z_A)^{\frac{1}{2}}\bar{G}_{\text{amp}}, \\ &= \sqrt{\bar{Z}_t}\sqrt{\bar{Z}_b}\sqrt{\bar{Z}_g}\bar{G}_{\text{amp}}, \\ \bar{Z}_{b,t} &= \tilde{Z}_{b,t}(1+\delta Z) \\ \bar{Z}_A &= \tilde{Z}_A(1+\delta Z_A)\end{aligned} \tag{5.16}$$

where $\bar{G}_{\text{amp}}$ is equivalent to G_{amp} except that no wavefunction renormalization counterterms are present and for the other counterterms we use those of eq.(5.15). The extra factors $(1+\delta Z)$ cancel unmatched vertex factors from the amputated external legs.

In the above we have resummed all the wavefunction renormalization counterterms. This potentially includes the top quark contribution to the gluon wavefunction renormalization at the QCD vertex. However it is preferable that the running QCD coupling depends only on the five light quark flavours. Therefore we choose $N_F = 5$ and cancel the top quark gluon self-energy by an explicit counterterm. We recognize the usual beta function of QCD in eq. (5.15). Note also that the pole parts of the mass and Yukawa coupling counterterms are related by

$$\delta y = \frac{\delta m}{m}, \tag{5.17}$$

the property that the finite part is not the same, is due to the fact that the Yukawa coupling is renormalised in the $\overline{\text{MS}}$ scheme, whereas the top quark mass is renormalised in the on-shell scheme. This relation stems from the fact that the neutral part of the Higgs sector is responsible for the mass of the quarks. The LSZ factors $\bar{Z}$-factors have to be calculated in this scheme, and will be UV divergent. We have $\bar{Z}_b = 1$ because of the absence of a counterterm, which can be seen as a cancellation between UV and IR divergences. The top quark $\bar{Z}_t$ factor is given by

$$\bar{Z}_t = \frac{\alpha_S}{4\pi}\left(2 + \ln\frac{\mu^2}{m^2}\right) \tag{5.18}$$

and, for the gluon we have

$$\bar{Z}_A = \frac{\alpha_S}{4\pi}\left(\frac{4}{9} - \frac{4}{3}\ln\frac{\mu^2}{m^2}\right). \tag{5.19}$$

Putting everything together, we find that the renormalized virtual corrections are given by

$$d\sigma^{(1),V} = C_\epsilon g^2 \left[-\frac{2}{\epsilon^2}(C_F + C_A) + \frac{2}{\epsilon}C_A\left(\ln\frac{s}{m^2} + \ln\frac{-t_1}{m^2} - \ln\frac{-u_1}{m^2}\right) + C_F\left(2\ln\frac{-u_1}{m^2} - 1\right)\right] d\sigma^{(0)} + d\sigma^{(1),V}_{\text{finite}}, \tag{5.20}$$

where

$$C_\epsilon = \frac{(4\pi e^{-\gamma_E})^\epsilon}{16\pi^2}\left(\frac{\mu^2}{m^2}\right)^\epsilon. \tag{5.21}$$

The poles in eq. (5.20) correspond to IR and COL singularities. These must be cancelled by the real emission contributions, to which we now turn.

5.1.2 Real diagram

The real emission diagrams at NLO are all tree diagrams, for the calculation of which several automated packages exists (e.g. MadGraph [77]). We chose to calculate the real emission graphs using FORM and checked the correctness of our result against MadGraph. The contribution to the cross section from real diagrams that are radiative corrections to the Born cross section is infinite due to IR/COL gluon emissions. Other real diagrams give a finite contribution. Due to the presence of only a single massive colored particle in the final state at the Born level, the IR/COL singularity structure is not overly complex. There are only collinear singularities from the initial parton collinear radiation, and an IR singularity. A collinear splitting of one of the initial partons is indistinguishable from a two to two process, because the collinear parton travels together with the remaining hadron and cannot be measured. The initial state collinear singularities are therefore factorized into the PDF's (as a process that happens inside the hadron). Therefore these divergences cancel against the process

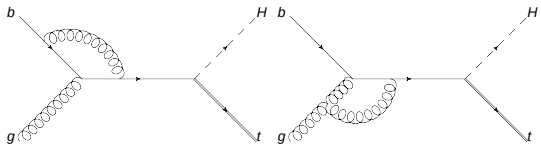

(a) QCD vertex correction diagrams.

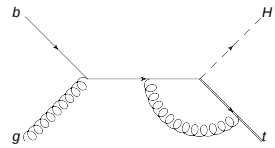

(b) Higgs vertex correction diagram.

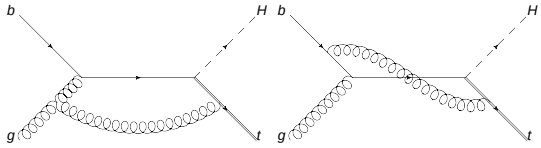

(c) Box diagrams.

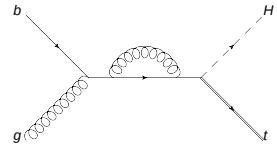

(d) Self-energy diagram.

Figure 5.3: s-channel virtual corrections.

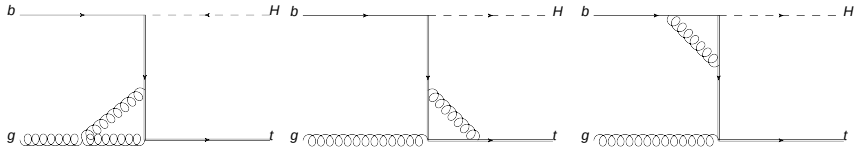

(a) QCD vertex correction diagrams.

(b) Higgs vertex correction diagram.

(c) Box diagram.

(d) Self energy diagram.

Figure 5.4: t-channel virtual corrections.

(a) Real correction to born s-channel.

(b) Real diagram contributing gg.

Figure 5.5: A sample of real diagrams.

independent collinear counterterms. The remaining IR divergences cancel against the virtual divergences for IR safe observables (see section 1.8). Nevertheless they presents a nuisance in numerical calculations, because a fully differential description will generate a final state with all momenta available. This requires a formalism in which the IR/COL divergences are cancelled analytically, leaving finite probabilities with only few negative weight events. This is achieved by the FKS formalism.

5.2 FKS subtraction formalism

Physical observables must be IR safe (see section 1.7), and this puts a demand on managing the divergences in higher order calculations. Schematically, the observable O (e.g. the p_t of a jet) is calculated at NLO according to

$$\langle O \rangle = \int d\Phi_2(\{k_i\}) O^{(2)}(\{k_i\}) \mathcal{M}^{(2)}(\{k_i\}) + \int d\Phi_3(\{k_i\}) O^{(3)}(\{k_i\}) \mathcal{M}^{(3)}(\{k_i\}), \quad (5.22)$$

where $\mathcal{M}^2$ and $\mathcal{M}^3$ are the two and three parton production probabilities respectively. In here O^2 and O^3 must be such that O^3 tends to O^2 in the collinear and infrared regions in phase space, which is the requirement that O is IR safe. Because of the limiting behavior of O we can separate phase space to obtain

$$\begin{aligned}\langle O \rangle = \int d\Phi_2(\{k_i\}) O^{(2)}(\{k_i\}) \mathcal{M}^{(2)}(\{k_i\}) + \int_{\text{singular}} d\Phi_3(\{k_i\}) O^{(2)}(\{k_i\}) \mathcal{M}^{(3)}(\{k_i\}) \\ + \int_{\text{non-singular}} d\Phi_3(\{k_i\}) O^{(3)}(\{k_i\}) \mathcal{M}^{(3)}(\{k_i\}), \quad (5.23)\end{aligned}$$

where we used to two-body phase space observable in the singular region.

There are two different types of methods to implement such a separation in practice. The *phase slicing method* [78, 79, 80] divides the phase space into hard and soft regions. Schematically we have

$$\begin{aligned}\int_0^1 dx\, x^{-1+\varepsilon} f(x) &\approx \int_0^\delta dx\, x^{-1+\varepsilon} f(0) + \int_\delta^1 dx\, x^{-1} f(x) \\ &\approx \frac{1}{\varepsilon} f(0) + f(0) \ln \delta + \int_\delta^1 dx\, x^{-1} f(x),\end{aligned} \quad (5.24)$$

where the integral symbolizes the phase space integration, regularized by dimensional regularization, and split into a soft ($x \approx 0$) and hard part. In the soft region, if δ is small, the integrand is well approximated by an analytical function that can be explicitly integrated, producing a pole that cancels the virtual poles. This method is conceptually close to the physics and easy to implement, but has the drawback of depending on δ being small. Moreover the total result then depends on the cancellation of large numbers (between the last two terms in (5.24)), leading to numerical instabilities. The *subtraction method* [81, 74, 82] works by introducing a counterterm that can

be integrated over the full phase space, schematically

$$\int_0^1 dx x^{-1+\varepsilon} f(x) = \int_0^1 dx x^{-1+\varepsilon} \left(f(x) - f(0)\right) + \frac{f(0)}{\varepsilon} = \int_0^1 dx [x^{-1}]_+ f(x) + \frac{f(0)}{\varepsilon}. \tag{5.25}$$

This method is exact and no large cancellation between real and virtual is required anymore [83] and presents, in this sense, a major advantage over the phase space slicing method.

We implement the cancellation of IR/COL poles through the so-called FKS subtraction scheme [74], which is particularly well suited for building a NLO Monte Carlo generator [84]. The divergence structure of the partonic cross sections is given by

$$d\hat{\sigma}_{ab}^{(0)}(k_1,k_2) = d\sigma_{ab}^{(0)}(k_1,k_2) \tag{5.26}$$

$$\begin{aligned} d\hat{\sigma}_{ab}^{(1)}(k_1,k_2) =& d\sigma_{ab}^{(1)}(k_1,k_2) + \frac{\alpha_S}{2\pi} \sum_d \int dx \left(\frac{1}{\bar{\varepsilon}} P_{da}(x) d\sigma_{db}^{(0)}(xk_1,k_2) \right) \\ &+ \frac{\alpha_S}{2\pi} \sum_d \int dx \left(\frac{1}{\bar{\varepsilon}} P_{db}(x) d\sigma_{ad}^{(0)}(k_1,xk_2) \right), \end{aligned} \tag{5.27}$$

where k_1, k_2 are the incoming partonic momenta and P is Altarelli-Parisi splitting function [85]. The starting point of the subtraction method is

$$d\sigma^{(r)} = d\sigma^{(\text{sing})} + d\sigma^{(\text{fin})}, \tag{5.28}$$

where we split the real cross section contribution into an analytical well-controlled singular part and a finite part. The singular part is from the region where the radiated gluon is soft or collinear to one of the initial state partons. The FKS method continues by introducing a particular representation for the momentum of the final state gluon

$$k = \frac{\sqrt{S}}{2} \xi \left(1, \sqrt{1-y^2}\vec{e}_T, y\right), \tag{5.29}$$

where $\xi \to 0$ parameterize the soft and $y \to \pm 1$ the collinear limits. Using this parameterization, the phase space measure of the gluon becomes in $d = 4 - 2\varepsilon$ dimensions

$$d\phi = \frac{d^{3-2\varepsilon}\vec{k}}{(2\pi)^{3-2\varepsilon} 2k^0} = \frac{1}{2(2\pi)^{3-2\varepsilon}} \left(\frac{\sqrt{S}}{2}\right)^{2-2\varepsilon} \xi^{1-2\varepsilon} (1-y^2)^{-\varepsilon} d\xi dy d\Omega^{2-2\varepsilon}. \tag{5.30}$$

The amplitude to be integrated with this measure is divergent in the limit $\xi \to 0$. We now insert $1 = \xi^2 \times \xi^{-2}$, absorbing the factor ξ^2 into the amplitude and ξ^{-2} in the measure, and obtain

$$\xi^{-2} d\phi = \frac{1}{2(2\pi)^{3-2\varepsilon}} \left(\frac{\sqrt{S}}{2}\right)^{2-2\varepsilon} \xi^{-1-2\varepsilon} (1-y^2)^{-\varepsilon} d\xi dy d\Omega^{2-2\varepsilon}. \tag{5.31}$$

Now we can use the distribution identity

$$\xi^{-1-2\varepsilon} = -\frac{\xi_{\text{cut}}^{-2\varepsilon}}{2\varepsilon}\delta(\xi) + \left[\frac{1}{\xi}\right]_c - 2\varepsilon\left[\frac{\ln\xi}{\xi}\right]_c + \mathcal{O}(\varepsilon^2), \tag{5.32}$$

where we defined the distribution $[f(\xi)]_c$ to satisfy

$$\int d\xi [f(\xi)]_c g(\xi) = \int_0^1 d\xi f(\xi)\left(g(\xi) - g(0)\theta(\xi_{\text{cut}} - \xi)\right). \tag{5.33}$$

ξ_{cut} is an arbitrary parameter. The result of calculation will not depend on the value of ξ_{cut} as long as it is below the resolution of the IR safe observable one calculates. The first term in eq. (5.32) isolates the IR pole and enters $d\sigma^{\text{sing}}$ in eq. (5.28). The Dirac delta function makes sure that the radiated gluon has no energy, which maps the three body observable onto the corresponding two body observable. The remaining terms in eq. (5.32) do not contain soft divergences but do still contain an collinear singularity. The remain collinear singularity can be treated analogously by multiplying and dividing by $(1-y^2)$. For the phase space measure we then use

$$(1-y^2)^{-1-2\varepsilon} = -\frac{(2\delta_I)^{-\varepsilon}}{2\varepsilon}\left[\delta(1-y) + \delta(1+y)\right] + \mathcal{P}_{\delta_I}(y) + \mathcal{O}(\varepsilon^2), \tag{5.34}$$

$$\mathcal{P}_{\delta_I}(y) = \frac{1}{2}\left[\left(\frac{1}{1-y}\right)_{\delta_I} + \left(\frac{1}{1+y}\right)_{\delta_I}\right]. \tag{5.35}$$

The divergence is again isolated at $y = \pm 1$, which makes the substitution of the two-body observable exact. This divergence again enters $d\sigma^{\text{sing}}$ in eq. (5.28).

Because all ε-poles have been isolated, one can add them to the virtual contribution, to obtain an finite result for both the two-to-two aand the two-to-three amplitudes. Using this one can calculate cross sections numerically producing fully differential NLO results.

We can use the NLO code to calculate various differential cross sections for top plus charged Higgs production. Before showing results, we discuss the implementation of our NLO calculation in the MC@NLO framework, in which parton showers are consistently added to the description. In the last section (5.4) we compare the NLO against the MC@NLO calculations for a variety of observables.

5.3 MC@NLO

The NLO description just achieved, while valid for calculating observables with at most one extra parton, cannot produce the fully exclusive events that a Monte Carlo (MC) event generator does. In order to do that we must interface the NLO code with a parton shower, which is the subject of this section.

A Monte Carlo event generator[1] is a computer program that attempts to generate events with a frequency corresponding to the probabilities that occur in nature[2]. Due to NLO corrections and MC counterterms, one has a small fraction of negative weighted events. By an event we mean the full set of final state particles being generated in an individual scattering process. Such an event generator can then be interfaced with a further simulation to incorporate detector effects. The increasing complexity of the processes and the detectors at the forefront of experimental particle physics, make these tools indispensible. The amount of particles being produced in events at the LHC is so large that huge amounts of complex data are being produced for each event. This presents a serious obstacle for understanding the underlying fundamental process. So instead of working backwards from data to get to the underlying hard interaction, the opposite approach is often taken in which a given hard interaction is generated, which is evolved forwards to model the data. This is achieved using Monte Carlo generators together with detector simulations. Another benefit of Monte Carlo simulations is that it provides an easy way of calculating observables with cuts applied.

The basic idea behind Monte Carlo generators is that soft and collinear radiation factorizes. As discussed in the introduction (section 1.9), the total scattering amplitude can be separated into a hard scattering combined with the effects of collinear and soft interactions. The total probability of an event is then given by

$$P(E) = \sum_H p(H)p(H \to E), \tag{5.36}$$

where H denotes the hard interaction. In this formula $p(H)$ is the probability for the particular hard interaction H to happen and $P(H \to E)$ is the probability to evolve from the end result of the hard interaction to the final event, i.e. each hard interaction is decoupled from any subsequent soft / collinear radiation. At leading order $p(H)$ is given by the Born differential cross-section and $p(H \to E)$ is calculated using parton showers (plus hadronization models, detector effects etc.). The parton shower radiates partons from the hard lines coming out of the hard interaction, according to well-known algorithms. The parton shower stops when the hard lines have radiated sufficient energy, governed by a non-perturbative cut-off parameter, after which the phase space is populated with many partons. The hadronization algorithm proceeds by clustering partons into colorless objects, which then decay to produce final state hadrons.

The Monte Carlo generator we use is Herwig [86], which, given the tree level cross section for the hard scattering, generates the hard scattering and performs the parton shower consistent with LO perturbation theory. However, at NLO we include real emissions, so that part of the tree level plus parton shower is already present in the real emission contributions. In a naive scheme of including NLO corrections in a MC this would introduce an overcounting of real emission contributions. This is not easily

[1] Example of much-used multi-purpose event generators are PYTHIA, Herwig, SHERPA and Ariadne.

[2] Such a description in terms of unweighted events is usually achieved using hit-and-miss and similar methods.

solved and prevented the use of NLO calculations in MC for a long time. In [84] a solution was presented, called MC@NLO. A similar but not quite equivalent method is adapted in the POWHEG [87] framework. In [84] a systematic subtraction of the real cross section is performed, such that there is no overcounting when the parton shower is included. The Monte Carlo counterterms, i.e. the terms that have to be subtracted because they represent the contribution of the shower at $\mathcal{O}(\alpha_S)$, have been calculated for Herwig. An efficient matching to this shower has been done within the FKS subtraction method, making this the preferred method for interfacing NLO with a Monte Carlo within the MC@NLO framework. The matching is such that the fully inclusive cross section of MC@NLO equals that of NLO.

Details of matching our NLO calculation of section 5.1 with the parton shower in MC@NLO framework are perfectly analogous to that of the Wt case in [88], so we shall not reproduce them here. We now rather turn to examine and compare the results of both our NLO and MC@NLO calculations for top plus charged Higgs production.

5.4 Results

In this section we present some results of our calculation. Having both a NLO and a MC@NLO calculations it is useful to compare them where possible. Of course we cannot compare multiparticle fully exclusive cross sections as NLO only has two or three final state partons. On the other hand for sufficiently inclusive observables there should be good agreement. We will here discuss some representative distributions, and we first describe the parameter choices used.

Firstly, it is conventional to write the charged Higgs coupling as [89]

$$-\frac{i}{v\sqrt{2}}V_{tb}[m_b \tan\beta(1-\gamma_5) + m_t \cot\beta(1+\gamma_5)], \tag{5.37}$$

where $v \simeq 246$GeV is the electroweak symmetry breaking scale, and $\tan\beta$ is the ratio of vacuum expectation values for the two Higgs doublets. Relating this to the form adopted for the coupling in eq. (5.4), one has

$$a = -\frac{i}{v\sqrt{2}}[m_b \tan\beta + m_t \cot\beta], \quad b = -\frac{i}{v\sqrt{2}}[m_t \cot\beta - m_b \tan\beta]. \tag{5.38}$$

Given that $\tan\beta$ is thought to be large [89], we choose $\tan\beta = 60$. Furthermore, the top and charged Higgs masses are set to 175GeV and 200GeV respectively. All results are presented for default (equal) factorisation and renormalisation scales of $(m_H + m_t)/2$, and we use MRST2002NLO [90] parton densities for both the LO and NLO results. With these choices, the LO and NLO cross-sections are 3.1pb and 4.2pb respectively i.e. a K-factor[3] of $\simeq 1.35$.

Next we consider kinematic distributions, beginning with the transverse momenta ($p_\perp$) of both the charged Higgs and the top. These do not show significant difference

[3]The K-factor is the ratio of the NLO to the LO cross section.

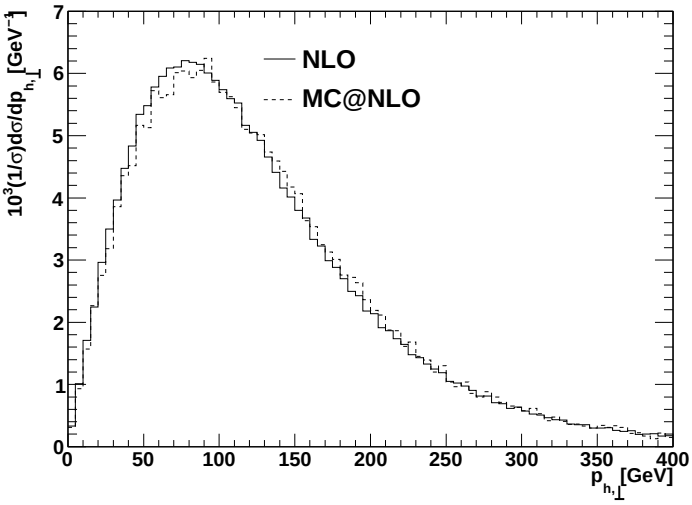

Figure 5.6: The transverse momentum ($(p_h)_\perp$) distribution of the charged Higgs boson.

between NLO and MC@NLO, as can be seen from figs. 5.6 and 5.7. For the $p_\perp$ of the Higgs this is expected as there is no showering of partons from the Higgs. For the top the showering has a mild effect given the large mass of the top (175 GeV), and the inclusive treatment of the recoil radiation in both calculations. Within the statistics there is no discernible difference between NLO and MC@NLO. In figs. 5.8 and 5.9 we show the rapidity distributions. The rapidity is the boost of the Higgs (or top) along the beam axis. Also here we do not observe any significant deviations between NLO and MC@NLO for reasons similar to that of the $p_\perp$ distributions. Any apparent asymmetry between positive and negative y should have a statistical origin, because there is complete symmetry in the center-of-mass frame for the Higgs (or top) to go into one of the two hemispheres defined by the beam. The distribution of the azimuthal angle between the top and the Higgs is shown in fig. 5.10. The azimuthal angle is the angle between the Higgs and the top particle in the transverse plane, which at leading order are necessarily back-to-back ($\phi = \pi$) by momentum conservation. Therefore the distribution of the cross section as function of the azimuthal angle is very sensitive to NLO corrections. Because the Monte Carlo parton shower radiates extra particles from the top, we expect to see extra decorrelation between the transverse directions of the two particles. Indeed, see fig. 5.10, one see an excess in the cross section at ϕ far from π in the case of MC@NLO.

Above distributions all match, with a slight deviation for the ϕ distribution. Not all observables show such good agreement between their NLO and MC@NLO description. One such distribution is the summed transverse momentum of the top and charged Higgs, which is zero at LO. NLO should produce a steeply rising real emis-

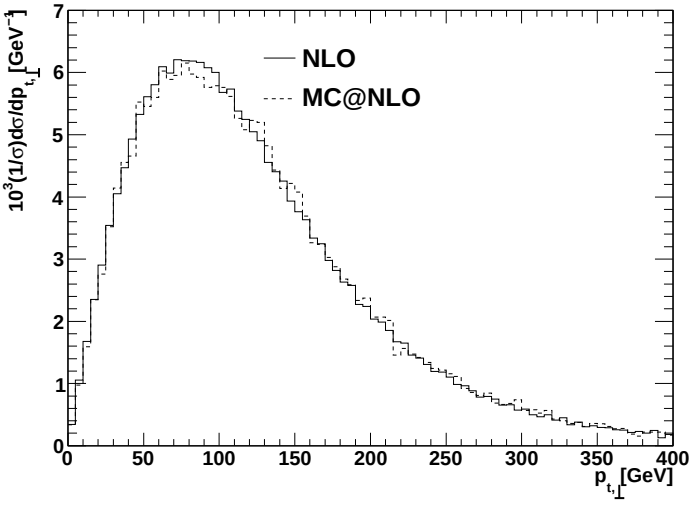

Figure 5.7: The transverse momentum ($(p_t)_\perp$) distribution of the top quark.

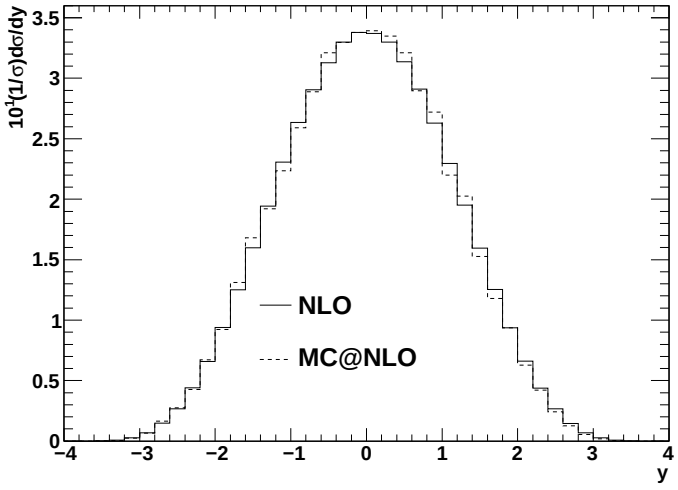

Figure 5.8: The rapidity (y) distribution of the charged Higgs boson.

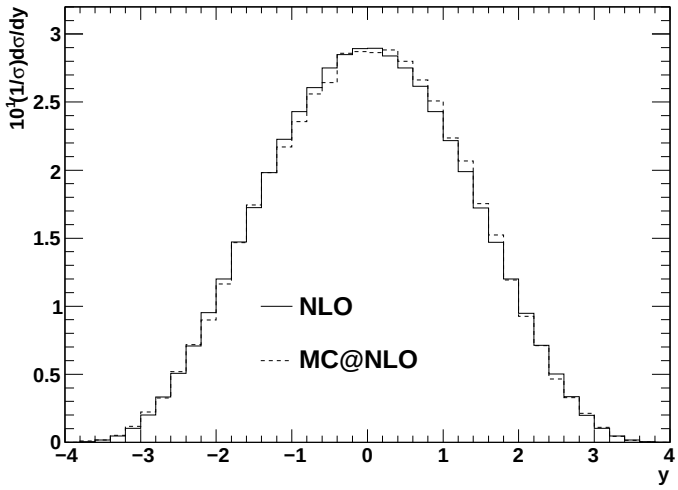

Figure 5.9: The rapidity (y) distribution of the top quark.

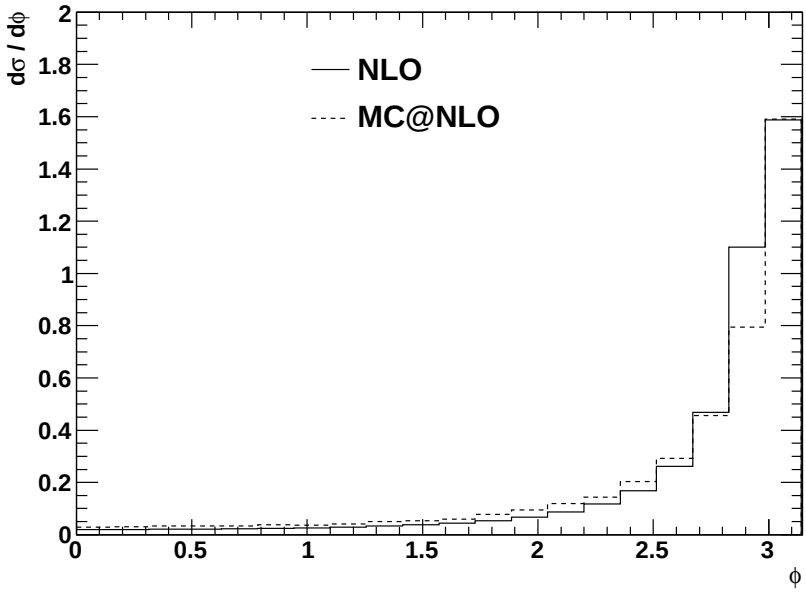

Figure 5.10: Distribution in azimuthal angle between top and Higgs at NLO and MC@NLO.

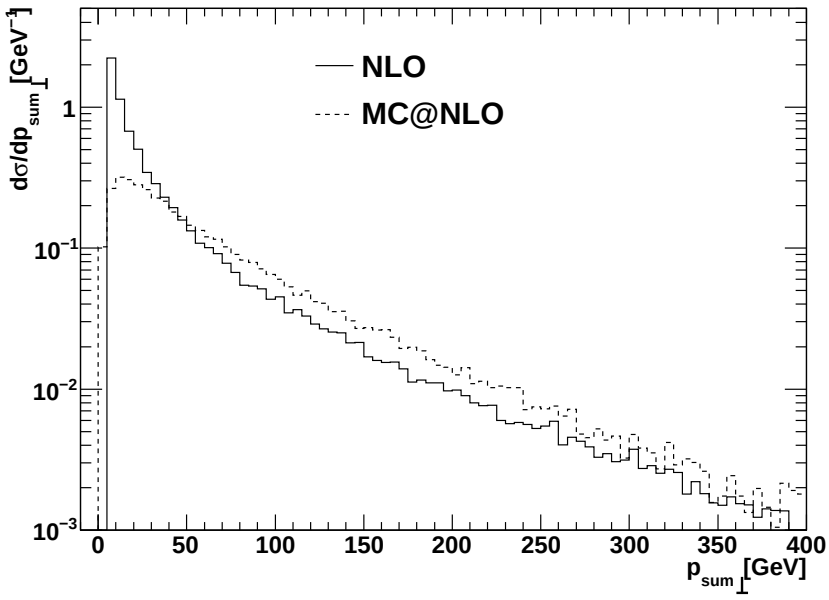

Figure 5.11: The distribution as function of the sum of the $p_\perp$ of the Higgs and top.

sion contribution for decreasing p_t, together with a large negative contribution at zero p_t from the virtual diagrams. We expect a more intuitive result from the MC@NLO distribution in which the Sudakov suppression present in the parton shower algorithm should lead to a smooth behavior towards $p_t = 0$. Both expected behaviors are indeed visible in fig.5.11. Moreover, at large p_t the NLO and MC@NLO calculations converge within the statistics, as can be seen from the tail of fig.5.11.

Chapter 6

Conclusion

In this thesis we have studied soft gluon radiation in QCD from various perspectives, and uncovered new patterns of exponentiation in perturbative descriptions of scattering amplitudes and cross sections. While the leading eikonal contributions from soft radiation and their all-order treatment have been understood for some time, almost nothing was known about next-to-eikonal contributions, defined by one extra power of soft gluon momentum. We have shown that such contributions also exponentiate. To this end we have developed new tools based both on path integrals and on new Feynman rules, that might also be useful beyond the purposes discussed here. The new insights have been applied to the Drell-Yan process in order to verify their validity and assess their predictive power.

In the introduction we recalled that in quantum field theory infinities arise from both small and large distance scales. Although these infinities cancel when treated correctly, their structure is instructive. In this thesis we focused on the infinities from large distance scales, i.e. infrared and collinear divergences. Remnants of these divergences can form numerically large perturbative corrections for physical observables in certain kinematical regimes, in particular near threshold: partonic cross sections diverge when all radiation is constrained to be soft. In such a threshold regime, characterized e.g. in Drell-Yan by $z \to 1$ or its Mellin moment $N \to \infty$, at order $\mathcal{O}(\alpha_S^n)$ perturbative coefficients grow as $\ln^{2n} N$. This endangers the predictive power of the perturbative series, which may be rescued by summing all-order perturbation theory into known analytical functions, an approach known as resummation. Using resummation we take into account the effect of arbitrary number of soft gluons radiated during the process. Such soft gluons can be treated in so-called eikonal approximation, in which the backreaction of the emission on the emitting particle is neglected. Using algebraic properties of the eikonal approximation it has been proved that the effect of all-order gluon radiation takes the form of an exponent. In chapters 2, 3 and 4 we extended this exponentiating structure to include terms generated by the next-to-eikonal contributions, characterized in Mellin space by terms $\mathcal{O}(\alpha_S^n \ln^k N/N)$.

More specifically, in chapter 2 we extended known resummation formulas by well-

motivated changes, in order to study the exponentiating structure of next-to-eikonal corrections. Indeed we found that we could reproduce all terms at one-loop and that we reproduced almost the next-to-eikonal next-to-leading logarithmic terms at two-loop order. The result gave confidence that also the next-to-eikonal part of the perturbation theory is governed by an all-order structure. In chapters 3 and 4 we indeed found such an all-order structure. In chapter 3 we analysed radiative scattering amplitudes using first-quantized path integrals. We derived a path-integral expression for a high momentum particle in a weak background gauge field. Using this powerful formalism we could indeed show that next-to-eikonal contributions exponentiate. In chapter 4 we rederive these results from a diagrammatic viewpoint, bringing the two approaches together.

In the last chapter we built a Monte Carlo event generator accurate to next-to-leading order (MC@NLO), for the scattering process producing a single top quark in association with charged Higgs boson in hadron collisions. This beyond the Standard Model process could be an important channel to discover new physics. The Monte Carlo algorithmically resums the effect of soft and collinear radiation thereby producing an accurate, well-normalized estimate for the events in this process. We showed and discussed some results of the both Monte Carlo and next-to-leading order calculations.

Taken together, the methods developed in this thesis should, besides yielding new insights into QCD perturbation theory, be beneficial towards more accurate predictions for scattering processes at particle colliders. Further study could include scattering processes with more colored lines and extension to various physical processes.

Bibliography

[1] Klaus Hepp. Proof of the Bogolyubov-Parasiuk theorem on renormalization. *Commun. Math. Phys.*, 2:301–326, 1966.

[2] Jean Zinn-Justin. *Quantum Field Theory and Critical Phenomena (International Series of Monographs on Physics)*. Clarendon Press, 4 edition, 2002.

[3] John C. Collins. *Renormalization. An introduction to renormalization, the renormalization group, and the operator product expansion*. Cambridge, Uk: Univ. Pr. (1984) 380p.

[4] W. Zimmermann. Convergence of Bogolyubov's method of renormalization in momentum space. *Commun. Math. Phys.*, 15:208–234, 1969.

[5] E. Brezin, Jean Zinn-Justin, and J. C. Le Guillou. Renormalization of the Nonlinear Sigma Model in (Two + Epsilon) Dimension. *Phys. Rev.*, D14:2615, 1976.

[6] Sidney R. Coleman. There are no Goldstone bosons in two-dimensions. *Commun. Math. Phys.*, 31:259–264, 1973.

[7] William A. Bardeen and Myron Bander. Phase Transition in an O(N) Gauge Model in Two- Dimensions. *Phys. Rev.*, D14:2117, 1976.

[8] L. D. Faddeev and V. N. Popov. Feynman diagrams for the Yang-Mills field. *Phys. Lett.*, B25:29–30, 1967.

[9] John C. Collins, Davison E. Soper, and George Sterman. Factorization of Hard Processes in QCD. *Adv. Ser. Direct. High Energy Phys.*, 5:1–91, 1988.

[10] Geoffrey T. Bodwin. Factorization of the Drell-Yan Cross-Section in Perturbation Theory. *Phys. Rev.*, D31:2616, 1985.

[11] T. D. Lee and M. Nauenberg. Degenerate Systems and Mass Singularities. *Phys. Rev.*, 133:B1549–B1562, 1964.

[12] V. V. Sudakov. Vertex parts at very high-energies in quantum electrodynamics. *Sov. Phys. JETP*, 3:65–71, 1956.

[13] George Sterman. Summation of Large Corrections to Short Distance Hadronic Cross-Sections. *Nucl. Phys.*, B281:310, 1987.

[14] S. Catani and L. Trentadue. Resummation of the QCD Perturbative Series for Hard Processes. *Nucl. Phys.*, B327:323, 1989.

[15] G. Parisi. Summing Large Perturbative Corrections in QCD. *Phys. Lett.*, B90:295, 1980.

[16] T. O. Eynck, Laenen E., and Magnea L. Exponentiation of the Drell-Yan cross section near partonic threshold in the DIS and MS-bar schemes. *JHEP*, 0306:057, 2003.

[17] Harry Contopanagos, Eric Laenen, and George Sterman. Sudakov factorization and resummation. *Nucl. Phys.*, B484:303–330, 1997.

[18] F. E. Low. Bremsstrahlung of very low-energy quanta in elementary particle collisions. *Phys. Rev.*, 110:974–977, 1958.

[19] T. H. Burnett and Norman M. Kroll. Extension of the low soft photon theorem. *Phys. Rev. Lett.*, 20:86, 1968.

[20] Vittorio Del Duca. High-energy bremsstrahlung theorems for soft photons. *Nucl. Phys.*, B345:369–388, 1990.

[21] M. Kramer, E. Laenen, and M. Spira. Soft gluon radiation in Higgs boson production at the LHC. *Nucl. Phys.*, B511:523, 1998.

[22] S. Catani, D. de Florian, and M. Grazzini. Higgs production in hadron collisions: Soft and virtual QCD corrections at NNLO. *JHEP*, 0105:025, 2001.

[23] Robert V. Harlander and William B. Kilgore. Soft and virtual corrections to p p $\rightarrow$ H + X at NNLO. *Phys. Rev.*, D64:013015, 2001.

[24] Stefano Catani, Daniel de Florian, Massimiliano Grazzini, and Paolo Nason. Soft-gluon resummation for Higgs boson production at hadron colliders. *JHEP*, 07:028, 2003.

[25] Rahul Basu, Eric Laenen, Anuradha Misra, and Patrick Motylinski. Soft-collinear effects in prompt photon production. *Phys. Rev.*, D76:014010, 2007.

[26] S. Moch, J. A. M. Vermaseren, and A. Vogt. The three-loop splitting functions in QCD: The non-singlet case. *Nucl. Phys.*, B688:101–134, 2004.

[27] Yu. L. Dokshitzer, G. Marchesini, and G. P. Salam. Revisiting parton evolution and the large-x limit. *Phys. Lett.*, B634:504–507, 2006.

[28] B. Basso and G. P. Korchemsky. Anomalous dimensions of high-spin operators beyond the leading order. *Nucl. Phys.*, B775:1–30, 2007.

[29] R. Hamberg, W. L. van Neerven, and T. Matsuura. A Complete calculation of the order alpha-s**2 correction to the Drell-Yan K factor. *Nucl. Phys.*, B359:343–405, 1991.

[30] E. B. Zijlstra and W. L. van Neerven. Order alpha-s**2 QCD corrections to the deep inelastic proton structure functions F2 and F(L). *Nucl. Phys.*, B383:525–574, 1992.

[31] J. A. M. Vermaseren, A. Vogt, and S. Moch. The third-order QCD corrections to deep-inelastic scattering by photon exchange. *Nucl. Phys.*, B724:3–182, 2005.

[32] Stefano Forte and Giovanni Ridolfi. Renormalization group approach to soft gluon resummation. *Nucl. Phys.*, B650:229–270, 2003.

[33] Lorenzo Magnea and George Sterman. Analytic continuation of the Sudakov form-factor in QCD. *Phys. Rev.*, D42:4222–4227, 1990.

[34] Simon Albino and Richard D. Ball. Soft resummation of quark anomalous dimensions and coefficient functions in MS-bar factorization. *Phys. Lett.*, B513:93–102, 2001.

[35] S. Catani, B. R. Webber, and G. Marchesini. QCD coherent branching and semi-inclusive processes at large x. *Nucl. Phys.*, B349:635–654, 1991.

[36] Eric Laenen and Lorenzo Magnea. Threshold resummation for electroweak annihilation from DIS data. *Phys. Lett.*, B632:270–276, 2006.

[37] Lance J. Dixon, Lorenzo Magnea, and George Sterman. Universal structure of subleading infrared poles in gauge theory amplitudes. *JHEP*, 08:022, 2008.

[38] G. Curci, W. Furmanski, and R. Petronzio. Evolution of Parton Densities Beyond Leading Order: The Nonsinglet Case. *Nucl. Phys.*, B175:27, 1980.

[39] S. Catani and M. Ciafaloni. Generalized Coherent State For Soft Gluon Emission. *Nucl. Phys.*, B249:301, 1985.

[40] G. P. Korchemsky and G. Marchesini. Resummation of large infrared corrections using Wilson loops. *Phys. Lett.*, B313:433–440, 1993.

[41] Gregory P. Korchemsky and George Sterman. Infrared factorization in inclusive B meson decays. *Phys. Lett.*, B340:96–108, 1994.

[42] Thomas Becher and Matthias Neubert. Threshold resummation in momentum space from effective field theory. *Phys. Rev. Lett.*, 97:082001, 2006.

[43] D. R. Yennie, Steven C. Frautschi, and H. Suura. The infrared divergence phenomena and high-energy processes. *Ann. Phys.*, 13:379–452, 1961.

[44] J. G. M. Gatheral. Exponentiation of eikonal cross-sections in nonabelian gauge theories. *Phys. Lett.*, B133:90, 1983.

[45] J. Frenkel and J. C. Taylor. Nonabelian eikonal exponentiation. *Nucl. Phys.*, B246:231, 1984.

[46] G. Sterman. Infrared divergences in perturbative QCD. (talk). *AIP Conf. Proc.*, 74:22–40, 1981.

[47] Carola Friederike Berger. *Soft gluon exponentiation and resummation*. PhD thesis, Stony Brook, 2003.

[48] Matthew J. Strassler. Field theory without Feynman diagrams: One loop effective actions. *Nucl. Phys.*, B385:145–184, 1992.

[49] Michael G. Schmidt and Christian Schubert. Worldline Green functions for multiloop diagrams. *Phys. Lett.*, B331:69–76, 1994.

[50] J. W. van Holten. Propagators and path integrals. *Nucl. Phys.*, B457:375–407, 1995.

[51] Zvi Bern and David C. Dunbar. A Mapping between Feynman and string motivated one loop rules in gauge theories. *Nucl. Phys.*, B379:562–601, 1992.

[52] Zvi Bern and David A. Kosower. The Computation of loop amplitudes in gauge theories. *Nucl. Phys.*, B379:451–561, 1992.

[53] A. I. Karanikas, C. N. Ktorides, and N. G. Stefanis. World-line techniques for resumming gluon radiative corrections at the cross-section level. *Eur. Phys. J.*, C26:445–455, 2003.

[54] M. Mezard, G. Parisi, and M. Virasoro. *Spin Glass Theory and Beyond*. World Scientific, 1987.

[55] Nikolaos Kidonakis. Collinear and soft gluon corrections to Higgs production at NNNLO. *Phys. Rev.*, D77:053008, 2008.

[56] L. Brink, P. Di Vecchia, and Paul S. Howe. A Locally Supersymmetric and Reparametrization Invariant Action for the Spinning String. *Phys. Lett.*, B65:471–474, 1976.

[57] A. G. Morgan. Second order fermions in gauge theories. *Phys. Lett.*, B351:249–256, 1995.

[58] C. S. Lam. Spinor helicity technique and string reorganization for multiloop diagrams. *Can. J. Phys.*, 72:415–438, 1994.

[59] G. Sterman. *An Introduction to quantum field theory*. Cambridge University Press, 1993.

[60] Eric Laenen, Lorenzo Magnea, and Gerben Stavenga. On next-to-eikonal corrections to threshold resummation for the Drell-Yan and DIS cross sections. *Phys. Lett.*, B669:173–179, 2008.

[61] Eric Laenen, Gerben Stavenga, and Chris D. White. Path integral approach to eikonal and next-to-eikonal exponentiation. *JHEP*, 03:054, 2009.

[62] Guido Altarelli, R. Keith Ellis, and G. Martinelli. Large Perturbative Corrections to the Drell-Yan Process in QCD. *Nucl. Phys.*, B157:461, 1979.

[63] T. Matsuura, S. C. van der Marck, and W. L. van Neerven. The Calculation of the Second Order Soft and Virtual Contributions to the Drell-Yan Cross-Section. *Nucl. Phys.*, B319:570, 1989.

[64] T. Matsuura, S. C. van der Marck, and W. L. van Neerven. The order alpha-s**2 contribution to the K factor of the Drell-Yan process. *Phys. Lett.*, B211:171, 1988.

[65] S. D. Drell and Tung-Mow Yan. Massive Lepton Pair Production in Hadron-Hadron Collisions at High-Energies. *Phys. Rev. Lett.*, 25:316–320, 1970.

[66] Eric Laenen, Lorenzo Magnea, Gerben Stavenga, and Chris D. White. Next-to-eikonal exponentiation of DY cross sections. in preparation.

[67] B. W. Harris, Eric Laenen, L. Phaf, Z. Sullivan, and S. Weinzierl. The fully differential single top quark cross section in next-to-leading order QCD. *Phys. Rev.*, D66:054024, 2002.

[68] Zack Sullivan. Understanding single-top-quark production and jets at hadron colliders. *Phys. Rev.*, D70:114012, 2004.

[69] Zack Sullivan. Angular correlations in single-top-quark and W j j production at next-to-leading order. *Phys. Rev.*, D72:094034, 2005.

[70] John M. Campbell, R. Keith Ellis, and Francesco Tramontano. Single top production and decay at next-to-leading order. *Phys. Rev.*, D70:094012, 2004.

[71] S. Zhu. Next-to-leading order QCD corrections to b g $\rightarrow$ t W- at the CERN Large Hadron Collider. *Phys. Lett.*, B524:283–288, 2002.

[72] John M. Campbell and Francesco Tramontano. Next-to-leading order corrections to W t production and decay. *Nucl. Phys.*, B726:109–130, 2005.

[73] G. Passarino and M. J. G. Veltman. One Loop Corrections for e+ e- Annihilation Into mu+ mu- in the Weinberg Model. *Nucl. Phys.*, B160:151, 1979.

[74] S. Frixione, Z. Kunszt, and A. Signer. Three jet cross-sections to next-to-leading order. *Nucl. Phys.*, B467:399–442, 1996.

[75] J. A. M. Vermaseren. New features of FORM. 2000.

[76] John C. Collins, Frank Wilczek, and A. Zee. Low-Energy Manifestations of Heavy Particles: Application to the Neutral Current. *Phys. Rev.*, D18:242, 1978.

[77] Johan Alwall et al. MadGraph/MadEvent v4: The New Web Generation. *JHEP*, 09:028, 2007.

[78] K. Fabricius, I. Schmitt, G. Kramer, and G. Schierholz. Higher Order Perturbative QCD Calculation of Jet Cross- Sections in e+ e- Annihilation. *Zeit. Phys.*, C11:315, 1981.

[79] H. Baer, J. Ohnemus, and J. F. Owens. A Next-To-Leading Logarithm Calculation of Jet Photoproduction. *Phys. Rev.*, D40:2844, 1989.

[80] W. T. Giele and E. W. Nigel Glover. Higher order corrections to jet cross-sections in e+ e- annihilation. *Phys. Rev.*, D46:1980–2010, 1992.

[81] R. Keith Ellis, D. A. Ross, and A. E. Terrano. Calculation of Event Shape Parameters in e+ e- Annihilation. *Phys. Rev. Lett.*, 45:1226–1229, 1980.

[82] S. Catani and M. H. Seymour. A general algorithm for calculating jet cross sections in NLO QCD. *Nucl. Phys.*, B485:291–419, 1997.

[83] Tim Oliver Eynck, Eric Laenen, Lukas Phaf, and Stefan Weinzierl. Comparison of phase space slicing and dipole subtraction methods for gamma* $\rightarrow$ Q anti-Q. *Eur. Phys. J.*, C23:259–266, 2002.

[84] Stefano Frixione and Bryan R. Webber. Matching NLO QCD computations and parton shower simulations. *JHEP*, 06:029, 2002.

[85] Guido Altarelli and G. Parisi. Asymptotic Freedom in Parton Language. *Nucl. Phys.*, B126:298, 1977.

[86] G. Corcella et al. HERWIG 6.5: an event generator for Hadron Emission Reactions With Interfering Gluons (including supersymmetric processes). *JHEP*, 01:010, 2001.

[87] Stefano Frixione, Paolo Nason, and Carlo Oleari. Matching NLO QCD computations with Parton Shower simulations: the POWHEG method. *JHEP*, 11:070, 2007.

[88] Stefano Frixione, Eric Laenen, Patrick Motylinski, Bryan R. Webber, and Chris D. White. Single-top hadroproduction in association with a W boson. *JHEP*, 07:029, 2008.

[89] Abdelhak Djouadi. The Anatomy of electro-weak symmetry breaking. II. The Higgs bosons in the minimal supersymmetric model. *Phys. Rept.*, 459:1–241, 2008.

[90] M. R. Whalley, D. Bourilkov, and R. C. Group. The Les Houches Accord PDFs (LHAPDF) and Lhaglue. 2005.

Samenvatting

In de subnucleaire wereld van de hedendaagse deeltjesfysica beschrijft kwantumchromodynamica de dominante kracht. De andere krachten die beschreven worden door het Standaard Model zijn de elektrische en zwakke kern kracht. In botsingsexperimenten, zoals die bijvoorbeeld gaan plaats vinden in de Large Hadron Collider (LHC) op het CERN, is het belangrijk om de gevolgen van deze kracht goed te begrijpen. Hoewel de hoge energie limiet van deze kracht zich, dankzij 'asymptotische vrijheid' (Nobelprijs 2007), adequaat laat beschrijven door perturbatietheorie is de lage energie limiet intrinsiek niet-perturbatief. Pertubatietheorie houdt in dat we de effecten van de kracht benaderen door er vanuit te gaan dat deze kracht zwak is en dat de deeltjes zich dus redelijk vrij kunnen bewegen. We kunnen dan systematisch een reeks van correctie-termen berekenen die beter en beter het effect van de kracht benaderen. Als de correctie-termen voldoende snel convergeren dan vormt dit een goede methode om accurate berekeningen uit te voeren.

Gelukkig is het mogelijk om de effecten van kwantumchromodynamica komend van laag-energetische interacties ('zachte straling') te scheiden van de harde, hoog-energetische, fundamentele interacties in een botsingsproces door middel van 'factorisatie'. Dit maakt het mogelijk om perturbatieve berekeningen te doen aan botsingsprocessen, waarbij de onberekenbare, niet-perturbatieve zachte correcties worden geparametriseerd door universele functies. Hoewel deze functies niet berekenbaar zijn, kunnen zij wel gemeten worden in specifieke experimenten om vervolgens gebruikt te worden om andere experimenten te verklaren. In dit proefschrift bestuderen wij de zachte aspecten van kwantumchromodynamica vanuit het perturbatieve standpunt. Alhoewel deze zachte straling niet-perturbatief is, kunnen we wel de lage energie limiet bestuderen van perturbatietheorie. De niet-perturbatieve natuur van de zachte straling is dan, in zekere zin, zichtbaar in perturbatietheorie door de grote correctie-termen. Deze grote correctie-termen verstoren de convergentie van de pertubatiereeks. Dit betekent dat hoge orde correctie-termen belangrijk zijn en wij willen daarom de effecten van alle ordes meenemen. De enige bekende manier om perturbatietheorie tot alle ordes te kunnen hanteren is door de reeks te sommeren tot bekende analytische functies. Deze procedure is met succes toegepast in verschillende berekeningen en staat bekend als hersommatie. In hoofdstuk 2 breiden we de bestaande hersommatie-formules uit met heuristische maar goed gemotiveerde termen en bestuderen de kwaliteit door de uitkomsten te vergelijken met bekende resultaten. Het

blijkt dat de uitgebreide formule inderdaad beter de structuur op alle ordes bevat en hersommeert, alhoewel niet alle termen correct gevonden worden. In hoofstukken 3 en 4 bestuderen we de structuur van de perturbatiereeks in het regime van zachte straling in meer detail en vinden een uitbreiding van de bekende structuur. Dit maakt het mogelijk om een exponentiële vorm voor de perturbatieve bijdrage van zachte straling te vinden, geldig tot op een extra orde in de zachte straling. Het uitgangspunt is dat de hoog-energetische deeltjes, die in botsingsprocessen gegenereerd worden, in een rechte lijn naar oneindig vliegen. Onze benadering bestaat uit het meenemen van kwantumfluctuaties rond dit pad. Deze fluctuaties kunnen belangrijke bedragen leveren aan bijvoorbeeld de productie van het Higgs deeltje.

In het laatste hoofdstuk 5 construeren we een computerprogramma waarmee we precieze voorspellingen kunnen doen voor de productie van een geladen Higgs geassocieerd met een single top quark. De moeilijkheid zit in het correct meenemen van de effecten van zachte straling. Het raamwerk waarbinnen we het computerprogramma opzetten, genaamd 'Monte Carlo at Next-to-Leading Order' (MC@NLO), maakt het mogelijk om het proces correct te berekenen tot op eerste orde in de kwantumchromodynamische correcties. Dit maakt het mogelijk om het proces te simuleren met alle deeltjes die gecreëerd worden. Hierbij wordt de ruimte gevuld met deeltjes die ontstaan door het splitsen van deeltjes met veel energie. Deze splitsingen worden gesimuleerd door klassieke kansprocessen en bieden daarom geen ruimte voor volledige kwantumcorrecties. Het MC@NLO raamwerk maakt het mogelijk om de eerste orde kwantumcorrectie op een consistente manier mee te nemen, om zo fysische grootheden uit te rekenen die accuraat zijn tot op eerste orde. Een dergelijk computer programma is van belang voor experimenten zoals die gedaan gaan worden met de LHC op het CERN.

Acknowledgments

My research has been done both at Utrecht University and at NIKHEF (National Institute for Subatomic Physics). As a guest at NIKHEF, I want to acknowledge their hospitality.

First and foremost I want to express my gratitude to Eric Laenen, my supervisor. I enjoyed the interesting discussions about physics and admire the effectiveness of your research. In case of research problems, you are able to quickly envision a path to obtain results. Furthermore you were always supportive and available for questions, tutoring or proof reading.

A special thanks goes to Chris White. We collaborated on multiple articles and I learned a lot from you. Working together was very enjoyable because of your humor and good spirit. Thanks, also, for your help during the write up of this thesis. Furthermore I like to thank Lorenzo Magnea for our collaboration. The weeks you visited were productive and funny.

Bernard de Wit and Biene Meijerman, I like to thank you for your support during the difficult period of my research. I also enjoyed assisting your Quantum Field Theory class.

My friends in Utrecht, Jaap, Jan, Lotte, Cornelis, Sander D, Sander, Pieter, Hendrik, Rudy, Mariska, Tom, my volleyball friends, thanks a lot for the good times and your support during the difficult time. Jan and Jaap, also my direct colleagues, it was always nice to discuss fun problems with you. As a life long friend and one of my paranimfs, I like to thank Martin van Breukelen.

I would like to thank all my colleagues both from Utrecht and Amsterdam and in particular my roommates Patrick, Gideon, Lisa, Sander, Tomas, Thomas, Mathijs and Reinier during these years.

At last I want to thank my family. Papa, bedankt voor je hulp en steun, ik voel me altijd weer helemaal rustig als ik bij jou ben. Vanzelfsprekend wil ik ook mama noemen die in het begin van de AIO periode, hoewel ziek, altijd mij gesteund heeft. Ik mis haar nog steeds. Boukje, Laura, Dieneke en Dick ik vind het erg leuk dat jullie er bij zijn gekomen. Verder wil ik omke Doekele bedanken die mij raad heeft raad heeft gegeven. Tenslotte wil ik mijn broer Jauke noemen. Wij hebben elkaar veel gezien tijdens mijn promotietraject. Ik vond het heel fijn dat je regelmatig bij mij was, zowel op het werk als thuis. Bedankt dat je mijn paranimf wilt zijn.

Curriculum Vitae

The author was born on June 25, 1980 in Delft, the Netherlands. In 1998 he obtained his VWO degree at Zandvliet College in The Hague. Ensuing, he started studying physics and mathematics at Utrecht University. He received his master's degree in theoretical physics (cum laude) in 2005. For his master's thesis research, he studied quantum chromodynamics under supervision of Eric Laenen. He continued his research in a PhD position, again under supervision of Eric Laenen. After completing his PhD, the author will continue his academic career at Fermilab for a postdoc position.